RĪGAS TEHNISKĀ UNIVERSITĀTE

**Anastasija Gaile**

# HINONU ATVASINĀJUMU MODIFIKĀCIJA REDOKSAKTĪVO MATERIĀLU IZVEIDEI

Promocijas darbs

# MODIFICATION OF QUINONE DERIVATIVES FOR THE DESIGN OF REDOX-ACTIVE MATERIALS

Doctoral Thesis

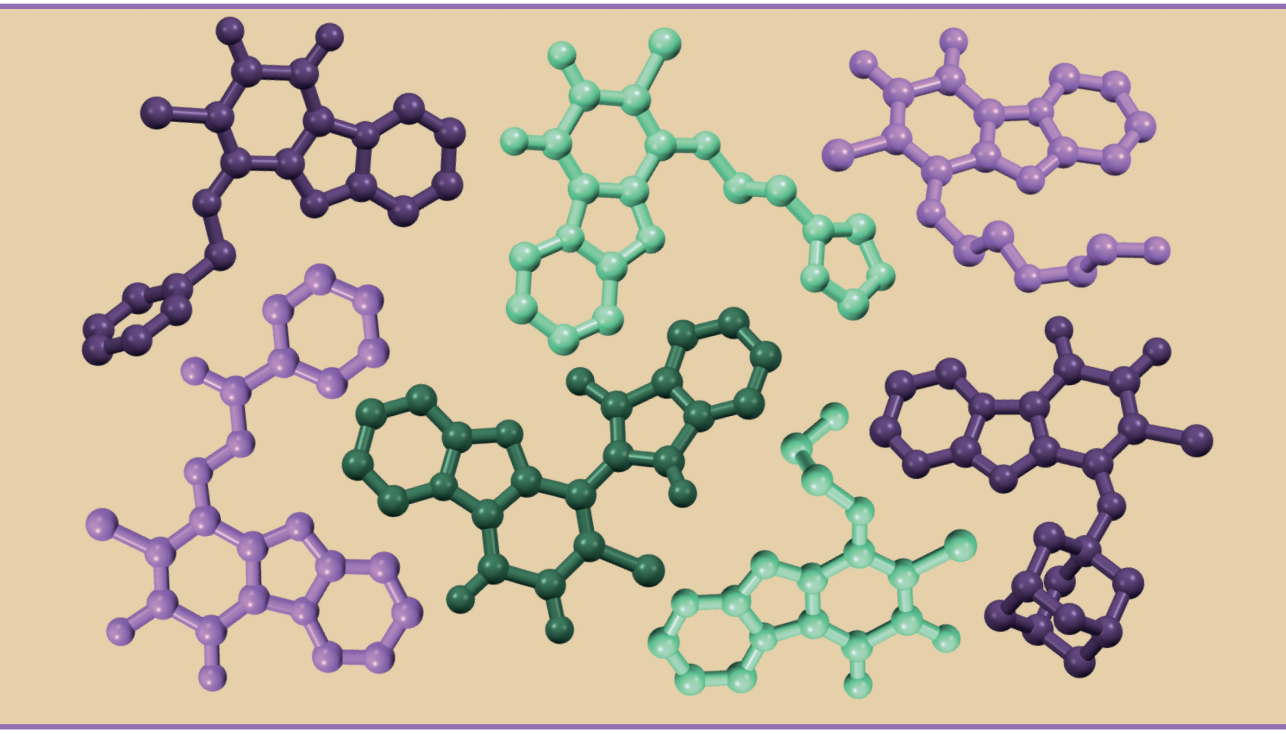

RTU Izdevniecība
RTU Press
Rīga 2024

**RĪGAS TEHNISKĀ UNIVERSITĀTE**
Dabaszinātņu un tehnoloģiju fakultāte
Ķīmijas un ķīmijas tehnoloģijas institūts

**RIGA TECHNICAL UNIVERSITY**
Faculty of Natural Sciences and Technology
Institute of Chemistry and Chemical Technology

**Anastasija Gaile**

Doktora studiju programmas "Ķīmija, materiālzinātne un tehnoloģijas" studente
Doctoral Student of the Study Programme "Chemistry, Materials Science and Engineering"

# HINONU ATVASINĀJUMU MODIFIKĀCIJA REDOKSAKTĪVO MATERIĀLU IZVEIDEI

# MODIFICATION OF QUINONE DERIVATIVES FOR THE DESIGN OF REDOX-ACTIVE MATERIALS

**Promocijas darbs**
**Doctoral Thesis**

Zinātniskā vadītāja / Scientific supervisor
asociētā profesore / Associate Professor
*Dr. chem.* NELLI BATENKO

RTU Izdevniecība
RTU Press
Rīga/Riga 2024

Gaile A. Hinonu atvasinājumu modifikācija redoksaktīvo materiālu izveidei. Promocijas darbs. – Rīga: RTU Izdevniecība, 2024. – 137 lpp.

Gaile, A. Modification of Quinone Derivatives for the Design of Redox-Active Materials. Doctoral Thesis. Riga: RTU Press, 2024. 137 p.

Publicēts saskaņā ar promocijas padomes "RTU P-01" 2024. gada 8. aprīļa lēmumu, protokols Nr. 04030-9.1/60.

Published in accordance with the decision of the Promotion Council "RTU P-01" of 8 April 2024, Minutes No. 04030-9.1/60.

Promocijas darbs izstrādāts ar Eiropas Sociālā fonda atbalstu darbības programmas "Izaugsme un nodarbinātība" 8.2.2. specifiskā atbalsta mērķa "Stiprināt augstākās izglītības institūciju akadēmisko personālu stratēģiskās specializācijas jomās" projektā Nr. 8.2.2.0/20/I/008 "Rīgas Tehniskās universitātes un Banku augstskolas doktorantu un akadēmiskā personāla stiprināšana stratēģiskās specializācijas jomās". Pētījums tapis ar Rīgas Tehniskās universitātes Doktorantūras grantu programmas atbalstu.

This research was supported by the European Social Fund within the Project No. 8.2.2.0/20/I/008, "Strengthening of PhD students and academic personnel of Riga Technical University and BA School of Business and Finance in the strategic fields of specialization" of the Specific Objective 8.2.2, "To Strengthen Academic Staff of Higher Education Institutions in Strategic Specialization Areas", of the Operational Programme "Growth and Employment" and by the Riga Technical University's Doctoral Grant Programme.

# PROMOCIJAS DARBS IZVIRZĪTS ZINĀTNES DOKTORA GRĀDA IEGŪŠANAI RĪGAS TEHNISKAJĀ UNIVERSITĀTĒ

Promocijas darbs zinātnes doktora (*Ph. D.*) grāda iegūšanai tiek publiski aizstāvēts 2024. gada 10. jūnijā Rīgas Tehniskās universitātes Dabaszinātņu un tehnoloģiju fakultātē, P. Valdena ielā 3, 272. auditorijā.

OFICIĀLIE RECENZENTI

Asociētais profesors *Dr. chem*. Artis Kinēns,
Latvijas Universitāte, Latvija

Asociētais profesors *Dr. chem.* Agris Bērziņš,
Latvijas Universitāte, Latvija

Vadošais pētnieks *Dr. chem.* Kārlis Pajuste,
Latvijas Organiskās sintēzes institūts, Latvija

APSTIPRINĀJUMS

Apstiprinu, ka esmu izstrādājusi šo promocijas darbu, kas iesniegts izskatīšanai Rīgas Tehniskajā universitātē zinātnes doktora (*Ph. D.*) grāda iegūšanai. Promocijas darbs zinātniskā grāda iegūšanai nav iesniegts nevienā citā universitātē.

Anastasija Gaile ……. (paraksts)

Datums: ……

Promocijas darbs sagatavots kā tematiski vienotu zinātnisko publikāciju kopa ar kopsavilkumu latviešu un angļu valodā. Tajā ietverti trīs zinātniskie oriģinālraksti un divi apskatraksti. Publikācijas zinātniskajos žurnālos uzrakstītas angļu valodā, to kopējais apjoms, ieskaitot pielikumus, ir 175 lpp.

# SATURS

4. Pielikums **Gaile, A**.; Batenko, N. Synthesis of Heterocyclic Ring-Fused Quinones (Microreview). *Chem. Heterocycl. Compd.* **2021**, *57* (11), 1076–1078. https://doi.org/10.1007/s10593-021-03027-w

5. Pielikums Batenko, N.; **Gaile, A**. Chemosensors Based on 5-Ethylidene-Substituted Barbituric Acid Derivatives (Microreview). *Chem. Heterocycl. Compd.* **2022**, *58* (2–3), 97–99. https://doi.org/10.1007/s10593-022-03061-2

6. Pielikums **Gaile, A.**; Dūrena, R.; Griščenko, Ņ.; Zukuls, A.; Batenko, N. Studies of cathode materials based on 6,7-dichloropyrido[1,2-*a*]benzimidazole-8,9-dione derivatives. *Nepublicēti rezultāti.*

# LIETOTIE SAĪSINĀJUMI

$\lambda_{max}$ – absorbcijas joslas maksimuma viļņa garums (nm)
δ – ķīmiskā nobīde (ppm)
ε – molārās absorbcijas koeficients
*BLA* – saišu garumu maiņa (*bond length alternation*)
*CM* – katoda materiāls (*cathode material*)
*CT* – lādiņa pārnese
CV – cikliskā voltampērmetrija
DBU – 1,8-diazabiciklo[5.4.0]undec-7-ēns
DCM – dihlormetāns
*DFT* – blīvuma funkcionāļa teorija (*density functional theory*)
DMF – *N,N*-dimetilformamīds
DMSO – dimetilsulfoksīds
Et – etil-
*FTIR* – infrasarkanā Furjē spektroskopija
h – stunda
H-saite – ūdeņraža saite
*HOMO* – augstākā aizņemtā molekulārā orbitāle
i. t. – istabas temperatūra
KMR – kodolu magnētiskā rezonanse
*LUMO* – zemākā neaizņemtā molekulārā orbitāle
Me – metil-
MT KMR – mainīgas temperatūras kodolu magnētiskā rezonanse
*PCM* – polarizējamā kontinuuma modelis (*polarizable continuum model*)
Ph – fenil-
ppm – miljonās daļas (*parts per million*)
PVDF – polivinilidēnfluorīds
RSA – rentgenstruktūranalīze
SEM – skenējošā elektronu mikroskopija
TFA – trifluoretiķskābe
UV-Vis – ultravioletās un redzamās gaismas (spektroskopija)

# PROMOCIJAS DARBA VISPĀRĒJS RAKSTUROJUMS

## Tēmas aktualitāte

Hinoni pārstāv konjugētu ciklisku diketonu klasi, kas sastopama dažādās dabas vielās. Šie savienojumi ir plaši zināmi, pateicoties to bioloģiskajai aktivitātei un fotofizikālajām īpašībām, kā arī citotoksisko un citoprotektīvo efektu dēļ.[1] Redoksīpašības nosaka hinona atvasinājumu būtisko nozīmi bioloģiskajos procesos (piemēram, šūnu elpošanā[2] un fotosintēzē[3]). Hinona strukturālie motīvi ir atrodami dažādās medicīnā lietotās vielās, piemēram, koenzīmā Q10,[4] menadionā,[5] K vitamīnā[6] un doksorubicīnā.[7]

Tajā pašā laikā hinona atvasinājumi tiek pētīti lietojumam enerģijas uzglabāšanas un enerģijas ievākšanas sistēmās.[8] Organiskie redoksaktīvie savienojumi tiek pētīti, pieaugošo prasību pēc enerģijas uzkrāšanas ierīcēm[9] dēļ, īpašu uzmanību veltot hinonu atvasinājumiem.[10, 11] Hinonu atvasinājumi pētīti kā aktīvās vielas organisko elektrodu materiāliem uzlādējamajās baterijās,[12] kā divu elektronu anolīti vai katolīti ūdens[13] un neūdens[10] redoksplūsmas (*redox flow*) baterijās, kā elektronu pārneses mediatori (*mediators*) metālu katalizētās reakcijās[14, 15] vai redoksmediatori litija sēra baterijās,[16] kā materiāls elektroķīmiskai $CO_2$ uztveršanai[17, 18] vai elektroķīmiskās ūdens sadalīšanas tehnoloģijās.[19]

Viens no perspektīvākajiem pētniecības virzieniem ir saistīts ar pētījumiem par hinonu izmantošanu elektrodu materiālos.[20] Tomēr pirms organisko elektrodu materiālu izmantošanas uzlādējamās baterijās joprojām ir jāuzlabo elektroķīmiskā efektivitāte, kā arī jāsamazina elektroda materiāla šķīdība elektrolītos un tilpuma izmaiņas (*volume change*), jo tam seko lādiņietilpības (*charge capacity*) zudumi.[21] Formāli hinonu atvasinājumus var iedalīt divās grupās – lielmolekulārie un mazmolekulārie atvasinājumi. Lielmolekulāro savienojumu (hinonu polimēri vai pie polimēriem saistīti hinoni) gadījumā samazinās šķīdība elektrolītā, taču no ekonomiskā viedokļa jāņem vērā arī substrātu un reaģentu izmaksas lielmolekulāro atvasinājumu sintēzei.[22] Turpretim mazmolekulāru hinonu materiālu priekšrocība ir zemākas izmaksas un vienkāršas sintēzes procedūras (1. att.).

Kontrolēta elektroķīmiskā veiktspēja un šķīdība ir izšķirošie faktori, lai iegūtu stabilus organisko elektrodu materiālus uz mazmolekulāro hinonu bāzes. Tādas īpašības kā šķīdība, ķīmiskā vai termiskā stabilitāte ir atkarīgas no hinona ķīmiskās struktūras, mijiedarbības ar saistvielām un iespējamās izomerizācijas. Turklāt salīdzinoši vājās nekovalentās starpmolekulārās mijiedarbības (ūdeņraža saites (H-saites), π-π mijiedarbības, van der Vālsa spēki, elektrostatiskie Kulona spēki) būtiski ietekmē morfoloģiju, dažādas fizikāli ķīmiskās īpašības (kušanas/viršanas temperatūra, blīvums, šķīdība), jonu difūziju, lādiņu transportu un organisko materiālu elektroķīmiskās īpašības.[23] Neapšaubāmi, vienlaikus var pastāvēt dažādas mijiedarbības, kas veicina pašsakārtotas struktūras (*self-assembled structure*).[24] Turklāt supramolekulāro sakārtojumu (*supramolecular assembly*) un kristalizāciju var kontrolēt, kombinējot dažādas starpmolekulārās mijiedarbības (piemēram, H-saites kopā ar π-π un/vai dipolārām mijiedarbībām), taču šāda kontrole joprojām nav izstrādāta.[25]

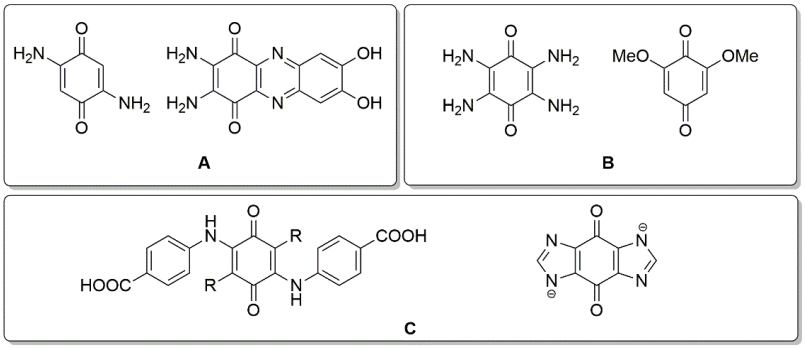


1. att. Mazmolekulāro hinona atvasinājumu piemēri,[25–30] kas pētīti potenciālai izmantošanai enerģijas uzkrāšanā, piemēram: (**A**) kandidāti $Li^+$ jonu baterijām; (**B**) kandidāti $Zn^{2+}$ jonu baterijām; (**C**) kandidāti izmantošanai redoksplūsmas (*redox flow*) baterijās.

Tādējādi sakarības starp hinona atvasinājumu struktūru un īpašībām, kā arī elektroķīmisko īpašību izpēte var noteikt savienojumu izmantošanas iespējas un ierobežojumus. Pieeja jaunu organisko materiālu izstrādei, iekļaujot vājas iekšmolekulārās un/vai starpmolekulārās mijiedarbības, kas var mainīt materiāla arhitektūru, palīdzēs uzlabot hinonu funkcionalizētu materiālu efektivitāti molekulārā līmenī.

Hinona atvasinājumu elektroķīmiskās un fizikāli ķīmiskās īpašības var uzlabot, modificējot mazas hinona molekulas ar funkcionālām grupām[21] vai kondensējot[31, 32] ar heterocikliem. Imidazo[1,2-*a*]piridīns ir izplatīts slāpekli saturošs heterocikls, kas tiek izmantots farmakoloģijas pētījumos,[33] kā arī pētīts materiālzinātnē.[34, 35] Imidazo[1,2-*a*]piridīna atvasinājumi var veidot spēcīgu iekšmolekulāru H-saiti starp protondonoru aizvietotāju un heterocikla slāpekli, kas veicina ierosinātā stāvokļa iekšmolekulāro protona pārneses (*excited-state intramolecular proton transfer, ESIPT*) izraisītu luminiscenci.[36,37] Turklāt imidazo[1,2-*a*]piridīna atvasinājumu pašsakārtoto fragmentu morfoloģiju (*morphologies of self-assembled motifs*) var ietekmēt, ja imidazo[1,2-*a*]piridīna sistēma tiek modificēta ar dažādām funkcionālajām grupām.[24]

Kā promocijas darba pamatstruktūra tika izvēlēts 6,7-dihlorpirido[1,2-*a*]benzimidazol-8,9-dions (2. att.), kas satur divu struktūrelementu kombināciju – *o*-hinona un imidazo[1,2-*a*]piridīna fragmentus. To var iegūt vienas stadijas sintēzē no komerciāli pieejamiem tetrahlor-1,4-benzohinona un 2-aminopiridīna.[38] No literatūras ir zināms,[38] ka 6,7-dihlorpirido[1,2-*a*]benzimidazol-8,9-dionu, tā atvasinājumus un analogus var viegli modificēt, selektīvi aizvietojot hlora atomu pie C(6) ar nukleofiliem, radot monoaizvietotu produktu. Tādējādi pirido[1,2-*a*]benzimidazol-8,9-diona atvasinājumi varētu sniegt iespēju izpētīt aizvietotāju ietekmi uz kopējo heterocikliskā hinona fragmenta struktūru un to fizikālajām un redoksīpašībām.

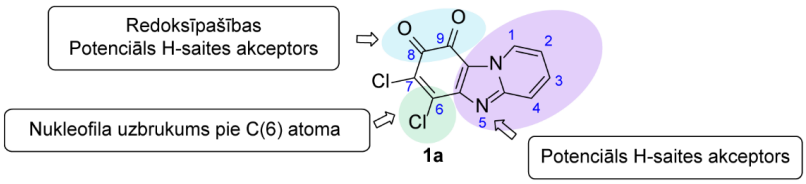


2. att. 6,7-Dihlorpirido[1,2-*a*]benzimidazol-8,9-diona struktūra (**1a**).

Promocijas darbs iedalīts divās daļās. Pirmajā daļā ir apkopoti dati, kas iegūti, modificējot izvēlētos heterocikliskos *o*-hinonus ar *C*-nukleofiliem, kā arī iegūto atvasinājumu struktūras pētījumi un redoksīpašības šķīdumā. Promocijas darba otrajā daļā aprakstīti 6,7-dihlorpirido[1,2-*a*]benzimidazol-8,9-diona modifikācijas rezultāti, izmantojot *N*-nukleofilus, un iegūto hinona atvasinājumu struktūras analīze (tautomērās formas), iekšmolekulāro un starpmolekulāro H-saišu un citu vāju nekovalentu mijiedarbību analīze. Elektrodu materiāli tika pagatavoti no heterocikliskā *o*-hinona un tā *p*-hinonimīna atvasinājuma, un to redoksīpašības tika analizētas. Šie strukturālie pētījumi tika veikti, lai atrastu potenciālas struktūru-īpašību sakarības, kas saista mazmolekulāro heterociklisko hinonu struktūru, iekšmolekulārās un starpmolekulārās mijiedarbības un fizikālās īpašības, nodrošinot datu kopumu turpmākajām materiālu izveides stratēģijām.

## Pētījuma mērķis un uzdevumi

Promocijas darba mērķis ir 6,7-dihlorpirido[1,2-*a*]benzimidazol-8,9-diona, tā atvasinājumu un analogu modifikācija, kā arī iegūto atvasinājumu strukturālie pētījumi un struktūru-īpašību sakarību izpēte.

Darba mērķa sasniegšanai definēti vairāki uzdevumi.

1. Modificēt 6,7-dihlorpirido[1,2-*a*]benzimidazol-8,9-dionu, tā atvasinājumus un analogus reakcijās ar *C*- un *N*-nukleofiliem.
2. Izmantojot rentgenstruktūranalīzes (RSA) datus, noskaidrot hinona atvasinājumu molekulāro struktūru un noteikt vājās nekovalentās mijiedarbības cietā stāvoklī.
3. Salīdzināt atvasinājumu molekulāro struktūru cietā stāvoklī un šķīdumā, izmantojot RSA, UV-Vis spektroskopijas un KMR spektroskopijas metodes kopā ar kvantu ķīmiskajiem aprēķiniem.
4. Izpētīt izvēlēto 6,7-dihlorpirido[1,2-*a*]benzimidazola-8,9-diona atvasinājumu redoksīpašības.

## Zinātniskā novitāte un galvenie rezultāti

Promocijas darbā gaitā tika iegūti 6,7-dihlorpirido[1,2-*a*]benzimidazol-8,9-diona atvasinājumi nukleofilās aizvietošanās reakcijās ar *C*- un *N*-nukleofiliem, ievadot aizvietotāju pie C(6). Reakcijā ar stēriski apjomīgiem *C*-nukleofiliem veidojās stabili

heterocikliskie *o*-hinona atvasinājumi. Gadījumā, ja tika izmantoti stēriski mazāki *C*-nukleofili, izveidotā produkta struktūru var aprakstīt pēc "saistīto polimetīnu" principa. Izmantojot aroilhidrazīdus kā *N*-nukleofilus, iegūti stabili *p*-hinonimīna atvasinājumi, bet reakcijās ar pirmējiem amīniem iegūtajiem produktiem piemīt merocianīna tipa struktūras. Iegūtajos savienojumos "klasiskā" heterocikliskā *o*-hinona struktūrelementa forma mainās atkarībā no ievadītā aizvietotāja, līdz ar to paplašinās savienojumu fizikālo īpašību diapazons.

Pamatojoties uz rentgenstruktūranalīzes un KMR spektroskopijas datiem, vairākos gadījumos savienojumos gan cietā stāvoklī, gan šķīdumā pastāv iekšmolekulārā H-saite (NH···N vai OH···N) starp ievadīto aizvietotāju un heterocikla slāpekli. Pateicoties vairākām vājām nekovalentām starpmolekulārām mijiedarbībām, iegūto *o*-hinona atvasinājumu kristālos tika novēroti dažādi molekulārās struktūras sakārtojumi. Nukleofilās aizvietošanās reakcijās ar pirmējiem amīniem izolēti 6-aminoaizvietoti *o*-hinona atvasinājumi (satur -NH-$CH_2$- struktūrelementu), kas var veidot centrosimetriskus ahirālus vai necentrosimetriskus hirālus kristālus, pateicoties kavētai rotācijai ap ogleklis-slāpeklis saiti. No 6,7-dihlorpirido[1,2-*a*]benzimidazol-8,9-diona un tā *p*-hinonimīna atvasinājumiem tika izgatavoti katoda materiāli un pārbaudīta redoksaktivitāte. Secināts, ka heterociklisko *o*-hinonu potenciāli var izmantot kā katoda materiālu ūdens elektrolītu baterijās.

## Darba struktūra un apjoms

Promocijas darbs sagatavots kā tematiski vienotu zinātnisko publikāciju kopa, kas veltīta 6,7-dihlorpirido[1,2-*a*]benzimidazol-8,9-diona un tā analogu un to atvasinājumu sintēzei, struktūras un īpašību izpētei cietā stāvoklī un/vai šķīdumā.

## Darba aprobācija un publikācijas

Promocijas darba galvenie rezultāti publicēti trīs zinātniskajos oriģinālrakstos. Promocijas darba izstrādes laikā sagatavoti divi apskatraksti. Pētījuma rezultāti prezentēti piecās zinātniskajās konferencēs.

**Zinātniskās publikācijas**

1. **Gaile, A.**; Belyakov, S.; Dūrena, R.; Griščenko, N.; Zukuls, A.; Batenko, N. Studies of the Functionalized α-Hydroxy-*p*-Quinone Imine Derivatives Stabilized by Intramolecular Hydrogen Bond. *Molecules* **2024**, *29* (7), 1613. https://doi.org/10.3390/molecules29071613
2. **Gaile, A.**; Belyakov, S.; Rjabovs, V.; Mihailovs, I.; Turovska, B.; Batenko, N. Investigation of Weak Noncovalent Interactions Directed by the Amino Substituent of Pyrido- and Pyrimido-[1,2-*a*]Benzimidazole-8,9-Diones. *ACS Omega* **2023**, *8* (43), 40960–40971. https://doi.org/10.1021/acsomega.3c07005
3. **Gaile, A.**; Belyakov, S.; Turovska, B.; Batenko, N. Synthesis of Asymmetric Coupled Polymethines Based on a 7-Chloropyrido[1,2-*a*]Benzimidazole-8,9-Dione Core. *J. Org. Chem.* **2022**, *87* (5), 2345–2355. https://doi.org/10.1021/acs.joc.1c02196

4. Batenko, N.; **Gaile, A**. Chemosensors Based on 5-Ethylidene-Substituted Barbituric Acid Derivatives (Microreview). *Chem. Heterocycl. Compd.* **2022**, *58* (2–3), 97–99. https://doi.org/10.1007/s10593-022-03061-2
5. **Gaile, A**.; Batenko, N. Synthesis of Heterocyclic Ring-Fused Quinones (Microreview). *Chem. Heterocycl. Compd.* **2021**, *57* (11), 1076–1078. https://doi.org/10.1007/s10593-021-03027-w

**Dalība konferencēs**

1. **Gaile, A**.; Belyakov, S.; Rjabovs, V.; Batenko, N. X-ray Crystallographic and Spectroscopic Studies of Heterocyclic *o*-Quinone Derivatives. 1st Aristotle Conference on Chemistry "Advances and Challenges in Chemistry 2023, Thessaloniki, Greece. November 12–15, **2023**.
2. **Gaile, A**.; Belyakov, S.; Batenko, N. NMR studies of 6-aminosubstituted pyrido- and pyrimido-[1,2-*a*]benzimidazole-8,9-diones. Riga Technical University 64th International Scientific Conference "Materials Science and Applied Chemistry", Riga, Latvia October 6, **2023**.
3. **Gaile, A**.; Belyakov, S.; Batenko, N. Investigation of Quinone Hydrazones/Thiosemicarbazones as Potential Bifunctional Ligands for Metal ion Complexation. Riga Technical University 63rd International Scientific Conference "Materials Science and Applied Chemistry", Riga, Latvia October 21, **2022**.
4. **Gaile, A**.; Belyakov, S.; Batenko, N. *o*-Quinone derivatives containing functionalized indane fragment: experimental and theoretical studies. Riga Technical University 62nd International Scientific Conference "Materials Science and Applied Chemistry", Riga, Latvia October 22, **2021**.
5. **Gaile A**, Belyakov S, Batenko A. Synthesis and structure investigation of benzimidazole-based 1,2- and 1,4-quinone derivatives. Riga Technical University 61th International Scientific Conference "Materials Science and Applied Chemistry 2020", Riga, Latvia, October 23, **2020**.

# PROMOCIJAS DARBA GALVENIE REZULTĀTI

Pētot mazmolekulāro hinonu funkcionalizēšanas virzienus, ir jāievēro hinona iespējamie tautomērie līdzsvari, kas var radīt jaunas savienojuma formas un īpašības. Piemēram, aizvietotāja ievadīšana *o*-benzohinona (**A**, **C**) C(4) pozīcijā var izraisīt tautomērās pārvērtības par *p*-hinonimīnu (**B**) vai *p*-hinonmetīdu (**D**) (3. att.), kas dažos gadījumos bioloģiskās sistēmās izraisa toksicitāti.[1] Daudzos nozīmīgos bioloģiskos procesos (piemēram, lignīna biosintēzē[39], kutikulāra sklerotizācijā[40] (*cuticular sclerotization*) kukaiņos vai melanīna[41] izveidē) *p*-hinonmetīda starpproduktiem ir izšķiroša nozīme kateholu atvasinājumu metaboliskajā oksidēšanā. *Land, E. J.* ar līdzautoriem[42] noskaidroja, ka, ievadot cianometilgrupu 1,2-naftohinona C(4) pozīcijā, novērots tautomērais līdzsvars un veidojas *p*-hinonmetīda forma. Ja aizvietošanās reakcijā izmanto pirmējo amīnu, var veidoties produktu maisījums galvenokārt tautomērā līdzsvara starp 4-amino-*o*-hinona un α-hidroksi-*p*-hinonimīna formām dēļ. Līdzsvars ir atkarīgs no šķīdinātāja polaritātes[43] un vides pH.[44]

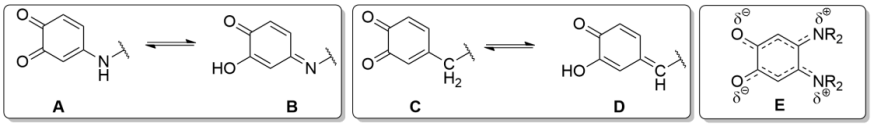


3. att. Tautomērais līdzsvars starp 4-amino-*o*-hinona (**A**) un α-hidroksi-*p*-hinonimīna (**B**) formām; tautomērais līdzsvars starp *o*-hinona (**C**) un α-hidroksi-*p*-hinonmetīda (**D**) formām; "saistītie polimetīni" (*coupled polymethines*) (**E**) uz *o*-hinona atvasinājuma bāzes.

Modificētos *o*-benzohinonus var raksturot arī kā "saistītos polimetīnus" (*coupled polymethines*) atkarībā no C(4) vai/un C(5) aizvietotāja rakstura, ja elektroni ir delokalizēti tikai starp karbonilgrupas skābekļa atomu un ievadīto aizvietotāju (aminoaizvietota savienojuma **E** gadījumā; 3. att.). Saskaņā ar *Dähne, S.* un līdzautoru pētījumiem,[45, 46] ja molekulā ir atrodamas divi polimetīna struktūrelementi (vai viens polimetīna un viens poliēna struktūrelements), tad tie nosaka savienojuma fotofizikālās īpašības.

## 1. Pirido[1,2-*a*]benzimidazol-8,9-diona fragmenta modifikācija reakcijā ar *C*-nukleofiliem

Ir zināms,[47] ka fotofizikālās un redoksīpašības korelē ar savienojuma struktūru, tajā skaitā planaritāti (starpplakņu leņķa (φ) vērtību), elektronu sadalījumu un redokspotenciāliem. Lai izpētītu aizvietotāja ietekmi uz 6,7-dihlorpirido[1,2-*a*]benzimidazol-8,9-diona (**1a**) struktūru, hinons **1a** tika modificēts ar plaši lietotiem *C*-nukleofiliem (1,3-indāndiona atvasinājumiem ar dažādu diciānometilēnvienību skaitu[48–50] (**2-4**), malononitrilu (**5**) un barbitūrskābi[51] (**6**)) trietilamīna klātbūtnē. Heterocikliskie hinona atvasinājumi (**7–11**) tika izolēti trietilamonija sāļu veidā (1. shēma). Savienojuma **10** sintēze tika veikta paaugstinātā temperatūrā, jo istabas temperatūrā reakciju iznākumi bija zemāki. Iegūtie produkti **7-11** ir krāsainas vielas, tumši zaļa krāsa piemīt

savienojumiem **7** un **11**, brūna – savienojumam **8**, zili violeta – savienojumiem **9**, **10**. Analizējot to struktūru, noskaidrots, ka trietilamonija sāļiem **7-11** piemīt dažādas hinona fragmenta formas.

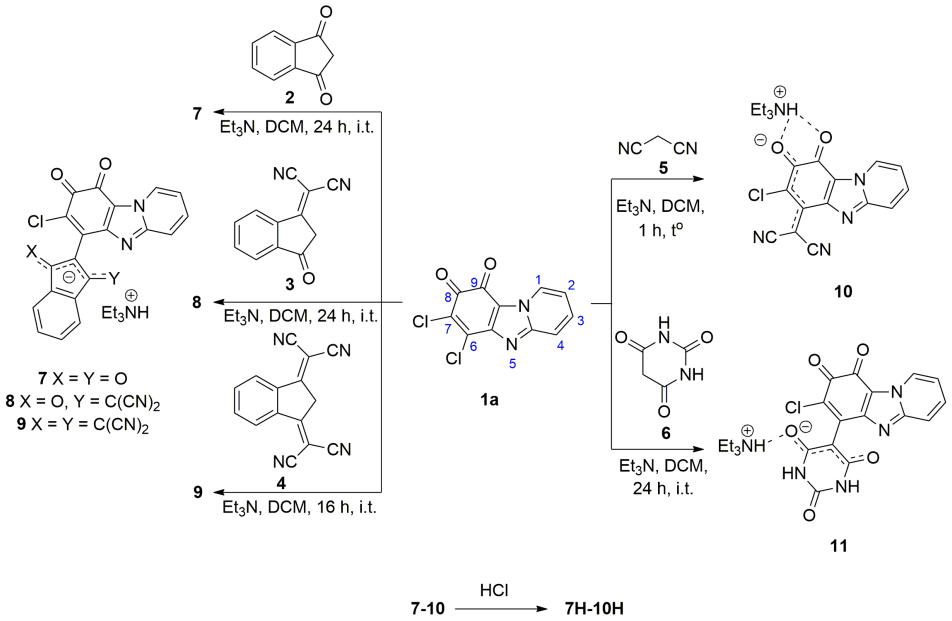


1. shēma. Savienojumu **7-11** un **7H-10H** sintēze.

Pēc trietilamonija sāļu **7-10** hidrolīzes skābā vidē izdalīti savienojumi **7H-10H**. Savienojuma **7H** gadījumā tika iegūta sarkana cieta viela, kas veidoja zaļas krāsas šķīdumu dimetilsulfoksīdā (DMSO). Sarkanās vielas *FTIR* spektrs uzrādīja absorbcijas joslas pie 1746 $cm^{-1}$ un 1702 $cm^{-1}$, kā arī netika novērota hidroksilgrupai raksturīgā absorbcijas josla. Secināts, ka hidrolīzes rezultātā veidojas produkts **7H**$^{keto}$ (cietā stāvoklī piemīt sarkanā krāsā), kur indāndiona fragments eksistē ketoformā. Tomēr sarkanās krāsas kristālu $^{1}$H KMR spektrā DMSO-$d_6$ šķīdumā eksistē tautomērais līdzsvars starp ketoformu (K) un enolformu (E) un tika novēroti divi signālu komplekti.[52] No $^{1}$H KMR spektra attiecība ketoforma/enolforma ir vienāda ar 0,45 : 1 (4. c att.).

Iztvaicējot šķīdinātāju no sāls **7** dihlormetāna (DCM) šķīduma, tika iegūti savienojuma **7H** (enolforma – **7H**$^{enol}$) zaļi kristāli. Savienojuma **7H**$^{enol}$ struktūra tika pieradīta ar rentgenstruktūranalīzes (RSA) metodi – kristaliskā stāvoklī heterocikliskais *o*-hinona fragments ir saistīts ar indāndiona fragmentu enolformā (4. a att.). Molekulu stabilizē ļoti spēcīga iekšmolekulārā ūdeņraža saite (H-saite) OH···N (N(5)···H = 1,172 Å, H···O = 1,379 Å, leņķa N(5)···H···O vērtība ir 157(6)°). Savienojuma **7H**$^{enol}$ kristāliskajā struktūrā tika konstatēta arī spēcīga starpmolekulārā σ-caurumu mijiedarbība starp C=O saites skābekli (indāndiona fragments) un hlora atomu; starpmolekulārās mijiedarbības rezultātā veidojās centrosimetriski molekulārie dimēri (4. b att.).

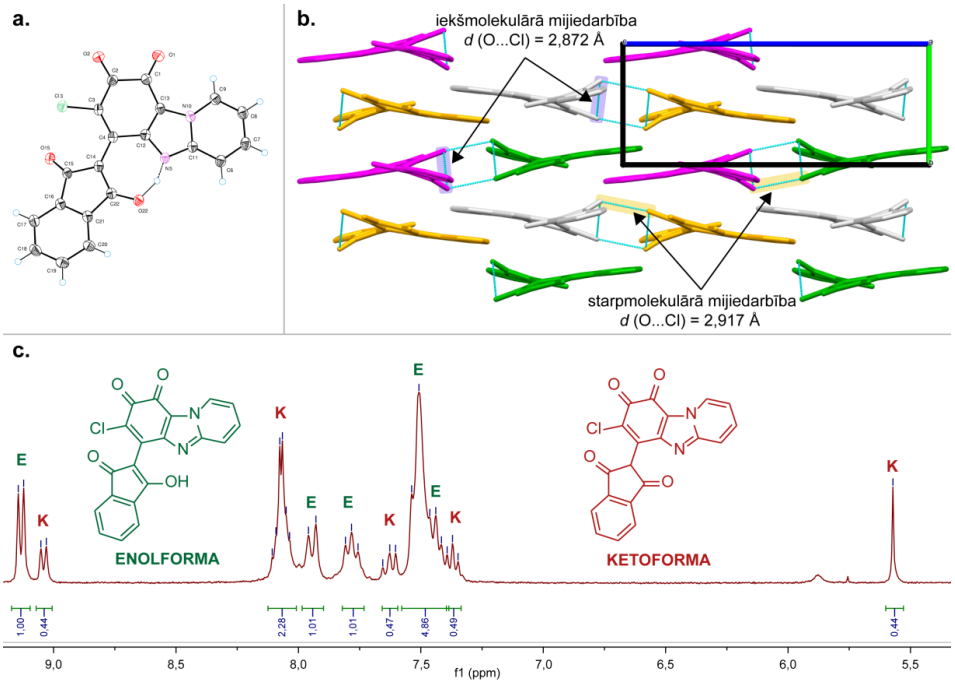


4. att. (a) Savienojuma **7H**$^{enol}$ asimetriskās vienības *ORTEP* diagramma, kas parāda termiskos elipsoīdus 50 % varbūtības līmenī; (b) savienojuma **7H**$^{enol}$ molekulu sakārtojums kristālā; gaiši zilas līnijas norāda O…Cl mijiedarbību; (c) $^{1}$H KMR spektra fragments (300 MHz, DMSO-$d_6$), enolformas (E) un ketoformas (K) struktūras.

Lai labāk izprastu aizvietotāja ietekmi uz heterocikliskā hinona fragmentu, savienojumiem **10-11** un **7H**$^{enol}$ tika veikta RSA datu analīze kopā ar *DFT* aprēķiniem (programma *ORCA*[53], *CAM-B3LYP/def2-TZVP* teorijas līmenis). Savienojumu **10-11** un **7H**$^{enol}$ heterocikliskā hinona fragmenta saišu garumi (RSA dati) tika salīdzināti savstarpēji un ar iepriekš publicēto[38] atvasinājumu ***o*-QCCN** (5. att.). No savienojumu saišu garumu analīzes cietā stāvoklī var secināt, ka hinona ciklu var sadalīt divos struktūrelementos, kurus atdala garas vienkāršas C-C saites *1* un *4* (saišu numerācija – 5. att.). Viens struktūrelements ietver saites *16-2-3* un sekojošās aizvietotāja saites. Iepriekš minētajiem 7-hlorpirido[1,2-*a*]benzimidazol-8,9-diona atvasinājumiem saišu *2* un *3* garumi mainās atkarībā no ievadītā aizvietotāja. Piemēram, savienojumos **11** un **7H**$^{enol}$ saitēm *2* un *3* bija izteikta vienkāršās/divkāršās saišu kārtas maiņa, kā ir "klasiskajā" *o*-benzohinona struktūrā,[54] savukārt savienojumos **10** un ***o*-QCCN** tika novērota saišu garumu vienlaikus izlīdzināšanās (saites *2* un *3*).

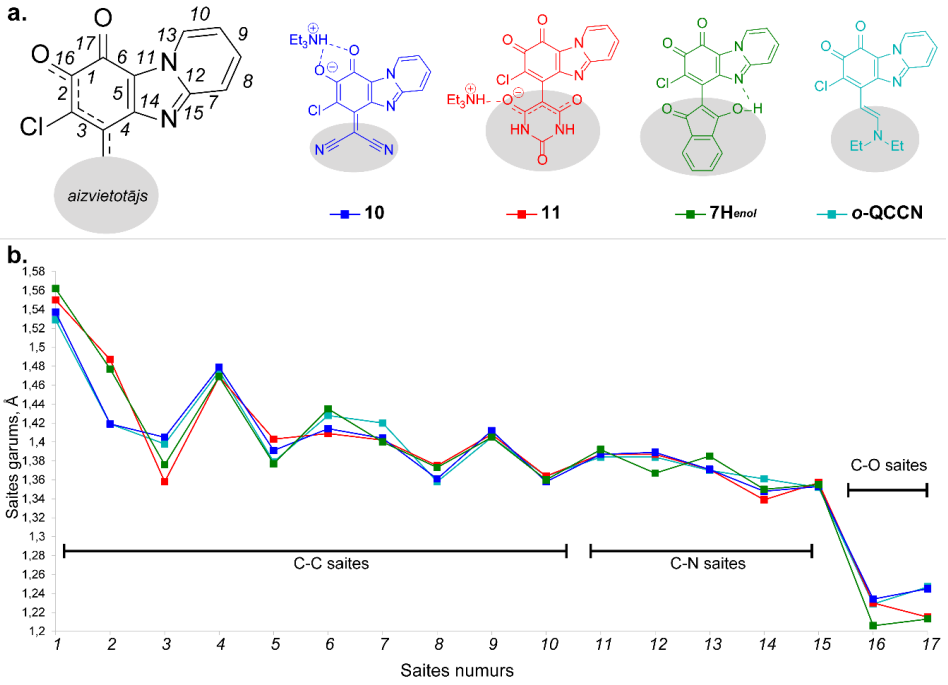


5. att. (a) Savienojumu **10-11**, **7H*enol*** un ***o*-QCCN** heterocikliskā hinona fragmenta shematiskais attēlojums ar saišu numerāciju; (b) saišu garumu salīdzinājums. Savienojuma ***o*-QCCN** saišu garumi tika ņemti no RSA datiem.[38]

Saites garuma maiņa (*bond length alternation*, *BLA*) tika aprēķināta struktūrelementam, kas satur saites *2-3-aizvietotājs* savienojumos **10-11**, **7H*enol***, ***o*-QCCN**. *BLA* parametra aprēķinam izmantoti RSA dati, kā arī kvantu ķīmisko aprēķinu dati no optimizētajām struktūru ģeometrijām (*DFT*; 1. tab.). Secināts, ka savienojumus **10** un ***o*-QCCN** var raksturot kā asimetriskus "sasaistītus polimetīnus" (*coupled polymethines*), jo oglekļa-oglekļa saitēm *2-3-aizvietotājs* *BLA* parametrs tuvojas nullei. Savienojumam **11** polimetīna fragments atrasts starp divām barbitūrskābes karbonilgrupām (izlīdzinātas saites ar π-elektronu delokalizāciju); savukārt saites *16-2-3-aizvietotājs* var raksturot kā poliēna fragmentu. Kopumā *o*-hinona formas stabilizāciju izsauc stēriski apjomīgs aizvietotājs, un negatīvā lādiņa delokalizācija notiek aizvietotāja fragmentā. Rezultātā konjugācija starp hinona ciklu un aizvietotāju pazūd. Otrs struktūrelements sastāv no heterocikla fragmenta (saites *5-15*) un blakus esošās karbonilgrupas (5. att., saite *17*). Savienojumu **10-11** un ***o*-QCCN** gadījumā *aizvietotājs* neietekmēja saišu *5-15* garumus. Hinona atvasinājumiem **10-11** un ***o*-QCCN** karbonilgrupas saites *17* garums bija līdzīgs atbilstošās saites garumam imidazo[1,2-*a*]piridīn-3-karbaldehīdā.[55] Tikai savienojuma **7H*enol*** gadījumā saite *17* bija nedaudz īsāka, jo spēcīga iekšmolekulāra H-saite (OH···N) ietekmēja π-elektronu sadalījumu molekulas heterocikliskajā daļā (saites *12-13*).

Tika salīdzināts trietilamonija sāļu **10** un **11** molekulu sakārtojums kristālā (6. att.). Novērots, ka savienojumam **10** raksturīga struktūra, kas stabilizēta ar π-π mijiedarbību (π-π *stacking*). Savienojuma **11** gadījumā kristāliskajai struktūrai ir raksturīga garu starpmolekulāro ķēžu veidošanās, pateicoties spēcīgām NH···O ūdeņraža saitēm starp barbitūrskābes fragmentiem, ar kuru anjoni ir savstarpēji saistīti.

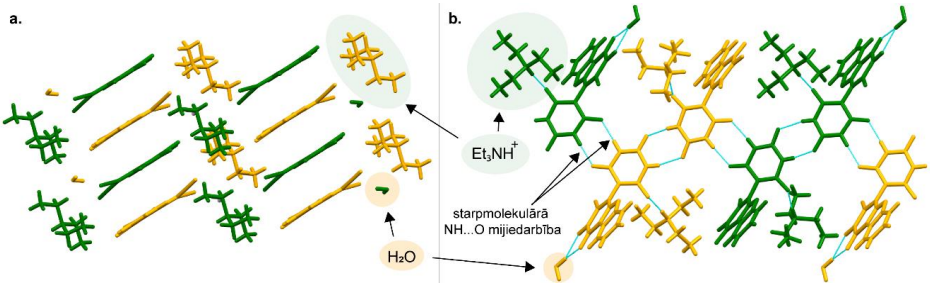


6. att. Savienojumu **10** (a) un **11** (b) sakārtojums kristālā, H-saites ir izceltas gaiši zilā krāsā.

Ar kvantu ķīmijas aprēķiniem *(DFT)* noteikta savienojumu optimizētā ģeometrija gan gāzes fāzē, gan šķīdumā (*PCM*). Iegūtie dati tika salīdzināti ar RSA eksperimentālajiem datiem (1. tab.). Savienojumu **10** un ***o*-QCCN** optimizētu struktūru ģeometrija paredz savienojumu izteiktu planaritāti, bet sāļiem **7-9** un **11** sagaidāmi 60 ± 10° starpplakņu leņķi starp ievadīto aizvietotāju plakni un heterocikliskā hinona plakni. Novērots, ka aprēķinātā optimizētā ģeometrija *CAM-B3LYP/def2-TZVP* līmenī DMF šķīdumā vislabāk atbilst eksperimentālajiem strukturālajiem parametriem (starpplakņu leņķiem un saišu garumiem no RSA datiem).

1. tabula

Savienojumu **10-11**, **7H** un ***o*-QCCN** starpplakņu leņķi ($\varphi$), saites garuma maiņa (*BLA*) un saites garums ($r$) starp plaknēm

| Savienojums | Metode | **11**[a] | **10** | **7H**$^{enol}$ | ***o*-QCCN** |
|---|---|---|---|---|---|
| Starpplakņu leņķis $\varphi$, ° | RSA | 60,79 (**11A**)<br>64,60 (**11B**) | 10,48 | 25,57 | 4,56 |
| | *DFT*[c] | 65,62 | 1,07 | 31,16 | 1,53 |
| $r_{C(6)\text{-}C(aizvietotājs)}$, Å | RSA | 1,468 (**11A**)<br>1,469 (**11B**) | 1,402 | 1,448 | 1,412 |
| | *DFT*[c] | 1,462 | 1,395 | 1,449 | 1,401 |
| *BLA* parametrs[b], Å | RSA | 0,0935 (**11A**)<br>0,0975 (**11B**) | 0,0055 | 0,0700 | 0,0245 |
| | *DFT*[c] | 0,0935 | 0,0070 | 0,0905 | 0,0260 |

[a] Sāls **11** kristāls sastāv no diviem anjoniem, kas ir apzīmēti kā anjoni **11A** un **11B**.

[b] *BLA* parametrs tika aprēķināts kā starpība starp formālās ogleklis-ogleklis vienkāršās un dubultās saites vidējo saišu garumu struktūras polimetīna/poliēna ķēdē (saites *2-3-aizvietotājs*).

[c] Ģeometrija optimizēta ar *CAM-B3LYP/def2-TZVP* metodi (DMF, *PCM*).

Trietilamonija sāļi **7-11** tika pētīti šķīdumā (DMSO-$d_6$), analizējot to $^{13}$C KMR spektrus. Tika salīdzinātas hinona karbonilgrupu signālu ķīmiskās nobīdes (δ C(8)=O un C(9)=O, atomu numerācija – 1. shēmā) $^{13}$C KMR spektros (7. a att.). Novērots, ka savienojuma **10** C(8) un C(9) signāli ir nobīdīti tuvāk viens otram ar Δδ(C=O) tikai 0,2 ppm, kas izskaidrojams ar līdzīgu elektronu blīvumu ap šiem oglekļa kodoliem, kā arī ar karbonilgrupu iesaistīšanos H-saitēs ar $Et_3NH^+$. Tomēr *o*-hinonu **7-9** un **11** $^{13}$C KMR spektros Δδ(C=O) tika aprēķināts kā 9,0 ppm, 11,5 ppm un 13,0 ppm un 11,1 ppm attiecīgi. Tika atrasta lineāra sakarība starp savienojumu **7-11** Δδ(C=O) (hinona fragments) $^{13}$C KMR spektros un aprēķināto starpplakņu leņķi (DMF) (7. b att.).

Vienādas ķīmiskās nobīdes konstatētas signāliem, kas attiecas uz 1,3-indāndiona fragmenta karbonilgrupu oglekļiem (δ(C=O) = 187,0 ppm) trietilamonija sāls **7** $^{13}$C KMR spektrā (DMSO-$d_6$). Tas liecina par vienādu ķīmisko apkārtni šiem atomiem, līdz ar to secināts, ka šķīdumā negatīvais lādiņš ir simetriski delokalizēts pa aizvietotāja fragmentu starp abām karbonilgrupām.

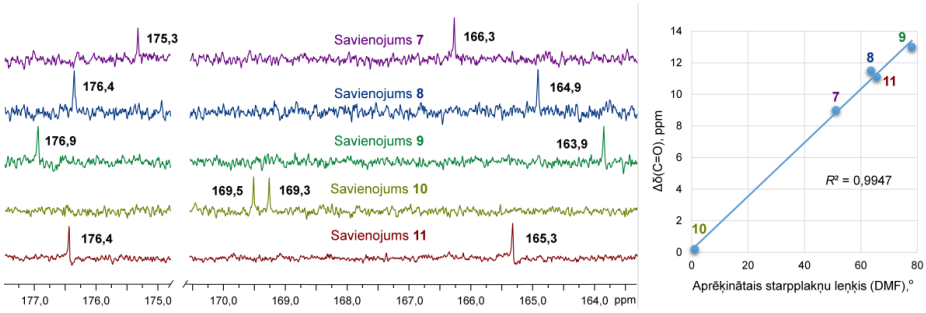


7. att. (a) Trietilamonija sāļu **7-11** $^{13}$C KMR (DMSO-$d_6$) spektru fragmenti; (b) korelācija starp savienojumu **7-11** aprēķināto starpplakņu leņķi (*CAM-B3LYP/def2-TZVP*, DMF, *PCM*) un starpību starp hinona C=O grupu ķīmiskām nobīdēm (Δδ(C=O)) $^{13}$C KMR spektros (DMSO-$d_6$).

Heterocikliskajam hinonam **1a** un tā atvasinājumiem **7-11**, kā arī ***o*-QCCN** tika aprēķinātas *HOMO*/*LUMO* enerģijas, izvietojums, kā arī to pārklāšanās vērtības (*DFT*). Salīdzinot ar izejvielu **1a** sintezētajiem savienojumiem, *HOMO* ir pārvietota no imidazo[1,2-*a*]piridīna fragmenta (8. att.) uz aizvietotāja daļu, kas liecina par savienojuma elektrondonorās daļas nobīdi. Hinona atvasinājumos **7-11** un ***o*-QCCN** *HOMO* tika izvietots molekulas polimetīna/poliēna struktūrelementā *16-2-3-aizvietotājs* (saišu apzīmējumi – 5. att), kas izskaidrojams ar negatīvā lādiņa delokalizāciju. *HOMO-LUMO* izvietojuma un pārklāšanās vērtību analīze parāda, ka savienojumiem **7-9** un **11** *HOMO* ir vairāk novietota donorajā aizvietotāja fragmentā, savukārt *LUMO* – akceptora daļā (hinona fragmentā) un ir iespējama iekšmolekulāra lādiņa pārnese (*charge transfer*, *CT*) no aizvietotāja uz hinona fragmentu. Tomēr savienojumiem **10** un ***o*-QCCN** *HOMO-LUMO* pārklāšanās vērtības ir lielākas, tāpēc šiem savienojumiem lādiņa pārneses raksturs ir mazāk izteikts (8. att.).

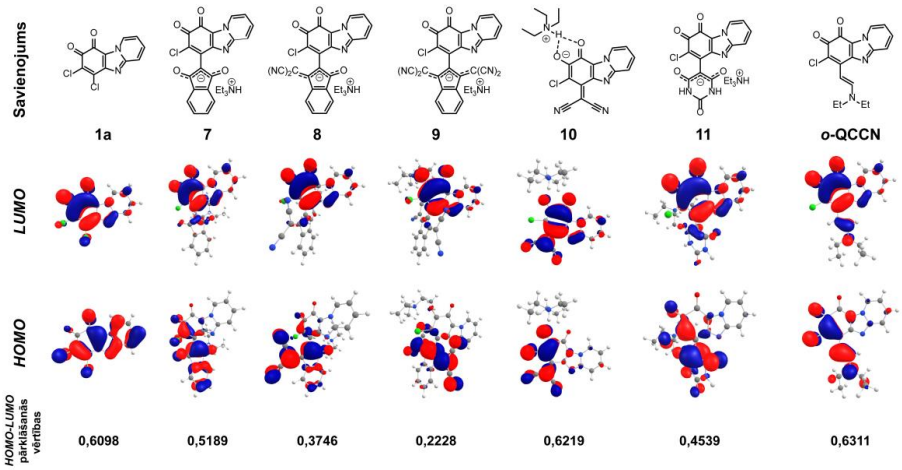


8. att. Savienojumu **1a**, **7-11** un ***o*-QCCN** frontālo orbitāļu un *HOMO-LUMO* pārklāšanās (pārklāšanās vērtības starp *HOMO* un *LUMO* tika aprēķinātas *CAM-B3LYP/def2- TZVP* līmenī DMF, izmantojot programmu *Multiwfn*).[56]

Iegūto savienojumu **7–11** īpašības šķīdumā tika pētītas, uzņemot UV-Vis spektrus šķīdinātājos ar dažādu polaritāti (DMF vai DCM), kā arī bāzes (DBU) un skābes (TFA) klātbūtnē (2. tab.). Iegūtajiem atvasinājumiem **7-9** atkarībā no ievadītā aizvietotāja novērota pozitīva vai negatīva solvatohromija. Piemēram, savienojumam **7** novērota pozitīva solvatohromija (garāko viļņu absorbcijas josla nobīdās hipsohromi, samazinoties šķīdinātāja polaritātei), savukārt sāļiem **8-9** bija novērota negatīva solvatohromija. Tas nozīmē, ka savienojumam **7** ierosinātais stāvoklis ir polārāks par pamatstāvokli, savukārt, ievadot divas (savienojums **8**) vai četras (savienojums **9**) cianogrupas, aizvietotājā ir novērojams pretējs gadījums, kad ierosinātais stāvoklis ir mazāk polārs nekā pamatstāvoklis. No tā var secināt, ka savienojumi **8-9** ir diezgan polāras molekulas pamatstāvoklī. Savienojumiem **10** un ***o*-QCCN** netika novērotas izteiktas izmaiņas UV-Vis spektros, mainoties šķīdinātāja polaritātei; abi savienojumi uzrādīja $\lambda_{max}$ diapazonā 630 ± 10 nm gan DMF, gan DCM šķīdumos. Abiem savienojumiem garo viļņu absorbcijas joslas neietekmēja bāzes klātbūtne, un novērota hipsohroma nobīde (ap 100 nm) skābos apstākļos, ko var attiecināt uz skābekļa protonēšanu pie C(8). Savukārt, pievienojot skābi atvasinājumu **7-9** DCM šķīdumiem, garāko viļņu absorbcijas josla pazūd. Līdz ar to secināts, ka sāļu **7-9** gadījumā anjona forma ir nepieciešama garāko viļņu absorbcijas joslai un protonēšana novērš iekšmolekulāro lādiņu pārnesi (2. tab.). Sāļiem **7-9** tika iegūta lineārā korelācija ($R^2$ = 0,99) starp absorbcijas joslas maksimuma viļņa garumu ($\lambda_{max}$ DCM šķīdumā) un *HOMO-LUMO* pārklāšanās vērtībām, kā arī starp $\lambda_{max}$ un aprēķināto starpplakņu leņķi. Papildus tika salīdzināti atvasinājumu **7-9** UV-Vis spektri ar izejvielu (*o*-hinona **1a** un indāna atvasinājumu **2-4**) spektriem DMF un DCM šķīdumos. Tika konstatēts, ka produkta **7-9** UV-Vis spektri sastāv no atsevišķu hromoforu absorbcijas joslām, tomēr to savstarpējā mijiedarbība rada jaunu garākā viļņa

absorbcijas joslu. Lielākā garo viļņu absorbcijas joslas batohromā nobīde tika novērota savienojumam **9** DCM šķīdumā (864 nm).

2. tabula

Savienojumu **7-11** un ***o*-QCCN** UV-Vis spektroskopijas dati

| Savienojums | $\lambda_{max}$ (lg ε) | | | |
|---|---|---|---|---|
| | DMF | DCM | DCM+TFA | DCM+DBU |
| **7** | 428 (3,99)<br>**690 (3,84)** | 411 (3,85)<br>**660 (3,30)** | 398 (3,74)<br>540 [a] | 434 (3,87)<br>681 (3,71) |
| **8** | 479 (4,08)<br>**697 (3,68)** | 462 (3,90)<br>**751 (3,42)** | 404 (3,60)<br>540 [a] | 482 (3,77)<br>710 (3,38) |
| **9** | 577 (4,36)<br>615 (4,22)<br>**740 (sh)** | 570 (4,37)<br>607 (4,23)<br>**864 (3,21)** | 346 (4,49)<br>430 [a]<br>510 [a] | 575 (4,40)<br>614 (4,27)<br>750 [a] |
| **10** | 409 (4,28)<br>**627 (3,97)** | 403 (4,40)<br>**641 (3,93)** | 367 (4,48)<br>541 (3,33) | 409 (4,22)<br>632 (3,87) |
| **11** | 661 (3,57) | – | – | – |
| ***o*-QCCN** | 414 (4,30)<br>**636 (4,06)** | 414 (4,23)<br>**640 (3,98)** | 382 (4,44)<br>559 (3,16) | 415 (4,25)<br>640 (4,00) |

[a] absorbcijas joslas "plecs".

Konstatēta lineāra korelācija starp savienojumu **10-11**, **7H*enol*** un ***o*-QCCN** garo viļņu absorbcijas joslas molārās absorbcijas koeficientiem (ε) DMF vai DMSO šķīdumos (9. att., 2. tab.) un to starpplakņu leņķa (φ) vērtībām (1. tab., RSA dati). Šī korelācija apstiprina secinājumu par garo viļņu joslas parādīšanās iemeslu. Jo izteiktāka elektronu delokalizācija starp hinona fragmentu un ievadīto aizvietotāju (ko apgrūtina liels starpplakņu leņķis), jo lielāks ir garāko viļņu absorbcijas joslas molārās absorbcijas koeficients.

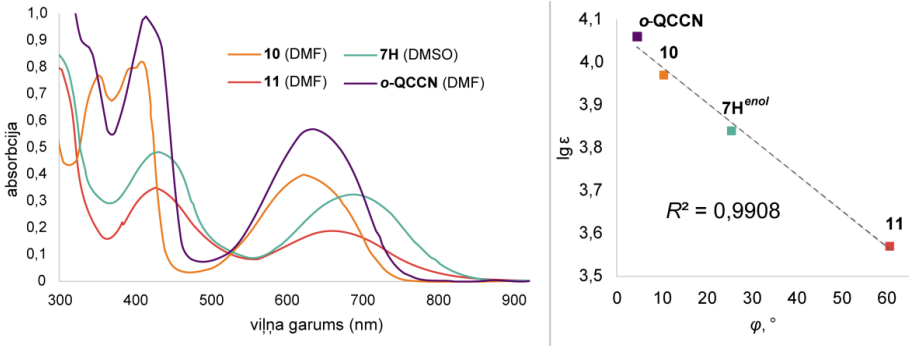


9. att. Savienojumu **10, 11, 7H*enol*** un ***o*-QCCN** UV absorbcijas spektri DMF/DMSO šķīdumos un korelācija starp to garo viļņu absorbcijas joslas molārās absorbcijas koeficientiem un starpplakņu leņķa lielumu (φ).

Sintezēto hinona atvasinājumu elektroķīmiskās īpašības acetonitrila (MeCN) šķīdumos tika pētītas ar ciklisko voltampērmetrijas metodi (CV), un atbilstošie elektroķīmiskās reducēšanas un oksidēšanās potenciāli ($E_{red}$, $E_{ox}$) apkopoti 3. tabulā. Ir zināms, ka

aizvietotāju ievadīšana hinonu atvasinājumos var izraisīt elektroķīmiskās reducēšanas potenciālu nobīdi.[57] No CV mērījumu rezultātiem tika konstatēts, ka hinona atvasinājumi **7** un **11** ir vieglāk reducējami (pirmie reducēšanas potenciāli $E^{I}_{red}$ ir –0,48 V un –0,44 V attiecīgi). Pieaugot cianogrupu skaitam sāls struktūrā (savienojumi **8-10**), pirmais reducēšanas potenciāls nobīdījās uz negatīvākām potenciāla vērtībām, kā arī uzrādīja neatgriezenisku oksidēšanās procesu.

3. tabula

Hinona atvasinājumu elektroķīmiskās īpašības. Reducēšanas ($E_{red}$) un oksidēšanās ($E_{ox}$) potenciāli (MeCN šķīdums, Ag/AgCl references elektrods)

| Savienojums | $E^{I}_{red}$, V | $E^{II}_{red}$, V | $E_{ox}$ V |
|---|---|---|---|
| Savienojumi ar negatīva lādiņa delokalizāciju aizvietotāja fragmentā | | | |
| **7** | –0,48 | – | 0,94 |
| **8** | –0,54 | –0,93 | 1,29 |
| **9** | –0,60 | –1,00 | 1,12 |
| **11** | –0,44 | –0,85 | 1,14 |
| Savienojumi ar negatīva lādiņa delokalizāciju polimetīna struktūrelementā (iekļaujot hinona fragmentu) | | | |
| ***o*-QCCN** | –0,59 | –1,12 | 1,01 |
| **10** | –0,50 | –0,74 | 0,96 |
| **10a** | –0,56 | –0,76 | 0,96 |
| **10b** | –0,43 | –0,59 | 1,04 |
| **10c** | –0,82 | –1,04 | 0,81 |
| **10d** | –0,81 | –0,92 | 0,83 |
| Produkti pēc hidrolīzes skābā vidē (**7H-10H**) | | | |
| **7H** | –0,34 | –0,72 | – |
| **8H** | –0,54 | –1,93 | 1,00 |
| **9H** | –0,68 | –1,51 | 0,86 |
| **10H** | –0,94 | – | 1,17 |

Savienojuma **10** atvasinājumi **10a-d** tika sintezēti, lai izpētītu heterocikla gredzena aizvietotāju ietekmi uz savienojumu elektroķīmiskajām īpašībām (2. shēma).

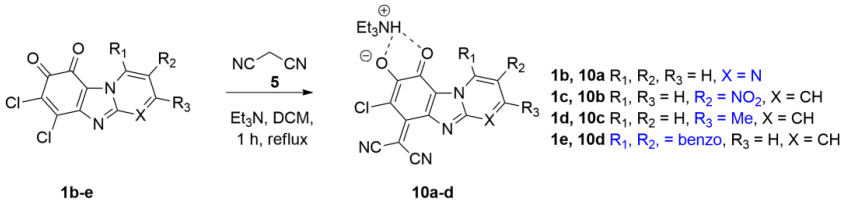


2. shēma. Savienojumu **10a-d** sintēze.

Savienojumi **10a-d** arī tika pētīti ar CV metodi (3. tab., 10. att.). Tika konstatēts, ka 4-CH aizstāšana ar N atomu (savienojums **10a**) heterociklā izraisīja tikai nenozīmīgas izmaiņas abu potenciālu vērtībās. Pirmo reducēšanas potenciālu un oksidēšanas potenciālu nobīdi uz negatīvākām potenciāla vērtībām ($E^{I}_{red}$ = –0,80 V un $E_{ox}$ = +0,80 V) izraisīja

metilgrupas ievadīšana pie C(3) (savienojums **10c**) vai arī aromātiskās sistēmas pagarināšana (savienojums **10d).** Elektronakceptoras grupas ievadīšana pie C(2) (**10b**) izraisīja pretēju efektu.

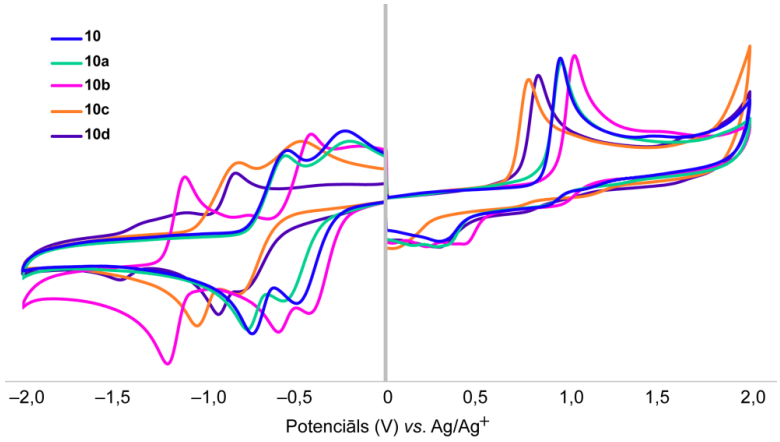


10. att. Savienojumu **10** un **10a-d** CV mērījumi MeCN šķīdumā.

Apkopojot iegūtos rezultātus, var secināt, ka, 6,7-dihlorpirido[1,2-*a*]benzimidazol-8,9-dionam reaģējot ar *C*-nukleofiliem, var iegūt atvasinājumus, kuros heterocikliskā hinona fragments var eksistēt dažādās formās. Pēc reakcijām ar stēriski lieliem *C*-nukleofiliem iegūtie 7-hlorpirido[1,2-*a*]benzimidazol-8,9-diona atvasinājumi ir stabili *o*-hinoni ar iespējamu negatīvā lādiņa delokalizāciju ievadītajā aizvietotajā (ja eksistē sāls formā). Šiem savienojumiem novērotā garo viļņu absorbcijas josla rodas no iekšmolekulāras lādiņa pārneses starp aizvietotāju un hinona fragmentiem, un šķīdumā var novērot pozitīvu vai negatīvu solvatohromiju.

Gadījumā, ja aizvietotāja un heterocikliskā hinona plaknes ir koplanāras, tad struktūrā var veidoties polimetīna fragments un rezultātā veidojas asimetriskie "sasaistītie polimetīni". Var secināt, ka, lai izprastu potenciālās lietošanas iespējas pētītājiem savienojumiem, ir nepieciešams analizēt arī telpisko struktūru, jo, mainoties molekulas planaritātei, notiek izmaiņas struktūrā un fizikālajās īpašībās. Turklāt modifikācijas iespēja ir mijiedarbība ar bāzēm, kas rezultātā rada atšķirīgas negatīvā lādiņa delokalizācijas.

Oriģinālpublikācija par šajā apakšnodaļā aprakstītajiem pētījumiem – 1. pielikumā.

## 2. Pirido[1,2-*a*]benzimidazol-8,9-diona fragmenta modifikācija reakcijā ar *N*-nukleofiliem

Halogēnaizvietoti hinoni reaģē ar amīniem, aminospirtiem un aminoskābēm – C-N saites veidošanās nerada jaunu hirālo centru, jo notiek secīgas pievienošanās/atšķelšanās reakcijas.[58] Kristalizējoties ahirāla organiskā molekula var spontāni veidot hirālus

kristālus.[59] Šādā gadījumā hiralitāte var veidoties, pateicoties kavētai rotācijai ap saiti molekulā vai spirālveidīgai supramolekulārai organizācijai kristālā. Ievadot mazkustīgā hinona "skeletā" konformacionāli lokanus aizvietotājus ar protondonorām īpašībām, var panākt supramolekulāro sistēmu veidošanos, ko stabilizē dažādas starpmolekulāras nekovalentās mijiedarbības.[60]

Hinona atvasinājumu gadījumā starp hinona karbonilgrupām un dažādām H-saites donoru grupām (piemēram, OH vai $NH_2$) var veidoties plašs starpmolekulāro H-saišu tīkls. Papildus tam struktūru var stabilizēt ne tikai starpmolekulārās H-saites, bet arī cieša starpslāņu π-π mijiedarbība, kas var rasties starp hinona cikliem, ja tie ir kondensēti ar aromātiskiem un/vai heterocikliskiem gredzeniem.[25] Vāju nekovalentu mijiedarbību rezultātā eksperimentāli pierādīta hinona atvasinājumu supramolekulārās struktūras stabilizācija,[44, 45] ko var kontrolēt ar ķīmisku modifikāciju un/vai aizvietotāju stēriskiem efektiem.

Halogenēto *o*-hinonu reakcijā ar pirmējiem amīniem var veidoties divi produkti – aizvietošanās produkts un/vai atvasinājums, kas veidojas pievienošanās reakcijā pie karbonilgrupas. Turklāt produktu maisījums var veidoties tautomēra līdzsvara dēļ starp 4-amino-*o*-hinonu un α-hidroksi-*p*-hinonimīnu.[44] Lai izveidotu materiālus, kuru pamatā ir hinons, ir nepieciešami dati par aizvietotāju ietekmi uz iekš/starpmolekulāro mijiedarbību un tautomēru veidošanas iespējām. Tādēļ veiktas 6,7-dihlorpirido-[1,2-*a*]benzimidazol-8,9-dionu reakcijas ar pirmējiem amīniem un benzhidrazīdiem, lai noskaidrotu aizvietotāja ietekmi, kā arī izpētītu iegūto produktu struktūru un īpašības.

### 2.1. Pirmējie amīni kā *N*-nukleofili

Iepriekšējos pētījumos[38] tika pierādīts, ka gadījumā, ja otrējais alifātiskais amīns (dietilamīns) tika izmantots kā nukleofilais reaģents reakcijā ar 6,7-dihlorpirido-[1,2-*a*]benzimidazol-8,9-dionu, tika iegūts *o*-hinona **1a** 6-dietilamino atvasinājums. Tas kristāliskā stāvoklī veidoja struktūru, kurā molekulas novietojas kolonnās. Šajā pētījumā pirido- un pirimido-[1,2-*a*]benzimidazol-8,9-dioni (**1a,b**) tika izvēlēti sākotnējā heterocikliskā *o*-hinona **1a** modifikācijai ar dažādiem pirmējiem amīniem (**12a-g**) (3. a shēma). Tika iegūti septiņu savienojumu **13c-g** un **14a,b** kristāli, kurus bija iespējams analizēt, izmantojot RSA metodi. No RSA datiem (4. tab.) ir redzams, ka slāpekļa atomam (N(11)) pie C(6) ir plakana ģeometrija visos pētāmajos savienojumos, jo leņķu α, β un γ summa (3. b shēma) ir vienāda vai tuvu 360°, kā arī tika novērota saišu izlīdzināšanas tendence fragmentā C(6)-C(7)-C(8).

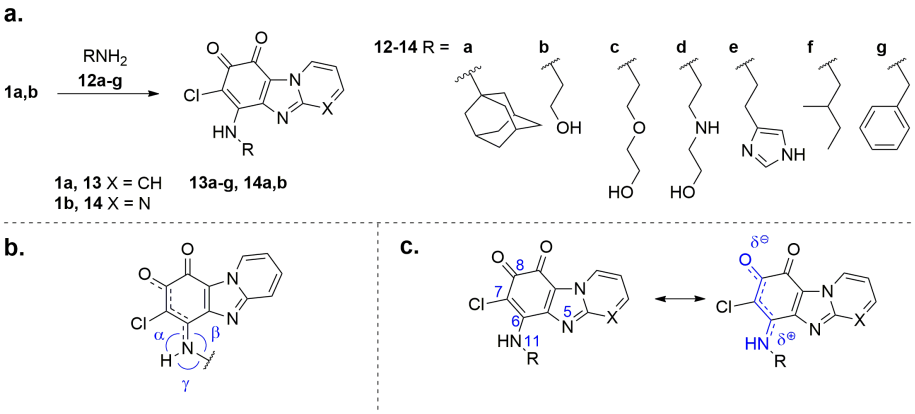


3. shēma. (a) Savienojumu **13a-g** un **14a,b** sintēze. Savienojumi **13d-e** tika izolēti kā hidrogēnhlorīdi; (b) savienojumu **13a-g** un **14a,b** saišu leņķi α, β un γ; (c) iegūto savienojumu **13a-g** un **14a,b** neitrālas un merocianīna tipa rezonanses formas.

Pamatojoties uz eksperimentālajiem datiem un savienojumu ģeometrijas no RSA, tika aprēķināta *Mayer* saišu kārta (*Mayer bond order*) saitei C(6)-N(11) (kvantu ķīmiska aprēķinu programma *Multiwfn*[56]) savienojumiem **13c-g** un **14a,b** un pierādīts daļējas dubultsaites raksturs (4. tab.). Tādējādi O=C(8)-C(7)-C(6)-N(11)H fragmentam ir merocianīna tipa struktūra (3. c shēma) un kavētā rotācija ap C(6)-N(11) saiti. Ir zināms,[63] ka merocianīna fragments var veicināt ūdeņraža saites veidošanos (*resonance-assisted hydrogen bond*).

4. tabula

Savienojumu **13c-g** un **14a,b** izvēlēto saišu garumu, saišu leņķu (α, β, γ) un torsijas leņķu (ϕ) vērtības (no RSA) un aprēķinātā *Mayer* saites kārta

| Sav. | Konformācija | $\phi_1$ [a,c] (C6-N11-C12-C13), ° | $\phi_2$ [b,c] (C6-N11-C12-C13), ° | C(6)-N attālums, Å | *Mayer* saites kārta | Saišu leņķu α, β un γ summa, ° |
|---|---|---|---|---|---|---|
| **13c** | sinklināla | 86,12 | – | 1,333 | 1,236 | 360,00 |
| **13d** | sinklināla | 75,15 | –75,15 | 1,340 | 1,197 | 359,41 |
| **13e** | antiklināla | 102,41 | –102,41 | 1,328 | 1,256 | 359,64 |
| **13f** | antiperiplanāra | 168,50$^{exo}$<br>152,21$^{endo}$ | –168,50$^{exo}$<br>–152,21$^{endo}$ | 1,338$^{exo}$<br>1,369$^{endo}$ | 1,236$^{exo}$<br>1,242$^{endo}$ | 359,74$^{exo}$<br>359,99$^{endo}$ |
| **13g** | antiperiplanāra | 164,62 | –164,62 | 1,333 | 1,231 | 359,21 |
| **14a** | – | – | – | 1,333 | 1,258 | 360,00 |
| **14b** | sinklināla | 73,57 | –73,57 | 1,342 | 1,258 | 360,00 |

[a] $\phi_1$ – torsijas leņķis molekulai ar (+) konformāciju.

[b] $\phi_2$ – torsijas leņķis molekulas inversijas ekvivalentam (ar (–) konformāciju) centrosimetriskā kristālā.

[c] *endo* formas gadījumā torsijas leņķi mēra saitēm C(6)-N(11')-C(12')-C(13') (12. att.).

Savienojums **13c** ir ahirāls, un molekulai bija sagaidāma fleksibilitāte (konformatīvā mobilitāte), pateicoties kustīgai sānu ķēdei. Pēc kristalizācijas savienojums **13c** spontāni izveidoja necentrosimetrisko hirālo kristālu ar telpisko grupu *P1*[64] un *Flack* parametru tuvu nullei (11. a-1 att.). Saskaņā ar RSA datiem (4. tab.) savienojuma **13c** kristāls satur tikai konformērus ar (+) sinklinālo konformāciju (saišu C(6)-N(11)-C(12)-C(13) torsijas leņķis; 11. a-2 att.). Desmit monokristālu (**13c**) analīze parādīja, ka četros kristālos hiralitāte sakrīt ar pētīto kristālu, tomēr atlikušos sešos hiralitāte ir pretēja. Tādējādi savienojumu **13c** var uzskatīt par racēmisku konglomerātu.[65, 66] Pārējie iegūtie atvasinājumi (**13d-g** un **14b**) kristalizējas, veidojot centrosimetriskus, ahirālus kristālus. No kristalogrāfijas viedokļa šādas struktūras var interpretēt kā vienu rotamēru (vienu no konformēriem, kas rodas kavētas rotācijas ap vienu saiti dēļ[67]), kas saistīts caur inversijas centru ar tā inversijas ekvivalentu (piemēram, savienojumi **14b** un **13g**, 11. b-2, c-2 att.).

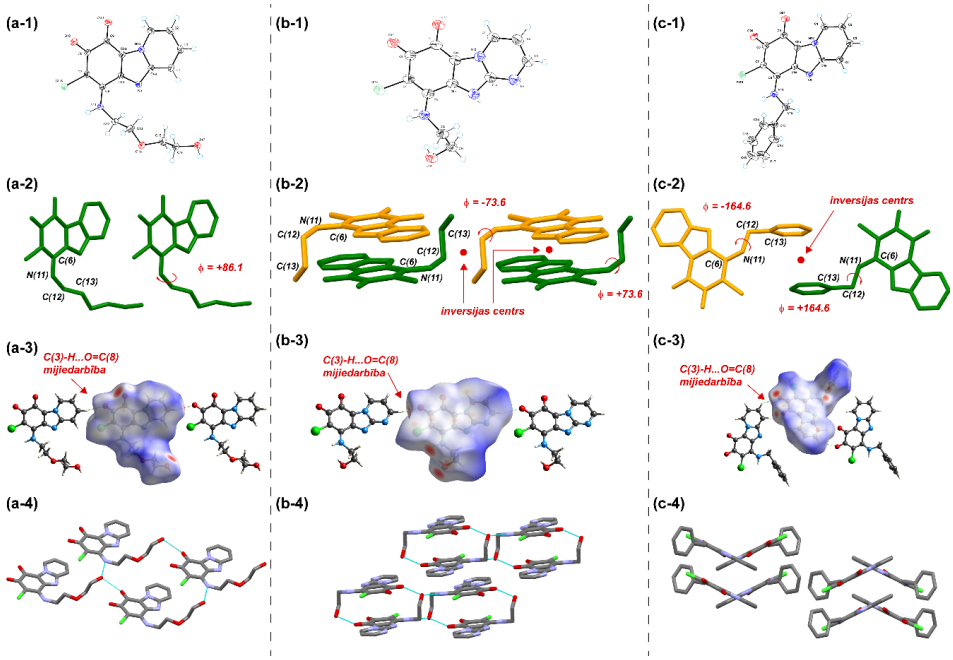


11. att. (a) Savienojuma **13c**; (b) savienojuma **14b**; (c) savienojuma **13g** kristālu: (1) *ORTEP* diagrammu asimetriskās vienības savienojumiem, kas parāda termiskos elipsoīdus 50 % varbūtības līmenī; (2) (+)-konformēra (zaļā krāsā) un (–)-konformēra (oranžā krāsā) torsijas leņķi (H atomi ir paslēpti); (3) Hiršfelda virsmas (*Hirshfeld surfaces*) un 1D molekulārās ķēdes ar C(8)=O…H-C(3) mijiedarbību; (4) kristāliskās struktūras sakārtojums (H-saites parādītas gaiši zilā krāsā).

Pateicoties C(6)-N(11)-C(12)-C(13) fragmenta torsijas leņķu atšķirībai, savienojumi centrisimetriskos kristālos ieņem dažādas konformācijas – savienojumi **13d** un **14b** sinklinālo (30°−90°, gan (+) gan (–)) konformāciju, savienojums **13e** – antiklinālo (90°−150°, (+) un (−)), savienojumi **13f,g** – antiperiplanāro (150°−180°(+) un (−)) (4. tab.).

Starpmolekulārā H-saite C(8)=O…H-C(3) (spēcīga vai vidēji spēcīga[68]) izraisīja 1D molekulāro ķēžu veidošanos savienojumu **13c-g** un **14a,b** kristāliskajās struktūrās. Saskaņā ar *Kikkawa, S., et al.*[69] klasifikāciju savienojumus var iedalīt divās grupās, ja salīdzina izveidoto 1D ķēžu H-saišu motīvus: taisns motīvs (*straight pattern*) ([(+) vai (–)] atsevišķas konformēru ķēdes) savienojumiem **13c-d,f** un **14b** (11. a-3, b-3 att.) un zigzagveida motīvs (*zig-zag pattern*) (ķēdes, kas veidojas gan no (+)- gan no (−)-konformēriem) savienojumiem **13e** un **13g**.

Pēc savienojuma **1a** reakcijas ar racēmisku reaģentu **12f** tika izolēts ahirāls savienojuma **13f** kristāls, kur abiem enantiomēriem tika atrastas divas molekulārās formas – *exo* un *endo* (12. att.). Kristālā 80 % no molekulām ieņēma *exo* formu, 20 % – *endo* formu, neskatoties uz N(11)H…N(5) iekšmolekulārās H-saites klātbūtni. *Endo* formas mazāko īpatsvaru var izskaidrot ar pagarināto C(6)-N(11') saiti (4. tab.), lai izveidotu iekšmolekulāro H-saiti.

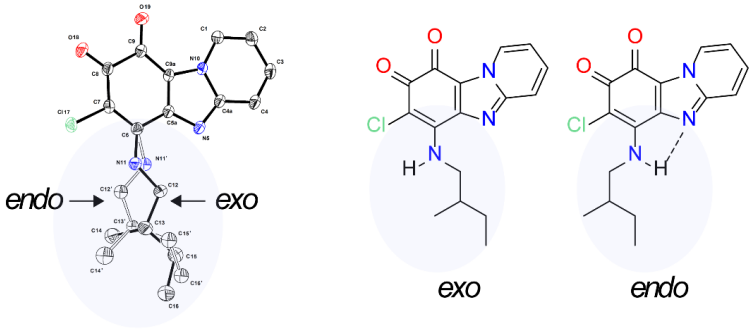


12. att. Savienojuma **13f** *ORTEP* diagramma, kas parāda *exo* un *endo* formas.

Ievērojot -NH-$CH_2$- fragmenta (kas nosaka *exo*/*endo* formas savienojuma **13f** kristālā) klātbūtni struktūrā, bija vērts izpētīt dažādu formu eksistenci šķīdumā. Turpmākajos struktūru pētījumos iegūtie savienojumi tika analizēti ar $^1$H KMR spektroskopijas metodi. Neskatoties uz ievadīto aizvietotāju dažādību, savienojumu **13b-g** un **14b** $^1$H KMR spektros (DMSO-$d_6$) tika novērotas divas iezīmes, kas atbilst -NH-α$CH_2$- (t.i., -N(11)H-C(12)$H_2$-) fragmentam. NH protonu signāli tika novēroti vājākos laukos (7,99–8,72 ppm diapazonā), kā arī α$CH_2$ protonu signāli tika paplašināti un nobīdīti vājākos laukos (13. att.). Savukārt šī parādība bija novērota tikai α$CH_2$ grupu signāliem, jo skaidra multiplicitāte bija redzama pārējo metilēngrupu signāliem, ieskaitot $\underline{CH_2}$ grupas signālus -NH-α$CH_2$-$\underline{CH_2}$ fragmentos savienojumos **13b-e** un **14b**. Savienojuma **13f** (satur diastereotopu $CH_2$ pie N(11) atoma) α$CH_2$ grupas diastereotopo protonu rezonanses signāli $^1$H KMR spektrā apstiprināti, izmantojot 2D $^1$H-$^1$H *COSY* un $^1$H-$^{13}$C *HSQC* KMR spektroskopijas metodes.

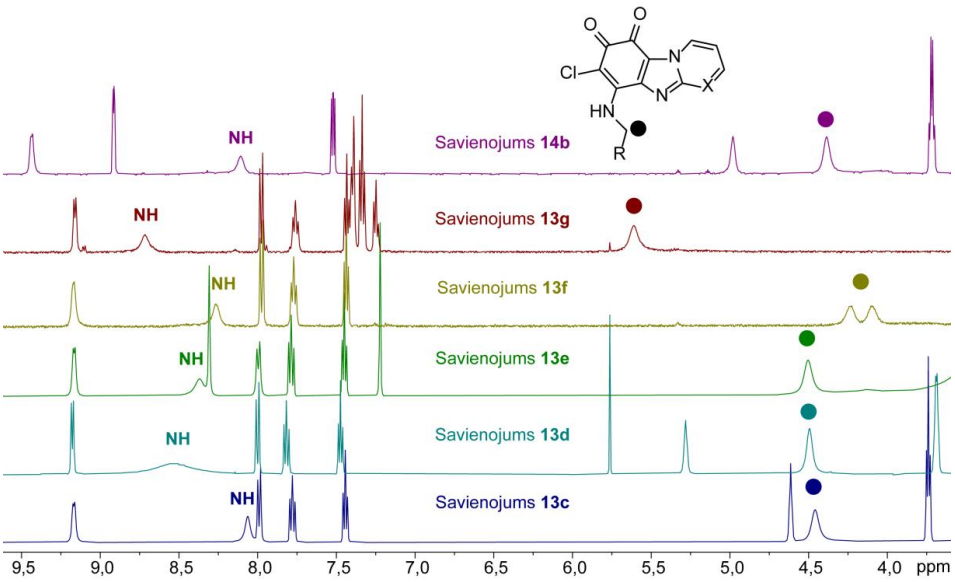


13. att. Savienojumu **13c-g**, **14b** $^1$H KMR (500 MHz, DMSO-$d_6$) spektri; $\alpha CH_2$ protonu signāli ir apzīmēti ar apļiem.

NH un $\alpha CH_2$ protonu ķīmiskās nobīdes var ietekmēt šķīdinātāja polaritāte, tāpēc tika izvēlēti savienojumi **13f-g**, lai izpētītu mijiedarbību ar šķīdinātājiem, kam piemīt dažāda polaritāte un H-saites bāziskums[70] ($\beta_1$, *hydrogen bond basicity*). Konstatēts, ka NH protona signāla ķīmiskā nobīde korelēja ar izmantotā šķīdinātāja $\beta_1$ vērtību (5. tab.). Savienojumu **13f-g** NH signālu nobīdi vājākā laukā DMSO-$d_6$ šķīdumā (salīdzinot ar ķīmisko nobīdi MeCN-$d_3$ un $CDCl_3$ šķīdumos) var izskaidrot ar starpmolekulārās mijiedarbības "viela-šķīdinātājs" (*solute-solvent*) veidošanos.[71]

Novērots, ka savienojumiem **13f-g** MeCN-$d_3$ un $CDCl_3$ šķīdumos $^1$H KMR spektrā parādās $\alpha CH_2$ grupas signālu paplašināšanās (5. tab.). Tomēr savienojuma **13f** spektros $CDCl_3$ šķīdumā atrasti *exo* un *endo* formu signāli; *exo* : *endo* attiecība (70 : 30) bija līdzīga kristāliskajā struktūrā novērotajai attiecībai (80 : 20), savukārt DMSO-$d_6$ un MeCN-$d_3$ šķīdumos istabas temperatūrā (298 K) izteikti *endo* formas signāli netika konstatēti. Tika pieņemts, ka savienojuma **13f** *exo* forma tiek stabilizēta, veidojot kompleksus "viela-šķīdinātājs", tādēļ vāja nekovalenta mijiedarbība ar šķīdinātāju konkurē ar *endo* formas stabilizāciju ar iekšmolekulārās H-saites veidošanos. Savienojuma **13g** $^1$H KMR spektros (298 K) visos izmantotajos šķīdinātājos *endo* formas signāli netika novēroti.

Ņemot vērā savienojuma **13f** divu formu klātbūtni (*exo*/*endo*) kristāliskajā stāvoklī, tālāk savienojumu **13f-g** formas šķīdumā tika pētītas, izmantojot mainīgas temperatūras $^1$H KMR spektroskopijas eksperimentus (MeCN-$d_3$ šķīdumos) (14. att.). Pazeminoties temperatūrai, $^1$H KMR spektros (248–253 K) novērotas izmaiņas – notiek visu plato signālu (NH, $\alpha CH_2$ grupas un C(1)-H) sašaurināšanās un sašķelšanās. Papildu zemas intensitātes signālu (atbilst *endo* formai) parādīšanās pierāda, ka šķīdumā eksistē divas formas.

5. tabula

Savienojumu **13f-g** ķīmiskās nobīdes (δ) $^1$H KMR spektros dažādu šķīdinātāju šķīdumos

| Sav. | Šķīdinātājs | Šķīdinātāja H-saites bāziskums ($\beta_1$)[70] | Ķīmiskā nobīde (δ), ppm | |
|---|---|---|---|---|
| | | | N<u>*H*</u> | HN-αC<u>*H*</u>$_2$ |
| **13f** | $CDCl_3$ | 0 | 6,24$^{exo}$<br>6,79$^{endo}$ | 4,09, 4,28$^{exo}$<br>3,74, 3,92$^{endo}$ |
| | MeCN-$d_3$ | 0,37 | 6,96 | 4,33, 4,13 |
| | DMSO-$d_6$ | 0,71 | 8,26 | 4,10, 4,23 |
| **13g** | $CDCl_3$ | 0 | 6,34 | 5,50 |
| | MeCN-$d_3$ | 0,37 | ~ 7,30 | 5,63 |
| | DMSO-$d_6$ | 0,71 | 8,72 | 5,69 |

Savienojumam **13g** zemākās temperatūrās abas formas novērotas šķīdumā (*exo* : *endo* formu attiecība 85 : 15), lai gan cietā stāvoklī tika konstatēta tikai *exo* forma (14. b att.). 253 K temperatūrā *exo* formas αCH$_2$ protoniem novērots dublets ($J$ = 7,1 Hz) pie 5,61 ppm kopā ar *endo* formas zemas intensitātes dubletu ($J$ = 7,2 Hz) pie 5,17 ppm.

Savienojumam **13f** novērotā *exo* : *endo* formu attiecība (248 K, MeCN-$d_3$ šķīdums) bija līdzīga (85 : 15), kas ir saskaņā ar *exo* : *endo* attiecību cietā stāvoklī (14. a att.). *Endo* formas diastereotopie metilēngrupas (αCH$_2$) protoni tika nobīdīti stiprākā laukā (ekranēti) attiecībā pret *exo* formas signāliem un uzrādīja signālus pie 3,67 ppm un 3,86 ppm ar skaidru multiplicitāti. Līdzīgi arī platais heterocikla C(1)-H protona signāls sašķēlās divos signālos. Turklāt zemas intensitātes NH grupas signāls (*endo* forma ar iekšmolekulāro H-saiti) parādās pie 7,41 ppm, savukārt *exo* formas NH grupas signāls tika novērots pie 7,17 ppm. Parasti NH protona signāliem, iesaistītiem starpmolekulārajā H-saitē, ir vairāk izteikta atkarība no temperatūras nekā iekšmolekulāri saistītiem NH grupas signāliem (jo iekšmolekulārā mijiedarbība ir spēcīgāka nekā starpmolekulārā H-saite[72]). Savienojuma **13f** gadījumā NH protona signāla (*exo* forma) ķīmiskā nobīde MeCN-$d_3$ šķīdumā lineāri korelēja ar temperatūru (248–333 K, $R^2$ = 0,97).

Savienojumam **13f** tika uzņemti mainīgas temperatūras $^1$H KMR spektri arī DMSO-$d_6$ šķīdumā, karsējot līdz 393 K, rezultātā tika konstatēta tikai monomēra *exo* forma (jo šajā temperatūrā H-saites stiprums ir samazināts). Lineāra korelācija tika atrasta starp NH protona ķīmisko nobīdi un temperatūru vielas **13f** šķīdumiem DMSO-$d_6$ (298 – 393 K, $R^2$ = 0,99).

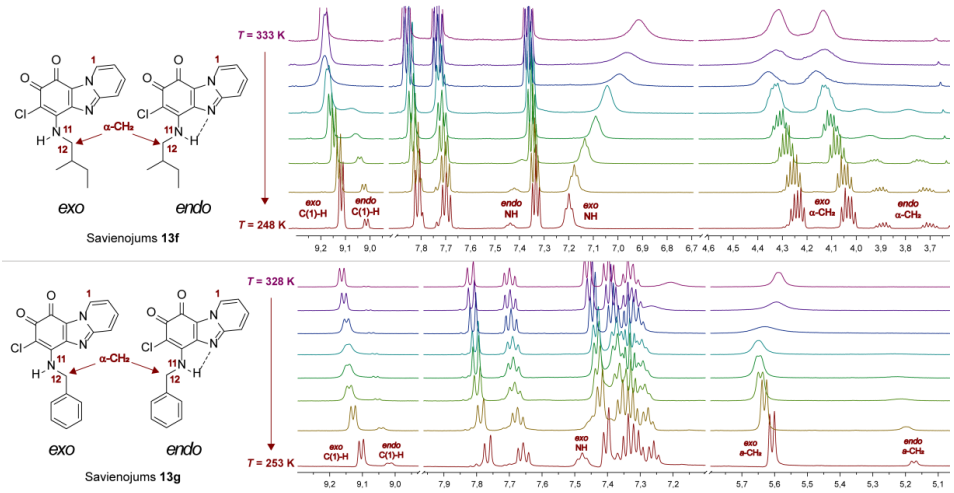


14. att. Mainīgas temperatūras $^1$H KMR spektra fragmenti (500 MHz, MeCN-$d_3$) (a) savienojumam **13f** temperatūras diapazonā no 248 K līdz 333 K; (b) savienojumam **13g** temperatūras diapazonā no 253 K līdz 328 K.

Apkopojot iegūtos rezultātus, var secināt, ka pēc 6,7-dihlorpirido[1,2-*a*]benzimidazol-8,9-diona un tā analoga reakcijām ar pirmējiem amīniem var iegūt atvasinājumus, kuros heterocikliskajam *o*-hinona fragmentam piemīt merocianīna tipa struktūra fragmentā O=C(8)-C(7)-C(6)-N(11)H. Daļējas dubultsaites raksturs piemīt ogleklis-slāpeklis saitei, kas saista heterociklisko hinonu un aizvietotāju. Pateicoties aizvietotāju protondonoro grupām un savienojumu dažādajiem elektroniskajiem efektiem, iegūto atvasinājumu kristālos varēja novērot dažāda veida starpmolekulārās mijiedarbības (tajā skaitā – vairākas H-saites un starpslāņu π-π mijiedarbības). Pārsvarā iegūti centrosimetriskie kristāli, tomēr viens no atvasinājumiem izveidoja hirālo kristālu bez inversijas ekvivalenta.

Iegūto produktu gadījumā kristāliskajā stāvoklī un šķīdumā dominē forma bez iekšmolekulārās ūdeņraža saites (*exo* forma). Otras formas (ar iekšmolekulāru H-saiti, *endo* forma) klātbūtne izskaidro novēroto $CH_2$ grupas (blakus NH) signāla paplašināšanos $^1$H KMR spektros šķīdumā istabas temperatūrā. NH protona signāla ķīmiskā nobīde ir atkarīga gan no šķīdinātāja H-saites bāziskuma, gan no temperatūras.

Oriģinālpublikācija par šajā apakšnodaļā aprakstītajiem pētījumiem – 2. pielikumā.

## 2.2. Benzhidrazīdi kā *N*-nukleofili

Hinona atvasinājumi **16a-f** tika iegūti hinonu **1a,c** reakcijā ar benzhidrazīdiem **15a-c** $Et_3N$ klātbūtnē (4. shēma). Iepriekšējā pētījumā, hinoniem **1a,b** reaģējot ar pirmējiem amīniem, tika iegūti 6-aminoaizvietotu produktu (**13a-g** un **14a,b**) zilas vai violetas krāsas kristāli, savienojumu **16a-c** gadījumā tika izolētas sarkani oranžas krāsas cietas vielas.

*o*-Hinona atvasinājumiem, kas satur aroil- vai acilhidrazīda fragmentu, ir iespējamas vairākas tautomērās struktūras.[73, 74] Pēc veiktajām analīzēm ($^1$H KMR un *FTIR*) iegūto savienojumu tautomērā forma netika pilnībā pierādīta. Lai precizētu hinona fragmenta formu cietā stāvoklī ar RSA metodi, savienojuma **16a** monokristāli tika izaudzēti no DCM šķīduma.

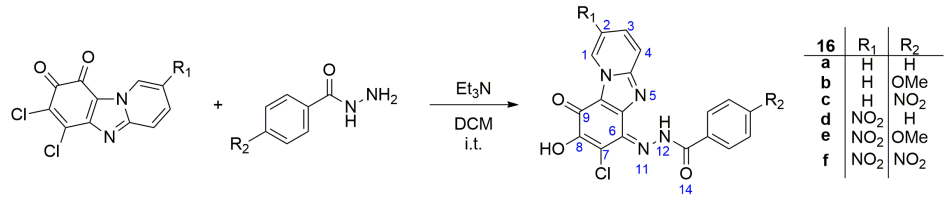


| 16 | $R_1$ | $R_2$ |
|---|---|---|
| a | H | H |
| b | H | OMe |
| c | H | $NO_2$ |
| d | $NO_2$ | H |
| e | $NO_2$ | OMe |
| f | $NO_2$ | $NO_2$ |

4. shēma. Savienojumu **16a-f** sintēze.

Pēc saišu garumu analīzes (RSA dati) tika konstatēta savienojuma **16a** α-hidroksi-*p*-hinonimīna forma. Molekulas **16a** *ORTEP* diagramma ar termiskajiem elipsoīdiem un atomu numerācijas shēmu redzama 15. a attēlā. Savienojuma **16a** struktūrā konstatētas divas iekšmolekulārās H-saites: N(12)H···N(5) un O(22)-H···O(23) (15. a att.). Turklāt hidroksilgrupa O(22)-H veido starpmolekulāru H-saiti O(22)-H···O'(23) ar otro savienojuma molekulu, veidojot centrosimetrisku molekulāro dimēru $R_2^2(10)$ (15. b att.). Konstatēta dimēru mijiedarbība starp slāņiem (15. c att.) pa kristalogrāfisko *a* asi, kā arī īss starpmolekulārais kontakts starp heterociklu (C(3)-H) un aizvietotāja amīda grupu.

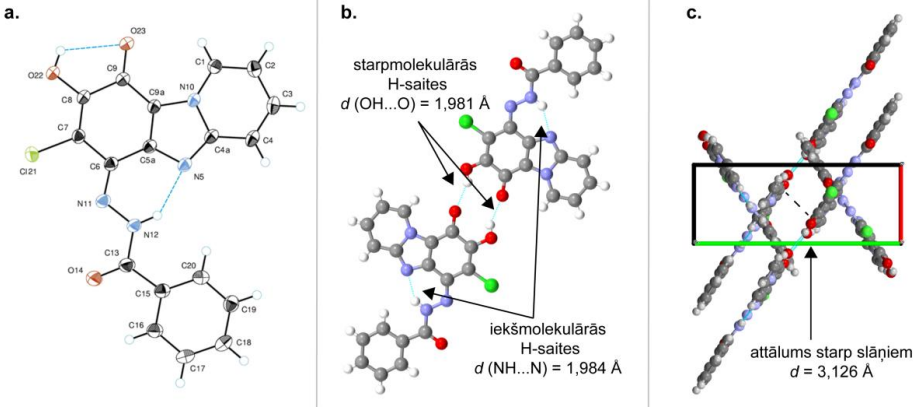


15. att. Savienojuma **16a** (**a**) *ORTEP* diagramma, kas parāda termiskos elipsoīdus 50 % varbūtības līmenī; (**b**) centrosimetriskais $R_2^2(10)$ molekulārais dimērs kristālā; (**c**) kristāliskās struktūras sakārtojums, skatoties pa *a* asi.

Iegūto savienojumu **16a-f** $^1$H KMR spektros DMSO-$d_6$ šķīdumā tika novēroti divi plati signāli, kas atbilst NH (pie 14,36–14,90 ppm) un OH (pie 10,95–11,41 ppm) protoniem. NH signāla nobīde vājākā laukā ļāva secināt, ka iekšmolekulārā saite N(12)-H···N(5)

saglabājās arī šķīdumā, jo šķīdinātājs neietekmēja savienojuma **16a** NH protona signāla ķīmisko nobīdi ($\delta_{NH}$ = 14,71 ppm (DMSO-$d_6$); $\delta_{NH}$ = 14,68 ppm ($CDCl_3$ – šķīdinātājs, kurā starpmolekulārā H-saite ir vājāka[75]). Tomēr šķīdinātāja maiņa no DMSO-$d_6$ uz $CDCl_3$ nobīda OH signālu stiprākā laukā no 10,99 ppm līdz 7,20 ppm. Ir zināms, ka α-hidroksi-*p*-naftohinona atvasinājumu gadījumā OH protoni ar iekšmolekulāro H-saiti uzrāda līdzīgu ķīmisko nobīdi (ap 7,30 ppm $CDCl_3$ šķīdumā).[76] Signāla nobīde vājākā laukā, izmantojot šķīdinātāju ar H-saites akceptora spējām[77] (DMSO-$d_6$), liecina par starpmolekulārās mijiedarbības veidošanos. Turklāt tika pētītas OH un NH signālu ķīmiskās nobīdes ($\delta_{OH}$ un $\delta_{NH}$ attiecīgi) $^1$H KMR spektros (DMSO-$d_6$) atkarībā no dažādu aizvietotāju ievadīšanu savienojuma **16a** struktūrā. Par aizvietotāju raksturlielumu tika ņemtas aizvietotāju *Hammett* konstantes ($\sigma_p$).[78] Rezultātā lineāras korelācijas ($R^2$ = 0,99) konstatētas savienojumiem **16a-c** ($R_1$ = H) un **16d-f** ($R_1$ = $NO_2$) starp aizvietotāju *Hammett* konstanti ($R_2$, fenilgredzena *para*-pozīcijā) un $\delta_{OH}$ (16. att.). Nitrogrupas klātbūtne heterocikliskajā fragmentā ($R_1$ = $NO_2$) izraisīja OH signāla nobīdi vājākā laukā, salīdzinot ar līdzīgām molekulām bez aizvietotāja ($R_1$ = H) heterociklā ($\Delta\delta_{OH} \approx$ 0,3 ppm). Tomēr NH signāls nobīdās stiprākā laukā, ja heterocikliskajā gredzenā ievada nitrogrupu ($R_1$ = $NO_2$), salīdzinot ar molekulu, kur tajā pašā pozīcijā ir ūdeņraža atoms ($R_1$ = H) ($\Delta\delta_{NH} \approx$ 0,3 ppm). Novērots, ka NH signāla nobīde vājākā laukā korelē lineāri ar aizvietotāja $R_2$ (fenilgredzena *para*-pozīcijā) raksturu, pārejot no elektrondora uz elektronakceptoru aizvietotāju (16. att.). Ir zināms,[79] ka spēcīgāka iekšmolekulārā H-saite nobīda NH protona signālu vājākā laukā. Tādējādi elektronakceptora grupa fenilgredzenā ($R_2$ = $NO_2$) palielina NH protona skābumu un iekšmolekulārās H-saites stiprumu, savukārt elektronakceptora grupa heterocikliskajā fragmentā ($R_1$ = $NO_2$) ietekmē elektronu blīvumu pie N(5) un iekšmolekulāro H-saiti.

Savienojumus **16a-c** var raksturot arī kā aroilhidrazonu strukturālos analogus.[74] No literatūras[80, 81] ir zināms, ka dažādiem hidrazonu atvasinājumiem ir raksturīga C=N konfigurācijas maiņa (*E*/*Z* izomerizācija) šķīdumā, ko var veicināt ķīmiski un/vai fotoķīmiski. Savienojuma **16a** $^1$H KMR spektros (DMSO-$d_6$ vai $CDCl_3$ šķīdumos) netika novēroti izomerizācijas produktu signāli. Tāpat netika novērota C=N dubultsaites konfigurācijas maiņa savienojumam **16b** (DMSO-$d_6$) pēc TFA pievienošanas (pārākumā) un pēc sekojošas apstarošanas ar UV gaismu (365 nm). Vienas konfigurācijas stabilitāti savienojumu **16a-c** gadījumā var izskaidrot ar iekšmolekulārās H-saites N(12)-H···N(5) klātbūtni.

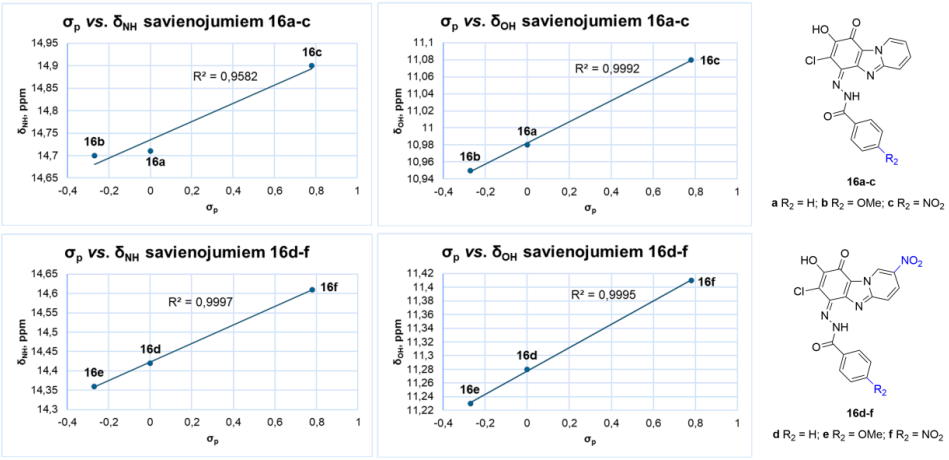


16. att. Savienojumu **16a-f** struktūras un korelācijas starp to aizvietotāja ($R_2$) *Hammett* konstanti ($\sigma_p$) un NH protona ($\delta_{NH}$) vai OH protona ($\delta_{OH}$) ķīmiskajām nobīdēm $^1$H KMR spektros (DMSO-$d_6$).

No savienojumu **16a-c** $^1$H KMR spektriem ir redzams, ka struktūrā ir divi skābi protoni. Lai izpētītu iespējamo iegūto savienojumu deprotonēšanas/protonēšanas procesu, tika veikts $^1$H KMR spektroskopijas titrēšanas eksperiments, kā paraugu izmantojot savienojumu **16b**. Deprotonēšanas process tika pētīts pēc secīgas bāzes (DBU) pievienošanas. Tiklīdz savienojuma **16b** DMSO-$d_6$ šķīdumam tika pievienoti 0,15 ekvivalenti bāzes, novērota pilnīga OH grupas signāla izzušana $^1$H KMR spektrā (17. att., iezīmēts sarkanā krāsā), kā arī dzeltenās krāsas šķīdums uzreiz kļuva tumši zils. Tajā pašā laikā parādījās $DBUH^+$ signāls pie 9,58 ppm (17. att., iezīmēts zilā krāsā). Tika pieņemts, ka deprotonētais savienojums **16b** veido H-saišu kompleksu ar $DBUH^+$. Tālāk, pievienojot bāzi, amīda fragmenta NH protona signāls kļūst šaurāks un tiek nobīdīts stiprākā laukā no 14,70 ppm līdz 14,51 ppm (17. att., iezīmēts dzeltenā krāsā). Pēc DBU pārākuma pievienošanās konstatēta vēl viena forma (17. att., iezīmēts zaļā krāsā; signālu attiecība 0,95 : 0,05). Jāatzīmē, ka līdzīgs process tika novērots arī savienojumu **16a** un **16c** gadījumā pēc mijiedarbības ar bāzi pārākumā. Pievienojot TFA pārākumu, novērotas sekojošas izmaiņas: atkal paradās OH grupas signāls, atgriežas šķīduma dzeltenā krāsa un pazūd otras (minorās) formas signāli. Līdz ar to secināts, ka skābes-bāzes līdzsvars ir atgriezenisks.

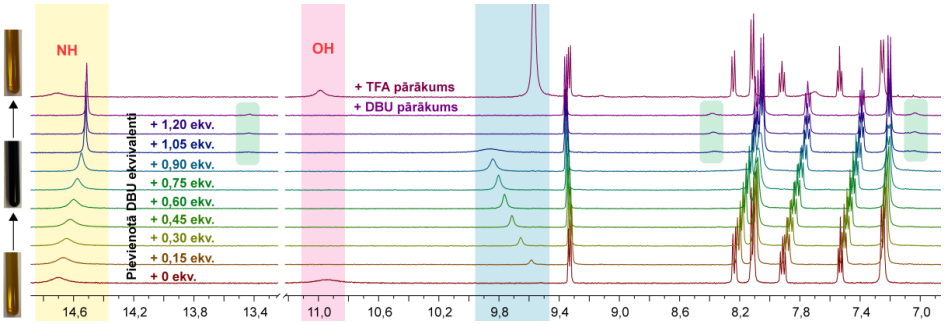


17. att. $^{1}$H KMR savienojuma **16b** skābju-bāzes titrēšana DMSO-$d_6$ šķīdumā (pēc secīgas bāzes (DBU) un skābes (TFA) pievienošanas).

Savienojuma **16a** UV-Vis absorbcijas spektri tika pētīti DCM un DMSO šķīdumos, un abos šķīdumos konstatēti divi absorbcijas maksimumi pie 381 nm un pie 446–449 nm. Pievienojot bāzi (DBU) savienojuma **16a** šķīdumam, pazūd absorbcijas josla pie ~ 450 nm un parādās jauna absorbcijas josla pie 556 nm dihlormetānā un pie 607 nm DMSO šķīdumā. Aizvietotāju ($R_1$ un $R_2$) ietekme uz garo viļņu absorbcijas maksimumu pārbaudīta, pievienojot DBU savienojumu **16a-c** (mainīgais $R_2$, $R_1$ = H) un **16d-f** (mainīgais $R_2$, $R_1$ = $NO_2$) $CHCl_3$ šķīdumam (6. tab.). Novērots, ka deprotonēto savienojumu **16d-f** garo viļņu absorbcijas joslai ir batohromā nobīde, salīdzinot ar savienojumiem **16a-c** (6. tab.). Turklāt hiperhromo efektu izraisīja nitrogrupas ievadīšana benzamīda fragmentā.

6. tabula

Savienojumu **16a-f** UV-Vis spektroskopijas dati DBU klātbūtnē ($CHCl_3$)

| Sav. | **16a** | **16b** | **16c** | **16d** | **16e** | **16f** |
|---|---|---|---|---|---|---|
| $\lambda_{max}$ (lg ε) | 365 (4,40)<br>380 (4,41)<br>**556** (3,87) | 368 (4,45)<br>382 (4,48)<br>**551** (3,89) | 377 (4,40)<br>**563** (3,91) | 371 (4,24)<br>**575** (3,73) | 365 (4,28)<br>**569** (3,76) | 361 (4,30)<br>**578** (3,86) |

Hinonimīni ir redoksaktīvi savienojumi, ko var reducēt līdz aminofenoliem.[82] Literatūrā[83] minēts, ka *o*-hinona modifikācija par tā *p*-hinonimīna analogu maina savienojuma redokspotenciālus un redoksīpašības, kā arī hinona un imīna grupu kombinācija vienā molekulā ir perspektīva pieeja organisko elektroenerģijas uzglabāšanas materiālu izveidei.[84] Turpmākajā pētījumā *o*-hinona **1a** (elektroķīmiski aktīvs savienojums MeCN šķīdumā[85]) un tā *p*-hinonimīna atvasinājuma **16a** redoksīpašības tika analizētas potenciālai lietošanai ūdens elektrolītu baterijās elektroda materiāla lomā.

Pirmkārt, tika pārbaudīta savienojumu **1a** un **16a** šķīdība ūdens vidē; savienojums **16a** nešķīst neitrālā un skābā vidē, savukārt savienojums **1a** nešķīst ūdens šķīdumos visā pH diapazonā. Līdz ar to analīzei tika izmantots neitrālais (0,5 M $K_2SO_4$) un skābais (0,5 M $H_2SO_4$) elektrolīts. Katoda materiāli **CM-1a** un **CM-16a** tika sagatavoti, kombinējot hinona atvasinājumus **1a** vai **16a** ar *Vulcan XC72 CB* (substrāts) un PVDF (saistviela) DMF šķīdumu. 18. attēlā redzami paraugu **CM-1a**, **CM-16a** un parauga bez aktīvā materiāla (substrāta) CV mērījumu rezultāti dažādos skenēšanas ātrumos neitrālā un skābā elektrolītā.

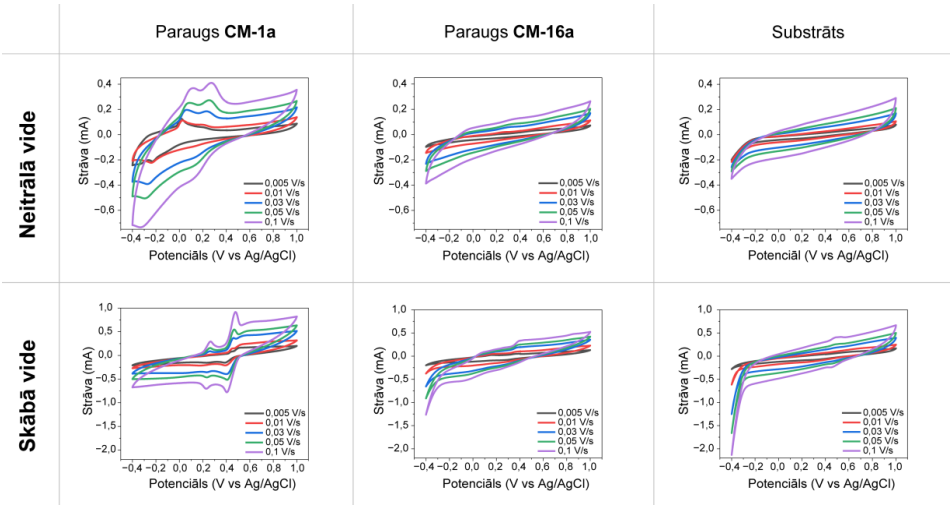


18. att. Paraugu **CM-1a**, **CM-16a** un substrāta CV mērījumu rezultāti dažādos skenēšanas ātrumos neitrālā (0,5 M $K_2SO_4$) elektrolītā un skābā (0,5 M $H_2SO_4$) elektrolītā.

Paraugam **CM-1a** CV mērījumos novēroti divi oksidēšanas un reducēšanas maksimumi (atbilst *o*-hinona fragmentam molekulā) skenēšanas potenciālu logā (*potential window*) gan neitrālā, gan skābā elektrolītā. Palielinot $H^+$ jonu koncentrāciju, novērota reakcijas potenciāla nobīde uz pozitīvākām potenciālu vērtībām. Skābā vidē abi potenciāli ir stabili, un to potenciālu starpība ir tikai 0,2 V, savukārt neitrālā vidē tikai viens potenciāls paliek nemainīgs pēc vairākiem CV cikliem. Tomēr paraugam **CM-16a** neitrālā elektrolītā nevar novērot nozīmīgus redoksprocesus; tikai skābā elektrolīta gadījumā var redzēt divus atgriezeniskus oksidēšanas potenciālus. Var secināt, ka, pārvēršot *o*-hinonu **1a** par α-hidroksi-*p*-hinonimīnu **16a**, elektroķīmiskā aktivitāte ir pazemināta.

Savienojumiem **1a** un **16a**, kā arī katodu materiāliem (**CM-1a**, **CM-16a**) tika uzņemti Ramana spektri pirms un pēc elektroķīmiskās ciklēšanas (*electrochemical cycling*) skābā un neitrālā elektrolītā (19. a att.). Iegūtie rezultāti parāda, ka pirms ciklēšanas un ciklētā katoda materiāla **CM-1a** spektri skābā elektrolītā sakrīt ar izejvielas **1a** spektru. Savukārt pēc parauga **CM-1a** ciklēšanas neitrālā elektrolītā spektrā var redzēt tikai oglekļa C un D joslas.[86, 87] Secināts, ka aktīvā viela šķīst elektrolītā un elektroķīmiskās reakcijas notiek šķīdumā (redoksprocesi šim paraugam novēroti CV mērījumos (18. att.)). Savukārt savienojums **16a** paliek katoda materiālā pēc CV mērījumiem, un tam nenovēro būtiskas izmaiņas, kā redzams no praktiski vienādiem Ramana spektriem vielai **16a** un paraugiem **CM-16a** pirms un pēc ciklēšanas, kas arī liecina par izteiktu stabilitāti ciklēšanas apstākļos.

Salīdzinot skenējošās elektronu mikroskopijas (SEM) attēlus (19. b att.) parauga **CM-1a** pirms un pēc ciklēšanas neitrālā vai skābā elektrolītā, var redzēt, ka tikai daļa no sākotnējās morfoloģijās saglabājās, kas apstiprināja informāciju no Ramana spektriem par aktīvas vielas šķīšanu elektrolītā. Paraugā **CM-16a** SEM attēlos pēc CV mērījumiem neitrālā un skābā elektrolītā var pamanīt nenozīmīgas izmaiņas morfoloģijā, ko var izskaidrot ar daļēju

aktīvās vielas izšķīšanu. Lielāka materiāla **CM-16a** stabilitāte, salīdzinot ar paraugu **CM-1a**, var būt izskaidrojama ar vāju nekovalentu mijiedarbību starp savienojumu **16a** un substrātu.

Apkopojot iegūtos rezultātus, var secināt, ka pēc 6,7-dihlorpirido[1,2-*a*]benzimidazol-8,9-diona reakcijām ar benzhidrazīdiem tika iegūti α-hidroksi-*p*-hinonimīna atvasinājumi ar vienu C=N saites konfigurāciju, ko stabilizē iekšmolekulārā H-saite. Tomēr iegūtie savienojumi pakļaujas deprotonēšanai un mijiedarbībai ar bāziskiem šķīdinātajiem skābā OH protona dēļ. Elektroda materiāla pagatavošanai parasti tiek izmantoti šķīdinātāji ar bāziskām īpašībām (piemēram, *N*-metil-2-pirolidons), tāpēc pirms materiāla pagatavošanas ir jāizanalizē savienojuma stabilitāti šādos apstākļos. Secināts, ka katoda materiāls, kura pamatā ir 6,7-dihlorpirido[1,2-*a*]benzimidazol-8,9-dions (**CM-1a**), varētu potenciāli efektīvi darboties elektrodos ūdens elektrolītu baterijās, ja tiks samazināta vielas šķīdība, piemēram, piesaistot pie polimēra matricas, kas varētu būt virziens tālākiem pētījumiem.

Oriģinālpublikācija par šajā apakšnodaļā aprakstītajiem pētījumiem – 3. pielikumā.

Lai paplašinātu katodu materiālu klāstu, no savienojumiem **7H**, **10** un 6-amino-7-hlorpirido[1,2-*a*]benzimidazol-8,9-diona tika izgatavoti katodu materiālu paraugi **CM-7H**, **CM-10** un **CM-Q-NH$_2$** attiecīgi (6. pielikums). Materiāliem veikti CV mērījumi skābā vidē, un uzņemti SEM attēli pirms un pēc elektroķīmiskās ciklēšanas. No iegūtajiem rezultātiem redzams, ka paraugu **CM-7H** CV mērījumos ir vairāki maksimumi, kas varētu liecināt par dažu formu klātbūtni (ņemot vērā to, ka materiālu izgatavošanas laikā tika izmantots polārs šķīdinātājs (DMF), kurā savienojumam **7H** bija pierādīta keto/enol tautomērija).

Neskatoties uz to, ka savienojumam **10** un to atvasinājumiem **10a-d** piemīt redoksīpašības šķīdumā (MeCN) (10. att., 3. tab.), CV mērījumi katoda materiālam **CM-10** skābā ūdens elektrolītā neparadīja līdzīgus rezultātus. Paraugiem **CM-7H** un **CM-10** SEM attēlos redzama parauga daļēja šķīšana pēc ciklēšanas. Paraugs **CM-Q-NH$_2$** CV mērījumos uzrādīja baterijas tipa īpašības ar salīdzinoši augstu strāvu un vislielāko stabilitāti ciklēšanas procesā.

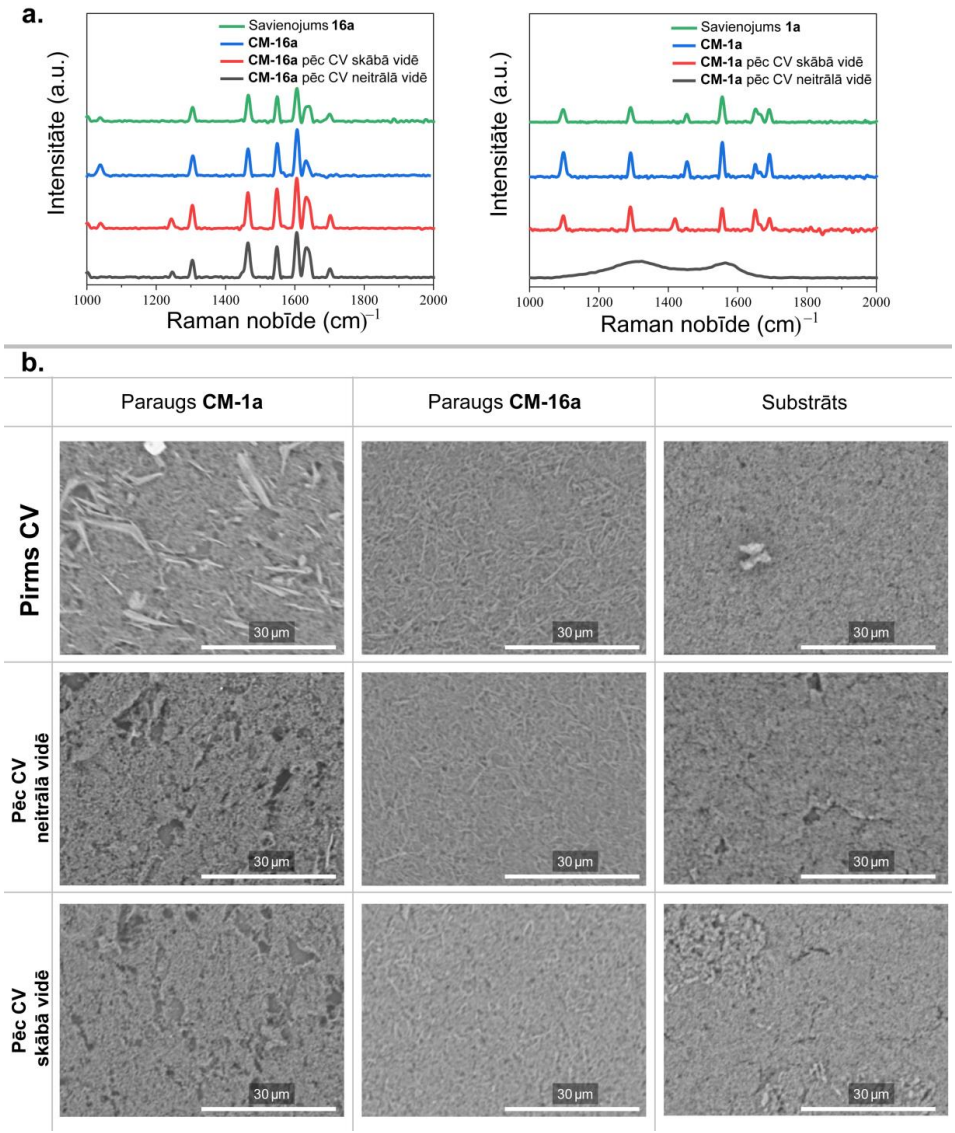


19. att. (a) Ramana spektri izejvielām **1a** un **16a** (zaļā līnija), katoda materiāliem (**CM-1a** un **CM-16a**) pirms (zilā līnija) un pēc to ciklēšanas skābā (sarkanā līnija) un neitrālā (pelēkā) līnija) elektrolītos; (b) sagatavoto katoda materiālu **CM-1a**, **CM-16a** un substrāta (pārklājums bez aktīvā materiāla) skenēšanas elektronu mikroskopijas attēli pirms un pēc CV mērījumiem neitrālā un skābā elektrolītā (2500× palielinājums).

# SECINĀJUMI

1. Strukturālie pētījumi parādīja, ka 6,7-dihlorpirido[1,2-*a*]benzimidazol-8,9-dions un tā analogi reakcijā ar nukleofiliem veido produktus, kuros hinona fragmentam piemīt dažādas formas: *o*-hinona (*C*-nukleofils – indāna atvasinājums vai barbitūrskābe) vai α-hidroksi-*p*-hinonimīna (*N*-nukleofils – benzhidrazīda atvasinājums) formas, kā arī var veidoties polimetīna (*C*-nukleofils – malononitrils) vai merocianīna (*N*-nukleofils – pirmējais amīns) tipa fragmenti.

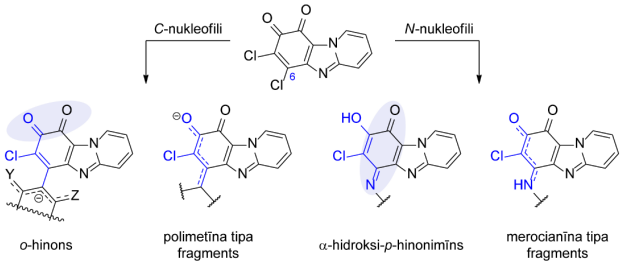


2. UV-Vis spektru datu analīze parādīja, ka iegūto 7-hlorpirido[1,2-*a*]benzimidazol-8,9-diona atvasinājumu spektroskopiskās īpašības šķīdumā ietekmē aizvietotāja raksturs, negatīvā lādiņa delokalizācija un planaritāte. Stēriski liels ārpus plaknes izgriezts funkcionalizēta indāna fragments padara savienojumu struktūru neplanāru, un var novērot izteikti pozitīvu (**7**) vai negatīvu (**8**, **9**) solvatohromiju. Gadījumā, ja heterocikliskā hinona un aizvietotāja fragmenti ir koplanāri (**10**), solvatohromijas efekts netiek novērots.

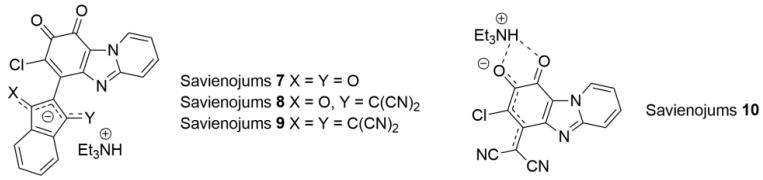


3. Gadījumā, ja 7-hlorpirido[1,2-*a*]benzimidazol-8,9-dionā ir ievadīts -NH-$CH_2$- fragments C(6) pozīcijā, veidojas merocianīna tipa struktūra. Šo atvasinājumu gadījumā cietā stāvoklī un šķīdumā dominē *exo* forma (bez iekšmolekulāras ūdeņraža saites). *Endo* formas klātbūtne (ar iekšmolekulāru H-saiti) izskaidro novēroto $CH_2$ grupas (blakus NH) signāla paplašināšanos $^1$H KMR spektros šķīdumā istabas temperatūrā.

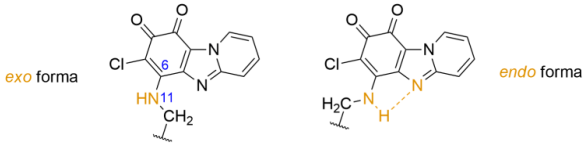


4. Pēc 6,7-dihlorpirido[1,2-*a*]benzimidazol-8,9-dionu reakcijas ar benzhidrazīdiem veidojas α-hidroksi-*p*-hinonimīnu atvasinājumi, kuros iekšmolekulārā H-saite starp

ievadīto aizvietotāju un heterocikla slāpekļa atomu (N(12)H…N(5)) stabilizē savienojuma C(6)=N(11) saites vienīgo konfigurāciju.

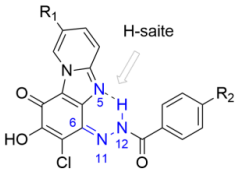


5. Katoda materiāli uz 6,7-dihlorpirido[1,2-*a*]benzimidazol-8,9-diona un to atvasinājumu bāzes potenciāli varētu darboties kā aktīvi elektroda materiāli ūdens elektrolītu baterijās.
6. 6,7-Dihlorpirido[1,2-*a*]benzimidazol-8,9-dions var kalpot kā daudzfunkcionāla platforma savienojumu iegūšanai ar plašu īpašību klāstu, ko potenciāli var izmantot materiālu jomā.

# DOCTORAL THESIS PROPOSED TO RIGA TECHNICAL UNIVERSITY FOR PROMOTION TO THE SCIENTIFIC DEGREE OF DOCTOR OF SCIENCE

To be granted the scientific degree of Doctor of Science (Ph. D.), the present Doctoral Thesis has been submitted for defence at the open meeting of the RTU Promotion Council on 10 June 2024 at the Faculty of Natural Sciences and Technology of Riga Technical University, 3 P. Valdena Street, Room 272.

OFFICIAL REVIEWERS

Associate Professor Dr. chem. Artis Kinēns,
University of Latvia, Latvia

Associate Professor Dr. chem. Agris Bērziņš,
University of Latvia, Latvia

Senior Researcher Dr. chem. Kārlis Pajuste,
Latvian Institute of Organic Synthesis, Latvia

## DECLARATION OF ACADEMIC INTEGRITY

I hereby declare that the Doctoral Thesis submitted for review to Riga Technical University for promotion to the scientific degree of Doctor of Science (Ph. D.) is my own. I confirm that this Doctoral Thesis has not been submitted to any other university for promotion to a scientific degree.

Anastasija Gaile ……. (signature)

Date: ……

The Doctoral Thesis has been prepared as a collection of thematically related scientific publications complemented by summaries in Latvian and English. The Doctoral Thesis unites three scientific publications and two microreviews. The scientific publications have been written in English with a total volume of 175 pages, including supplementary data.

# TABLE OF CONTENTS



Appendix 1 **Gaile, A**.; Belyakov, S.; Turovska, B.; Batenko, N. Synthesis of Asymmetric Coupled Polymethines Based on a 7-Chloropyrido[1,2-*a*]Benzimidazole-8,9-Dione Core. *J. Org. Chem.* **2022**, *87* (5), 2345–2355. https://doi.org/10.1021/acs.joc.1c02196

Appendix 2 **Gaile, A**.; Belyakov, S.; Rjabovs, V.; Mihailovs, I.; Turovska, B.; Batenko, N. Investigation of Weak Noncovalent Interactions Directed by the Amino Substituent of Pyrido- and Pyrimido-[1,2-*a*]Benzimidazole-8,9-Diones. *ACS Omega* **2023**, *8* (43), 40960–40971. https://doi.org/10.1021/acsomega.3c07005

Appendix 3 **Gaile, A**.; Belyakov, S.; Dūrena, R.; Griščenko, Ņ.; Zukuls, A.; Batenko, N. Studies of the Functionalized α-Hydroxy-*p*-Quinone Imine Derivatives Stabilized by Intramolecular Hydrogen Bond. *Molecules* **2024**, *29* (7), 1613. https://doi.org/10.3390/molecules29071613

Appendix 4 **Gaile, A**.; Batenko, N. Synthesis of Heterocyclic Ring-Fused Quinones (Microreview). *Chem. Heterocycl. Compd.* **2021**, *57* (11), 1076–1078. https://doi.org/10.1007/s10593-021-03027-w

Appendix 5 Batenko, N.; **Gaile, A**. Chemosensors Based on 5-Ethylidene-Substituted Barbituric Acid Derivatives (Microreview). *Chem. Heterocycl. Compd.* **2022**, *58* (2–3), 97–99. https://doi.org/10.1007/s10593-022-03061-2

Appendix 6 **Gaile, A**.; Dūrena, R.; Griščenko, Ņ.; Zukuls, A.; Batenko, N. Studies of cathode materials based on 6,7-dichloropyrido[1,2-*a*]benzimidazole-8,9-dione derivatives. *Unpublished results.*

# ABBREVIATIONS

$\lambda_{max}$ – wavelength of maximum absorption (nm)
δ – chemical shift (ppm)
ε – molar absorption coefficient
BLA – bond length alternation
CM – cathode material
CT – charge transfer
CV – cyclic voltammetry
DBU –1,8-diazabicyclo[5.4.0]undec-7-ene
DCM – dichloromethane
DFT – density functional theory
DMF – *N*,*N*-dimethylformamide
DMSO – dimethylsulfoxide
Et – ethyl
FTIR - Fourier-transform infrared
H-bond – hydrogen bond
HOMO – highest occupied molecular orbital
LUMO – lowest unoccupied molecular orbital
Me – methyl
NMR – nuclear magnetic resonance
PCM – polarizable continuum model
Ph – phenyl
ppm – parts per million
PVDF – polyvinylidene fluoride
r.t. – room temperature
SEM – scanning electron microscopy
TFA – trifluoroacetic acid
UV – ultraviolet
VT – variable temperature

# GENERAL OVERVIEW OF THE THESIS

## Introduction

Quinones are ubiquitous small molecules that represent a class of conjugated cyclic diketones commonly found in various natural products. These compounds are known for their physiological and photophysical properties as well as cytotoxic and cytoprotective effects[1] due to their versatile redox activity. Also, quinone derivatives play an essential role in biological processes (e.g., cellular respiration[2] and photosynthesis[3]) and quinone structural motifs are found in various biologically active compounds such as Coenzyme Q10,[4] Menadione,[5] Vitamin K,[6] Doxorubicin.[7]

At the same time quinone derivatives have been investigated for numerous applications in energy-storage and energy-harvesting systems.[8] Environmental issues and increasing demands on renewable energy-powered vehicles and energy storage devices for portable electronics[9] explain the rise of the attention to the research directions of organic redox active compounds in general and quinones in particular.[10,11] Quinone molecules have been extensively explored as organic electrode[12] materials for different types of rechargeable batteries, as two-electron anolytes or catholytes for aqueous[13] and non-aqueous[10] redox flow batteries, as electron-transfer mediators in metal-catalyzed reactions[14,15] or redox mediators in lithium-sulfur batteries,[16] as material for electrochemical $CO_2$ capture[17,18] or in electrochemical water-splitting technology.[19]

One of the most promising research directions is related to the application of quinones as electrode materials.[20] Nevertheless, several essential issues (electronic conductivity, solubility in electrolytes, large volume change, etc.) should still be improved before organic electrode materials can be extensively applied in secondary batteries.[21] In general, quinone derivatives can be divided into two groups: high-molecular and low-molecular derivatives. In the case of high-molecular compounds (quinone polymers or quinone-functionalized polymers), the solubility in the electrolyte decreases, but the cost of substrates and reagents for complex quinone-functionalized materials should also be considered from the economic prospects.[22] In contrast, small molecule quinones benefit from lower cost and simple preparation procedures (Fig. 1).

Controlled electrochemical performance and solubility are crucial factors for the achievement of stable organic cathode materials on the base of small molecule quinones. Properties such as solubility and chemical or thermal stability depend on the chemical structure of the quinone motif, interaction with media and possible isomerization. Moreover, the relatively weak noncovalent intermolecular interactions (hydrogen bonds (H-bonds), π-π interactions, van der Waals forces, electrostatic Coulomb forces) significantly influence the morphologies, different physicochemical properties (melting/boiling point, density, solubility), the ionic diffusion, the charge transport, and the electrochemical properties of organic materials.[23] Undoubtedly, various interactions may exist simultaneously leading to a self-assembled structure.[24] Additionally, supramolecular assembly and crystallization can

be controlled by the combination of different inter/intramolecular interactions but such control is still under development.[25]

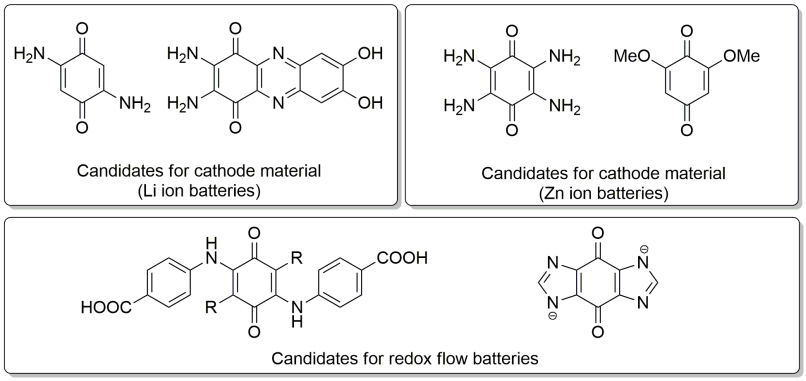


Fig. 1. Several examples[25–30] of small molecule quinone derivatives investigated for potential application in energy storage.

Thus, investigating the structure/property relationships and electrochemical behavior of quinone derivatives can detect the ranges when considering an application. An approach to the design of new organic materials by incorporating weak intra/intermolecular interactions allows modifying the architecture of the material and will help to tune the performance of quinone-functionalized materials at the molecular level.

Electrochemical and physicochemical properties can be adjusted by the modification of small quinone molecules with functional groups[21] or condensation with heterocycles.[31,32] Nitrogen-bridgehead heterocycle imidazo[1,2-*a*]pyridine is a valuable heterocyclic scaffold that is used in pharmacology research[33] and is investigated in material science[34,35] as well. Imidazo[1,2-*a*]pyridine derivatives tend to form strong intramolecular H-bond between the hydrogen atom of a donor group and nitrogen of the heterocycle, which facilitate the excited-state intramolecular proton transfer (ESIPT) luminescence.[36,37] Additionally, morphologies of self-assembled motifs can be affected if the imidazo[1,2-*a*]pyridine system is modified by the incorporation of variable functional groups.[24]

6,7-Dichloropyrido[1,2-*a*]benzimidazole-8,9-dione is a heterocyclic *o*-quinone that contains a combination of two structural subunits: *o*-quinone fragment and imidazo[1,2-*a*]pyridine core (Fig. 2). It can be obtained in one-step synthesis from commercially available tetrachloro-1,4-benzoquinone and 2-aminopyridine.[38] It is known[38] that 6,7-dichloropyrido[1,2-*a*]benzimidazole-8,9-dione, its derivatives and analogs can be easily modified via selective nucleophilic substitution of a chlorine atom at C(6) position providing monosubstituted product. Hence, on the base of pyrido[1,2-*a*]benzimidazole-8,9-dione core, a set of derivatives was synthesized, which provides the opportunity to investigate the influence of the substituents on the overall structure of quinone core and physical/redox properties.

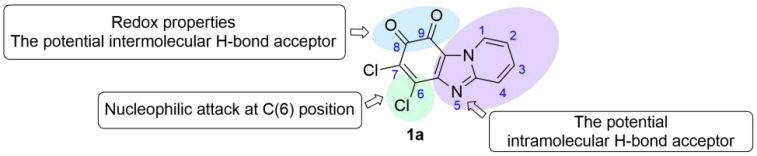


Fig. 2. The structure of 6,7-dichloropyrido[1,2-*a*]benzimidazole-8,9-dione (**1a**).

The Doctoral Thesis comprises two chapters. Chapter 1 covers data obtained from modification of the selected heterocyclic quinones with *C*-nucleophiles, structural studies, and redox properties of the obtained derivatives in solution. Chapter 2 provides results of the modification using *N*-nucleophiles, analysis of structural aspects of quinone derivatives (tautomerization), the effect of intra/intermolecular H-bonds and other weak noncovalent interactions as well as the studies of redox properties of starting *o*-quinone and obtained *p*-quinone imine derivative in solid state. These investigations were conducted to find generalizable connections relating to small heterocyclic quinone molecule structure, intra/intermolecular interactions, and properties, providing a framework for future design strategies, rather than proposing specific new material candidates.

## Aims and objectives

The aim of the Thesis is the modification of 6,7-dichloropyrido[1,2-*a*]benzimidazole-8,9-dione, its derivatives and analogs, as well as structural studies and the investigation of structure–property relationships of the obtained derivatives.

The following tasks were set:

1. To modify 6,7-dichloropyrido[1,2-*a*]benzimidazole-8,9-diones and its analogs via substitution reaction with *C*- and *N*-nucleophiles.
2. To define the molecular structure of quinone derivatives and to establish weak non-covalent interactions in solid state using X-ray crystallography data.
3. To compare data on the molecular structure of derivatives in solid state obtained from X-ray crystallography analysis and behavior in solution using UV-Vis spectroscopy and NMR spectroscopy methods accompanied by quantum chemical calculations.
4. To explore redox properties of selected 6,7-dichloropyrido[1,2-*a*]benzimidazole-8,9-dione derivatives.

## Scientific novelty and main results

During the course of the Thesis, the derivatives of 6,7-dichloropyrido[1,2-*a*]benzimidazole-8,9-dione were synthesized by nucleophilic substitution with *C*- and *N*-nucleophiles at C(6) position. In the case of bulky *C*-nucleophiles, stable heterocyclic *o*-quinone derivatives with sterically hindered substituents were found, on the other hand, the use of less bulky *C*-nucleophiles led to the formation of coupled polymethines. Stable *p*-quinone imine structures were obtained by using aroyl hydrazides as *N*-nucleophiles as

well as merocyanine-type structures were isolated in the case of aliphatic primary amines. In the resulting compounds, the form of the "classical" heterocyclic *o*-quinone structural unit changes depending on the introduced substituent, thereby expanding the range of physical properties of the compounds.

Using a combination of NMR spectroscopy and X-ray crystallography, the study revealed some features of *o*-quinone derivatives: in several cases, the introduced substituent formed an intramolecular H-bond with the nitrogen of heterocycle (N-H···N or O-H···N type) as well as weak intermolecular non-covalent interactions were observed leading to different architectures of molecular self-assembly. Substitution with primary amines led to a set of 6-aminosubstituted *o*-quinone derivatives containing -NH-$CH_2$- moiety that can form non-centrosymmetric chiral (racemic conglomerate) or centrosymmetric achiral crystals. Cathode materials were prepared from 6,7-dichloropyrido[1,2-*a*]benzimidazole-8,9-dione and its *p*-quinone imine derivative and tested for redox activity. It was found that the heterocyclic *o*-quinone has the potential for application as cathode material in aqueous electrolyte batteries.

## Structure of the Thesis

The Thesis is a collection of thematically related scientific publications devoted to the investigation of the synthesis, structure and properties of 6,7-dichloropyrido[1,2-*a*]benzimidazole-8,9-dione and its analogs and their derivatives in solid state and/or in solution.

## Publications and approbation of the Thesis

The results of the Thesis have been published in three scientific publications and two microreviews. Additionally, the results have been disseminated at five scientific conferences.

**Publications**

1. **Gaile, A.**; Belyakov, S.; Dūrena, R; Griščenko, Ņ; Zukuls, A.; Batenko, N. Studies of the Functionalized α-Hydroxy-*p*-Quinone Imine Derivatives Stabilized by Intramolecular Hydrogen Bond. *Molecules* **2024**, *29* (7), 1613. https://doi.org/10.3390/molecules29071613
2. **Gaile, A.**; Belyakov, S.; Rjabovs, V.; Mihailovs, I.; Turovska, B.; Batenko, N. Investigation of Weak Noncovalent Interactions Directed by the Amino Substituent of Pyrido- and Pyrimido-[1,2-*a*]Benzimidazole-8,9-Diones. *ACS Omega* **2023**, *8* (43), 40960–40971. https://doi.org/10.1021/acsomega.3c07005
3. **Gaile, A.**; Belyakov, S.; Turovska, B.; Batenko, N. Synthesis of Asymmetric Coupled Polymethines Based on a 7-Chloropyrido[1,2-*a*]Benzimidazole-8,9-Dione Core. *J. Org. Chem.* **2022**, *87* (5), 2345–2355. https://doi.org/10.1021/acs.joc.1c02196

4. Batenko, N.; **Gaile, A**. Chemosensors Based on 5-Ethylidene-Substituted Barbituric Acid Derivatives (Microreview). *Chem. Heterocycl. Compd.* **2022**, *58* (2–3), 97–99. https://doi.org/10.1007/s10593-022-03061-2
5. **Gaile, A**.; Batenko, N. Synthesis of Heterocyclic Ring-Fused Quinones (Microreview). *Chem. Heterocycl. Compd.* **2021**, *57* (11), 1076–1078. https://doi.org/10.1007/s10593-021-03027-w

**Conference participation**

1. **Gaile, A**.; Belyakov, S.; Rjabovs, V.; Batenko, N. X-ray Crystallographic and Spectroscopic Studies of Heterocyclic *o*-Quinone Derivatives. 1st Aristotle Conference on Chemistry "Advances and Challenges in Chemistry 2023, Thessaloniki, Greece. November 12–15, **2023**.
2. **Gaile, A**.; Belyakov, S.; Batenko, N. NMR studies of 6-aminosubstituted pyrido- and pyrimido-[1,2-a]benzimidazole-8,9-diones. Riga Technical University 64th International Scientific Conference "Materials Science and Applied Chemistry", Riga, Latvia October 6, **2023**.
3. **Gaile, A**.; Belyakov, S.; Batenko, N. Investigation of Quinone Hydrazones/Thiosemicarbazones as Potential Bifunctional Ligands for Metal ion Complexation. Riga Technical University 63rd International Scientific Conference "Materials Science and Applied Chemistry", Riga, Latvia October 21, **2022**.
4. **Gaile, A**.; Belyakov, S.; Batenko, N. *o*-Quinone derivatives containing functionalized indane fragment: experimental and theoretical studies. Riga Technical University 62nd International Scientific Conference "Materials Science and Applied Chemistry", Riga, Latvia October 22, **2021**.
5. **Gaile A**, Belyakov S, Batenko A. Synthesis and structure investigation of benzimidazole-based 1,2- and 1,4-quinone derivatives. Riga Technical University 61st International Scientific Conference "Materials Science and Applied Chemistry 2020", Riga, Latvia, October 23, **2020**.

# MAIN RESULTS OF THE THESIS

The ability of quinone molecules to undergo tautomerization is an important issue due to the significant impact of different forms on the properties of the resulting compounds. The understanding and control of the process can lead to new and potentially desirable characteristics of quinone derivatives or to avoid non-desirable properties. For example, modification of the *o*-benzoquinone (**A, C**) fragment at the C(4) position may involve tautomerization into *p*-quinone imine (**B**) or *p*-quinone methide (**D**) (Fig. 3) in biological systems leading to toxicity in some cases.[1] For many significant biological processes (e.g., lignin biosynthesis,[39] cuticular sclerotization[40] in insects or melanization[41]) quinone methide intermediates play a crucial role in the metabolic oxidation of catechol derivatives. A study by Land E. J. et al.[42] revealed that the structure of *o*-quinone undergoes facile tautomerism to *p*-quinone methide form by introducing cyanomethyl moiety at C(4) position of 1,2-naphthoquinone. When a primary aliphatic amine is used in the substitution reaction, a product mixture can be formed, mainly due to a tautomeric equilibrium between 4-amino-*o*-quinone and α-hydroxy-*p*-quinone imine forms. Equilibrium is sensitive to solvent[43] and pH[44] of the media.

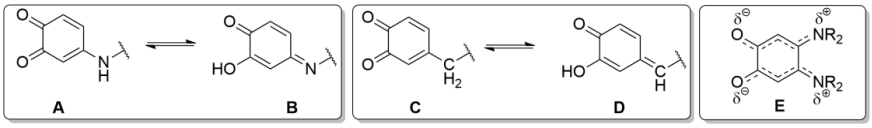


Fig. 3. Tautomeric equilibrium between 4-amino-*o*-quinone (**A**) and α-hydroxy-*p*-quinone imine (**B**) forms; tautomeric equilibrium between *o*-quinone (**C**) and α-hydroxy-*p*-quinone methide (**D**) forms; coupled polymethine (**E**) on the base of *o*-quinone derivative.

Modified *o*-benzoquinones can be characterized also as coupled polymethines depending on the nature of the substituent at C(4) or/and C(5) if electrons are delocalized exclusively between the oxygen atom of carbonyl group and introduced substituent (amino substituent in the case of compound **E**, Fig. 3). According to Dähne, S. et al.,[45,46] if two polymethine structural units (or one polymethine and one polyene chains) are found in the molecule, it generally exhibits a coupling effect that determines photophysical properties of the compound.

## 1. Modification of pyrido[1,2-*a*]benzimidazole-8,9-dione core by reaction with *C*-nucleophiles

Different photophysical and electrochemical properties can be obtained by varying planarization (interplanar angle ($\varphi$) values), electron distribution and redox potentials of the compound.[47] To investigate the effect of a substituent on the structure, quinone **1a** was modified by commonly used *C*-nucleophiles (1,3-indandione derivatives with different numbers of dicyanomethylene units[48–50](**2-4**), malononitrile (**5**) and barbituric acid[51] (**6**)) in the presence of triethylamine. A series of heterocyclic quinone derivatives (**7**−**11**) was

isolated as triethylammonium salts (Scheme 1). Synthesis of compound **10** was carried out under reflux since poor yields were obtained at ambient temperature. All obtained products **7-11** are deeply colored compounds: compounds **7** and **11** have a dark green color, compound **8** – brown, and compounds **9** and **10** – purple or dark blue. The different delocalization of the negative charge and diverse forms of quinone core in triethylammonium salts **7-11** were established.

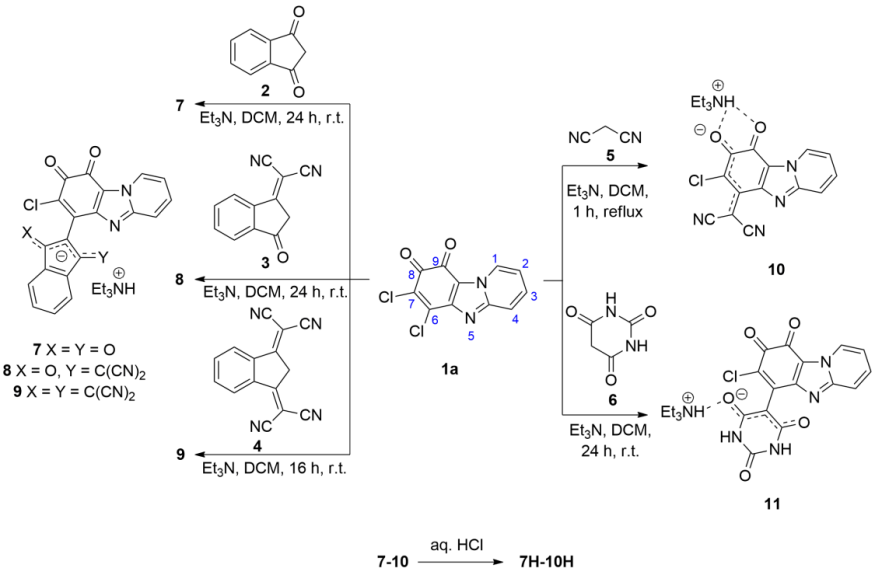


Scheme 1. Synthesis of compounds **7-11** and **7H-10H**.

After acidic hydrolysis of triethylammonium salts **7-10**, a set of compounds **7H-10H** was isolated and analyzed. An interesting feature was observed in the case of compound **7H**: a red solid was obtained; however, dissolved in DMSO, the solid formed a green-colored solution. FTIR spectrum of red solid showed absorption bands at 1746 and 1702 $cm^{-1}$ and the absence of an absorption band characteristic of a hydroxyl group. It can be concluded that acidic hydrolysis of salt **7** led to product **7H**$^{keto}$ (red-colored in solid state) with diketo form of indandione moiety. However, $^1$H NMR spectrum of red-colored crystals in DMSO-$d_6$ solution exhibited two sets of signals caused the by keto/enol tautomeric equilibrium[52] of the indandione fragment. From the $^1$H NMR spectrum, the keto/enol form ratio is equal to 0.45 : 1 (Fig. 4 c).

Green-colored crystals of enol form of compound **7H** (**7H**$^{enol}$) were obtained unexpectedly by slow evaporation of DCM solution of salt **7**. The structure of compound **7H**$^{enol}$ was confirmed by X-ray crystallography: in solid state, the heterocyclic *o*-quinone fragment is connected to the enolic form of indandione (Fig. 4 a). The molecule was stabilized by a very strong intramolecular H-bond of OH···N type (N(5)···H = 1.172 Å, H···O = 1.379 Å, the value of N(5)···H···O angle is equal 157(6)$^o$). In the crystal structure of **7H**$^{enol}$, a strong intermolecular σ-hole interaction was found between the oxygen of C=O

bond (indandione fragment) and chlorine atom; in the crystal structure, centrosymmetric molecular dimers were formed (Fig. 4 b).

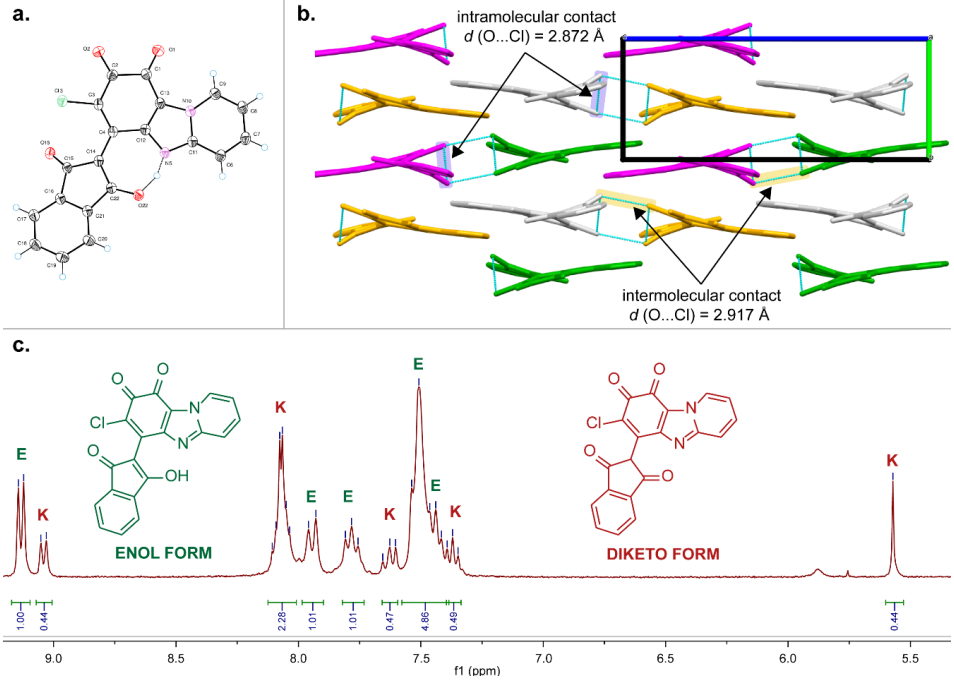


Fig. 4. a – ORTEP diagram of the asymmetric unit for compound **7H*enol*** showing thermal ellipsoids at the 50 % probability level. b – Molecular packing of compound **7H*enol*** in solid state; light blue lines indicate O…Cl interactions. c – Expansion of $^{1}$H NMR spectrum (300 MHz, DMSO-$d_6$), showing enol (E) and diketo (K) forms.

To better understand the effect of the substituent on the parent structure, the X-ray crystallography data analysis of compounds **10-11** and **7H*enol*** was conducted along with DFT calculations (*ORCA*[53] software, CAM-B3LYP/def2-TZVP level of theory). Bond lengths (X-ray crystallography data) of the heterocyclic quinone core of compounds **10-11** and **7H*enol*** were compared to each other and to previously reported[38] benzimidazole-based quinone derivative ***o*-QCCN** (Fig. 5). Analysis of the bond lengths of the selected compounds in solid state led to the conclusion that quinone cycle can be divided into two structural units separated by long single C-C bonds *1* and *4* (see Fig. 5 a for the bond numbering). One structural unit includes bonds *16-2-3-substituent* and the length of bonds *2* and *3* of 7-chloropyrido[1,2-*a*]benzimidazole-8,9-dione derivatives varied depending on the *substituent* introduced. For example, in compounds **11** and **7H*enol***, bonds *2* and *3* displayed a pronounced single/double bond alternation like in the "classical" *o*-benzoquinone,[54] whereas in compounds **10** and ***o*-QCCN**, a simultaneous equalization of the lengths (bonds *2* and *3*) was found.

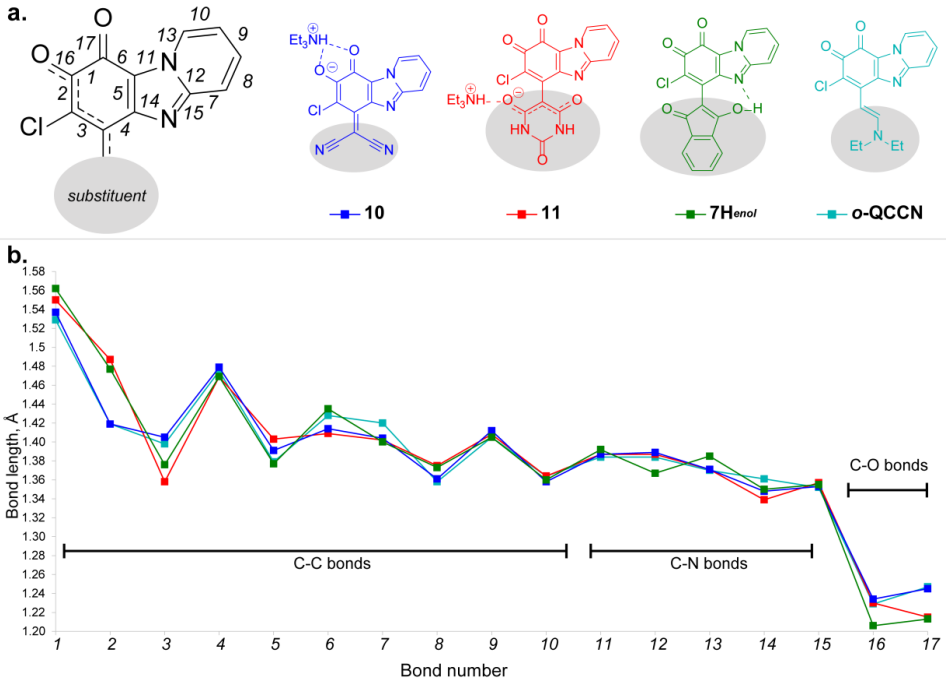


Fig. 5. a – The schematic representation of heterocyclic quinone core of compounds **10-11, 7H$^{enol}$,** and ***o*-QCCN** with bond numbering. b – A comparison of the bond lengths of the selected compounds. Bond lengths of compound ***o*-QCCN** were confirmed by single crystal X-ray data.[38]

The bond length alternation (BLA) was calculated for bonds *2-3-substituent* using data obtained from X-ray crystallography analysis as well as for the optimized geometries (DFT calculations) of compounds **10-11, 7H$^{enol}$, *o*-QCCN** (Table 1). It was concluded that compounds **10** and ***o*-QCCN** can be characterized as asymmetric "coupled polymethines" because of the BLA vanishing over the selected structural unit. On the other hand, for compound **11** a polymethine fragment was found between two carbonyl groups of barbituric acid (equalized bonds with extensive distribution of π-electrons); however, bonds *16-2-3-substituent* can be characterized as a polyene fragment. Overall, the delocalization of the negative charge over a sterically hindered *substituent* provides the stabilization of *o*-quinone form. As a result, the conjugation between the quinone cycle and substituent disappeared. Another structural unit consists of the heterocycle moiety (bonds *5-15*) and a nearby carbonyl group (bond *17*) (Fig. 5). In the case of compounds **10-11** and ***o*-QCCN**, lengths of the bonds *5-15* were not affected by the introduced *substituent*. Also, the length of bond *17* in quinone derivatives was similar to the length of the carbonyl group bond in imidazo[1,2-*a*]pyridine-3-carbaldehyde derivative.[55] Only in the case of compound **7H$^{enol}$**, bond *17* was slightly shorter since strong intramolecular H-bond N···HO affected π-electron distribution in the heterocyclic part (bonds *12-13*) of the molecule.

The crystal packing motifs of triethylammonium salts **10** and **11** were compared (Fig. 6). Noteworthy, head-to-tail columnar packing stabilized by π-π-stacking was found in the crystal structure of compound **10**. The formation of the chains was observed in the case of compound **11** where anions are associated by means of H-bonds of NH···O type between barbituric acid moieties.

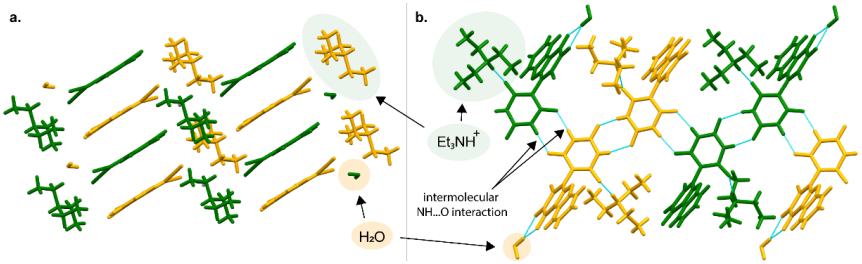


Fig. 6. Crystal packing of compounds **10** (a) and **11** (b), H-bonds are highlighted in light blue color.

DFT calculations were carried out to optimize the geometry of the obtained compounds (in gas phase as well as in solution, PCM model). The obtained data was compared to the experimental data from X-ray crystallography analysis (Table 1). For DFT-optimized compounds **10** and ***o*-QCCN**, calculations predict coplanarity of all atoms, but for salts **7-9** and **11**, interplanar angles of 60±10° are expected between the introduced substituent plane and heterocyclic quinone plane. Interestingly, optimized geometry at CAM-B3LYP/def2-TZVP level in DMF solution gave the best agreement to experimental structural parameters (interplanar angle and bond lengths).

Table 1

Interplanar angles ($\varphi$), bond length alternation (BLA), and bond length ($r$) between planes of compounds **10**-**11**, **7H** and ***o*-QCCN**

| Compound | Method | **11**[a] | **10** | **7H**$^{enol}$ | ***o*-QCCN** |
|---|---|---|---|---|---|
| Interplanar angle $\varphi$, ° | X-ray | 60.79 (**11A**)<br>64.60 (**11B**) | 10.48 | 25.57 | 4.56 |
| | Calculations[c] | 65.62 | 1.07 | 31.16 | 1.53 |
| $r_{C(6)\text{-}C(substituent)}$, Å | X-ray | 1.468 (**11A**)<br>1.469 (**11B**) | 1.402 | 1.448 | 1.412 |
| | Calculations[c] | 1.462 | 1.395 | 1.449 | 1.401 |
| BLA[b], Å | X-ray | 0.0935 (**11A**)<br>0.0975 (**11B**) | 0.0055 | 0.0700 | 0.0245 |
| | Calculations[c] | 0.0935 | 0.0070 | 0.0905 | 0.0260 |

[a] Crystal of salt **11** consists of two anions that are marked as anions **11A** and **11B**.

[b] BLA parameter was calculated as the difference between the average bond lengths of the formal C-C single and double bonds in the polymethine/polyene chain for the structure (bonds *2-3* and following bonds of the introduced substituent).

[c] Geometry optimized at the CAM-B3LYP/def2-TZVP level of theory (DMF solvent, PCM).

The structure of triethylammonium salts **7-11** was investigated in solution by the analysis of their $^{13}$C NMR spectra. Chemical shifts of quinone carbonyl group's signals (δ of C(8) and C(9)) in $^{13}$C NMR spectra were compared (Fig. 7 a). It was observed that C(8) and C(9) signals of compound **10** were shifted close to each other with Δδ(C=O) equal to 0.2 ppm, which was explained by the similar electron density of these carbon atoms; additionally, δ(C=O) are affected by H-bonding with $Et_3NH^+$. However, Δδ(C=O) in $^{13}$C NMR spectra of *o*-quinones **7-9** and **11** were found to be 9.0 ppm, 11.5 ppm, 13.0 ppm, and 11.1 ppm, respectively. A linear relationship was found between Δδ(C=O) (quinone fragment) in $^{13}$C NMR spectra of compounds **7-11** and calculated interplanar angle (DMF) (Fig. 7 b).

One signal at a single chemical shift was observed for carbons of carbonyl groups of 1,3-indandione moiety in $^{13}$C NMR spectra (DMSO-$d_6$) of triethylammonium salt **7** (δ(C=O) = 187.0 ppm). This indicates an equal electron density distribution; thus, in solution, the negative charge is symmetrically delocalized over the substituent fragment (between two carbonyl groups).

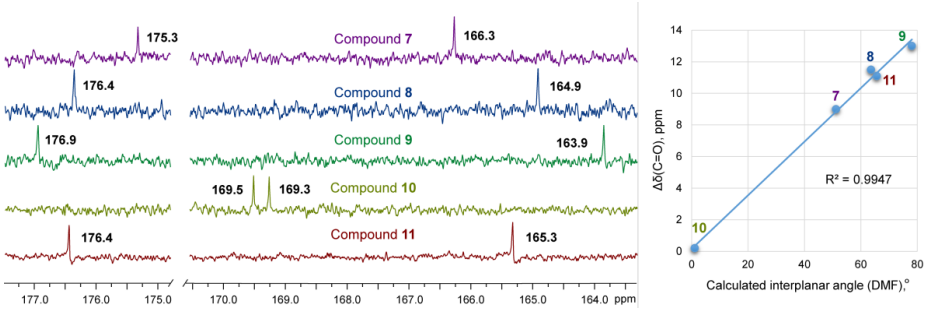


Fig. 7. a – A fragment of $^{13}$C NMR (DMSO-$d_6$) spectra of triethylammonium salts **7-11**. b – A correlation between calculated interplanar angle in DMF (CAM-B3LYP/def2-TZVP, PCM) and difference between shifts of quinone C=O groups (Δδ(C=O)) in $^{13}$C NMR spectra of compounds **7-11** in DMSO-$d_6$.

Frontier orbitals were calculated (DFT) for heterocyclic quinone **1a** and its derivatives **7-11** and ***o*-QCCN** as well. HOMO was shifted from imidazo[1,2-*a*]pyridine fragment (Fig. 8, initial quinone **1a**) towards substituent moiety of triethylammonium salts **7-11** and compound ***o*-QCCN**, indicating a shift of the electron-donating part of the compound. In quinone derivatives **7-11** and ***o*-QCCN**, HOMO was spread over the polymethine/polyene structural unit of the molecule: *16-2-3-substituent* (see Fig. 5 a for the bond numbering), which can be explained by the delocalization of the negative charge over this segment. Analysis of frontier orbitals and HOMO-LUMO overlap values showed that for compounds **7-9** and **11**, HOMO is located more in the donor substituent fragment, but LUMO – in the acceptor part (quinone fragment), and intramolecular charge transfer from substituent to the quinone fragment is possible. However, for compounds **10** and ***o*-QCCN** HOMO-LUMO overlap values are higher; thus, the charge transfer character seems to be weak (Fig. 8).

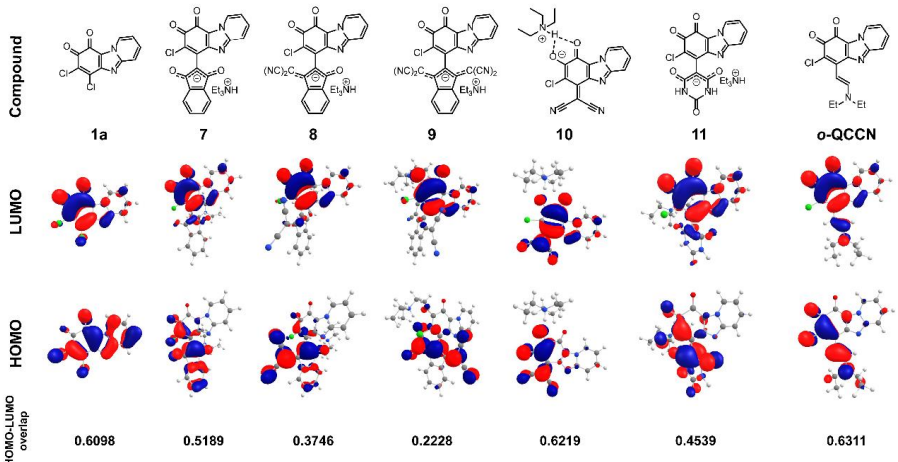


Fig. 8. Frontier orbitals and HOMO-LUMO overlap at the CAM-B3LYP/def2-TZVP level for compounds **1a, 7-11** and ***o*-QCCN** (overlap integrals between the HOMO and LUMO were calculated at the CAM-B3LYP/def2-TZVP level in DMF using *Multiwfn*[56] software).

To study the properties of the resulting compounds in solution, UV-Vis spectra for salts **7**−**11** were recorded in solvents with different polarities (DMF or DCM) under basic (DBU) and acidic (TFA) conditions (Table 2). Depending on the introduced substituent, positive or negative solvatochromism was observed for derivatives **7-9**. For instance, compound **7** exhibited positive solvatochromism (the longest wavelength absorption band shifts hypsochromically as the polarity of the solvent decreases); by contrast, salts **8-9** exhibited negative solvatochromic behavior. This means that for compound **7**, the excited state is more polar than the ground state while introducing two (compound **8**) or four (compound **9**) cyano groups into the substituent shows the opposite effect – the excited state is less polar than the ground state. It can be concluded that compounds **8-9** are quite polar molecules in the ground state. However, compounds **10** and ***o*-QCCN** showed $\lambda_{max}$ in a range of 630±10 nm in both DMF or DCM solutions (exhibited practically no solvatochromism) and showed no changes under basic conditions. Both compounds exhibit hypsochromic shift of *ca.* 100 nm under acidic conditions that can be attributed to the protonation of oxygen at C(8). The addition of TFA to the DCM solution of compounds **7-9** caused the disappearance of the longest wavelength transitions. It was concluded that the presence of the anionic form of salts **7-9** is necessary for the longwave absorption band and protonation induces quenching of the intramolecular charge transfer (Table 2). In the case of derivatives **7-9**, a clear correlation ($R^2$ = 0.99) was obtained between $\lambda_{max}$ (DCM) and HOMO-LUMO overlap as well as between $\lambda_{max}$ and calculated interplanar angle. Additionally, UV-Vis spectra of derivatives **7-9** were compared with spectra of substrates (*o*-quinone **1a** and indane derivatives **2-4**) in DMF and DCM solutions. It was found that UV-Vis spectra of products **7-9** consist of its chromophore units absorption, and the interaction between them leads to a new longwave

absorption band. The largest bathochromic shift of the longwave absorption band was observed in the case of compound **9** in DCM solution (864 nm).

Table 2

UV-Vis spectral data of compounds **7-11** and ***o*-QCCN**

| Compound | $\lambda_{max}$ (lgε) | | | |
|---|---|---|---|---|
| | DMF | DCM | DCM+TFA | DCM+DBU |
| **7** | 428 (3.99)<br>**690 (3.84)** | 411 (3.85)<br>**660 (3.30)** | 398 (3.74)<br>540 (sh) | 434 (3.87)<br>681 (3.71) |
| **8** | 479 (4.08)<br>**697 (3.68)** | 462 (3.90)<br>**751 (3.42)** | 404 (3.60)<br>540 (sh) | 482 (3.77)<br>710 (3.38) |
| **9** | 577 (4.36)<br>615 (4.22)<br>**740 (sh)** | 570 (4.37)<br>607 (4.23)<br>**864 (3.21)** | 346 (4.49)<br>430 (sh)<br>510 (sh) | 575 (4.40)<br>614 (4.27)<br>750 (sh) |
| **10** | 409 (4.28)<br>**627 (3.97)** | 403 (4.40)<br>**641 (3.93)** | 367 (4.48)<br>541 (3.33) | 409 (4.22)<br>632 (3.87) |
| **11** | 661 (3.57) | - | - | - |
| ***o*-QCCN** | 414 (4.30)<br>**636 (4.06)** | 414 (4.23)<br>**640 (3.98)** | 382 (4.44)<br>559 (3.16) | 415 (4.25)<br>640 (4.00) |

A correlation was found for molar absorption coefficients (ε) of the longwave absorption band of compounds **10-11**, **7H*$^{enol}$*** and ***o*-QCCN** in DMF/DMSO solutions (Fig. 9, Table 2) and experimental value of interplanar angle ($\varphi$) (Table 1, X-ray crystallography data). This result supports the observed appearance of the longwave absorption band. As the interplanar angle between the quinone subunit and substituent decreases, a greater extent of electron delocalization can be found. This enhanced delocalization leads to a higher molar absorption coefficient of the longest wavelength absorption band.

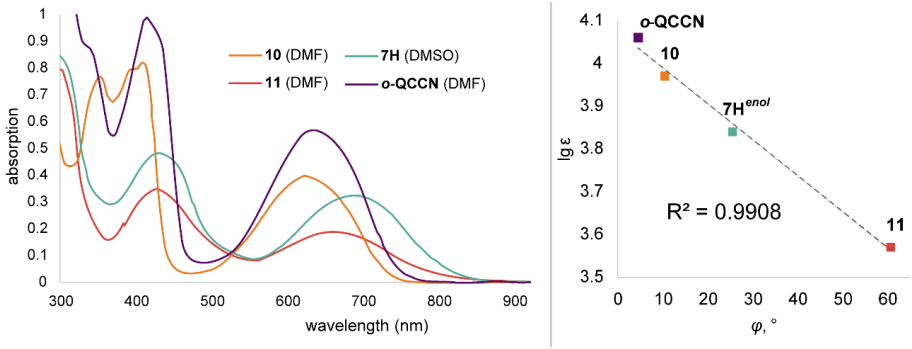


Fig. 9. UV absorption spectra of compounds **10, 11, 7H*$^{enol}$*** and ***o*-QCCN** in DMF/DMSO solutions and correlation between their molar absorption coefficients of the longwave absorption band and the size of interplanar angle ($\varphi$).

The electrochemical properties of the synthesized quinone derivatives in MeCN solutions were investigated by cyclic voltammetry (CV) and electrochemical reduction and oxidation potentials ($E_{red}$, $E_{ox}$) are listed in Table 3. It is known that the electrochemical

reduction of the quinone system is sensitive to the integration of substituents.[57] From the results of CV measurements it was found that quinone derivatives **7** and **11** can be more easily reduced (the first reduction potentials $E^{I}_{red}$ are –0.48 V and –0.44, respectively). With the increasing number of cyano groups in the salt structure (compounds **8-10**) the first reduction potential shifted toward more negative potential values with an irreversible oxidation wave.

Table 3

Electrochemical properties of the quinone derivatives: reduction ($E_{red}$) and oxidation ($E_{ox}$) potentials (MeCN solution, Ag/AgCl reference electrode)

| Compound | $E^{I}_{red}$, V | $E^{II}_{red}$, V | $E_{ox}$ V |
|---|---|---|---|
| Compounds with negative charge distribution over the introduced substituent | | | |
| **7** | –0.48 | - | 0.94 |
| **8** | –0.54 | –0.93 | 1.29 |
| **9** | –0.60 | –1.00 | 1.12 |
| **11** | –0.44 | –0.85 | 1.14 |
| Compounds with negative charge distribution over the polymethine structural unit of quinone | | | |
| ***o*-QCCN** | –0.59 | –1.12 | 1.01 |
| **10** | –0.50 | –0.74 | 0.96 |
| **10a** | –0.56 | –0.76 | 0.96 |
| **10b** | –0.43 | –0.59 | 1.04 |
| **10c** | –0.82 | –1.04 | 0.81 |
| **10d** | –0.81 | –0.92 | 0.83 |
| Hydrolyzed products (**7H-10H**) of triethylammonium salts **7-10** | | | |
| **7H** | –0.34 | –0.72 | - |
| **8H** | –0.54 | –1.93 | 1.00 |
| **9H** | –0.68 | –1.51 | 0.86 |
| **10H** | –0.94 | - | 1.17 |

Derivatives of compound **10** were prepared to investigate the effect of the substituent at the heterocycle ring of quinone on electrochemical properties (Scheme 2).

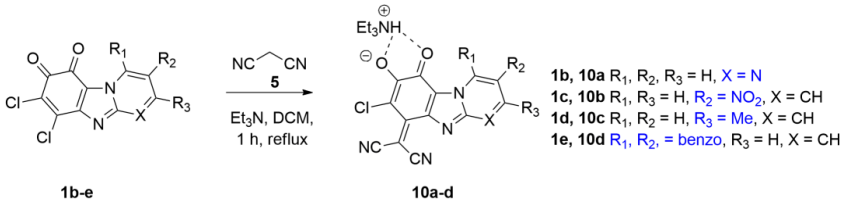


Scheme 2. Synthesis of compounds **10a-d**.

Compounds **10a-d** were investigated by CV (Table 3, Fig. 10). It was found that replacing 4-CH to N (**10a**) in the heterocycle caused only insignificant changes in both

potential values. The shift of the first reduction potentials and oxidation potentials toward more negative potential values (*ca.* $E^{I}_{red}$ = –0.80 V and $E_{ox}$ = +0.80 V) was caused by the introduction of the methyl group at C(3) (**10c**) or by elongation of the aromatic system (**10d).** The introduction of the electron-withdrawing group at C(2) (**10b**) showed the opposite effect.

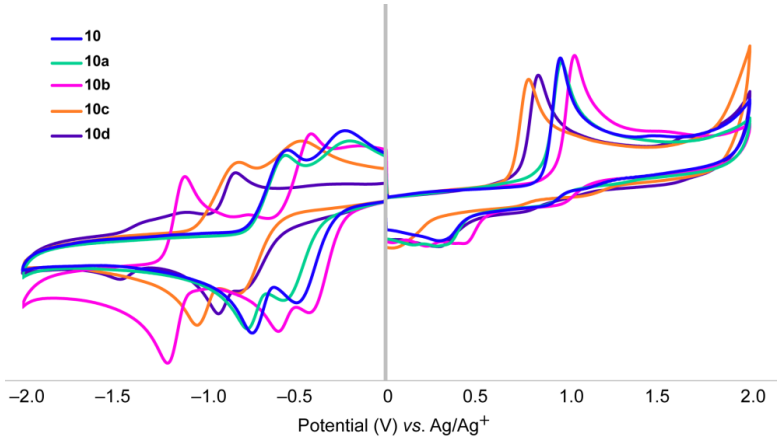


Fig. 10. Cyclic voltammograms of compounds **10** and **10a-d** in MeCN solution.

To summarize, the reaction of 6,7-dichloropyrido[1,2-*a*]benzimidazole-8,9-dione with *C*-nucleophiles in the presence of $Et_3N$ led to the formation of salts where the quinone fragment can exist in different forms. After reactions with bulky *C*-nucleophiles, the resulting 7-chloropyrido[1,2-*a*]benzimidazol-8,9-diones are stable *o*-quinones connected by the C-C bond with the substituent, which is out-of-plane. In this case, the negative charge is delocalized in the introduced substituent. The longwave absorption band observed for these compounds arises from intramolecular charge transfer between the substituent and the quinone moieties, and positive or negative solvatochromism can be observed in solution.

When the introduced substituent and heterocyclic quinone fragments are coplanar, two structural units can be found in the molecule; as a result, asymmetric "coupled polymethines" are formed, and the intramolecular charge transfer character of the molecule seems to be weak. To understand the potential applications of the investigated compounds, it is necessary to analyze the spatial structure because changes in the planarity of the molecule are followed by changes in the structure and in the physical properties. An additional possibility of modification is the interaction with bases, which in turn leads to various delocalizations of the negative charge.

The scientific publication of the research described in this chapter can be found in Appendix 1.

## 2. Modification of pyrido[1,2-*a*]benzimidazole-8,9-dione core by reaction with *N*-nucleophiles

Quinones with replaceable halide substituents react with amines, amino alcohols, and amino acids: the formation of the C-N bond does not produce a new chirality center since it proceeds via the addition/elimination sequence.[58] It is known[59] that chirality of achiral organic molecules in solid state can result from restricted rotation of bonds and/or spiral packing in the structure. By incorporation of conformationally flexible moieties with proton-donating properties at the quinone "backbone", the formation of supramolecular systems stabilized by various intermolecular non-covalent interactions can be achieved.[60]

In the case of quinone derivatives, an extensive network of intermolecular H-bonds can be formed between carbonyl groups of quinones and different H-bond donor groups (e.g., OH or $NH_2$). Also, close interlayer π-π interactions can occur between quinone rings when they are fused with aromatic and/or heterocyclic rings; as a result, ordered redox-active molecular solids can be created.[25] Stabilization of the supramolecular structure of quinone derivatives by synergistic noncovalent forces can be controlled by chemical modification and/or steric effects of substituents that were demonstrated experimentally.[44, 45]

In general, halogenated *o*-quinones reaction with primary amines can give two main products: a substitution product and/or a derivative formed by nucleophilic addition to the carbonyl group. Additionally, a mixture of the products can be formed due to tautomeric equilibrium between 4-amino-*o*-quinone and α-hydroxy-*p*-quinone imine.[44] For the rational design of quinone-based materials a data collection on intra/intermolecular interactions and substituent effects on supramolecular structure is needed. Thus, the reactions of 6,7-dichloropyrido-[1,2-*a*]benzimidazole-8,9-diones with primary amines and benzohydrazides were carried out and the structure and properties of obtained products were explored.

### 2.1. Primary amines as *N*-nucleophiles

As it was previously reported[38] when a secondary aliphatic amine (diethylamine) was used as a nucleophilic reagent in the reaction with 6,7-dichloropyrido-[1,2-*a*]benzimidazole-8,9-dione, 6-diethylamino derivative of *o*-quinone **1a** was obtained and columnar stacking in crystal state was found. Pyrido- and pyrimido-[1,2-*a*]benzimidazole-8,9-diones (**1a,b**) were selected for the modification of the initial core with primary aliphatic amines and flexible amino alcohols (**12a-g**) (Scheme 3a). Crystals of seven compounds (**13c-g** and **14a,b**) were obtained and analyzed using X-ray crystallography analysis. The analysis of X-ray data (Table 4) revealed that nitrogen N(11) at the C(6) position of all studied compounds has a planar configuration as the sum of angles α, β and γ (Scheme 3 b) is almost 360° and the tendency to the bond equalization in the fragment C(6)-C(7)-C(8) was observed.

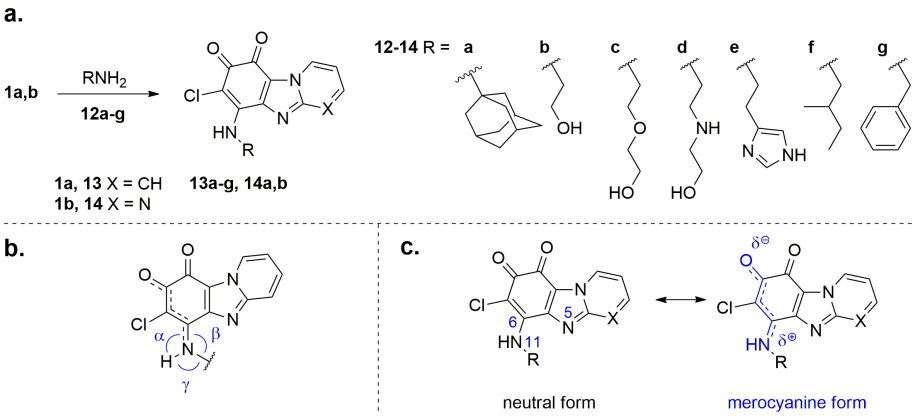


Scheme 3. a – Synthesis of compounds **13a-g** and **14a,b.** Compounds **13d-e** were isolated as hydrochlorides. b – Bond angles α, β and γ of compounds **13a-g** and **14a,b.** c – Neutral and merocyanine-type resonance forms of obtained compounds **13a-g** and **14a,b.**

On the basis of experimental data, the Mayer bond order of C(6)-N(11) bond (*Multiwfn*[56] software) for compounds **13c-g** and **14a,b** was calculated and a partial double bond character was proved (Table 4). Thus, O=C(8)-C(7)-C(6)-N(11)H fragment has a merocyanine-type structure (Scheme 3 c) and restricted rotation along the C(6)-N(11) axis. Also, the merocyanine fragment can facilitate the formation of resonance-assisted hydrogen bond.[63]

Table 4

Crystallographic parameters and calculated Mayer bond order from single crystal X-ray analysis of compounds **13c-g** and **14a,b**

| Cmpd. | Conformation | $\phi_1$ [a,c] (C6-N11-C12-C13), ° | $\phi_2$ [b,c] (C6-N11-C12-C13), ° | C(6)-N distance, Å | Mayer bond order | The sum of the angles α, β and γ, ° |
|---|---|---|---|---|---|---|
| **13c** | synclinal | 86.12 | - | 1.333 | 1.236 | 360.00 |
| **13d** | synclinal | 75.15 | –75.15 | 1.340 | 1.197 | 359.41 |
| **13e** | anticlinal | 102.41 | –102.41 | 1.328 | 1.256 | 359.64 |
| **13f** | antiperiplanar | $168.50^{exo}$<br>$152.21^{endo}$ | $-168.50^{exo}$<br>$-152.21^{endo}$ | $1.338^{exo}$<br>$1.369^{endo}$ | $1.236^{exo}$<br>$1.242^{endo}$ | $359.74^{exo}$<br>$359.99^{endo}$ |
| **13g** | antiperiplanar | 164.62 | –164.62 | 1.333 | 1.231 | 359.21 |
| **14a** | - | - | - | 1.333 | 1.258 | 360.00 |
| **14b** | synclinal | 73.57 | –73.57 | 1.342 | 1.258 | 360.00 |

[a] $\phi_1$ – torsion angle for a molecule with (+) conformation.

[b] $\phi_2$ – torsion angle for the inversion equivalent of the molecule in a centrosymmetric crystal (with (–) conformation).

[c] in the case of *endo* form, the torsion angle is measured along bonds C(6)-N(11')-C(12')-C(13') (Fig. 12).

Compound **13c** crystallized spontaneously into a non-centrosymmetric chiral crystal (Fig. 11 a-1) with space group *P*1[64] (Flack parameter close to zero) although compound **13c** is achiral and sidechain was expected to be conformationally flexible. According to the X-ray data analysis (Table 4), compound **13c** crystal contains only (+) synclinal conformers (Fig. 11 a-2). Screening of ten single crystals (**13c**) showed that the chirality of four of them corresponds to that of the crystal structure. For six single crystals, the crystal structure was inverted. Thus, compound **13c** represents a racemic conglomerate.[65,66] Other obtained derivatives (**13d-g** and **14b**) crystallized with the formation of centrosymmetric, achiral crystals. From a crystallography point of view, such structures can be interpreted as a single rotamer (one of a set of conformers arising from the restricted rotation about a single bond[67]) accompanied by its inverse equivalent (e.g., compounds **14b** and **13g** in Fig. 11 b-2, c-2).

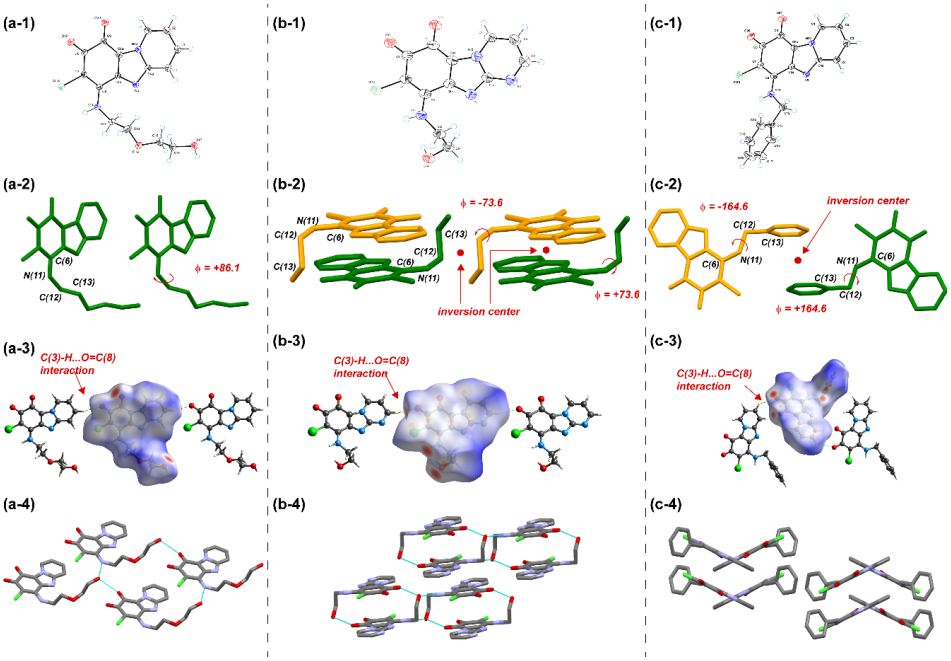


Fig. 11. Crystal structures of (a) compound **13c,** (b) compound **14b**, and (c) compound **13g** were chosen as representatives of the (1) ORTEP diagrams of the asymmetric unit for compounds showing thermal ellipsoids at the 50 % probability level (2) torsion angles of (+)-conformer (colored in green) and (–)-conformer (colored in orange) (for the sake of clarity, all hydrogen atoms were omitted) (3) top view of Hirshfeld surfaces and 1D molecular chains with C(8)=O…H-C(3) contacts (4) crystal packing (H-bonds shown in light blue color).

Centrosymmetric crystals of compounds **13d** and **14b** acquire both (+) and (−) synclinal (30°−90°) conformations while molecules of compound **13e** – (+) and (−) anticlinal (90°−150°), and molecules of compounds **13f,g** – (+) and (−) antiperiplanar (150°−180°) conformations due to torsional differences at C(6)-N(11)-C(12)-C(13) fragment (Table 4).

Strong to moderate[68] C(8)=O…H-C(3) H-bond led to the formation of 1D molecular chains in the crystal structures of compounds **13c-g** and **14a,b**. According to Kikkawa, S., et al.,[69] classification compounds could be divided into two groups along 1D chains: a straight pattern ([(+) or (−)] single conformer chains formed by H-bonds) for compounds **13c-d,f** and **14b** (Fig. 11 a-3, b-3) and a zig-zag pattern (chains that are formed through H-bonds and consisted of (+)- and (−)-conformers alternately associated with a glide) for compounds **13e** and **13g** (Fig. 11 c-3).

After the reaction of compound **1a** with racemic reagent **12f**, crystals of compound **13f** were isolated, where two molecular forms of each enantiomer were found in crystals: *exo* and *endo* (Fig. 12). In the crystal, the main *exo* form occupies 80 %, while the *endo* form occupies 20 % despite the presence of intramolecular H-bond of N(11)H…N(5) type, which can be explained by the elongation of C(6)-N(11) bond (Table 4) in order to form intramolecular H-bond.

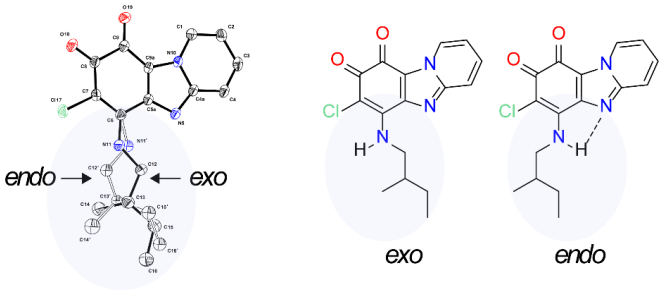


Fig. 12. ORTEP diagram of compound **13f** showing *exo* and *endo* forms.

Noting the presence of the -NH-$CH_2$- fragment in the structure (which determines the *exo*/*endo* forms of compound **13f** in the crystal), it was worth investigating the presence of different forms in the solution. In further structure studies, the obtained compounds were analyzed by the $^1$H NMR spectroscopy method. Despite the variety of introduced substituents, $^1$H NMR spectra of compounds **13b-g** and **14b** in DMSO-$d_6$ solutions showed two features corresponding to the -NH-α$CH_2$- (*i.e.*, -N(11)H-C(12)$H_2$-) fragment: NH proton signals were observed in 7.99–8.72 ppm range and protons of α$CH_2$ appeared as broad downfield signals (Fig. 13). The broadening of α$CH_2$ signal is not affected by the rest of the sidechain since compounds **13b-e** and **14b** have -NH-α$CH_2$-$\underline{CH_2}$ fragment and signals of $\underline{CH_2}$ group had clear multiplicity. Resonance signals of diastereotopic protons of α$CH_2$ group of compound **13f** (contains branched aminoalkyl substituent at C(6) position with diastereotopic $CH_2$ group attached to N(11)H) were identified in $^1$H NMR spectrum using 2D $^1$H-$^1$H COSY and $^1$H-$^{13}$C HSQC NMR spectra.

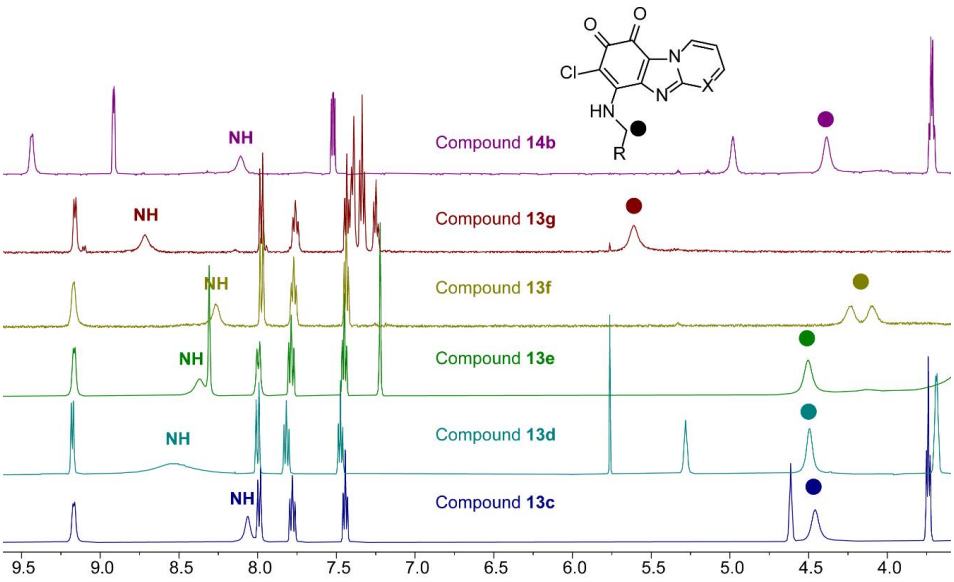


Fig. 13. $^1$H NMR (500 MHz, DMSO-$d_6$) spectra of compounds **13c-g**, **14b**; signals of $\alpha CH_2$ protons are marked with circles.

Since chemical shifts of NH and $\alpha CH_2$ protons can be sensitive to the solvent, compounds **13f-g** were chosen for the investigation of solute-solvent interactions using solvents with different polarity and H-bond basicity.[70] Signal of NH proton showed solvent-dependent chemical shift, which correlated well with $\beta_1$ value (H-bond basicity)[70] of the solvents used (Table 5). The downfield shift of NH signals in DMSO-$d_6$ relative to those in MeCN-$d_3$ and $CDCl_3$ for compounds **13f-g** can be explained by the formation of the solute-solvent complexes.[71]

It was observed that protons of the $\alpha CH_2$ group appeared as broad signals for compounds **13f-g** in MeCN-$d_3$ and $CDCl_3$ solutions as well (Table 5). In $^1$H NMR spectra of compound **13f** in $CDCl_3$ solution signals of *exo* and *endo* forms were found; *exo* : *endo* ratio (70 : 30) was close to the ratio observed in the crystal structure (80:20), but in DMSO-$d_6$ and MeCN-$d_3$ solutions at room temperature (298 K) signals of *endo* form were not detected. It was supposed that *exo* form of compound **13f** was stabilized by the formation of solute-solvent complexes in DMSO, and weak non-covalent interactions compete with *endo* form stabilization by intramolecular H-bond. Interestingly, in all three solvents, compound **13g** showed no separate signals of *endo* form in $^1$H NMR spectra (298 K).

The existence of *exo*/*endo* forms of compound **13f** in the solid state prompted us to examine the behavior of compounds **13f-g** (soluble in MeCN-$d_3$) in solution using variable temperature (VT) $^1$H NMR spectroscopy experiments (Fig. 14). $^1$H NMR spectra (248–253 K) showed narrowing and splitting of all broad signals (NH, $\alpha CH_2$ group and C(1)-H protons). The existence of two forms was proved by the appearance of an additional set of signals of low intensity that corresponded to the *endo* form.

Table 5

Chemical shifts (δ) of compounds **13f-g** in $^1$H NMR spectra using solvents with different hydrogen-bond basicity parameters

| Cmpd. | Solvent | H-bond basicity of solvents ($\beta_1$)[70] | Chemical shifts (δ), ppm | |
|---|---|---|---|---|
| | | | N<u>*H*</u> | HN-αC<u>*H*</u>$_2$ |
| **13f** | $CDCl_3$ | 0 | 6.24$^{exo}$<br>6.79$^{endo}$ | 4.09, 4.28$^{exo}$<br>3.74, 3.92$^{endo}$ |
| | MeCN-$d_3$ | 0.37 | 6.96 | 4.33, 4.13 |
| | DMSO-$d_6$ | 0.71 | 8.26 | 4.10, 4.23 |
| **13g** | $CDCl_3$ | 0 | 6.34 | 5.50 |
| | MeCN-$d_3$ | 0.37 | ~7.30 | 5.63 |
| | DMSO-$d_6$ | 0.71 | 8.72 | 5.69 |

For compound **13g**, both forms were observed in MeCN solution at lower temperatures (*exo*:*endo* form ratio 85:15) although only the *exo* form was found in solid state (Fig. 14 b). At 253 K αCH$_2$, protons of *exo* form showed a doublet ($J$ = 7.1 Hz) at 5.61 ppm accompanied by low-intensity doublet ($J$ = 7.2 Hz) of *endo* form at 5.17 ppm.

For compound **13f**, the observed *exo:endo* forms ratio (248 K, MeCN-$d_3$ solution) was similar (85:15) and is in good agreement with *exo:endo* ratio in the solid state (Fig. 14 a). Diastereotopic protons of *endo* form (αCH$_2$) were shifted upfield (shielded) relative to the signals of *exo* form and showed clearly identifiable signals at 3.67 ppm and 3.86 ppm (same multiplicities as *exo* αCH$_2$). Similarly, the signal of the C(1)-H proton of the heterocycle splits into two signals. Additionally, the low-intensity signal of the intramolecularly H-bonded NH group of *endo* form appeared at 7.41 ppm, while the NH group of *exo* form was observed at 7.17 ppm. Generally, signals of NH proton involved in intermolecular H-bonding are more temperature dependent than signals of intramolecularly bonded NH group (stronger interaction than intermolecular H-bonding[72]). The chemical shift of NH proton (*exo* form) in the MeCN-$d_3$ solution correlated linearly with temperature (248–333 K, $R^2$ = 0.97).

For compound **13f** VT $^1$H NMR spectra were also recorded in DMSO-$d_6$ solution upon heating up to 393 K. It can be supposed that only monomer *exo* form was found since H-bonds are weakened at elevated temperatures. Linear correlation was found between the chemical shift of NH proton (*exo* form) and the temperature for solutions in DMSO-$d_6$ (298–393 K, $R^2$ = 0.99).

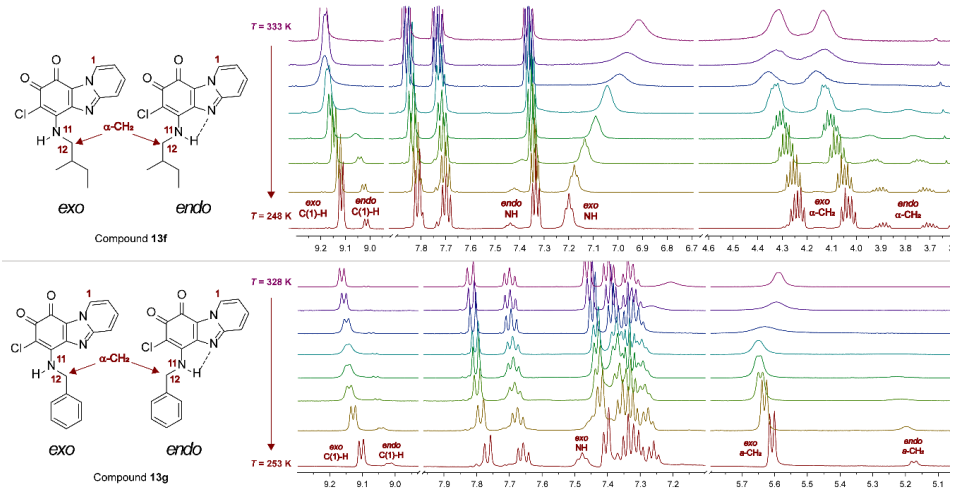


Fig. 14. Fragments of VT $^1$H NMR spectrum (500 MHz, MeCN-$d_3$) (a) of compound **13f** in the temperature range of 248–333 K; (b) of compound **13g** in the temperature range of 253–328 K.

To summarize, after the reaction of 6,7-dichloropyrido[1,2-*a*]benzimidazol-8,9-dione (or its analog) with primary amines, derivatives obtained have a merocyanine-type structure in the fragment O=C(8)-C(7)-C(6)-N(11)H. The carbon-nitrogen bond that connects the heterocyclic quinone and the substituent has a partial double bond character. Proton-donating groups attached to a flexible sidechain, as well as electronic effects of the substituent, led to different types of intermolecular interactions (several H-bonds and interlayer π-π interactions) which could be observed in the crystal packing of the obtained derivatives. Centrosymmetric crystals were mostly obtained, however, one of the derivatives formed a chiral crystal without an inversion equivalent.

Among this set of derivatives, the form without an intramolecular hydrogen bond (*exo* form) predominates in solid state and in solution. The presence of the second form (with an intramolecular H-bond, *endo* form) explains the observed broadening of the signal of the $CH_2$ group (adjacent to NH) in $^1$H NMR spectra in solution at room temperature. The chemical shift of the NH proton signal correlates with both the H-bond basicity of the solvent and temperature.

The scientific publication of the research described in this chapter can be found in Appendix 2.

## 2.2. Benzohydrazides as *N*-nucleophiles

Quinone derivatives **16a-f** were obtained by nucleophilic substitution of quinones **1a,c** by benzohydrazides **15a-c** in the presence of $Et_3N$ (Scheme 4). Interestingly, when quinones **1** reacted with amines, deep-blue colored crystals of 6-amino-substituted products were

obtained, but in the case of compounds **16a-f**, red-orange-colored solids were isolated. It is known that several tautomeric structures are possible for the quinone derivatives containing aroyl- or acyl hydrazide fragment attached to the quinone core.[73,74] To establish the exact form of quinone, core crystals of compound **16a** were grown from DCM solution for single-crystal X-ray crystallography analysis since the tautomeric form of the obtained compounds was still under consideration after routine identification procedures (e.g., $^1$H-NMR and FTIR).

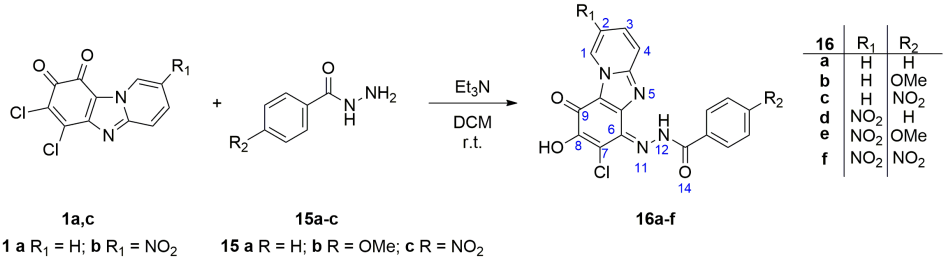


Scheme 4. Synthesis of compounds **16a-f.**

After the inspection of the bond length, an α-hydroxy-*p*-quinone imine form was confirmed. Figure 15 a shows a perspective view of molecule **16a** with thermal ellipsoids and the atom-numbering scheme. Two intramolecular hydrogen bonds were found in the structure of compound **16a**: N(12)H···N(5) and O(22)-H···O(23) (Fig. 15 a). Moreover, hydroxy group O(22)-H forms bifurcated H-bonds, and centrosymmetric $R_2^2(10)$ molecular dimer was formed with the second molecule of the compound through intermolecular bond O(22)-H···O'(23) (Fig. 15 b). Additionally, stacking of the dimers along the crystallographic *a*-axis (Fig. 15 c), as well as a short intermolecular contact between heterocycle (C(3)-H) and the amide group of the substituent, were found.

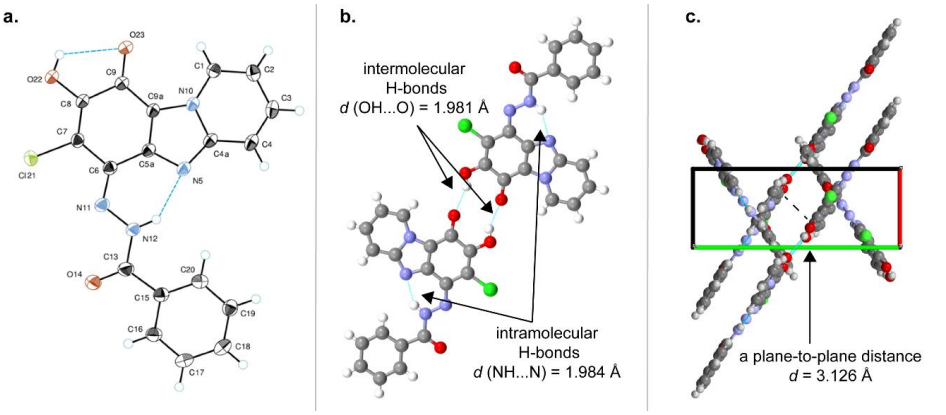


Fig. 15. **a** – ORTEP diagram of compound **16a** showing thermal ellipsoids at the 50 % probability level. **b** – The centrosymmetric $R_2^2(10)$ molecular dimer in the crystal structure of compound **16a**. **c** – Crystal packing of compound **16a** along *a*-axis.

In $^1$H NMR spectra of the obtained compounds **16a-f** in DMSO-$d_6$ solution, a set of two broad signals corresponding to NH (at 14.36–14.90 ppm) and OH (at 10.95–11.41 ppm) protons was observed. It can be concluded that intramolecular bond N(12)-H···N(5) found in solid state persists in solution as well since the position of the NH proton of compound **16a** was not affected by the solvent ($\delta_{NH}$ = 14.71 ppm (DMSO-$d_6$); $\delta_{NH}$ = 14.68 ppm ($CDCl_3$ – a solvent in which H-bonding interactions are expected to be weaker[75]). However, for a signal of OH proton, a distinguishable shift was observed, changing the DMSO-$d_6$ solution (10.99 ppm) to $CDCl_3$ solution (7.20 ppm). It is known that in the case of α-hydroxy-*p*-naphthoquinone derivatives, an intramolecularly H-bonded OH proton signal appears at 7.30 ppm in $CDCl_3$ solution.[76] A downfield shift in a solvent (DMSO-$d_6$) with H-bond acceptor abilities[77] indicates the formation of additional intermolecular interactions. In addition, to establish the effect of different substituents ($R_1$ and $R_2$), chemical shifts of OH and NH signals ($\delta_{OH}$ and $\delta_{NH}$, respectively) in $^1$H NMR spectra (DMSO-$d_6$) of compounds **16a-f** were analyzed. The Hammett constants ($\sigma_p$) were taken as the characteristic of the substituents.[78] As a result, linear correlations ($R^2$ = 0.99) were found between the Hammett substituent constants ($R_2$, substituent at the phenyl ring) and $\delta_{OH}$ (Fig. 16) for compounds **16a-c** (variable $R_2$ while $R_1$ = H) and **16d-f** (variable $R_2$ while $R_1$ = $NO_2$). The presence of the nitro group in the heterocyclic fragment ($R_1$ = $NO_2$) caused a downfield shift of OH signal compared to compounds without a substituent ($R_1$ = H) at the heterocycle ($\Delta\delta_{OH} \approx 0.3$ ppm). However, the presence of the nitro group in the heterocyclic ring ($R_1$ = $NO_2$) resulted in an upfield shift of NH signal ($\Delta\delta_{NH} \approx 0.3$ ppm) compared to molecules with a hydrogen atom at the same position ($R_1$ = H). The variation of the electronic character of the substituent in the *para*-position of the phenyl ring (Fig. 16) led to the downfield shift of the NH signal going from electron-donating to electron withdrawing group. It is known,[79] that the NH proton signal is more shifted downfield when the intramolecular H-bond is stronger. Thus, the electron-withdrawing group of the phenyl ring ($R_2$ = $NO_2$) increases the acidity of the NH proton and the strength of the intramolecular H-bond, while the electron-withdrawing group at the heterocyclic fragment ($R_1$ = $NO_2$) affects the electron density at N(5), which also modulates the intramolecular H-bond.

In general, compounds **16a-f** could be described as a structural analog of aroyl hydrazones.[74] Hydrazone derivatives activated by chemical inputs and/or light irradiation are known to undergo *E*/*Z* isomerization in solution.[80,81] In this work, no signals of isomerization products were observed in $^1$H NMR spectra of DMSO-$d_6$ or $CDCl_3$ solutions of compound **16a** as well as no configurational switching was observed for compound **16b** (DMSO-$d_6$) after the addition of the excess of TFA and following irradiation (365 nm). In the case of compounds **16a-f**, the presence of strong intramolecular H-bond N(12)-H···N(5) can explain the existence of a single configuration.

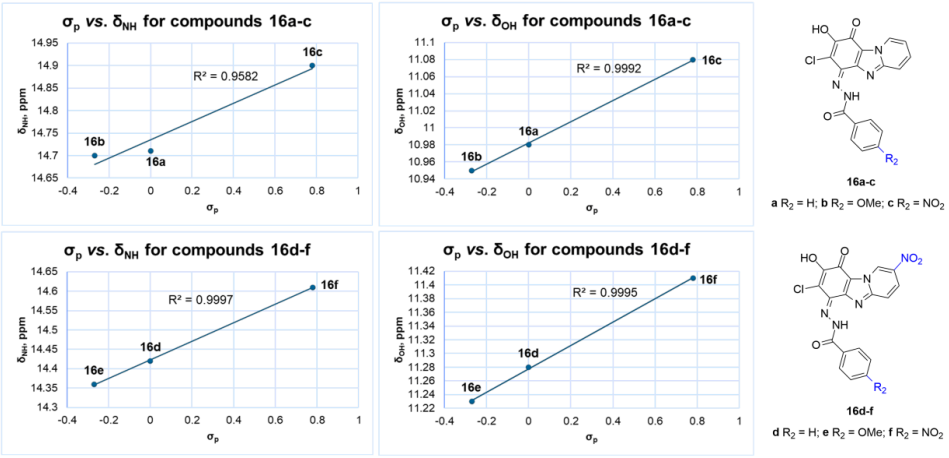


Fig. 16. Structures of compounds **16a-f** and correlations between the Hammett constant of $R_2$ substituent ($\sigma_p$) and the chemical shifts of NH proton ($\delta_{NH}$) or OH proton ($\delta_{OH}$) in $^1$H NMR spectra (DMSO-$d_6$) of compounds **16a-f**.

The structure of compounds **16a-f** contains two acidic protons, as seen from their $^1$H NMR spectra. To explore possible protonation/deprotonation of the obtained compounds, $^1$H NMR titration experiment was carried out using compound **16b** as a representative. The deprotonation was investigated upon sequential addition of the base (DBU). As soon as 0.15 equivalents of the base were added to the DMSO-$d_6$ solution of compound **16b**, a broad signal of OH proton completely disappeared, and the yellow-colored solution immediately became dark blue (Fig. 17, highlighted in red). It was supposed that deprotonated compound **16b** formed a hydrogen-bonded complex with protonated DBU. At the same time, a signal of $DBUH^+$ appeared at 9.58 ppm (Fig. 17, highlighted in blue). Upon further addition of the base, the signal of the NH proton (amide fragment) sharpens and undergoes an upfield shift from 14.70 ppm to 14.51 ppm (Fig. 17, highlighted in yellow). The addition of the excess of DBU caused the appearance of a second minor form of the compound (Fig. 17, highlighted in green) (ratio major/minor proton signal was found 0.95: 0.05). Noteworthy, a similar process was detected in the case of compounds **16a** and **16c** after interaction with excess of DBU. The reversibility of the acid-base equilibrium was proved by the sequential addition of TFA (excess): the signal of OH proton was restored (as well as the yellow color of the solution), and signals of the minor form disappeared.

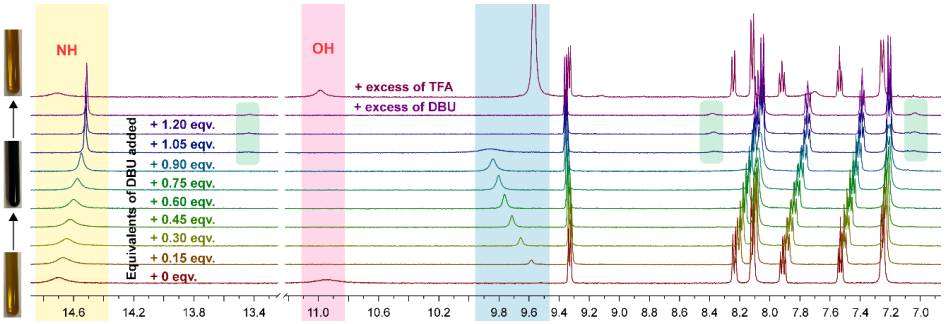


Fig. 17. $^1$H NMR acid-base titration of compound **16b** in DMSO-$d_6$ solution (upon sequential addition of base (DBU) and acid (TFA)).

The UV-Vis absorption spectra of compound **16a** were studied in DCM and DMSO solutions and two absorption maximums at 381 nm and at 446–449 nm were found in both solutions. When a base (DBU) was added to a solution of compound **16a**, the absorption band *ca*. 450 nm disappeared and, simultaneously, a new band appeared at 556 nm in DCM and at 607 nm in DMSO. The effect of substituents ($R_1$ and $R_2$) on the longwave absorption band was examined by the addition of DBU to the $CHCl_3$ solution of compounds **16a-c** (variable $R_2$ while $R_1$ = H) and **16d-f** (variable $R_2$ but $R_1$ = $NO_2$) (Table 6). A bathochromic shift was observed for the $\lambda_{max}$ of the deprotonated derivatives **16d–f** compared to deprotonated compounds **16a–c** (Table 6). In addition, the hyperchromic effect was caused by the introduction of the nitro group into the benzamide fragment ($R_2$).

Table 6

UV-Vis data of compounds **16a-f** in the presence of DBU ($CHCl_3$)

| Compound | **16a** | **16b** | **16c** | **16d** | **16e** | **16f** |
|---|---|---|---|---|---|---|
| $\lambda_{max}$ (lg ε) | 365 (4.40)<br>380 (4.41)<br>**556** (3.87) | 368 (4.45)<br>382 (4.48)<br>**551** (3.89) | 377 (4.40)<br>**563** (3.91) | 371 (4.24)<br>**575** (3.73) | 365 (4.28)<br>**569** (3.76) | 361 (4.30)<br>**578** (3.86) |

In general, *p*-quinone imines are redox-active molecules that are known to undergo a redox cycle through aminophenols.[82] It was reported[83] that converting *o*-quinone into its *p*-quinone imine analogue changes the entire redox system and this transformation can be observed electrochemically. A combination of redox-active quinone and imine groups has shown promising results for electrical energy storage materials.[84] Redox properties of *o*-quinone **1a** (electrochemically active compound in MeCN solution[85]) and quinone imine **16a** were analyzed for potential application in aqueous electrolyte batteries as electrode material.

First, the solubility of compounds **1a** and **16a** in aqueous media was tested; compound **16a** was insoluble in neutral and acidic environments while compound **1a** was insoluble in aqueous solutions of the whole pH range. Then cathode materials **CM-1a** or **CM-16a** were prepared by the combination of quinone derivatives **1a** or **16a** with *Vulcan XC72 CB* (substrate) and a binder solution of PVDF/DMF. Figure 18 shows the results of CV

measurements at varying scanning speeds for samples **CM-1a** and **CM-16a** and a sample without active material (substrate) in neutral and acidic electrolytes.

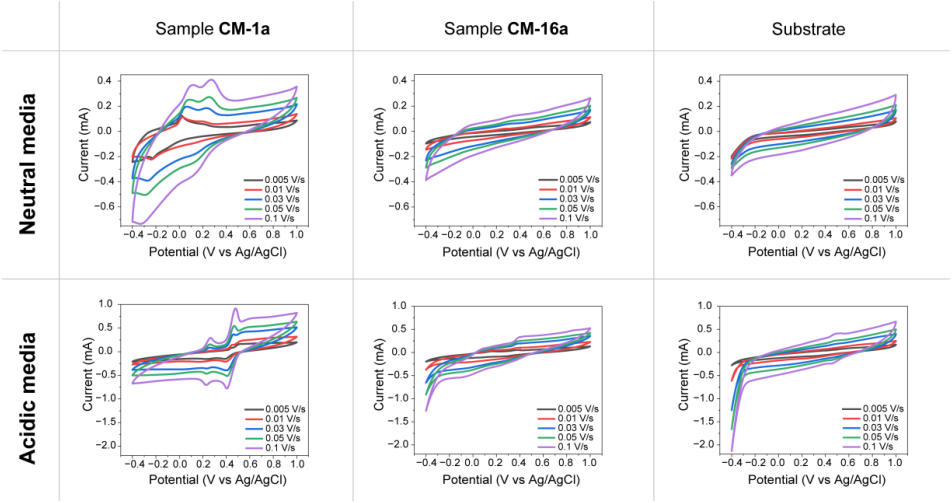


Fig. 18. CV results at varying scanning speeds for samples **CM-1a**, **CM-16a** and substrate in neutral (0.5 M $K_2SO_4$) electrolyte and in acidic (0.5 M $H_2SO_4$) electrolyte.

Sample **CM-1a** has distinct two redox maxima (corresponding to the *o*-quinone fragment in the molecule) in the scanned potential window in both neutral and acidic electrolytes. By increasing $H^+$ ion concentration a shift in reaction potential to more positive values was observed. Moreover, in the acidic environment, both peaks are stable (the potential difference is only up to 0.2 V), while in a neutral environment, only one of them is stable and remains unchanged after several CV cycles. However, for sample **CM-16a** in a neutral electrolyte, no significant redox processes can be observed. In the case of acidic electrolyte, upon closer inspection, two reversible oxidation peaks can be seen. It can be concluded that by converting *o*-quinone **1a** to α-hydroxy-*p*-quinone imine **16a** the electrochemical activity as cathode material has been greatly suppressed.

Raman spectra of pure compounds (**1a**, **16a**) as well as prepared cathodes (**CM-1a**, **CM-16a)** before and after electrochemical cycling in acidic and neutral electrolytes were received (Fig. 19 a). The obtained results showed that spectra for the prepared and cycled cathode sample **CM-1a** in acidic electrolyte remain as an initial spectrum of pure compound **1a**. However, only C and D bands of carbon[86,87] can be seen in the spectrum if sample **CM-1a** is cycled in neutral electrolyte. It can be concluded that the active material was dissolved from the electrode and gone through the electrochemical reactions from the solution since CV measurements showed redox processes for this sample (Fig. 18). On the other hand, compound **16a** was preserved in the cathode before and after CV and did not go through any chemical changes, as seen from unchanged Raman spectra for prepared and cycled samples **CM-16a**.

Obtained data from scanning electron microscopy (SEM) (Fig. 19 b) supports findings from Raman spectroscopy that the active compound **1a** dissolves from the sample **CM-1a** in electrolytes and goes through electrochemical reactions from the solution. Only a part of the original morphologies can be seen after the sample **CM-1a** was cycled. For sample **CM-16a**, structures of active material can be found in images after CV in neutral electrolyte and in acidic electrolyte with some partial dissolution. The greater stability of **CM-16a** in comparison to **CM-1a** can be explained by the formation of non-covalent interactions between compound **16a** and substrate.

To summarize, α-hydroxy-*p*-quinonimine derivatives were formed after reactions of 6,7-dichloropyrido[1,2-*a*]benzimidazole-8,9-dione with benzohydrazides. A single imine bond configuration was found, which is stabilized by an intramolecular H-bond. However, the obtained compounds are prone to deprotonation and interaction with basic solvents due to the acidic OH proton. Knowing that solvents with basic properties (e.g., *N*-methyl-2-pyrrolidone) are usually used to prepare the electrode material, the stability of the compound under such conditions should be analyzed before the material is prepared. It was concluded that cathode material based on 6,7-dichloropyrido[1,2-*a*]benzimidazole-8,9-dione (**CM-1a)** could act as a potential effective active electrode in aqueous electrolyte batteries if the dissolution of the sample is inhibited, for example, by the attachment to the polymer backbone.

The scientific publication of the research described in this chapter can be found in Appendix 3.

To expand the range of the investigated cathode materials, samples of cathode material **CM-7H**, **CM-10**, and **CM-Q-NH2** were prepared from compounds **7H**, **10**, and 6-amino-7-chloropyrido[1,2-*a*]benzimidazole-8,9-dione, respectively (see Appendix 6). The redox properties of obtained samples were tested by CV measurements in an acidic electrolyte and SEM images were obtained before and after cycling. The initial CV measurements of the sample **CM-7H** revealed multiple redox waves, suggesting the presence of different forms of compound **7H** (possibly due to the known keto/enol tautomeric equilibrium of compound **7H** in the polar DMF solvent that was used during preparation of the material).

While compound **10** and its derivatives **10a–d** exhibit redox activity in MeCN solution (Fig. 10, Table 3), the cathode material prepared from compound **10** exhibited different electrochemical behavior in the acidic electrolyte, as seen from the CV measurements. SEM images revealed partial dissolution of the active material from samples **CM-7H** and **CM-10** after cycling. However, sample **CM-Q-NH2** displayed promising battery-like behavior with relatively high current and good stability during electrochemical cycling.

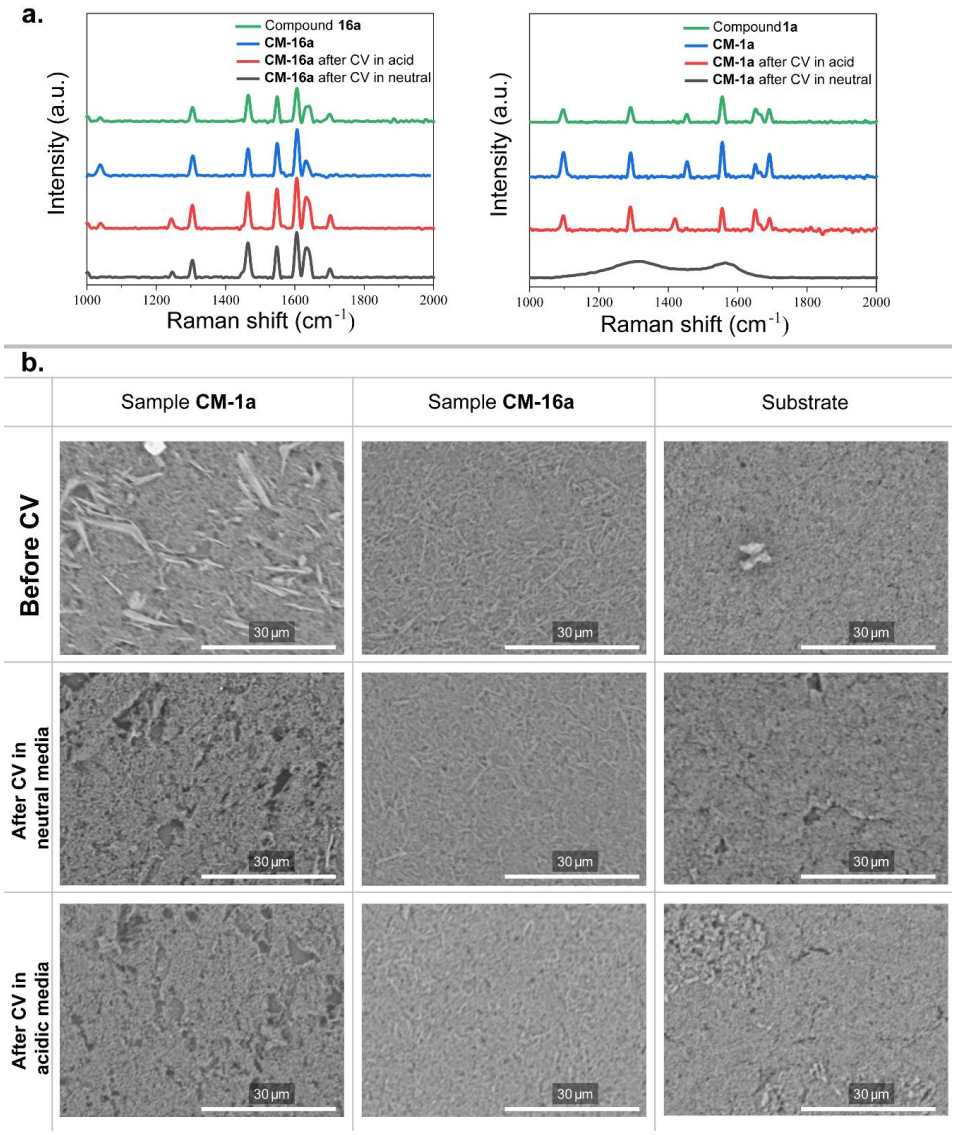


Fig. 19. a – Raman spectra of pure compounds **1a** and **16a** (green line), prepared cathodes (**CM-1a** and **CM-16a**) before (blue line) and after cycling in acidic (red line) and neutral (grey line) electrolytes. b – Scanning electron microscopy images of prepared cathode surfaces **CM-1a**, **CM-16a** and substrate (coating without active material) before and after CV measurements in neutral and acidic electrolytes (magnification of ×2500).

# CONCLUSIONS

1. Structural studies showed that in the reaction of 6,7-dichloropyrido[1,2-*a*]benzimidazol-8,9-dione and its analogs with nucleophiles the obtained compounds can exist in different forms: *o*-quinone (*C*-nucleophile – indane derivative or barbituric acid) or α-hydroxy-*p*-quinone imine (*N*-nucleophile – benzohydrazide derivative), as well as polymethine (*C*-nucleophile – malononitrile) or merocyanine (*N*-nucleophile – primary amine) type structures can also be formed.

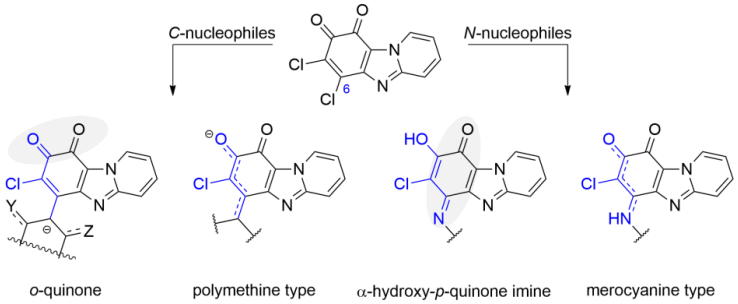


2. The analysis of UV-Vis spectroscopy data revealed that the spectroscopic properties of the obtained 7-chloropyrido[1,2-*a*]benzimidazole-8,9-dione derivatives in solution are affected by the substituent type, delocalization of negative charge, and molecular planarity. Introducing a bulky substituent fragment derived from functionalized indane disrupts the molecule's planarity, leading to positive (**7**) or negative (**8, 9**) solvatochromism. In the case when heterocyclic quinone and substituent fragments are coplanar (**10**), the solvatochromic behavior was not observed.

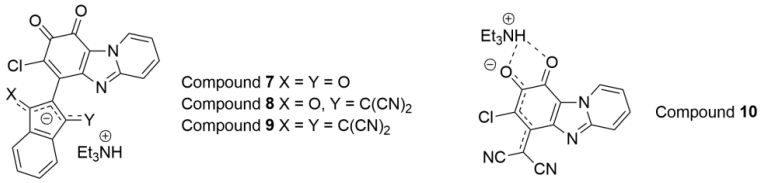


3. On the base of 7-chloropyrido[1,2-*a*]benzimidazole-8,9-dione core containing -NH-$CH_2$- fragment at C(6) position merocyanine-type structure is formed. In the case of these derivatives, a form without intramolecular H-bond (*exo* form) dominates in solid state and in solution. The presence of minor *endo* form (with intramolecular H-bond) explains the observed broadening of the $CH_2$ group signal (adjacent to NH) in $^1$H NMR spectra in solution at room temperature.

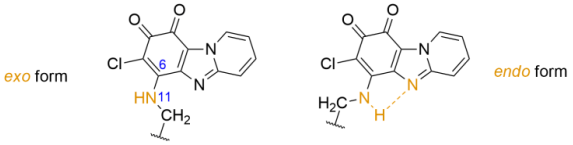

4. The study revealed that an intramolecular H-bond between an introduced substituent and nitrogen atom of a heterocycle (N(12)H…N(5)) stabilizes a single configuration of C(6)=N(11) bond of α-hydroxy-*p*-quinone imine derivative in solid state and in solution.

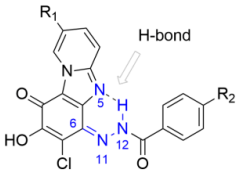


5. Material based on 6,7-dichloropyrido[1,2-*a*]benzimidazole-8,9-dione derivatives could act as a potential effective active cathode in aqueous electrolyte batteries.
6. The 7-chloropyrido[1,2-*a*]benzimidazole-8,9-dione core can serve as a multifunctional platform for obtaining compounds with valuable properties for material design and development.

# ATSAUCES/REFERENCES


(1) Bolton, J. L.; Dunlap, T. Formation and Biological Targets of Quinones: Cytotoxic versus Cytoprotective Effects. *Chem. Res. Toxicol.* **2017**, *30* (1), 13–37. https://doi.org/10.1021/acs.chemrestox.6b00256.

(2) Anand, A.; Chen, K.; Yang, L.; Sastry, A. V.; Olson, C. A.; Poudel, S.; Seif, Y.; Hefner, Y.; Phaneuf, P. V.; Xu, S.; Szubin, R.; Feist, A. M.; Palsson, B. O. Adaptive Evolution Reveals a Tradeoff between Growth Rate and Oxidative Stress during Naphthoquinone-Based Aerobic Respiration. *Proc. Natl. Acad. Sci.* **2019**, *116* (50), 25287–25292. https://doi.org/10.1073/pnas.1909987116.

(3) Cao, P.; Bracun, L.; Yamagata, A.; Christianson, B. M.; Negami, T.; Zou, B.; Terada, T.; Canniffe, D. P.; Shirouzu, M.; Li, M.; Liu, L. N. Structural Basis for the Assembly and Quinone Transport Mechanisms of the Dimeric Photosynthetic RC–LH1 Supercomplex. *Nat. Commun.* **2022**, *13* (1), 1–12. https://doi.org/10.1038/s41467-022-29563-3.

(4) Ernster, L.; Dallner, G. Biochemical, Physiological and Medical Aspects of Ubiquinone Function. *Biochim. Biophys. Acta - Mol. Basis Dis.* **1995**, *1271* (1), 195–204. https://doi.org/10.1016/0925-4439(95)00028-3.

(5) Calderon, P.; Cadrobbi, J.; Marques, C.; Hong-Ngoc, N.; Jamison, J.; Gilloteaux, J.; Summers, J.; Taper, H. Potential Therapeutic Application of the Association of Vitamins C and K3 in Cancer Treatment. *Curr. Med. Chem.* **2002**, *9* (24), 2271–2285. https://doi.org/10.2174/0929867023368674.

(6) Vos, M.; Esposito, G.; Edirisinghe, J. N.; Vilain, S.; Haddad, D. M.; Slabbaert, J. R.; Van Meensel, S.; Schaap, O.; De Strooper, B.; Meganathan, R.; Morais, V. A.; Verstreken, P. Vitamin K 2 Is a Mitochondrial Electron Carrier That Rescues Pink1 Deficiency. *Science (80-. ).* **2012**, *336* (6086), 1306–1310. https://doi.org/10.1126/science.1218632.

(7) Wellington, K. W. Understanding Cancer and the Anticancer Activities of Naphthoquinones – a Review. *RSC Adv.* **2015**, *5* (26), 20309–20338. https://doi.org/10.1039/C4RA13547D.

(8) Son, E. J.; Kim, J. H.; Kim, K.; Park, C. B. Quinone and Its Derivatives for Energy Harvesting and Storage Materials. *J. Mater. Chem. A* **2016**, *4* (29), 11179–11202. https://doi.org/10.1039/c6ta03123d.

(9) Simon, P.; Gogotsi, Y. Perspectives for Electrochemical Capacitors and Related Devices. *Nat. Mater.* **2020**, *19* (11), 1151–1163. https://doi.org/10.1038/s41563-020-0747-z.

(10) Mansha, M.; Anam, A.; Akram Khan, S.; Saeed Alzahrani, A.; Khan, M.; Ahmad, A.; Arshad, M.; Ali, S. Recent Developments on Electroactive Organic Electrolytes for Non-Aqueous Redox Flow Batteries: Current Status, Challenges, and Prospects. *Chem. Rec.* **2024**, *24* (1). https://doi.org/10.1002/tcr.202300233.

(11) Go, C. Y.; Shin, J.; Choi, M. K.; Jung, I. H.; Kim, K. C. Switchable Design of Redox-Enhanced Nonaromatic Quinones Enabled by Conjugation Recovery. *Adv. Mater.* **2023**. https://doi.org/10.1002/adma.202311155.

(12) Shea, J. J.; Luo, C. Organic Electrode Materials for Metal Ion Batteries. *ACS Appl. Mater. Interfaces* **2020**, *12* (5), 5361–5380. https://doi.org/10.1021/acsami.9b20384.

(13) Fornari, R. P.; Mesta, M.; Hjelm, J.; Vegge, T.; De Silva, P. Molecular Engineering Strategies for Symmetric Aqueous Organic Redox Flow Batteries. *ACS Mater. Lett.* **2020**, *2* (3), 239–246. https://doi.org/10.1021/acsmaterialslett.0c00028.

(14) Piera, J.; Bäckvall, J.-E. Catalytic Oxidation of Organic Substrates by Molecular Oxygen and Hydrogen Peroxide by Multistep Electron Transfer – A Biomimetic Approach. *Angew. Chemie Int. Ed.* **2008**, *47* (19), 3506–3523. https://doi.org/10.1002/anie.200700604.

(15) Salazar, C. A.; Flesch, K. N.; Haines, B. E.; Zhou, P. S.; Musaev, D. G.; Stahl, S. S. Tailored Quinones Support High-Turnover Pd Catalysts for Oxidative C–H Arylation with O 2. *Science (80-. ).* **2020**, *370* (6523), 1454–1460. https://doi.org/10.1126/science.abd1085.

(16) Tsao, Y.; Lee, M.; Miller, E. C.; Gao, G.; Park, J.; Chen, S.; Katsumata, T.; Tran, H.; Wang, L.-W.; Toney, M. F.; Cui, Y.; Bao, Z. Designing a Quinone-Based Redox Mediator to Facilitate Li2S Oxidation in Li-S Batteries. *Joule* **2019**, *3* (3), 872–884. https://doi.org/10.1016/j.joule.2018.12.018.

(17) Simeon, F.; Stern, M. C.; Diederichsen, K. M.; Liu, Y.; Herzog, H. J.; Hatton, T. A. Electrochemical and Molecular Assessment of Quinones as CO2-Binding Redox Molecules for Carbon Capture. *J. Phys. Chem. C* **2022**, *126* (3), 1389–1399. https://doi.org/10.1021/acs.jpcc.1c09415.

(18) Voskian, S.; Hatton, T. A. ELECTROCHEMICAL PROCESS FOR GAS SEPARATION. US 2017/0113182 A1, 2017.

(19) Wang, F.; Sheng, H.; Li, W.; Gerken, J. B.; Jin, S.; Stahl, S. S. Stable Tetrasubstituted Quinone Redox Reservoir for Enhancing Decoupled Hydrogen and Oxygen Evolution. *ACS Energy Lett.* **2021**, 1533–1539. https://doi.org/10.1021/acsenergylett.1c00236.

(20) Han, C.; Li, H.; Shi, R.; Zhang, T.; Tong, J.; Li, J.; Li, B. Organic Quinones towards Advanced Electrochemical Energy Storage: Recent Advances and Challenges. *J. Mater. Chem. A* **2019**, *7* (41), 23378–23415. https://doi.org/10.1039/c9ta05252f.

(21) Wu, Z.; Liu, Q.; Yang, P.; Chen, H.; Zhang, Q.; Li, S.; Tang, Y.; Zhang, S. Molecular and Morphological Engineering of Organic Electrode Materials for Electrochemical Energy Storage. *Electrochem. Energy Rev.* **2022**, *5* (s1), 1–67. https://doi.org/10.1007/s41918-022-00152-8.

(22) Hasan, F.; Mahanta, V.; Abdelazeez, A. A. Quinones for Aqueous Organic Redox Flow Battery: A Prospective on Redox Potential, Solubility, and Stability. *Adv. Mater. Interfaces* **2023**, *10* (24), 1–25. https://doi.org/10.1002/admi.202300268.

(23) Wang, C. Weak Intermolecular Interactions for Strengthening Organic Batteries. *Energy Environ. Mater.* **2020**, *3* (4), 441–452. https://doi.org/10.1002/eem2.12076.

(24) Brar, S. K.; Kumar, S.; Pandey, S. K.; Bhasin, K. K.; Wangoo, N.; Sharma, R. K. Fabrication of Self-Assembled Imidazo[1,2-a]Pyridine Based Materials: Understanding the Impact of Solvent and Chemical Modulation. *J. Mol. Liq.* **2018**, *254*, 208–215. https://doi.org/10.1016/j.molliq.2018.01.090.

(25) Langis-Barsetti, S.; Maris, T.; Wuest, J. D. Triptycene 1,2-Quinones and Quinols: Permeable Crystalline Redox-Active Molecular Solids. *J. Org. Chem.* **2018**, *83* (24), 15426–15437. https://doi.org/10.1021/acs.joc.8b02706.

(26) Sieuw, L.; Jouhara, A.; Quarez, É.; Auger, C.; Gohy, J.-F.; Poizot, P.; Vlad, A. A H-Bond Stabilized Quinone Electrode Material for Li–Organic Batteries: The Strength of Weak Bonds. *Chem. Sci.* **2019**, *10* (2), 418–426. https://doi.org/10.1039/C8SC02995D.

(27) Li, C.; Hu, L.; Ren, X.; Lin, L.; Zhan, C.; Weng, Q.; Sun, X. Asymmetric Charge Distribution of Active Centers in Small Molecule Quinone Cathode Boosts High-Energy and High-Rate Aqueous Zinc-Organic Batteries. **2024**, 2313241. https://doi.org/10.1002/adfm.202313241.

(28) Lin, Z.; Shi, H. Y.; Lin, L.; Yang, X.; Wu, W.; Sun, X. A High Capacity Small Molecule Quinone Cathode for Rechargeable Aqueous Zinc-Organic Batteries. *Nat. Commun.* **2021**, *12* (1), 1–9. https://doi.org/10.1038/s41467-021-24701-9.

(29) Jethwa, R. B.; Zhao, E. W.; Kerber, R. N.; Jónsson, E.; Wright, D. S.; Grey, C. P. Designing for Conjugate Addition: An Amine Functionalised Quinone Anolyte for Redox Flow Batteries. *J. Mater. Chem. A* **2021**, *9* (27), 15188–15198. https://doi.org/10.1039/d1ta02870g.

(30) Jethwa, R. B.; Hey, D.; Kerber, R. N.; Bond, A. D.; Wright, D. S.; Grey, C. P. Exploring the Landscape of Heterocyclic Quinones for Redox Flow Batteries. *ACS Appl. Energy Mater.* **2024**, *7* (2), 414–426. https://doi.org/10.1021/acsaem.3c02223.

(31) Gaile, A.; Batenko, N. Synthesis of Heterocyclic Ring-Fused Quinones (Microreview). *Chem. Heterocycl. Compd.* **2021**, *57* (11), 1076–1078. https://doi.org/10.1007/s10593-021-03027-w.

(32) Miroshnikov, M.; Divya, K. P.; Babu, G.; Meiyazhagan, A.; Reddy Arava, L. M.; Ajayan, P. M.; John, G. Power from Nature: Designing Green Battery Materials from Electroactive Quinone Derivatives and Organic Polymers. *J. Mater. Chem. A* **2016**, *4* (32), 12370–12386. https://doi.org/10.1039/c6ta03166h.

(33) Kwong, H. C.; Chidan Kumar, C. S.; Mah, S. H.; Mah, Y. L.; Chia, T. S.; Quah, C. K.; Lim, G. K.; Chandraju, S. Crystal Correlation Of Heterocyclic Imidazo[1,2-a]Pyridine Analogues and Their Anticholinesterase Potential Evaluation. *Sci. Rep.* **2019**, *9* (1), 1–15. https://doi.org/10.1038/s41598-018-37486-7.

(34) Anupriya; Thomas, K. R. J.; Nagar, M. R.; Shahnawaz; Jou, J.-H. Imidazo[1,2-a]Pyridine Based Deep-Blue Emitter: Effect of Donor on the Optoelectronic Properties. *J. Mater. Sci. Mater. Electron.* **2021**, *32* (22), 26838–26850. https://doi.org/10.1007/s10854-021-07060-5.

(35) Mathur, C.; Gupta, R.; Bansal, R. K.; Swami, S.; Sheoran, A.; Salunke, D. B. Preparation and Physicochemical Properties of Organic Semiconducting Materials from the Reaction of Imidazo[1,2-a]Pyridines with Tetracyanoethylene. *ChemistrySelect* **2023**, *8* (41). https://doi.org/10.1002/slct.202302954.

(36) Mutai, T.; Muramatsu, T.; Yoshikawa, I.; Houjou, H.; Ogura, M. Development of Imidazo[1,2- a ]Pyridine Derivatives with an Intramolecular Hydrogen-Bonded Seven-Membered Ring Exhibiting Bright ESIPT Luminescence in the Solid State.

*Org. Lett.* **2019**, *21* (7), 2143–2146. https://doi.org/10.1021/acs.orglett.9b00455.

(37) Stasyuk, A. J.; Cywiński, P. J.; Gryko, D. T. Excited-State Intramolecular Proton Transfer in 2′-(2′-Hydroxyphenyl)Imidazo[1,2-a]Pyridines. *J. Photochem. Photobiol. C Photochem. Rev.* **2016**, *28*, 116–137. https://doi.org/10.1016/j.jphotochemrev.2016.05.003.

(38) Batenko, N.; Belyakov, S.; Kiselovs, G.; Valters, R. Synthesis of 6,7-Dichloropyrido[1,2-a]Benzimidazole-8,9-Dione and Its Analogues and Their Reactions with Nucleophiles. *Tetrahedron Lett.* **2013**, *54* (35), 4697–4699. https://doi.org/10.1016/j.tetlet.2013.06.094.

(39) Zhu, X.; Akiyama, T.; Yokoyama, T.; Matsumoto, Y. Stereoselective Formation of β-O-4 Structures Mimicking Softwood Lignin Biosynthesis: Effects of Solvent and the Structures of Quinone Methide Lignin Models. *J. Agric. Food Chem.* **2019**, *67*, 6950–6961. https://doi.org/10.1021/acs.jafc.9b01968.

(40) Sugumaran, M. Unified Mechanism for Sclerotization of Insect Cuticle. *Adv. In Insect Phys.* **1998**, *27* (C), 229–334. https://doi.org/10.1016/S0065-2806(08)60014-4.

(41) Sugumaran, M. Reactivities of Quinone Methides versus O-Quinones in Catecholamine Metabolism and Eumelanin Biosynthesis. *Int. J. Mol. Sci.* **2016**, *17* (9), 1–23. https://doi.org/10.3390/ijms17091576.

(42) Land, E. J.; Ramsden, C. A.; Riley, P. A.; Yoganathan, G. 4-Cyanomethyl-Ortho-Quinone Tautomerism and the Structure of the Dienophile in Gates' Morphine Synthesis. *Tetrahedron* **2003**, *59* (48), 9547–9554. https://doi.org/10.1016/j.tet.2003.10.008.

(43) Abakumov, G. A.; Cherkasov, V. K.; Kocherova, T. N.; Druzhkov, N. O.; Kurskii, Y. A.; Abakumova, L. G. Quinonimines and Aminoquinones, the Reaction Products of 3,6-Di(Tert-Butyl)-o-Benzoquinone with Primary and Secondary Amines. *Russ. Chem. Bull.* **2006**, *55* (7), 1195–1199. https://doi.org/10.1007/s11172-006-0398-5.

(44) Ribeiro, R. C. B.; Ferreira, P. G.; De A. Borges, A.; Da S. M. Forezi, L.; De Carvalho da Silva, F.; Ferreira, V. F. 1,2-Naphthoquinone-4-Sulfonic Acid Salts in Organic Synthesis. *Beilstein J. Org. Chem.* **2022**, *18*, 53–69. https://doi.org/10.3762/bjoc.18.5.

(45) Dähne, S.; Leupold, D. Coupling Principles in Organic Dyes. *Angew. Chemie Int. Ed. English* **1966**, *5* (12), 984–993. https://doi.org/10.1002/anie.196609841.

(46) Berger, S.; Hertl, P.; Rieker, A. Physical and Chemical Analysis of Quinones. In *The Quinonoid Compounds (1988)*; John Wiley & Sons, Ltd, 1988; pp. 29–78. https://doi.org/https://doi.org/10.1002/9780470772119.ch2.

(47) Barnsley, J. E.; Pelet, W.; McAdam, J.; Wagner, K.; Hayes, P.; Officer, D. L.; Wagner, P.; Gordon, K. C. When "Donor-Acceptor" Dyes Delocalize: A Spectroscopic and Computational Study of D-A Dyes Using "Michler's Base." *J. Phys. Chem. A* **2019**, *123* (28), 5957–5968. https://doi.org/10.1021/acs.jpca.9b03275.

(48) Telitel, S.; Dumur, F.; Kavalli, T.; Graff, B.; Morlet-Savary, F.; Gigmes, D.; Fouassier, J.-P.; Lalevée, J. The 1,3-Bis(Dicyanomethylidene)Indane Skeleton as a (Photo) Initiator in Thermal Ring Opening Polymerization at RT and Radical or Cationic Photopolymerization. *RSC Adv.* **2014**, *4* (31), 15930. https://doi.org/10.1039/C3RA42819B.

(49) Huang, J.; Tang, H.; Yan, C.; Li, G. 1,1-Dicyanomethylene-3-Indanone End-Cap Engineering for Fused-Ring Electron Acceptor-Based High-Performance Organic Photovoltaics. *Cell Reports Phys. Sci.* **2021**, *2* (1), 100292. https://doi.org/10.1016/j.xcrp.2020.100292.

(50) Francos, J.; García-Garrido, S. E.; Borge, J.; Suárez, F. J.; Cadierno, V. Butadiene Dyes Based on 3-(Dicyanomethylidene)Indan-1-One and 1,3-Bis(Dicyanomethylidene)Indane: Synthesis, Characterization and Solvatochromic Behaviour. *RSC Adv.* **2016**, *6* (9), 6858–6867. https://doi.org/10.1039/c5ra27005g.

(51) Batenko, N.; Gaile, A. Chemosensors Based on 5-Ethylidene-Substituted Barbituric Acid Derivatives (Microreview). *Chem. Heterocycl. Compd.* **2022**, *58* (2–3), 97–99. https://doi.org/10.1007/s10593-022-03061-2.

(52) Sigalov, M.; Lemcoff, N. G.; Shainyan, B.; Chipanina, N.; Aksamentova, T. Enol Forms of 1,3-Indanedione, Their Stabilization by Strong Hydrogen Bonding, and Zwitterion-Assisted Interconversion. *European J. Org. Chem.* **2010**, No. 14, 2800–2811. https://doi.org/10.1002/ejoc.201000026.

(53) Neese, F. The ORCA Program System. *Wiley Interdiscip. Rev. Comput. Mol. Sci.* **2012**, *2* (1), 73–78. https://doi.org/10.1002/wcms.81.

(54) Skancke, A.; Skancke, N. *The Chemistry of Quinonoid Compounds*; Patai, S., Rappoport, Z., Eds.; John Wiley & Sons Ltd, 1988.

(55) Anaflous, A.; Albay, H.; Benchat, N. E.; El Bali, B.; Dušek, M.; Fejfarová, K. 2-Phenyl-Imidazo[1,2-a]Pyridine-3-Carbaldehyde. *Acta Crystallogr. Sect. E Struct. Reports Online* **2008**, *64* (5). https://doi.org/10.1107/S1600536808011306.

(56) Lu, T.; Chen, F. Multiwfn: A Multifunctional Wavefunction Analyzer. *J. Comput. Chem.* **2012**, *33* (5), 580–592. https://doi.org/10.1002/jcc.22885.

(57) Aguilar-Martinez, M.; Macias-Ruvalcaba, N.; Bautista-Martinez, J.; Gomez, M.; Gonzalez, F.; Gonzalez, I. Review: Hydrogen Bond and Protonation as Modifying Factors of the Quinone Reactivity. *Curr. Org. Chem.* **2004**, *8* (17), 1721–1738. https://doi.org/10.2174/1385272043369548.

(58) Formen, J. S. S. K.; Wolf, C. Chiroptical Switching and Quantitative Chirality Sensing with (Pseudo)Halogenated Quinones. *Angew. Chemie Int. Ed.* **2021**, *60* (52), 27031–27038. https://doi.org/10.1002/anie.202111542.

(59) Matsumoto, A.; Kaimori, Y.; Kawasaki, T.; Soai, K. Asymmetric Autocatalysis Initiated by Crystal Chirality of Achiral Compounds. In *Advances in Asymmetric Autocatalysis and Related Topics*; Elsevier, 2017; pp. 337–355. https://doi.org/10.1016/B978-0-12-812824-4.00018-6.

(60) Helmers, I.; Ghosh, G.; Albuquerque, R. Q.; Fernández, G. Pathway and Length Control of Supramolecular Polymers in Aqueous Media via a Hydrogen Bonding Lock. *Angew. Chemie Int. Ed.* **2021**, *60* (8), 4368–4376. https://doi.org/10.1002/anie.202012710.

(61) Tuttle, M. R.; Davis, S. T.; Zhang, S. Synergistic Effect of Hydrogen Bonding and π–π Stacking Enables Long Cycle Life in Organic Electrode Materials. *ACS Energy Lett.* **2021**, *6* (2), 643–649. https://doi.org/10.1021/acsenergylett.0c02604.

(62) Zheng, S.; Shi, D.; Sun, T.; Zhang, L.; Zhang, W.; Li, Y.; Guo, Z.; Tao, Z.; Chen, J. Hydrogen Bond Networks Stabilized High-Capacity Organic Cathode for Lithium-Ion Batteries. *Angew. Chemie Int. Ed.* **2023**, *62* (9). https://doi.org/10.1002/anie.202217710.

(63) Steiner, T. The Hydrogen Bond in the Solid State. In *Angewandte Chemie International Edition*; 2002; Vol. 41, pp. 48–76. https://doi.org/10.1002/1521-3773(20020104)41:1<48::AID-ANIE48>3.0.CO;2-U.

(64) Adawy, A. Functional Chirality: From Small Molecules to Supramolecular Assemblies. *Symmetry (Basel).* **2022**, *14* (2), 292. https://doi.org/10.3390/sym14020292.

(65) Flack, H. D. Chiral and Achiral Crystal Structures. *Helv. Chim. Acta* **2003**, *86* (4), 905–921. https://doi.org/10.1002/hlca.200390109.

(66) Thompson, A. L.; Watkin, D. J. X-Ray Crystallography and Chirality: Understanding the Limitations. *Tetrahedron Asymmetry* **2009**, *20* (6–8), 712–717. https://doi.org/10.1016/j.tetasy.2009.02.025.

(67) Eliel, L. E.; Wilen, H. S. *Stereochemistry of Organic Compounds*; 1994.

(68) Giacovazzo, C.; Monaco, H. .; Artioli, G.; Viterbo, D.; Ferraris, G.; Gilli, G.; Zanotti, G.; Catti, M. *Fundamentals of Crystallography 2nd Edition*; Oxford University Press; 2nd edition (July 15, 2002), 2002.

(69) Kikkawa, S.; Masu, H.; Katagiri, K.; Okayasu, M.; Yamaguchi, K.; Danjo, H.; Kawahata, M.; Tominaga, M.; Sei, Y.; Hikawa, H.; Azumaya, I. Characteristic Hydrogen Bonding Observed in the Crystals of Aromatic Sulfonamides: 1D Chain Assembly of Molecules and Chiral Discrimination on Crystallization. *Cryst. Growth Des.* **2019**, *19* (5), 2936–2946. https://doi.org/10.1021/acs.cgd.9b00159.

(70) Laurence, C.; Legros, J.; Chantzis, A.; Planchat, A.; Jacquemin, D. A Database of Dispersion-Induction DI, Electrostatic ES, and Hydrogen Bonding α 1 and β 1 Solvent Parameters and Some Applications to the Multiparameter Correlation Analysis of Solvent Effects. *J. Phys. Chem. B* **2015**, *119* (7), 3174–3184. https://doi.org/10.1021/jp512372c.

(71) Sigalov, M.; Shainyan, B.; Chipanina, N.; Ushakov, I.; Shulunova, A. Intra- and Intermolecular N□H···O Hydrogen Bonds in Pyrrolyl Derivatives of Indane-1,3-Dione - Experimental and Theoretical Study. *J. Phys. Org. Chem.* **2009**, *22* (12), 1178–1187. https://doi.org/10.1002/poc.1573.

(72) Cierpicki, T.; Otlewski, J. Amide Proton Temperature Coefficients as Hydrogen Bond Indicators in Proteins. *J. Biomol. NMR* **2001**, *21* (3), 249–261. https://doi.org/10.1023/A:1012911329730.

(73) Carroll, F. I.; Miller, H. W.; Meck, R. Thiosemicarbazone and Amidinohydrazone Derivatives of Some 1,4-Naphthoquinones. *J. Chem. Soc. C Org.* **1970**, *3* (15), 1993. https://doi.org/10.1039/j39700001993.

(74) Dudley, K. H.; Miller, H. W.; Schneider, P. W.; McKee, R. L. Potential Naphthoquinone Antimalarials. 2-Acylhydrazino-1,4-Naphthoquinones and Related Compounds. *J. Org. Chem.* **1969**, *34* (9), 2750–2755. https://doi.org/10.1021/jo01261a058.

(75) Catalán, J. Toward a Generalized Treatment of the Solvent Effect Based on Four Empirical Scales: Dipolarity (SdP, a New Scale), Polarizability (SP), Acidity (SA), and Basicity (SB) of the Medium. *J. Phys. Chem. B* **2009**, *113* (17), 5951–5960. https://doi.org/10.1021/jp8095727.

(76) Shapet'ko, N. N.; Shigorin, D. N. NMR Study of Intramolecular Hydrogen Bond Protons in Quinoid Structures. *Zhurnal Strukt. Khimii* **1967**, *8* (3), 538–540.

(77) Kamlet, M. J.; Taft, R. W. Solvent Hydrogen-Bond Acceptor (HBA) Basicities. *J. Am. Chem. Soc.* **1975**, *98* (2), 377–383. https://doi.org/10.1021/ja00418a009.

(78) Hansch, C.; Leo, A.; Taft, R. W. A Survey of Hammett Substituent Constants and Resonance and Field Parameters. *Chem. Rev.* **1991**, *91* (2), 165–195. https://doi.org/10.1021/cr00002a004.

(79) Su, X.; Lõkov, M.; Kütt, A.; Leito, I.; Aprahamian, I. Unusual Para-Substituent Effects on the Intramolecular Hydrogen-Bond in Hydrazone-Based Switches. *Chem. Commun.* **2012**, *48* (85), 10490. https://doi.org/10.1039/c2cc35860c.

(80) Su, X.; Aprahamian, I. Hydrazone-Based Switches, Metallo-Assemblies and Sensors. *Chem. Soc. Rev.* **2014**, *43* (6), 1963–1981. https://doi.org/10.1039/c3cs60385g.

(81) Johnson, J. E.; Morales, N. M.; Gorczyca, A. M.; Dolliver, D. D.; McAllister, M. A. Mechanisms of Acid-Catalyzed Z / E Isomerization of Imines. *J. Org. Chem.* **2001**, *66* (24), 7979–7985. https://doi.org/10.1021/jo010067k.

(82) Klopčič, I.; Dolenc, M. S. Chemicals and Drugs Forming Reactive Quinone and Quinone Imine Metabolites. *Chem. Res. Toxicol.* **2019**, *32* (1), 1–34. https://doi.org/10.1021/acs.chemrestox.8b00213.

(83) Almeida, R. G.; Valença, W. O.; Rosa, L. G.; De Simone, C. A.; De Castro, S. L.; Barbosa, J. M. C.; Pinheiro, D. P.; Paier, C. R. K.; De Carvalho, G. G. C.; Pessoa, C.; Goulart, M. O. F.; Kharma, A.; Da Silva Júnior, E. N. Synthesis of Quinone Imine and Sulphur-Containing Compounds with Antitumor and Trypanocidal Activities: Redox and Biological Implications. *RSC Med. Chem.* **2020**, *11* (10), 1145–1160. https://doi.org/10.1039/d0md00072h.

(84) Chen, T.; Banda, H.; Yang, L.; Li, J.; Zhang, Y.; Parenti, R.; Dincă, M. High-Rate, High-Capacity Electrochemical Energy Storage in Hydrogen-Bonded Fused Aromatics. *Joule* **2023**, *7* (5), 986–1002. https://doi.org/10.1016/j.joule.2023.03.011.

(85) Batenko, N.; Kricka, A.; Belyakov, S.; Turovska, B.; Valters, R. A Novel Method for the Synthesis of Benzimidazole-Based 1,4-Quinone Derivatives. *Tetrahedron Lett.* **2016**, *57* (3), 292–295. https://doi.org/10.1016/j.tetlet.2015.12.002.

(86) Kudin, K. N.; Ozbas, B.; Schniepp, H. C.; Prud'homme, R. K.; Aksay, I. A.; Car, R. Raman Spectra of Graphite Oxide and Functionalized Graphene Sheets. *Nano Lett.* **2008**, *8* (1), 36–41. https://doi.org/10.1021/nl071822y.

(87) Saravanan, M.; Ganesan, M.; Ambalavanan, S. An in Situ Generated Carbon as Integrated Conductive Additive for Hierarchical Negative Plate of Lead-Acid Battery. *J. Power Sources* **2014**, *251*, 20–29. https://doi.org/10.1016/j.jpowsour.2013.10.143.

# PATEICĪBAS

Vēlos izteikt pateicību:

- *Dr. phys.* Sergejam Beļakovam (LOSI) par rentgenstruktūranalīzes datu iegūšanu izvēlētajiem savienojumiem;
- *Mg*. Ramonai Dūrenai, *Bc.* Ņikitam Griščenko, *Ph. D*. Anzelmam Zukulam (RTU) par katoda materiāla izgatavošanu, CV mērījumiem, Ramana spektriem un SEM attēliem;
- *Dr. chem*. Baibai Turovskai (LOSI) par iegūto savienojumu cikliskās voltammetrijas mērījumiem MeCN šķīdumos;
- *Dr. chem.* Vitālijam Rjabovam (RTU) par mainīgas temperatūras $^{1}$H KMR spektroskopijas eksperimentu.

Paldies Rīgas Tehniskajai universitātei un Ķīmijas un ķīmijas tehnoloģijas institūtam par visām sniegtajām iespējām doktorantūras studiju laikā! Paldies kolēģiem par sniegtajām zināšanām un prasmēm, ka arī par padomiem un sniegto atbalstu! Visdziļākā pateicība promocijas darba vadītājai asociētai profesorei *Dr. chem*. Nelli Batenko par zinātniskajām idejām, diskusijām, motivāciju un ticību manām spējām visu šo gadu laikā! Sirsnīgs paldies manai ģimenei un draugiem par milzīgu atbalstu, rūpēm un iedrošinājumu!

# ACKNOWLEDGEMENT

I would like to express my gratitude to:

- Dr. phys. Sergey Belyakov (LIOS) for obtaining X-ray crystallography data for selected compounds;
- Mg. Ramona Dūrena, Bc. Ņikita Griščenko, and Ph. D. Anzelms Zukuls (RTU) for cathode material preparation, CV measurements, Raman spectra and SEM images;
- Dr. chem. Baiba Turovska (LIOS) for cyclic voltammetry measurements in MeCN solutions of obtained compounds;
- Dr. chem. Vitālijs Rjabovs (RTU) for variable temperature $^{1}$H NMR experiment.

I am grateful to Riga Technical University and the Institute of Chemistry and Chemical Technology for all the opportunities provided during my doctoral studies. I am thankful to my colleagues for the knowledge and skills they shared, as well as for their advice and support! My deepest gratitude to my supervisor, Associate Professor Dr. chem. Nelli Batenko, for the scientific ideas, insightful discussions, constant motivation, and for always believing in my abilities! Sincere thanks to my family and friends for their immense support, care, and encouragement!

# PIELIKUMI/APPENDICES

1. Pielikums
Appendix 1

Anastasija Gaile, Sergey Belyakov, Baiba Turovska, Nelli Batenko

# Synthesis of Asymmetric Coupled Polymethines Based on a 7-Chloropyrido[1,2-*a*]benzimidazole-8,9-dione Core

*J. Org. Chem*. **2022**, 87, 2345−2355.

DOI: 10.1021/acs.joc.1c02196

JOC The Journal of Organic Chemistry

pubs.acs.org/joc Article

# Synthesis of Asymmetric Coupled Polymethines Based on a 7-Chloropyrido[1,2-*a*]benzimidazole-8,9-dione Core

Anastasija Gaile, Sergey Belyakov, Baiba Turovska, and Nelli Batenko*

Cite This: *J. Org. Chem.* 2022, 87, 2345−2355 Read Online

ACCESS | Metrics & More | Article Recommendations | Supporting Information

**ABSTRACT:** A synthesis of 7-chloropyrido[1,2-*a*]benzimidazole-8,9-dione derivatives bearing fragments of widely used acceptor units has been performed, and their structures were investigated using the principle of coupled polymethines. Their electronic and electrochemical properties have also been studied. Compounds were isolated in both salt and neutral forms and depending on the introduced substituent can exist as *o*-quinone or *p*-quinone methide.

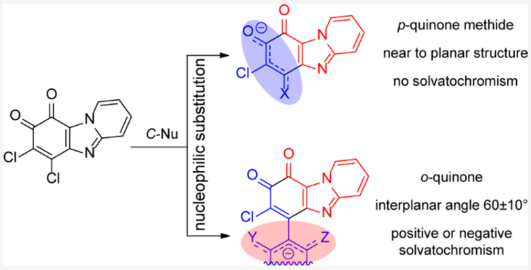




## INTRODUCTION

Quinone derivatives have been widely used due to their unique electrochemical properties that can enhance the efficiencies of energy-harvesting and energy-storage systems.[1]

When considering an application of quinone derivatives, it is important to note that the chemical stability, properties, and solubility depend on the chemical structure, interaction with media, and changes upon isomerization. It is known from the literature[2,3] that modification of the *o*-quinone fragment at the C(4) position may involve isomerization into *p*-quinone methide or *p*-quinone imine in biological systems, in some cases leading to toxicity. Inter- and intramolecular hydrogen bonds (H-bonds) affect the electrochemical properties and solubility of quinone derivatives and can be controlled by chemical modification or steric hindering to create stable molecular crystal materials and electrodes for battery applications.[4] Among many parameters relevant to the design of organic redox materials, the planarity or nonplanarity of the molecules is also an important factor.[5]

Quinones can be used as ligands to design coordination complexes[6,7] or metal−organic frameworks[8] featuring original photophysical and redox properties. Functionalization of the quinone molecules and tuning the bonds formed between quinone ligands and metal ions as well as delocalized electron distributions endow the metal−organic frameworks (MOFs) with chemical and electrochemical stability, which are essential for organic electrode materials to have the desirable properties. Thus, quinone structure isomerization or condensation with heterocycles can lead to a different metal−ligand binding mechanism as well as to new properties of the compound.[9,10]

Hence, studies of the relationship between quinone's molecular structure and its photophysical and electrochemical behavior are extremely important as they may provide further insights into the chemical engineering of quinone molecules for a specific application.

Imidazo[1,2-*a*]pyridine is a common nitrogen-bridgehead heterocycle used in pharmacology research because of the biological activities of its derivatives[11] and has also found applications in material science.[12] Some imidazo[1,2-*a*]-pyridine derivatives serve as excited-state intramolecular proton transfer (ESIPT) fluorophores[12] due to H-bond formation properties and can coordinate with metal ions.[13]

Quinone **1** contains an imidazo[1,2-*a*]pyridine fragment fused with an *o*-quinone moiety, and substituents can be introduced selectively at the C(6) position.[14] According to the literature,[15,16] *o*-benzoquinones, depending on the nature of the substituent at C(4)/C(5), can be characterized using a coupled polymethine concept. Two polymethine chains separated from each other are found in the structure, and the optical and photophysical properties of the molecules differ from the "classical" quinone properties. It was previously reported[14] that after the introduction of electron-donating substituents at the C(6) position of quinone **1** a new strong longwave absorption band was observed in their UV spectra.

Keeping these features in mind, we synthesized quinone derivatives (**2**−**6** and **3H**−**6H**) by combining heterocyclic *o*-quinone **1** with commonly used acceptor end groups such as barbituric acid[17,18] (**7**), 1,3-indandione analogues with differ-

**Received:** September 8, 2021
**Published:** January 31, 2022




https://doi.org/10.1021/acs.joc.1c02196
*J. Org. Chem.* 2022, 87, 2345−2355

**Scheme 1. Synthesis of Compounds 2−6 and 3H−6H**

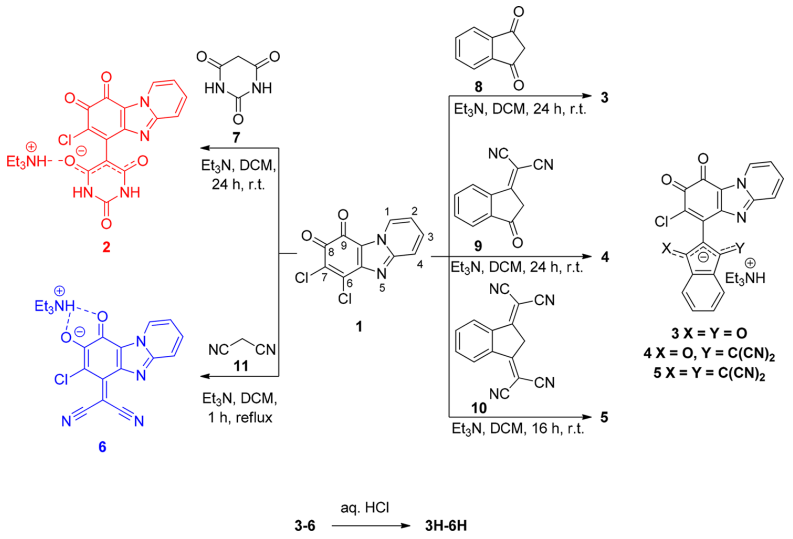


ent numbers of dicyanomethylene units[19−21] (**8**−**10**), and malononitrile (**11**) (Scheme 1) and investigated their structure−property relationships. We explored how substitution at C(6) of quinone **1** affected the bond lengths of quinone and fused imidazo[1,2-*a*]pyridine moieties as well as the planarity or nonplanarity of the resulting compounds using X-ray crystallography data. Connection of donor and acceptor moieties by only one C−C bond is used to design molecules with a small HOMO/LUMO gap.[22] A minimized distance provides less conjugation between donor and acceptor units, but such a combination may affect both parts of the molecule: the heterocyclic quinone and the introduced substituent.

It is known[6] that combination of different chelating sites in the same molecule should enhance the coordination abilities of a compound. For example, the ligand could gain the ability to form heterometallic complexes with different metals at both sites simultaneously.[23] The investigated quinone derivatives could be promising because *o*-quinones and imidazo[1,2-*a*]pyridine are known as metal binding fragments and combination of such fragments could lead to multifunctional ligands. Such species would be interesting from the viewpoint of the redox properties or sensor activity, self-assembly of ordered structures in a crystal phase, the formation of a hydrogen-bonded organic framework[24] or the formation of MOFs.

## RESULTS AND DISCUSSION

**Synthesis.** Heterocyclic quinone derivatives were prepared by nucleophilic substitution of a chlorine atom at C(6) of quinone **1** in the presence of triethylamine, which led to isolation of compounds **2**−**6** as triethylammonium salts with different localizations of the negative charge (Scheme 1). Despite the fact that all quinone derivatives were isolated in the salt form, compounds **2**−**5** exist in the *o*-quinone form and compound **6** and its derivatives **6a**−**d** in the *p*-quinone methide form. Isolation of compound **6** at ambient temperature was unsuccessful, and the product was obtained under reflux.

Salts **6a**−**d** were obtained using the same procedure by nucleophilic substitution of quinone derivatives **1a**−**d**[14] with malononitrile (Scheme 2).

**Scheme 2. Synthesis of Compounds 6a−d**

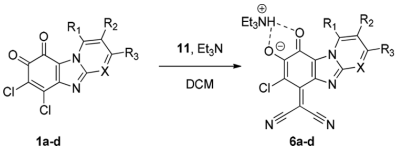


The conclusion about the form (*o*-quinone or *p*-quinone methide) of the isolated compounds was reached by using X-ray crystallography (vide infra) and NMR data analysis. Shifts of quinone carbonyl groups in $^{13}$C NMR spectra indicated that salts **2**−**5** are likely to exist as *o*-quinones because the differences in their C═O shifts are 11.1, 9.0, 11.5, and 13.0 ppm, respectively (Figures S2, S4, S6, and S8). These values are greater than that of *o*-quinone **1** (8.7 ppm).[14] Nevertheless, for compound **6**, the C═O group shifts were closer to each other with a difference of only 0.2 ppm (at 169.3 and 169.5 ppm). A similar trend was observed in NMR spectra of compounds **6a**−**c** (C═O shifts have 0.3−1.8 ppm differences) and compound **6d** (3.9 ppm). On the basis of the literature,[25] we concluded that the electron density on the C(8) atom for compounds **6** and **6a**−**d** was greater but on the C(9) atom was smaller than on the same atoms of compounds **1**−**5**. An intermolecular H-bond with O(8) and O(9) atoms could explain unsuccessful attempts to obtain a tetracyanoquinodimethane derivative from compound **6**. Probably, in the case of *o*-quinone derivatives, the difference in the chemical shifts of carbonyl groups in the $^{13}$C NMR spectrum can be used to analyze the hydrogen bonding effect.

It is noteworthy that both carbonyl groups of the barbituric acid moiety of compound **2** and the indandione moiety of compound **3** arise at one signal in $^{13}$C NMR spectra (162.4


https://doi.org/10.1021/acs.joc.1c02196
J. Org. Chem. 2022, 87, 2345−2355

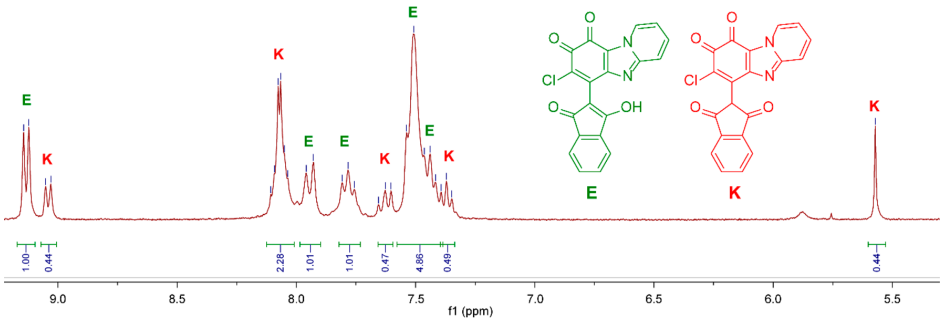


**Figure 1.** Expansion of the $^1$H NMR spectrum (300 MHz, DMSO-$d_6$), showing enol (E) and diketo (K) forms of compound **3H**. From the $^1$H NMR spectrum, the enol:diketo ratio is equal to 1:0.45.

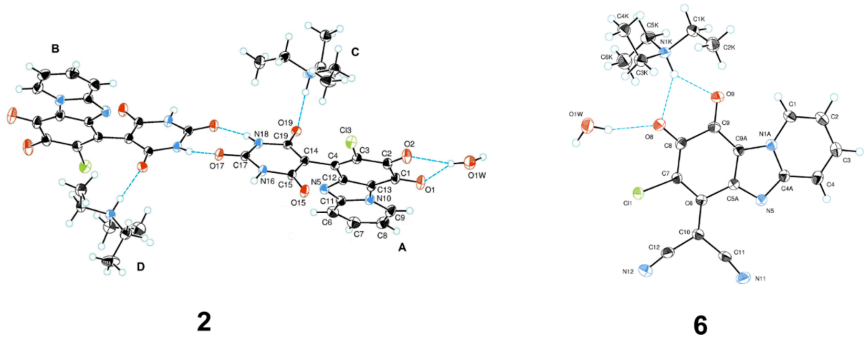


**Figure 2.** ORTEP structures of compounds **2** and **6**. All non-hydrogen atoms are depicted as thermal ellipsoids at the 50% probability level.

and 187.0 ppm, respectively), confirming the delocalization of the negative charge between carbonyl groups and the symmetry of the nucleophile fragment.

Surprisingly, green crystals of compound **3H** were obtained by slow evaporation of the solvent from the solution of salt **3** in DCM. X-ray crystallography confirmed the structure of compound **3H** as *o*-quinone connected to the enolic form of indandione (Figure S31), which was stabilized by a strong intramolecular H-bond (vide infra). However, acidic hydrolysis of salt **3** led to product **3H** (red in solid state) with the diketo form of the indandione moiety as shown by analysis of the IR spectrum: absorption bands at 1702 and 1746 cm$^{-1}$ and absence of the OH absorption band. The $^1$H NMR spectrum (DMSO-$d_6$) of compound **3H** (red in solid state) exhibited two sets of signals caused by the keto−enol tautomeric equilibrium of the indandione fragment (Figure 1). According to the literature,[26] the aromatic protons of the diketo moiety resonate in the range of 8.0−8.2 ppm but aromatic protons of the enol fragment are shifted upfield to approximately 7.3−7.5 ppm. The shift of the keto−enol equilibrium from the diketo form (red) to the enol form (green) in DMF and DMSO can be observed by the naked eye; the color of the solution was green (Figure S36).

Compounds **4H−6H** were also obtained from acidic hydrolysis of salts **4−6**, respectively, that was evidenced by the absence of $Et_3NH^+$ signals in their $^1$H NMR spectra.

It is worth noting that for the enol form of compound **3H** there was no OH group signal and no OH or CH signal was observed in the $^1$H NMR spectrum of compounds **4H−6H** at ambient temperature. Due to fast exchange, only one signal was observed for both the proton and water, which was concluded from downfielded signal of water in the $^1$H NMR spectrum of compounds **4H−6H** in a DMSO-$d_6$ solution. This can be attributed to deprotonation and anionic structure stabilization by the solvation in polar media.[27] Theoretically, the formation of a betaine with a protonated N(5) and negative charge delocalized over the acceptor fragment cannot be excluded.

**X-ray Crystal Structure Analysis.** ORTEP drawings of salts **2** and **6** are shown in Figure 2. The asymmetric unit of the salt **2** crystal consists of two anions, two cations ($Et_3NH^+$), and one water molecule. Single-crystal X-ray data confirmed that the negative charge of anion **2** was delocalized in the fragment of barbituric acid equally in the O(19)−C(19)−C(14)−C(15)−O(15) moiety (C−C bond lengths of 1.407 and 1.421 Å and C−O bond lengths of 1.242 and 1.254 Å) and formed an intermolecular H-bond between $Et_3NH^+$ and the oxygen atom of barbituric acid. In the crystal structure of salt **2**, the anions are associated by strong hydrogen bonds of the NH···O type.

Compound **6**, which was more likely to exist in the *p*-quinone methide form, formed a forklike intermolecular H-bond between $Et_3NH^+$ and both oxygen atoms of the quinone fragment. It was shown that the bond lengths of the carbonyl groups [C(8)−O(8), 1.245 Å; C(9)−O(9), 1.234 Å] are greater than the standard C═O bond length and H···O distances [H···O(8), 2.18(3) Å; H···O(9), 2.21(3) Å] that are equal within the error limits. Therefore, the negative charge of


https://doi.org/10.1021/acs.joc.1c02196
J. Org. Chem. 2022, 87, 2345−2355

the anion is delocalized between two oxygen atoms, which agreed with $^{13}C$ NMR data analysis (vide supra).

In this work, a comparison of X-ray crystallography data of compounds **2**, **6**, and **3H** with those previously reported[14,28] for benzimidazole-based *o*- and *p*-quinone derivatives (*o*-**QN**, *o*-**QCCN**, and *p*-**Q**) was carried out (Figure 3).

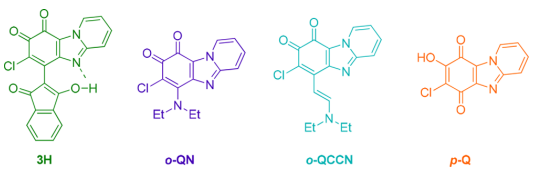


**Figure 3.** Structures of compounds **3H**, *o*-**QN**,[14] *o*-**QCCN**,[14] and *p*-**Q**[28] confirmed by single-crystal X-ray data.

The bond lengths determined for the quinone cycle established two parts linked by long single bonds 1 and 4 (Figure 4). The length of bonds 2 and 3 varied depending on

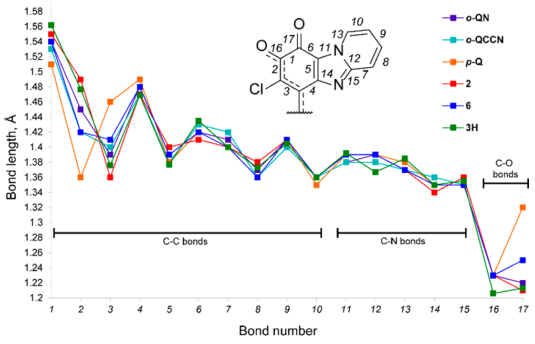


**Figure 4.** Bond lengths and schematic representation of the heterocyclic quinone core of compounds **2**, **6**, **3H**, *o*-**QN**, *o*-**QCCN**, and *p*-**Q** with bond numbering.

the substituent introduced at C(6) or the change from *o*- to *p*-quinone structure. For example, in compounds **6** and *o*-**QCCN**, bonds 2 and 3 are almost equal, while in compounds **2** and **3H**, the same bonds displayed a pronounced single-bond/double-bond alternation like in the "classical" *o*-benzoquinone.[29]

Analysis of the X-ray data of compounds **2**, **6**, *o*-**QN**, *o*-**QCCN**, and *p*-**Q** showed that the bond lengths of the heterocyclic fragment [bonds 5−15 (Figure 4)] were not affected by the introduced substituent, structural changes between *o*- and *p*-quinone, or the existence of the compound in the salt form. Moreover, the bond lengths in the heterocyclic part of the molecule did not differ from the bond lengths of different imidazo[1,2-*a*]pyridine derivatives in the solid state,[11] and they were almost the same as imidazo[1,2-*a*]pyridine-3-carbaldehyde derivative[30] bond lengths, where bonds 14 and 15 were equalized like in compounds **2**, **6**, *o*-**QN**, *o*-**QCCN**, and *p*-**Q**. The length of the carbonyl group bond in the imidazo[1,2-*a*]pyridine-3-carbaldehyde derivative was equal to the length of bond 17 in quinone derivatives studied via single-crystal X-ray, although bond 17 of compound **3H** was shorter. In the structure of **3H** (Figure S31), a very strong intramolecular H-bond of the OH···N type with a length of 2.502(4) Å was found. The N(5)···H···O angle is 157(6)° [N(5)···H, 1.172 Å; H···O, 1.379 Å]. A hydrogen atom lying almost in the middle of the N···O line affected the distribution of $\pi$-electrons in the heterocyclic part of the molecule and the nearby carbonyl group (bond 17). In the crystal structure of **3H** (green in solid state), there was also a strong inter- and intramolecular $\sigma$-hole interaction between the oxygen of the C═O bond in the indandione fragment and the chlorine atom; the O···Cl distances are 2.917 and 2.872 Å, respectively (Figure 5). By means of this interaction, centrosymmetric molecular dimers were formed in the crystal structure.

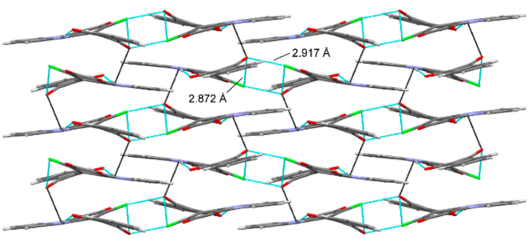


**Figure 5.** Molecular packing in the crystal of compound **3H**. Light blue lines indicate $\sigma$-hole interaction, and black lines correspond to interaction between N(5) and the indandione C═O group.

Interplanar angles between the heterocyclic quinone plane and the introduced substituent plane (in the solid state) of compounds **2**, **6**, **3H**, and *o*-**QCCN** can be compared (Table 1). The bulky barbituric acid moiety is rotated away from the quinone cycle plane around the C−C bond that can be seen from the larger interplanar angle $\varphi$, the fact that the symmetry of the p orbitals is lower, and the interaction between the quinone and barbituric acid moieties is weaker. On the contrary, in the case of compounds **6** and *o*-**QCCN**, the C−C bond between the planes has more double bond character and $\varphi$ is smaller.

On the basis of the analysis of the molecular geometry in the solid state and the coupling principle of polymethine dyes,[15] the structures of *o*-quinone **1** derivatives can be theoretically divided into two parts. The first part includes the heterocycle moiety and a nearby carbonyl group (bonds 5−15 and 17), and the second part bonds 16-2-3 and the following bonds of the substituent introduced at C(6). Because of the vanishing bond length alternation (BLA) in the second part of the molecule compounds **6** and *o*-**QCCN** can be characterized as "coupled polymethines". For compound **2**, bonds 16-2-3 and the following bonds to the substituent at C(6) can be characterized as the polyene fragment but equal bonds with delocalized negative charge between two carbonyl groups of barbituric acid can be characterized as the polymethine fragment.

Despite separation by long single bonds 1 and 4, an introduced substituent can influence the heterocyclic part through the formation of an intramolecular H-bond, as seen from analysis of the structure of compound **3H** in the solid state.

**DFT Calculations.** DFT calculations were carried out to optimize the geometries of the studied compounds in the gas phase and solvents (DCM or DMF, the conductor-like polarizable continuum model (PCM)) using the CAM-B3LYP functional with the def2-TZVP basis set. For compounds **2**, **6**, **3H** and *o*-**QCCN** the geometries were


https://doi.org/10.1021/acs.joc.1c02196
J. Org. Chem. 2022, 87, 2345−2355

**Table 1. Interplanar Angles ($\varphi$), Bond Length Alternation (BLA), and Bond Lengths ($r$) between the Planes of Compounds 2, 6, 3H, and *o*-QCCN**

| compd | method | solvent[b] | interplanar angle $\varphi$ (deg) | $r_{C(6)-C(Nu)}$ (Å) | BLA[c] (Å) |
|---|---|---|---|---|---|
| **2**[a] | X-ray (**2A**) | | 60.79 | 1.468 | 0.0935 |
| | X-ray (**2B**) | | 64.60 | 1.469 | 0.0975 |
| | CAM-B3LYP/def2-TZVP | DMF | 65.62 | 1.462 | 0.0935 |
| | | vacuum | 60.39 | 1.453 | 0.093 |
| | B3LYP/6-311G** | vacuum | 55.94 | 1.450 | 0.0505 |
| **6** | X-ray | | 10.48 | 1.402 | 0.0055 |
| | CAM-B3LYP/def2-TZVP | DMF | 1.07 | 1.395 | 0.007 |
| | | DCM | 1.4 | 1.392 | −0.0015 |
| | | vacuum | 1.56 | 1.373 | −0.05 |
| | B3LYP/6-311G** | vacuum | 0.34 | 1.394 | −0.0315 |
| **3H**[d] | X-ray | | 25.57 | 1.448 | 0.07 |
| | CAM-B3LYP/def2-TZVP | DMF | 31.16 | 1.449 | 0.0905 |
| | | vacuum | 32.87 | 1.454 | 0.107 |
| | B3LYP/6-311G** | vacuum | 32.01 | 1.454 | 0.09 |
| ***o*-QCCN** | X-ray | | 4.56 | 1.412 | 0.0245 |
| | CAM-B3LYP/def2-TZVP | DMF | 1.53 | 1.401 | 0.026 |
| | | DCM | 1.6 | 1.407 | 0.037 |
| | | vacuum | 2.7 | 1.429 | 0.0825 |
| | B3LYP/6-311G** | vacuum | 1.99 | 1.431 | 0.0705 |

[a]The crystal of salt **2** consists of two anions that are marked as anions **2A** and **2B**. [b]Depends on the solubility of the compound. [c]The BLA parameter was calculated as the difference between the average bond lengths of the formal C−C and C═C bonds in the polymethine/polyene chain for the structure (bonds 2 and 3 and following bonds of the introduced substituent). [d]Enol form of **3H**.

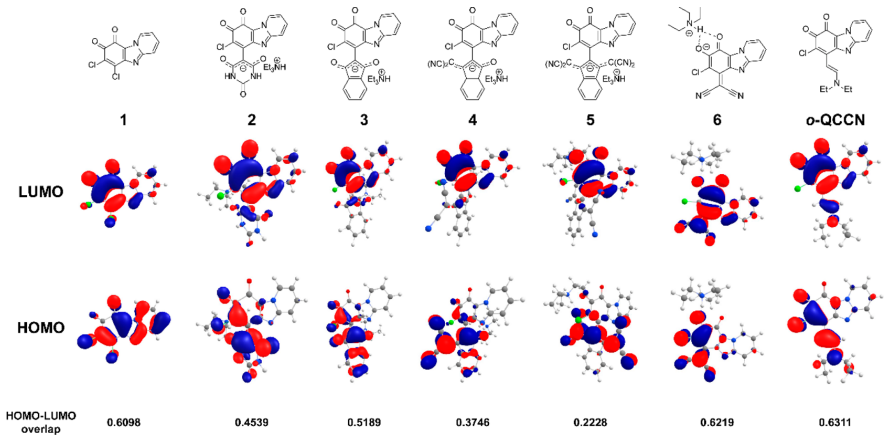


**Figure 6.** Frontier orbitals and HOMO−LUMO overlap at the CAM-B3LYP/def2-TZVP level for compounds **1**−**6** and ***o*-QCCN** (overlap integrals between the HOMO and LUMO were calculated at the CAM-B3LYP/def2-TZVP level in DMF using Multiwfn[32]).

optimized in the gas phase using also B3LYP functional with 6-311G** basis set for comparison.

For salts **2**−**5**, DFT calculations predicted similar interplanar angles (60 ± 10°) in the gas phase between the heterocyclic quinone and the introduced substituent planes that can be explained by steric congestion, but for salt **6** bearing a malononitrile fragment, the calculation predicts the coplanarity of all atoms. Typically, derivatives with bulky substituents were likely to exist in *o*-quinone form with negative charge distributed in the introduced substituent. Upon introduction of sterically less hindered substituents at the C(6) position, conjugation between the quinone and substituent appeared. As one can see, there is a linear relationship ($R^2$ = 0.995) between the calculated (DMF) interplanar angle and the chemical shift differences of C═O groups (quinone fragment) in $^{13}$C NMR spectra of compounds **2**−**6** in DMSO-$d_6$ (Figure S40).

DFT calculations showed that interplanar angles and bond lengths of compounds **2**, **6**, **3H**, and ***o*-QCCN** followed a trend that is consistent with the X-ray crystallography data (Table 1). However, for salt **6** and compound ***o*-QCCN** in the solid state, the interplanar angle is larger than the calculated value because of the intermolecular H-bonds that were formed between the compound and surrounding molecules ($Et_3NH^+$ and/or water molecules) in the crystal packing (Figure S30). On the contrary, the interplanar angle of compound **3H** in the solid state was smaller because of the strong inter- and intramolecular interactions in the crystal. This means that the planarity or nonplanarity of the compound and the interplanar angle are affected by a combination of different factors,


https://doi.org/10.1021/acs.joc.1c02196
J. Org. Chem. 2022, 87, 2345−2355

including the steric hindrance of the substituent, the presence of the H-bond donor and acceptor centers in the structure, and intermolecular interactions in crystal packing. Hence, the form of the investigated quinone derivatives could be different in solution due to interaction with solvent molecules as in case of **3H**.

The HOMO of salts **2**−**6** and compound *o*-**QCCN** was spread over the introduced substituent and 16-2-3 bonds of the quinone showing the polymethine/polyene part of the molecule from the "coupled polymethine" concept, including one carbonyl group of quinone at C(8). It should be noted that the $\pi$-electron distribution in the HOMO level of salts **2**−**6** differs from that of the initial quinone **1** and is shifted from the imidazo[1,2-*a*]pyridine fragment toward the substituent moiety. The LUMO includes the quinone cycle and both carbonyl groups of quinone (Figure 6).

Theoretically, the HOMO is dominated by the donor moiety while the LUMO by the acceptor moiety.[31] In the case of compounds **2**−**5**, the HOMO is spread over the introduced substituent that can be explained by delocalization of negative charge over the fragment.

Judging from the frontier orbitals and HOMO−LUMO overlap values of salts **3**−**5**, these compounds exhibit an effective $\pi$-electron distribution over the larger substituent fragment and intramolecular charge transfer from the substituent to the quinone. However, for compounds **6** and *o*-**QCCN**, the charge transfer character seems to be weak because the HOMO−LUMO overlap values are higher (Figure 6).

Despite the fact that compound **6** can be characterized as a coupled polymethine, its calculated HOMO/LOMO gap is similar to the HOMO/LUMO gap of derivatives **2**−**5** possessing disrupted $\pi$-conjugation systems between the quinone and substituent moiety.

Calculated HOMO/LUMO gaps for salts **3**−**6** were smaller than for hydrolyzed compounds **3H**−**6H**, meaning that deprotonation generates a negative charge distribution between the quinone and substituent or mainly in the substituent part.

The geometries of **2**−**6** were optimized in the gas phase and two solvents (DCM and DMF). The solvent-mediated effect resulted in a change in the interplanar angle of the compounds. As expected, the increase in interplanar angle $\varphi$ was accompanied by a decrease in the HOMO−LUMO overlap (Table S6).

Time-dependent density functional theory (TD-DFT) calculations were conducted on the ground state optimized geometries of compounds using the PCM. The calculated spectra predicted a batochromic shift of the HOMO−LUMO transition band for compound **3** going from the gas phase to the polar solvent, negative solvatochromic behavior for compounds **4** and **5**, and no significant effect for salt **6**. This result is consistent with the UV-vis absorption spectra (vide infra).

**UV−Vis Properties.** The calculated bandgap decreases in the order **2** → **3** → **4** → **5**, and in the same order, the bathochromic shift of the longest wavelength absorption bands in the UV-vis spectra in DMF solutions shifted, going from 661 nm for salt **2** to the low-intensity shoulder at 740 nm for salt **5**. The longwave absorption band of salt **3** was shifted to a shorter wavelength with a decrease in the polarity of the solvent (positive solvatochromism); however, salts **4** and **5** exhibited negative solvatochromic behavior because the absorption was red-shifted in DCM to 751 and 864 nm, respectively. A clear correlation ($R^2$ = 0.99) resulted for derivatives **3**−**5** between absorption maxima (DCM) and their HOMO−LUMO overlap as well as between the absorption maxima (DCM) and the calculated interplanar angle ($R^2$ = 0.99) (Figure S41).

The absorption properties of salts **2**−**6** were recorded under basic (DBU) and acidic (TFA) conditions in polar (DMF) and nonpolar (DCM) solvents (Table S2, Figure S34, and Figure S35). Absorption spectra of compounds **3**−**5** in DCM after addition of DBU exhibited almost identical absorption maxima as in DMF, meaning that a polar solvent with hydrogen bond accepting abilities tends to stabilize the anionic form. On the contrary, after the addition of TFA to a DCM solution the longest wavelength transitions of salts **3**−**5** disappeared. Protonation-induced quenching of the intramolecular charge transfer means that the anion form is necessary for the longwave absorption (Figure 7a,b).

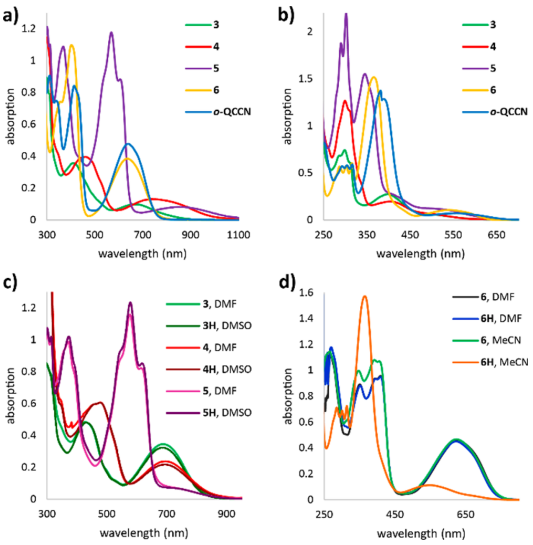


**Figure 7.** UV-vis absorption spectra for (a) salts **3**−**6** and compound *o*-**QCCN** in DCM, (b) salts **3**−**6** and compound *o*-**QCCN** in DCM after the addition of TFA, (c) compounds **3**−**5**, and **3H**−**5H** in DMF/DMSO, and (d) compounds **6** and **6H** in DMF and MeCN.

Interestingly, compound **5** exhibited strong absorption at approximately 580 nm similar to that of the initial nucleophile **10**, which in polar solvents exists in its deprotonated form.[27] Hence, UV-vis absorption spectra of compounds **3**−**5** were compared to the UV-vis spectra of their individual components before the reaction: *o*-quinone **1** and Indane derivatives **8**−**10** in DMF and DCM solutions (Figure S37). The UV-vis spectra of derivatives **3**−**5** consist of the spectra of its constituent chromophores and new longest wavelength absorption band, which is expected to arise from the interaction between both chromophore units. On the basis of the molar extinction coefficients of these bands in a DCM solution, we concluded that in the case of compound **5** ($\varepsilon$ = 1600 $M^{-1}$ $cm^{-1}$) the interaction between two units is less pronounced than in compounds **3** ($\varepsilon$ = 2000 $M^{-1}$ $cm^{-1}$) and **4** ($\varepsilon$ = 2600 $M^{-1}$ $cm^{-1}$); the lowest $\varepsilon$ value was estimated for compound **5** with the largest HOMO−LUMO separation.


https://doi.org/10.1021/acs.joc.1c02196
J. Org. Chem. 2022, 87, 2345−2355

After the addition of TFA to the DCM solution, the UV spectra of compounds **3**−**5** were virtually identical to the superposition of the spectra of isolated chromophores (Figure S37), indicating protonation of a compound at the functionalized Indane moiety and almost no electronic coupling between the units in the ground state. The theoretically calculated ground-state geometry of compounds **3H**−**5H** bearing a CH unit at the Indane moiety predicted an almost 90° interplanar angle between the heterocyclic quinone and introduced substitution planes, meaning that p orbitals are orthogonal and there is no conjugation between two chromophore units.

Compounds **3H**−**6H** each exhibited the same absorption as its analogue salts **3**−**6**, respectively, in DMSO and DMF solvents due to the H-bond accepting properties[33] of these solvents and were not affected by the addition of DBU (Figure 7c,d). The forms of compounds **3H**−**6H** were expected to be close to the forms of salts **3**−**6**, respectively, due to intermolecular interaction with hydrogen bond acceptor solvents. $Et_3NH^+$ as a cation does not make a significant contribution to the absorption properties of compounds **3**−**6** in DMF/DMSO; otherwise, UV spectra would be different for **3**−**6** and **3H**−**6H** in these solvents.

Surprisingly, salt **6** and compound ***o*-QCCN** had absorption at approximately 630 nm in DMF and at 640 nm in DCM and showed no changes under basic conditions. However, despite the vanishing BLA in the merocyanine part of **6** and ***o*-QCCN** (Table 1) in the solid state, their absorption spectra did not show a typical intense, narrow transition characteristic of "cyanine electronic structure"[25,34] when charge is perfectly delocalized through the polymethine fragment and exhibited practically no solvatochromism (Figure S38). Thus, in case of compounds **6** and ***o*-QCCN** cyanine structure does not dominate in solutions. Both compounds exhibit similar behavior under acidic conditions (a hypsochromic shift of ∼100 nm) that was attributed to the protonation of oxygen at C(8), after which compounds are expected to exist in the *p*-quinone methide form.

Substitution at the heterocyclic ring did not have a significant effect on the absorption spectra of compounds **6a**−**d** in DCM or DMF, because these compounds did not show shifts in their absorption maxima of >20 nm compared to that of parent compound **6**. Only compound **6d** with an elongated aromatic system after addition of TFA showed a bathochromic shift (44 nm) in comparison with that of parent compound **6** (Table S4).

Despite compounds **2**, **6**, **3H**, and ***o*-QCCN** existing in different forms, the molar extinction coefficients of their longwave absorption band in DMF/DMSO solutions correlated inversely to the size of $\varphi$ from X-ray crystallography data (Table 1 and Figure 8). That agreed with the conclusion about the longwave band appearance due to the electron delocalization between the quinone and substituent and its dependence on the interplanar angle.

**Electrochemical Properties.** As a reference, quinone **1** presents two reversible reduction steps (−0.36 and −1.15 V). As expected, cyclic voltammograms of the quinone derivatives showed that the most easily reduced salts were **2** and **3** (−0.44 and −0.48 V, respectively), while the first reduction potential shifted to the lower voltages with an increase in the number of cyano groups in the salt structure (for compounds **4**−**6**, −0.54, −0.60, and −0.50 V, respectively) and all of them showing an irreversible oxidation wave.

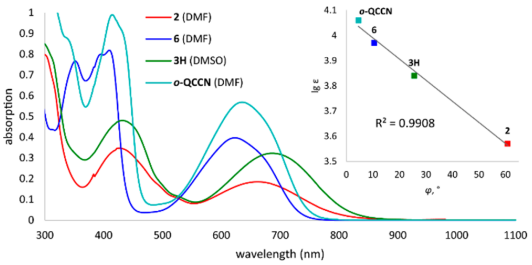


**Figure 8.** UV absorption spectra of compounds **2**, **6**, **3H**, and ***o*-QCCN** in DMF/DMSO solutions and correlation between their molar extinction coefficients of the longwave absorption and the size of $\varphi$.

Substitution at the quinone heterocyclic ring did affect the electrochemical properties of compounds **6a**−**d**. The introduction of an electron-withdrawing group (**6a**) shifts the reduction to higher voltages (−0.43 V), but introduction of a methyl group (**6b**) or elongation of the aromatic system (**6d**) shifts the reduction to lower voltages (approximately −0.80 V); also, replacing CH with N (**6c**) in the cycle did not show any effect (Figure S43 and Table S8). Compound **6H** exhibited the largest electrochemical gap compared to those of salt **6** and all other studied compounds.

## CONCLUSION

We have synthesized heterocyclic *o*-quinone derivatives connected with widely used acceptors by C−C bonds. These compounds can exist in the *o*-quinone or *p*-quinone methide form depending on the sterical factors and inter- and intramolecular interactions. Planar compounds bearing sterically less hindered substituents at C(6) can be characterized by the principle of coupling polymethines with electron delocalization between the quinone and substituent, but compounds with bulky substituents at C(6) have extensive charge delocalization in the substituent part of the molecule with less pronounced interaction between the quinone and substituent due to large interplanar angles. The obtained quinone derivatives, depending on the introduced substituent, could exhibit positive, negative, or no solvatochromic behavior.

The presence of hydrogen donor/acceptor fragments in the obtained quinone derivatives [at the *o*-quinone, the N(5) atom of the imidazo[1,2-*a*]pyridine moiety, and at the substituent] enables various intra- and intermolecular interactions that could be formed in different parts of the molecule. The heterocyclic part of the molecule may be affected by the formation of a strong intramolecular hydrogen bond to N(5).

In broader terms, derivatives that are based on the 7-chloropyrido[1,2-*a*]benzimidazole-8,9-dione core could be further investigated from the viewpoint of the construction of hydrogen-bonded organic frameworks[24] or coordination with metal ions at different chelating sites.

## EXPERIMENTAL SECTION

All reagents except for **1**, **1a**−**d**, ***o*-QN**, ***o*-QCCN**, ***p*-Q**, **9**, and **10** were obtained from commercial suppliers and used as received. Compounds **1**, **1a**−**d**, ***o*-QN**, ***o*-QCCN**, and ***p*-Q** are known and were prepared by previously described methods.[14,28] Compounds **9** and **10** were synthesized according to the reported procedures.[35] The reactions with heating were performed using a heating plate. Melting points were measured on a Kruess KSP 11 melting point analyzer. $^1$H


https://doi.org/10.1021/acs.joc.1c02196
J. Org. Chem. 2022, 87, 2345−2355

NMR and $^{13}C$ NMR spectra were recorded on a Bruker Avance 300 spectrometer at 300 and 75 MHz, respectively, in DMSO-$d_6$ solutions. For $^{13}C$ NMR, the attached proton test (APT) experiment was performed, which yields quaternary (C↑) and methylene ($CH_2$↑) signals positive and methine (CH↓) and methyl ($CH_3$↓) signals negative. Chemical shifts were expressed in parts per million ($\delta$) relative to the solvent signal (DMSO-$d_6$, 2.50 ppm for $^1H$ and 39.5 ppm for $^{13}C$).[36] Elemental CHN analysis was carried out on a Euro Vector EA 3000 analyzer. IR spectra were recorded on a PerkinElmer Spectrum 100 FTIR spectrometer equipped with an attenuated total reflectance Universial ATR Sampling Accessory. The UV−vis absorption spectra were recorded with a PerkinElmer 35 UV−vis spectrometer using 1 cm quartz cuvettes with a compound concentration ($c$) of $5 \times 10^{-5}$ M. Low-resolution mass spectra were recorded on a Waters EMD 1000MS mass detector (ESI + mode, voltage of 30 V) with an Xterra MS C18 5 $\mu$m, 2.1 mm × 100 mm column in gradient eluent mode using 0.1% HCOOH in deionized water and MeCN or MeOH.

**Triethylammonium 5-(7-Chloro-8,9-dioxo-8,9-dihydrobenzo[4,5]imidazo[1,2-*a*]pyridin-6-yl)-2,4,6-trioxohexahydropyrimidin-5-ide (2).** 6,7-Dichloropyrido[1,2-*a*]-benzimidazole-8,9-dione (**1**) (0.15 g, 0.56 mmol) was dissolved in DCM (250 mL). Then barbituric acid (**7**, 0.07 g, 0.56 mmol) dissolved in DMF (5 mL) and $Et_3N$ (0.16 mL, $\rho$ = 0.73 g/cm$^3$, 1.12 mmol) were added to the solution at room temperature. The mixture was stirred for 24 h. The obtained precipitate was filtered and recrystallized from EtOH. Yield: 0.12 g (48%), dark green crystalline solid. Mp: >300 °C. MS: after the hydrolysis of triethylammonium salt $C_{15}H_7ClN_4O_5$ requires $[M + H]^+$ 359.02; found $[M + H^+]^+$ 359.20. $^1H$ NMR (300 MHz, DMSO-$d_6$): $\delta$ 9.39 (br. s, 2H, exchange with $D_2O$, NH), 9.07 (d, $J$ = 6.6 Hz, 1H, H-1), 8.86 (br. s, 1H, exchange with $D_2O$, NH), 7.88 (d, $J$ = 8.9 Hz, 1H, H-4), 7.70 (t, $J$ = 8.0 Hz, 1H, H-3), 7.34 (t, $J$ = 6.7 Hz, 1H, H-2), 3.09 (q, $J$ = 7.2 Hz, 6H, $CH_2$), 1.16 (t, $J$ = 7.3 Hz, 9H, $CH_3$). $^{13}C\{^1H\}$ NMR (75 MHz, DMSO-$d_6$): $\delta$ 176.4, 165.3, 162.4, 155.3, 152.6, 149.3, 146.0, 132.2 (CH), 130.4, 128.5 (CH), 118.9, 118.8 (CH), 117.9 (CH), 84.8, 46.2 ($CH_2$), 9.1 ($CH_3$). IR (neat, cm$^{-1}$): 3561, 3493, 3126, 2974, 1680 (C═O), 1648 (C═O), 1610, 1573. Anal. Calcd for $C_{21}H_{22}ClN_5O_5 \cdot 0.5H_2O$: C, 53.79; H, 4.94; N, 14.94. Found: C, 53.46; H, 5.13; N, 14.84.

**General Method for the Preparation of Compounds 3 and 4.** 6,7-Dichloropyrido[1,2-*a*]benzimidazole-8,9-dione (**1**) (0.15 g, 0.56 mmol) was dissolved in DCM (250 mL). Then the DCM (10 mL) solution of 1,3-indandione (**8**) (0.08 g, 0.56 mmol) or the MeCN (40 mL) solution of 3-(dicyanomethylene)indan-1-one (**9**) (0.07 g, 0.56 mmol) was added at room temperature followed by the addition of $Et_3N$ (0.16 mL, 1.12 mmol). The reaction mixture was stirred for 24 h. The solution was filtered, and the filtrate was evaporated. The obtained precipitate was recrystallized from THF.

*Triethylammonium 2-(7-Chloro-8,9-dioxo-8,9-dihydrobenzo-[4,5]imidazo[1,2-a]pyridin-6-yl)-1,3-dioxo-2,3-dihydro-1H-inden-2-ide (**3**).* Yield: 0.13 g (62%), dark green solid. Mp: 152−155 °C. MS: after the hydrolysis of triethylammonium salt $C_{20}H_9ClN_2O_4$ requires $[M + H]^+$ 377.03; found $[M + H^+]^+$ 377.20. $^1H$ NMR (300 MHz, DMSO-$d_6$): $\delta$ 9.10 (d, $J$ = 6.5 Hz, 1H, H-1), 9.02 (br. s, 1H, exchange with $D_2O$, NH), 7.84 (d, $J$ = 8.9 Hz, 1H, H-4), 7.68 (m, 1H, H-3), 7.42 (dt, $J$ = 7.1, 3.6 Hz, 2H, $H_{Indane}$), 7.35 (m, 3H, H-2 + 2$H_{Indane}$), 3.09 (m, 6H, $CH_2$), 1.17 (t, $J$ = 7.3 Hz, 9H, $CH_3$). $^{13}C\{^1H\}$ NMR (75 MHz, DMSO-$d_6$): $\delta$ 187.0, 175.3, 166.3, 154.3, 149.1, 143.4, 141.6, 131.9 (CH), 130.9 (CH), 128.4 (CH), 124.8, 119.3, 119.1 (CH), 118.8 (CH), 117.8 (CH), 104.6, 46.1 ($CH_2$), 9.1 ($CH_3$). IR (neat, cm$^{-1}$): 2982, 2668, 2501, 1710 (C═O), 1638 (C═O), 1627, 1608, 1553. Anal. Calcd for $C_{26}H_{24}ClN_3O_4 \cdot 0.5H_2O$: C, 64.13; H, 5.17; N, 8.63. Found: C, 64.47; H, 5.16; N, 8.35.

*Triethylammonium 2-(7-Chloro-8,9-dioxo-8,9-dihydrobenzo-[4,5]imidazo[1,2-a]pyridin-6-yl)-1-(dicyanomethylene)-3-oxo-2,3-dihydro-1H-inden-2-ide (**4**).* Yield: 0.25 g (85%), dark brown solid. Mp: 188−190 °C. MS: after the hydrolysis of triethylammonium salt $C_{23}H_9ClN_4O_3$ requires $[M + H]^+$ 425.04; found $[M + H^+]^+$ 425.20. $^1H$ NMR (300 MHz, DMSO-$d_6$): $\delta$ 9.22 (br.s, 1H, exchange with $D_2O$, NH) 9.12 (d, $J$ = 6.5 Hz, 1H, H-1), 8.09 (d, $J$ = 7.3 Hz, 1H, $H_{Indane}$), 7.95 (d, $J$ = 8.9 Hz, 1H, H-4), 7.76 (t, $J$ = 7.6 Hz, 1H, H-3), 7.50 (td, $J$ = 7.3, 1.7 Hz, 1H, H-2) 7.45 (d, $J$ = 7.6 Hz, 1H, $H_{Indane}$), 7.40 (d, $J$ = 7.0 Hz, 2H, $H_{Indane}$), 3.09 (m, 6H, $CH_2$), 1.18 (t, $J$ = 7.3 Hz, 9H, $CH_3$). $^{13}C\{^1H\}$ NMR (75 MHz, DMSO-$d_6$): $\delta$ 185.7, 176.4, 164.9, 157.9, 154.8, 149.6, 141.2, 140.7, 139.5, 136.4, 132.8 (CH), 131.8 (CH), 130.5 (CH), 128.7 (CH), 121.5 (CH), 120.6, 120.5 (CH), 119.3, 119.1 (CH), 118.6 (CH), 84.6, 55.4, 46.1 ($CH_2$), 9.0 ($CH_3$). IR (neat, cm$^{-1}$): 2985, 2888, 2707, 2194, 1649 (C═O), 1623, 1597. Anal. Calcd for $C_{29}H_{24}ClN_5O_3 \cdot H_2O$: C, 64.03; H, 4.82; N, 12.87. Found: C, 64.35; H, 5.05; N, 12.86.

**Triethylammonium 2-(7-Chloro-8,9-dioxo-8,9-dihydrobenzo[4,5]imidazo[1,2-*a*]pyridin-6-yl)-1,3-bis-(dicyanomethylene)-2,3-dihydro-1*H*-inden-2-ide (5).** 6,7-Dichloropyrido[1,2-*a*]benzimidazole-8,9-dione (**1**) (0.15 g, 0.56 mmol) was dissolved in DCM (250 mL). 1,3-Bis(dicyanomethylene)-indane (**10**) (0.14 g, 0.56 mmol) in MeCN (50 mL) and $Et_3N$ (0.16 mL, 1.12 mmol) were added to the solution at room temperature. The mixture was stirred for 16 h. The solution was filtered, and the filtrate was evaporated. The obtained precipitate was dissolved in MeCN, and an aqueous solution of $FeCl_3$ (10%, 50 mL) was added. The product was extracted using DCM (100 mL). The organic layer was dried over $CaCl_2$ and filtered. The filtrate was concentrated under reduced pressure to a residual volume of 10 mL, and then 20 mL of hot hexane was added. The separated dark solid was filtered off and dried under air. Yield: 0.2 g (62%), dark solid. Mp: 125−127 °C. MS: after the hydrolysis of triethylammonium salt $C_{26}H_9ClN_6O_2$ requires $[M + H]^+$ 473.05; found $[M + H^+]^+$ 473.30. $^1H$ NMR (300 MHz, DMSO-$d_6$): $\delta$ 9.17 (d, $J$ = 6.5 Hz, 1H, H-1), 8.90 (br. s, 1H, exchange with $D_2O$, NH), 8.17 (dd, $J$ = 5.6, 3.1 Hz, 2H, $H_{Indane}$), 8.04 (d, $J$ = 9.0 Hz, 1H, H-4), 7.85 (t, $J$ = 8.0 Hz, 1H, H-3), 7.55 (dd, $J$ = 5.5, 3.2 Hz, 2H, $H_{Indane}$), 7.49 (t, $J$ = 7.2 Hz, 1H, H-2), 3.09 (m, 6H, $CH_2$), 1.17 (t, $J$ = 7.3 Hz, 9H, $CH_3$). $^{13}C\{^1H\}$ NMR (75 MHz, DMSO-$d_6$): $\delta$ 176.9, 163.9, 155.6, 154.6, 150.2, 139.4, 137.7, 134.3, 133.8 (CH), 131.3 (CH), 129.2 (CH), 122.6 (2 × CH), 119.5 (CH), 118.5, 118.3, 117.4 (CN), 107.0 (CN), 52.9, 46.2 ($CH_2$), 9.1 ($CH_3$). IR (neat, cm$^{-1}$): 3059, 2985, 1686 (C═O), 1645 (C═O), 1556. Anal. Calcd for $C_{32}H_{24}N_7O_2Cl \cdot 2H_2O$: C, 63.10; H, 4.47; N, 16.10. Found: C, 63.47; H, 4.63; N, 15.83.

**General Method for Preparation of Compounds 6 and 6a−d.** Malononitrile (**11**, 3.0 equiv) and $Et_3N$ (2.0 equiv) were added to a hot solution of 6,7-dichloropyrido[1,2-*a*]benzimidazole-8,9-dione (**1**) or its analogue (**1a−d**) (1.0 equiv) in DCM (50−200 mL). The mixture was refluxed while being stirred for 1−4 h and then cooled to room temperature. The solution was filtered, and the filtrate was evaporated. The crude product was purified by recrystallization from ethanol to give the products as dark blue solids.

*Triethylammonium 7-Chloro-6-(dicyanomethylene)-9-oxo-6,9-dihydrobenzo[4,5]imidazo[1,2-a]pyridin-8-olate (**6**).* 6,7-Dichloropyrido[1,2-*a*]benzimidazole-8,9-dione (**1**) (0.2 g, 0.75 mmol), malononitrile (**11**) (0.15 g, 2.25 mmol), and $Et_3N$ (0.2 mL, 1.5 mmol). Yield: 0.2 g (70%), dark blue solid. Mp: 181−183 °C. MS: after the hydrolysis of triethylammonium salt $C_{14}H_5ClN_4O_2$ requires $[M + H]^+$ 297.02; found $[M + H^+]^+$ 297.17. $^1H$ NMR (300 MHz, DMSO-$d_6$): $\delta$ 9.15 (d, $J$ = 6.5 Hz, 1H, H-1), 8.82 (br. s, 1H, exchange with $D_2O$, NH), 7.88 (d, $J$ = 8.9 Hz, 1H, H-4), 7.69 (t, $J$ = 7.9 Hz, 1H, H-3), 7.35 (t, $J$ = 6.8 Hz, 1H, H-2), 3.10 (m, 6H, $CH_2$), 1.18 (t, $J$ = 7.2 Hz, 9H, $CH_3$). $^{13}C\{^1H\}$ NMR (75 MHz, DMSO-$d_6$): $\delta$ 169.5, 169.3, 150.0, 147.6, 141.4, 131.4 (CH), 128.0 (CH), 120.63, 120.62, 119.0, 118.6 (CH), 117.6 (CH), 108.8, 46.1 ($CH_2$), 9.4 ($CH_3$). IR (neat, cm$^{-1}$): 3555, 3465, 3024, 2864, 2191, 1645 (C═O), 1619, 1565, 1523 Anal. Calcd for $C_{20}H_{20}N_5O_2Cl \cdot H_2O$: C, 57.76; H, 5.33; N, 16.84. Found: C, 57.68; H, 5.40; N, 16.70.

*Triethylammonium 7-Chloro-6-(dicyanomethylene)-2-nitro-9-oxo-6,9-dihydrobenzo[4,5]imidazo[1,2-a]pyridin-8-olate (**6a**).* 6,7-Dichloro-2-nitropyrido[1,2-*a*]benzimidazole-8,9-dione (**1a**) (0.15 g, 0.48 mmol), malononitrile (**11**) (0.10 g, 1.44 mmol), and $Et_3N$ (0.13 mL, 0.96 mmol). Yield: 0.08 g (38%), dark blue solid. Mp: 223−225 °C. MS: after the hydrolysis of triethylammonium salt $C_{14}H_4ClN_5O_4$ requires $[M + H]^+$ 342.00; found $[M + H^+]^+$ 342.20. $^1H$ NMR (300


https://doi.org/10.1021/acs.joc.1c02196
J. Org. Chem. 2022, 87, 2345−2355

MHz, DMSO-$d_6$): $\delta$ 9.90 (d, $J$ = 2.2 Hz, 1H, H-1), 8.83 (br. s, 1H, exchange with $D_2O$, NH), 8.32 (dd, $J$ = 9.8, 2.3 Hz, 1H, H-3), 8.03 (d, $J$ = 9.9 Hz, 1H, H-4), 3.11 (m, 6H, $CH_2$), 1.18 (t, $J$ = 7.3 Hz, 9H, $CH_3$). $^{13}C\{^1H\}$ NMR (75 MHz, DMSO-$d_6$): $\delta$ 170.3, 168.5, 151.9, 147.7, 142.4, 140.4, 139.5, 127.3 (CH), 124.6 (CH), 120.2, 120.1, 118.3 (CH), 106.2, 46.2 ($CH_2$), 9.1 ($CH_3$). IR (neat, $cm^{-1}$): 3468, 3033, 2870, 2188, 1652 (C═O), 1611, 1577, 1560. Anal. Calcd for $C_{20}H_{19}ClN_6O_4$: C, 54.24; H, 4.32; N, 18.98. Found: C, 54.32; H, 4.38; N, 18.80.

*Triethylammonium 7-Chloro-6-(dicyanomethylene)-3-methyl-9-oxo-6,9-dihydrobenzo[4,5]imidazo[1,2-a]pyridin-8-olate (**6b**).* 6,7-Dichloro-3-methylpyrido[1,2-*a*]benzimidazole-8,9-dione (**1b**) (0.15 g, 0.53 mmol), malononitrile (**11**) (0.11 g, 1.59 mmol), and $Et_3N$ (0.15 mL, 1.06 mmol). Yield: 0.13 g (59%), dark blue solid. Mp: 188−189 °C. MS: after the hydrolysis of triethylammonium salt $C_{15}H_7ClN_4O_2$ requires $[M + H]^+$ 311.03; found $[M + H^+]^+$ 311.10. $^1H$ NMR (300 MHz, DMSO-$d_6$): $\delta$ 9.01 (d, $J$ = 6.8 Hz, 1H, H-1), 8.84 (br. s, 1H, exchange with $D_2O$, NH), 7.70 (s, 1H, H-4), 7.20 (dd, $J$ = 6.8, 1.2 Hz, 1H, H-2) 3.10 (m, 6H, $CH_2$), 2.46 (s, 3H, $CH_3$), 1.17 (t, $J$ = 7.3 Hz, 9H, $CH_2-\underline{CH_3}$). $^{13}C\{^1H\}$ NMR (75 MHz, DMSO-$d_6$): $\delta$ 169.4, 169.1, 166.8, 150.3, 148.0, 142.8, 141.4, 127.2 (CH), 120.7, 120.6, 119.7 (CH), 118.7, 117.3 (CH), 46.1 ($CH_2$), 21.4 ($CH_3$), 9.2 ($CH_3$). IR (neat, $cm^{-1}$): 3005, 2883, 2737, 2195, 1636 (C═O), 1566, 1523, 1460. Anal. Calcd for $C_{21}H_{22}ClN_5O_2$: C, 61.24; H, 5.38; N, 17.00. Found: C, 61.27; H, 5.47; N, 16.97.

*Triethylammonium 8-Chloro-9-(dicyanomethylene)-6-oxo-6,9-dihydrobenzo[4,5]-imidazo[1,2-a]pyrimidin-7-olate (**6c**).* 6,7-Dichloropyrimido[1,2-*a*]benzimidazole-8,9-dione (**1c**) (0.15 g, 0.56 mmol), malononitrile (**11**) (0.11 g, 1.68 mmol), and $Et_3N$ (0.16 mL, 1.12 mmol). Yield: 0.08 g (36%), dark blue solid. Mp: 192−193 °C. MS: after the hydrolysis of triethylammonium salt $C_{13}H_4ClN_5O_2$ requires $[M + H]^+$ 298.01; found $[M + H^+]^+$ 298.30. $^1H$ NMR (300 MHz, DMSO-$d_6$): $\delta$ 9.40 (dd, $J$ = 6.6, 1.9 Hz, 1H, H-1), 8.84 (br. s, 1H, exchange with $D_2O$, NH), 8.84 (dd, $J$ = 4.1, 1.7 Hz, 1H, H-3), 7.42 (dd, $J$ = 6.6, 4.4 Hz, 1H, H-2), 3.10 (q, $J$ = 7.2 Hz, 6H, $CH_2$), 1.18 (t, $J$ = 7.3 Hz, 9H, $CH_3$). $^{13}C\{^1H\}$ NMR (75 MHz, DMSO-$d_6$): $\delta$ 170.1, 168.7, 155.2 (CH), 150.7, 150.3, 141.0, 136.3 (CH), 120.5, 120.3, 117.5, 113.4 (CH), 109.0, 46.2 ($CH_2$), 9.1 ($CH_3$). IR (neat, $cm^{-1}$): 3017, 2860, 2742, 2193, 2179, 1654 (C═O), 1613, 1569, 1522, 1457. Anal. Calcd for $C_{19}H_{19}ClN_6O_2$: C, 57.22; H, 4.80; N, 21.07. Found: C, 57.23; H, 4.73; N, 21.05.

*Triethylammonium 9-Chloro-8-(dicyanomethylene)-11-oxo-8,11-dihydrobenzo[4,5]imidazo[1,2-a]quinolin-10-olate (**6d**).* 6,7-Dichlorobenzimidazo[1,2-*a*]quinoline-10,11-dione (**6e**) (0.15 g, 0.47 mmol), malononitrile (**11**) (0.09 g, 1.41 mmol), and $Et_3N$ (0.13 mL, 0.94 mmol). Yield: 0.1 g (48%), dark blue solid. Mp: 183−184 °C. MS: after the hydrolysis of triethylammonium salt $C_{18}H_7ClN_4O_2$ requires $[M + H]^+$ 347.03; found $[M + H^+]^+$ 347.20. $^1H$ NMR (300 MHz, DMSO-$d_6$): $\delta$ 9.17 (d, $J$ = 8.7 Hz, 1H, H-1), 8.85 (br. s, 1H, exchange with $D_2O$, NH), 8.13 (m, 2H, H-4 and H-5), 7.87 (t, $J$ = 7.3 Hz, 1H, H-2), 7.80 (d, $J$ = 9.3 Hz, 1H, H-6), 7.70 (t, $J$ = 7.4 Hz, 1H, H-3), 3.10 (m, 6H, $CH_2$), 1.17 (t, $J$ = 7.3 Hz, 9H, $CH_3$). $^{13}C\{^1H\}$ NMR (75 MHz, DMSO-$d_6$): $\delta$ 173.7, 169.8, 167.1, 149.3, 148.6, 146.3, 133.7, 133.2 (CH), 129.8 (CH), 129.7 (CH), 127.1 (CH), 126.4, 125.3, 121.7, 120.5 (CH), 117.7 (CH), 109.2, 46.2 ($CH_2$), 9.1 ($CH_3$). IR (neat, $cm^{-1}$): 3036, 2984, 2877, 2167, 1658 (C═O), 1602, 1558, 1542. Anal. Calcd for $C_{24}H_{22}ClN_5O_2{\cdot}0.5H_2O$: C, 63.09; H, 5.07; N, 15.33. Found: C, 63.43; H, 4.90; N, 15.70.

**General Method for the Preparation of Compounds 3H and 4H.** 6,7-Dichloropyrido[1,2-*a*]benzimidazole-8,9-dione (**1**) (0.15 g, 0.56 mmol) was dissolved in DCM (250 mL). Then a solution of 1,3-indandione (**8**) (0.08 g, 0.56 mmol) in DCM (10 mL) or a solution of 3-(dicyanomethylene)indan-1-one (**9**) (0.11 g, 0.56 mmol) in MeCN (40 mL) was added at room temperature followed by the addition of $Et_3N$ (0.16 mL, 1.12 mmol). The reaction mixture was stirred for 24 h and then washed with a diluted HCl solution (0.1 M, 2 × 100 mL). The organic layer was separated, dried over $CaCl_2$, filtered, and concentrated under reduced pressure. The residue was recrystallized from MeCN.

*7-Chloro-6-(1,3-dioxo-2,3-dihydro-1H-inden-2-yl)benzo[4,5]-imidazo[1,2-a]pyridine-8,9-dione (**3H**).* Yield: 0.12 g (57%), red solid. Mp: >300 °C dec. MS: $C_{20}H_9ClN_2O_4$ requires $[M + H]^+$ 377.03; found $[M + H^+]^+$ 377.20. Both forms [enol (green) and diketo (red)] gave the same $^1H$ NMR spectra. $^1H$ NMR (300 MHz, DMSO-$d_6$) for the enol form: $\delta$ 9.13 (d, $J$ = 6.5 Hz, 1H, H-1), 7.94 (d, $J$ = 9.1 Hz, 1H, H-4), 7.78 (m, 1H, H-3), 7.46 (m, 5H, H-2 + $4H_{Indane}$). $^1H$ NMR (300 MHz, DMSO-$d_6$) for the diketo form: $\delta$ 9.04 (d, $J$ = 6.7 Hz, 1H, H-1), 8.07 (m, 5H, H-4 + $4H_{Indane}$), 7.63 (m, 1H, H-3), 7.37 (t, $J$ = 6.7 Hz, 1H, H-2), 5.57 (s, 1H, exchange with $D_2O$, CH). The compound is not soluble enough to record the $^{13}C$ NMR spectrum. IR (neat, $cm^{-1}$): 3096, 3025, 2959, 2923, 2851, 1746 (C═O), 1702 (C═O), 1656 (C═O), 1626, 1605, 1528. Anal. Calcd for $C_{20}H_9ClN_2O_4{\cdot}0.5MeCN$: C, 63.49; H, 2.66; N, 8.81. Found: C, 63.63; H, 2.77; N, 8.56.

*2-[2-(7-Chloro-8,9-dioxo-8,9-dihydrobenzo[4,5]imidazo[1,2-a]-pyridin-6-yl)-3-hydroxy-1H-inden-1-ylidene]malononitrile (**4H**).* Yield: 0.15 g (63%), dark solid. Mp: 270−272 °C. MS: $C_{23}H_9ClN_4O_3$ requires $[M + H]^+$ 425.04; found $[M + H^+]^+$ 425.20. $^1H$ NMR (300 MHz, DMSO-$d_6$): $\delta$ 9.12 (d, $J$ = 6.6 Hz, 1H, H-1), 8.09 (d, $J$ = 7.2 Hz, 1H, $H_{Indane}$), 7.95 (d, $J$ = 8.9 Hz, 1H, H-4), 7.77 (m, 1H, H-3), 7.50 (td, $J$ = 7.3, 1.9 Hz, 1H, H-2), 7.45 (d, $J$ = 7.0 Hz, 1H, $H_{Indane}$), 7.41 (dd, $J$ = 5.1, 3.3 Hz, 2H, $H_{Indane}$). $^{13}C\{^1H\}$ NMR (75 MHz, DMSO-$d_6$): $\delta$ 185.7, 176.3, 164.9, 158.0, 154.4, 149.3, 140.8, 140.6, 136.4, 132.9 (CH), 131.8 (CH), 130.6 (CH), 128.8 (CH), 121.6 (CH), 120.6 (CH), 120.6, 119.2, 118.9, 118.6 (CH), 118.5 (CH), 106.2, 80.4. IR (neat, $cm^{-1}$): 3105, 3072, 3050, 2210, 1678 (C═O), 1651 (C═O), 1615, 1601, 1569. Anal. Calcd for $C_{23}H_9ClN_4O_3{\cdot}0.5MeCN$: C, 64.73; H, 2.38; N, 14.15. Found: C, 64.93; H, 2.57; N, 13.83.

**2,2′-[2-(7-Chloro-8,9-dioxo-8,9-dihydrobenzo[4,5]imidazo-[1,2-*a*]pyridin-6-yl)-1*H*-indene-1,3(2*H*)-diylidene]-dimalononitrile (5H).** Compound **5** (0.1 g, 0.25 mmol) was dissolved in 100 mL of DCM and washed with a diluted HCl solution (0.1 M, 4 × 100 mL). The organic layer (without drying) was left for 12 h for compound **5H** to crystallize. The formed precipitate was filtered, and the crude solid was washed with DCM (2 × 25 mL) to afford the product as a beige solid. Yield: 0.05 g (61%), beige solid. Mp: >300 °C. MS: $C_{26}H_9ClN_6O_2$ requires $[M + H]^+$ 473.05; found $[M + H^+]^+$ 473.23. $^1H$ NMR (300 MHz, DMSO-$d_6$): $\delta$ 9.16 (d, $J$ = 6.5 Hz, 1H, H-1), 8.16 (dd, $J$ = 5.6, 3.1 Hz, 2H, $H_{Indane}$), 8.04 (d, $J$ = 8.8 Hz, 1H, H-4), 7.85 (t, $J$ = 6.9 Hz, 1H, H-3), 7.55 (dd, $J$ = 5.5, 3.2 Hz, 2H, $H_{Indane}$), 7.49 (t, $J$ = 8.0 Hz, 1H, H-2). $^{13}C\{^1H\}$ NMR (75 MHz, DMSO-$d_6$): $\delta$ 176.9, 163.8, 155.6, 154.6, 150.1, 139.4, 137.7, 134.3, 133.8 (CH), 131.3 (CH), 129.2 (CH), 122.6 (2 × CH), 119.5 (CH), 118.5, 118.3, 117.4 (CN), 107.0 (CN), 52.9. IR (neat, $cm^{-1}$): 3096, 2956, 2202, 1691 (C═O), 1663, 1645 (C═O), 1594. Anal. Calcd for $C_{26}H_9ClN_6O_2{\cdot}0.33$ DCM: C, 63.11; H, 1.94; N, 16.77. Found: C, 63.31; H, 2.23; N, 16.63.

**2-[7-Chloro-8-hydroxy-9-oxobenzo[4,5]imidazo[1,2-*a*]-pyridin-6(9*H*)ylidene]malononitrile (6H).** Compound **6** (0.1 g, 0.25 mmol) was dissolved in 100 mL of a 1:1 MeCN/DCM mixture and washed with a diluted HCl solution (0.1 M, 2 × 100 mL). The organic layer (without drying) was concentrated under reduced pressure. The resulting precipitate was dried and recrystallized from MeCN. Yield: 0.07 g (94%), brown solid. Mp: >300 °C. MS: $C_{14}H_5ClN_4O_2$ requires $[M + H]^+$ 297.02; found $[M + H^+]^+$ 297.20. $^1H$ NMR (300 MHz, DMSO-$d_6$): $\delta$ 9.15 (d, $J$ = 6.7 Hz, 1H, H-1), 7.89 (d, $J$ = 9.0 Hz, 1H, H-4), 7.71 (m, 1H, H-3), 7.36 (t, $J$ = 6.8 Hz, 1H, H-2). $^{13}C\{^1H\}$ NMR (75 MHz, DMSO-$d_6$): $\delta$ 168.9, 165.1, 154.5, 148.6, 147.68, 142.6, 131.7 (CH), 128.1 (CH), 119.1, 118.8, 118.7 (CH), 117.9 (CH), 109.3. IR (neat, $cm^{-1}$): 3224, 2216, 1643 (C═O), 1633, 1587, 1557. Anal. Calcd for $C_{14}H_5ClN_4O_2$: C, 56.68; H, 1.70; N, 18.89. Found: C, 56.79; H, 1.93; N, 18.59.

## ■ ASSOCIATED CONTENT

### Supporting Information

The Supporting Information is available free of charge at https://pubs.acs.org/doi/10.1021/acs.joc.1c02196.



https://doi.org/10.1021/acs.joc.1c02196
J. Org. Chem. 2022, 87, 2345−2355

Additional experimental data, $^{1}H$ and $^{13}C\{^{1}H\}$ NMR and UV−vis absorption spectra, crystallographic data for compounds **2**, **6**, and **3H**, and calculation data (Cartesian coordinates, computed total energies of optimized structures, and TD-DFT-calculated UV−vis absorption data) (PDF)

### Accession Codes

CCDC 2079503−2079505 contain the supplementary crystallographic data for this paper. These data can be obtained free of charge via www.ccdc.cam.ac.uk/data_request/cif, or by emailing data_request@ccdc.cam.ac.uk, or by contacting The Cambridge Crystallographic Data Centre, 12 Union Road, Cambridge CB2 1EZ, UK; fax: +44 1223 336033.

## AUTHOR INFORMATION


### Corresponding Author

**Nelli Batenko** − *Riga Technical University, Riga LV-1048, Latvia*; Email: nelli.batenko@rtu.lv

### Authors

**Anastasija Gaile** − *Riga Technical University, Riga LV-1048, Latvia*; orcid.org/0000-0001-7268-573X

**Sergey Belyakov** − *Latvian Institute of Organic Chemistry, Riga LV-1006, Latvia*

**Baiba Turovska** − *Latvian Institute of Organic Chemistry, Riga LV-1006, Latvia*

Complete contact information is available at: https://pubs.acs.org/10.1021/acs.joc.1c02196


### Notes

The authors declare no competing financial interest.

## ACKNOWLEDGMENTS

This research/publication was supported by Riga Technical University's Doctoral Grant programme (34-14800-DOK.LĶI/20) and "Development of innovative face cosmetics with controlled release of active ingredients by use of Metal Organic Frameworks or Cocrystals" (ERAF Project 1.1.1.1/18/A/176). The authors thank Prof. V. Kampars for the guidance and valuable support and Mg. chem. Igors Mihailovs for assistance with the calculations.

## REFERENCES


(1) Son, E. J.; Kim, J. H.; Kim, K.; Park, C. B. Quinone and Its Derivatives for Energy Harvesting and Storage Materials. *J. Mater. Chem. A* **2016**, *4* (29), 11179−11202.

(2) Sugumaran, M. Reactivities of Quinone Methides versus O-Quinones in Catecholamine Metabolism and Eumelanin Biosynthesis. *Int. J. Mol. Sci.* **2016**, *17* (9), 1576.

(3) Bolton, J. Quinone Methide Bioactivation Pathway: Contribution to Toxicity and/or Cytoprotection? *Curr. Org. Chem.* **2014**, *18* (1), 61−69.

(4) Sieuw, L.; Jouhara, A.; Quarez, É.; Auger, C.; Gohy, J. F.; Poizot, P.; Vlad, A. A H-Bond Stabilized Quinone Electrode Material for Li-Organic Batteries: The Strength of Weak Bonds. *Chem. Sci.* **2019**, *10* (2), 418−426.

(5) Che, Y.; Perepichka, D. F. Quantifying Planarity in the Design of Organic Electronic Materials. *Angew. Chemie - Int. Ed.* **2021**, *60* (3), 1364−1373.

(6) Norkov, S. V.; Cherkasov, A. V.; Shavyrin, A. S.; Arsenyev, M. V.; Kuropatov, V. A.; Cherkasov, V. K. Annulation of a 1,3-Dithiole Ring to a Sterically Hindered o-Quinone Core. Novel Ditopic Redox-Active Ligands. *Beilstein J. Org. Chem.* **2021**, *17*, 273−282.

(7) Albold, U.; Hoyer, C.; Neuman, N. I.; Sobottka, S.; Hazari, A. S.; Lahiri, G. K.; Sarkar, B. Isolable Cu(I) Complexes of Extremely Electron-Poor, Completely Unreduced o-Quinone and "Di- o-Quinone" Ligands Stabilized through $\pi$-$\pi$ Interactions in the Secondary Coordination Sphere. *Inorg. Chem.* **2019**, *58* (6), 3754−3763.

(8) Nielson, K. V.; Zhang, L.; Zhang, Q.; Liu, T. L. A Strategic High Yield Synthesis of 2,5-Dihydroxy-1,4-Benzoquinone Based MOFs. *Inorg. Chem.* **2019**, *58* (16), 10756−10760.

(9) Kubanik, M.; Lam, N. Y. S.; Holtkamp, H. U.; Söhnel, T.; Anderson, R. F.; Jamieson, S. M. F.; Hartinger, C. G. Quinoline-Para-Quinones and Metals: Coordination-Assisted Formation of Quinoline-Ortho-Quinones. *Chem. Commun.* **2018**, *54* (8), 992−995.

(10) Ansari, M. A.; Beyer, K.; Schwederski, B.; Kaim, W.; Lahiri, G. K. Diruthenium Complexes of P-Benzoquinone−Imidazole Hybrid Ligands: Innocent or Noninnocent Behavior of the Quinone Moiety. *Chem. - An Asian J.* **2018**, *13* (19), 2947−2955.

(11) Kwong, H. C.; Chidan Kumar, C. S.; Mah, S. H.; Mah, Y. L.; Chia, T. S.; Quah, C. K.; Lim, G. K.; Chandraju, S. Crystal Correlation Of Heterocyclic Imidazo[1,2-*a*]Pyridine Analogues and Their Anticholinesterase Potential Evaluation. *Sci. Rep.* **2019**, *9* (1), 1−15.

(12) Stasyuk, A. J.; Cywiński, P. J.; Gryko, D. T. Excited-State Intramolecular Proton Transfer in 2′-(2′-Hydroxyphenyl)Imidazo-[1,2-*a*]Pyridines. *J. Photochem. Photobiol. C Photochem. Rev.* **2016**, *28*, 116−137.

(13) Srivastava, S.; Thakur, N.; Singh, A.; Shukla, P.; Maikhuri, V. K.; Garg, N.; Prasad, A.; Pandey, R. Development of a Fused Imidazo[1,2-*a*] Pyridine Based Fluorescent Probe for $Fe^{3+}$ and $Hg^{2+}$ in Aqueous Media and HeLa Cells. *RSC Adv.* **2019**, *9* (51), 29856−29863.

(14) Batenko, N.; Belyakov, S.; Kiselovs, G.; Valters, R. Synthesis of 6,7-Dichloropyrido[1,2-*a*]Benzimidazole-8,9-Dione and Its Analogues and Their Reactions with Nucleophiles. *Tetrahedron Lett.* **2013**, *54* (35), 4697−4699.

(15) Dähne, S.; Leupold, D. Coupling Principles in Organic Dyes. *Angew. Chem., Int. Ed. Engl.* **1966**, *5* (12), 984−993.

(16) Berger, S.; Hertl, P.; Rieker, A. Physical and Chemical Analysis of Quinones. In *The Quinonoid Compounds*; John Wiley & Sons, Ltd., 1988; pp 29−78.

(17) Schade, A.; Schreiter, K.; Rüffer, T.; Lang, H.; Spange, S. Interactions of Enolizable Barbiturate Dyes. *Chem. - A Eur. J.* **2016**, *22* (16), 5734−5748.

(18) Mohammadi Ziarani, G.; Aleali, F.; Lashgari, N. Recent Applications of Barbituric Acid in Multicomponent Reactions. *RSC Adv.* **2016**, *6* (56), 50895−50922.

(19) Telitel, S.; Dumur, F.; Kavalli, T.; Graff, B.; Morlet-Savary, F.; Gigmes, D.; Fouassier, J.-P.; Lalevée, J. The 1,3-Bis-(Dicyanomethylidene)Indane Skeleton as a (Photo) Initiator in Thermal Ring Opening Polymerization at RT and Radical or Cationic Photopolymerization. *RSC Adv.* **2014**, *4* (31), 15930.

(20) Huang, J.; Tang, H.; Yan, C.; Li, G. 1,1-Dicyanomethylene-3-Indanone End-Cap Engineering for Fused-Ring Electron Acceptor-Based High-Performance Organic Photovoltaics. *Cell Reports Phys. Sci.* **2021**, *2* (1), 100292.

(21) Francos, J.; García-Garrido, S. E.; Borge, J.; Suárez, F. J.; Cadierno, V. Butadiene Dyes Based on 3-(Dicyanomethylidene)-Indan-1-One and 1,3-Bis(Dicyanomethylidene)Indane: Synthesis, Characterization and Solvatochromic Behaviour. *RSC Adv.* **2016**, *6* (9), 6858−6867.

(22) Shimizu, A.; Ishizaki, Y.; Horiuchi, S.; Hirose, T.; Matsuda, K.; Sato, H.; Yoshida, J. I. HOMO-LUMO Energy-Gap Tuning of $\pi$-Conjugated Zwitterions Composed of Electron-Donating Anion and Electron-Accepting Cation. *J. Org. Chem.* **2021**, *86* (1), 770−781.

(23) Poddel'sky, A. I.; Druzhkov, N. O.; Fukin, G. K.; Cherkasov, V. K.; Abakumov, G. A. Bifunctional Iminopyridino-Catechol and Its o-Quinone: Synthesis and Investigation of Coordination Abilities. *Polyhedron* **2017**, *124*, 41−50.

(24) Lin, R. B.; He, Y.; Li, P.; Wang, H.; Zhou, W.; Chen, B. Multifunctional Porous Hydrogen-Bonded Organic Framework Materials. *Chem. Soc. Rev.* **2019**, *48* (5), 1362−1389.
(25) Pascal, S.; Haefele, A.; Monnereau, C.; Charaf-Eddin, A.; Jacquemin, D.; Le Guennic, B.; Andraud, C.; Maury, O. Expanding the Polymethine Paradigm: Evidence for the Contribution of a Bis-Dipolar Electronic Structure. *J. Phys. Chem. A* **2014**, *118* (23), 4038−4047.
(26) Sigalov, M.; Lemcoff, N. G.; Shainyan, B.; Chipanina, N.; Aksamentova, T. Enol Forms of 1,3-Indanedione, Their Stabilization by Strong Hydrogen Bonding, and Zwitterion-Assisted Interconversion. *Eur. J. Org. Chem.* **2010**, *2010*, 2800−2811.
(27) Heo, J.; Lim, C. K.; Whang, D. R.; Shin, J.; Jeong, S. Y.; Park, S. Y.; Kwon, I. C.; Kim, S. Self-Deprotonation and Colorization of 1,3-Bis(Dicyanomethylidene)Indan in Polar Media: A Facile Route to a Minimal Polymethine Dye for NIR Fluorescence Imaging. *Chem. - A Eur. J.* **2012**, *18* (28), 8699−8704.
(28) Batenko, N.; Kricka, A.; Belyakov, S.; Turovska, B.; Valters, R. A Novel Method for the Synthesis of Benzimidazole-Based 1,4-Quinone Derivatives. *Tetrahedron Lett.* **2016**, *57* (3), 292−295.
(29) Skancke, A.; Skancke, P. N. General and Theoretical Aspects of Quinones. In *The Quinonoid Compounds*; John Wiley & Sons, Ltd., 1988; pp 1−28.
(30) Anaflous, A.; Albay, H.; Benchat, N. E.; El Bali, B.; Dušek, M.; Fejfarová, K. 2-Phenyl-Imidazo[1,2-a]Pyridine-3-Carbaldehyde. *Acta Crystallogr., Sect. E: Crystallogr. Commun.* **2008**, *64* (5), o927.
(31) Chen, T.; Zheng, L.; Yuan, J.; An, Z.; Chen, R.; Tao, Y.; Li, H.; Xie, X.; Huang, W. Understanding the Control of Singlet-Triplet Splitting for Organic Exciton Manipulating: A Combined Theoretical and Experimental Approach. *Sci. Rep.* **2015**, *5* (May), 1−11.
(32) Lu, T.; Chen, F. Multiwfn: A Multifunctional Wavefunction Analyzer. *J. Comput. Chem.* **2012**, *33* (5), 580−592.
(33) Kamlet, M. J.; Taft, R. W. Solvent Hydrogen-Bond Acceptor (HBA) Basicities. *J. Am. Chem. Soc.* **1976**, *98* (2), 377−383.
(34) Pascal, S.; Haefele, A.; Monnereau, C.; Charaf-Eddin, A.; Jacquemin, D.; Le Guennic, B.; Maury, O.; Andraud, C. On the Versatility of Electronic Structures in Polymethine Dyes. *Opt. Photonics Counterterrorism, Crime Fight. Def. X; Opt. Mater. Biomater. Secur. Def. Syst. Technol. XI* **2014**, *9253*, 92531A.
(35) Bello, K. A.; Cheng, L.; Griffiths, J. Near-Infrared Absorbing Methine Dyes Based on Dicyanovinyl Derivatives of Indane-1,3-Dione. *J. Chem. Soc. Perkin Trans. 2* **1987**, *6*, 815−818.
(36) Gottlieb, H. E.; Kotlyar, V.; Nudelman, A. NMR Chemical Shifts of Common Laboratory Solvents as Trace Impurities. *J. Org. Chem.* **1997**, *62*, 7512−7515.





https://doi.org/10.1021/acs.joc.1c02196
*J. Org. Chem.* 2022, 87, 2345−2355

2. Pielikums

Appendix 2

Anastasija Gaile, Sergey Belyakov, Vitālijs Rjabovs, Igors Mihailovs,
Baiba Turovska, and Nelli Batenko

# Investigation of Weak Noncovalent Interactions Directed by the Amino Substituent of Pyrido- and Pyrimido-[1,2-*a*]benzimidazole-8,9-diones

*ACS Omega* **2023**, *8*, 40960−40971

DOI: 10.1021/acsomega.3c07005

ACS OMEGA

Open Access



http://pubs.acs.org/journal/acsodf

Article

# Investigation of Weak Noncovalent Interactions Directed by the Amino Substituent of Pyrido- and Pyrimido-[1,2-*a*]benzimidazole-8,9-diones

Anastasija Gaile, Sergey Belyakov, Vitālijs Rjabovs, Igors Mihailovs, Baiba Turovska, and Nelli Batenko*

Cite This: *ACS Omega* 2023, 8, 40960−40971

Read Online

ACCESS | Metrics & More | Article Recommendations | Supporting Information

**ABSTRACT:** Quinones are small redox-active molecules that are able to form intra- and intermolecular interactions both in the solid state and in solution. On the basis of 6-amino-substituted pyrido- and pyrimido-[1,2-*a*]benzimidazole-8,9-diones, weak interactions were investigated by single-crystal X-ray and $^1$H NMR spectroscopy methods. Crystallization of quinone derivatives containing a −NH−$CH_2$− fragment led to the formation of both chiral and achiral crystals. The presence of two forms with (*endo* form) and without (*exo* form) an intramolecular hydrogen bond was experimentally detected by X-ray crystallography analysis and variable-temperature (VT) $^1$H NMR experiments in the cases of *iso*pentylamino- and benzylamino-substituted derivatives. Interestingly, the *exo* form dominates both in the solid state and in solution.

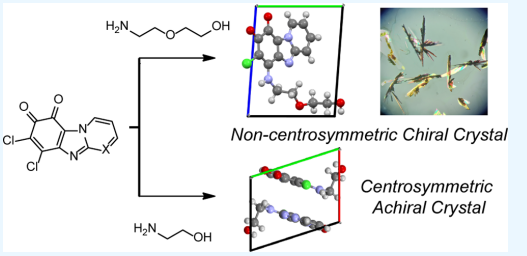




## INTRODUCTION

Quinones and quinone derivatives are small molecules involved in numerous significant biological processes such as photosynthesis,[1] cellular respiration,[2] intra- and extracellular signaling,[3] and metabolic transformations with cytotoxic or cytoprotective effects.[4] Quinones are used as cocatalysts in palladium catalysis[5] and electron-transfer mediators in metal catalyzed reactions,[6] as well as redox reservoirs in water electrolysis processes.[7] Promising results were achieved for the application of quinone derivatives as quinone electrode materials[8,9] for Li−organic batteries,[10,11] zinc−organic[12] batteries, and metal-free symmetric quinone-acid cells.[13]

It is known[14] that the relatively weak intra- and intermolecular interactions influence different physicochemical properties such as the melting/boiling point, the solubility, the morphologies, and the charge transport in organic materials. As quinones are conjugated cyclic diketones, their carbonyl groups can form hydrogen bonds (H-bonds) with different groups (e.g., −OH or $-NH_2$). As a result, stabilization of the supramolecular structure of quinone derivatives by a network of synergistic noncovalent forces (H-bonding and $\pi-\pi$ stacking) was observed.[10,11,15] For example, thermal stability and low solubility of 2,5-diamino-1,4-benzoquinone[10] in battery electrolytes were demonstrated and explained by the formation of a H-bond between amino and carbonyl groups polarized by electronic delocalization. Another example is a stabilization of the supramolecular structure of 2,3-diamino-7,8-dihydroxyphenazine-1,4-dione[11] by intermolecular interactions and $\pi-\pi$ stacking. The rational design of quinone derivatives can be used for the construction of ordered redox-active molecular solids.[16] It was demonstrated[17,18] that crystallization and supramolecular assembly can be controlled by the combination of different inter- and intramolecular interactions, but the use of such a control is still a complex problem.

It was reported[19] that quinones with replaceable halide substituents react with amines, amino alcohols, and amino acids: the formation of a carbon−nitrogen bond does not produce a new chirality center as it proceeds via an addition/elimination sequence. Conformationally flexible fragments with proton-donating abilities may allow the stabilization of different modes of H-bonds[20] that in turn can affect the formation of supramolecular systems as well as physical properties of the resulting compounds. The development of a generalized data set of substituents with the ability to form multiple H-bonds in the solid state as well as in solution is essential. Therefore, there remains a demand to establish possible weak intra- and intermolecular interactions of quinone derivatives because understanding such interactions can provide a useful approach to designing new materials in general and crystal engineering in particular.[21]

**Received:** September 13, 2023
**Accepted:** September 26, 2023
**Published:** October 19, 2023





https://doi.org/10.1021/acsomega.3c07005
*ACS Omega* 2023, 8, 40960−40971

We selected pyrido- and pyrimido-[1,2-*a*]benzimidazole-8,9-diones for the investigation of the formation of intra- and intermolecular interactions upon modification of the initial core with amines and amino alcohols. Initial compounds (**1a,b**) contain a combination of *o*-quinone and imidazo[1,2-*a*]pyridine (H-bond acceptor) fragments. Imidazo[1,2-*a*]-pyridine derivatives tend to form intramolecular H-bonds between the substituent and nitrogen of the heterocycle.[22] It was observed that derivatives of pyrido- and pyrimido[1,2-*a*]benzimidazole-8,9-dione (Scheme 1a) possessing an electron-withdrawing group at the C(6) position can form H-bonded dimers[23] as well as $\pi-\pi$ stacking interactions in the solid state.[24]

**Scheme 1. (a) Synthesis of Compounds 3a−g and 4a,b (Compounds 3d,e Were Isolated as Hydrochloride Salts); (b) Mesomeric Forms of Derivatives 3a−g and 4a,b**

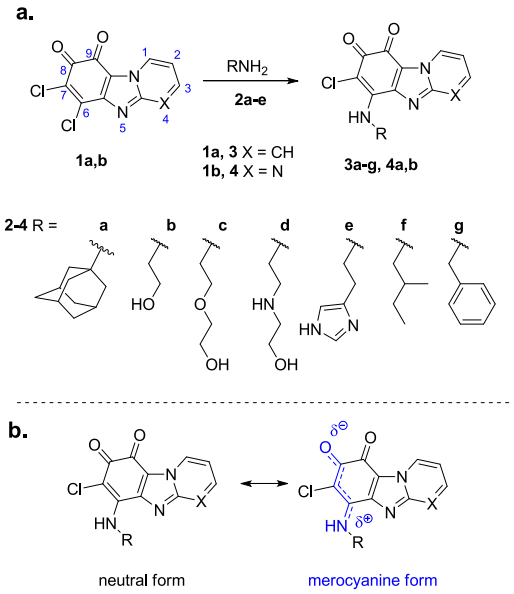


## RESULTS AND DISCUSSION

**Synthesis.** In this work, quinone derivatives **3a−g** and **4a,b** were obtained via a simple one-step nucleophilic substitution reaction using different amines **2a,e−g**, aminoethanol (**2b**), and its elongated analogues 2-(2-aminoethoxy)ethanol (**2c**) and 2-((2-aminoethyl)amino)ethanol (**2d**) (Scheme 1a). The choice of primary amines was based on (i) the presence of a H-bond-donating group and (ii) different numbers of $CH_2$ groups attached to $NH_2$. All of these features can affect the formation of H-bonds and properties of the resulting compounds. It is known[24] that in the case of heterocyclic quinones **1a,b** nucleophilic substitution (carried out in an aprotic solvent) proceeds selectively and provides only the C(6) substituted product.

Compounds **3a−g** and **4a,b** possess H-bond-acceptor functionality (carbonyl groups) at one part and H-donor functionality (NH) at the opposite part of the molecule. In the case of compounds **3b−e** and **4b**, functional groups of the side chain can provide additional sites for the formation of H-bonds.

It is known[25] that hydrolysis of 6-*N*,*N*-diethylaminopyrido-[1,2-*a*]benzimidazole-8,9-dione led to the formation of the 1,4-quinone core. Interestingly, compound **5** (with an *o*-quinone core) was obtained during recrystallization of compound **3g** from ethanol (Scheme 2).

**Scheme 2. Formation of Compound 5**

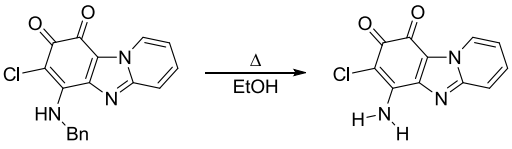


Additionally, signals of compound **5** and benzaldehyde were detected in a DMSO-$d_6$ solution of **3g** after 2 weeks by analysis of the $^1$H NMR spectrum (Figure S36). The existence of the amino group was proved by $^1$H NMR, two-dimensional (2D) $^1$H−$^1$H nuclear Overhauser effect spectroscopy (NOESY), and 2D $^1$H−$^1$H exchange spectroscopy (EXSY) NMR and Fourier-transform infrared (FTIR) spectra. It is worth mentioning that protons of the amino group were observed as two broad signals at 8.16 and 8.65 ppm ($^1$H NMR spectra in DMSO-$d_6$ solution, Figure S31), but addition of molecular sieves led to the coalescence of signals to one broad one that appeared at 8.41 ppm (Figure S35).

**Single-Crystal X-ray Studies.** The most demonstrative evidence of a H-bond existing in a crystal structure is the detection of close contacts via X-ray analysis. Diffraction data were collected at low temperatures on a Rigaku, XtaLAB Synergy, Dualflex, HyPix (Hybrid Pixel Array Detector) diffractometer using monochromated Cu−K$\alpha$ radiation ($\lambda$ = 1.54184 Å). An empirical absorption correction was performed using spherical harmonics, implemented in the SCALE3 ABSPACK scaling algorithm. The crystal structures were solved by direct methods using intrinsic phasing and refined by full-matrix least squares. All nonhydrogen atoms were refined in anisotropical approximation; hydrogen atoms involved in H-bonds were refined isotropically, and other H atoms were refined by the riding model. All calculations were performed with the help of Olex2 software.[26] Single-crystal X-ray crystallography data of compounds **3c−g** and **4a,b** can be found in the Supporting Information (Table S2, Figures S37−S51). For further details, see the crystallographic data for the compounds deposited at the Cambridge Crystallographic Data Centre (see Accession Codes in Supporting Information).

To avoid the formation of H-bonding between the *o*-quinone derivative and a protic solvent, aprotic solvent or solvents mixture (*n*-hexane, toluene, DCM, or acetonitrile) was used for the crystallization step. Only crystals of compound **3e** were obtained from methanol due to the poor solubility in aprotic solvents. Hirshfeld surfaces (for compounds **3c−d,g** and **4a,b**) and energy framework calculations[27] (for compounds **3c,g** and **4a,b**) were obtained (except for compounds **3e** and **3f** due to disorder of the crystal structure) in a whole-of molecule approach to explore intermolecular interactions in the crystal packing using the B3LYP/6-31G(d,p) energy model


https://doi.org/10.1021/acsomega.3c07005
ACS Omega 2023, 8, 40960−40971

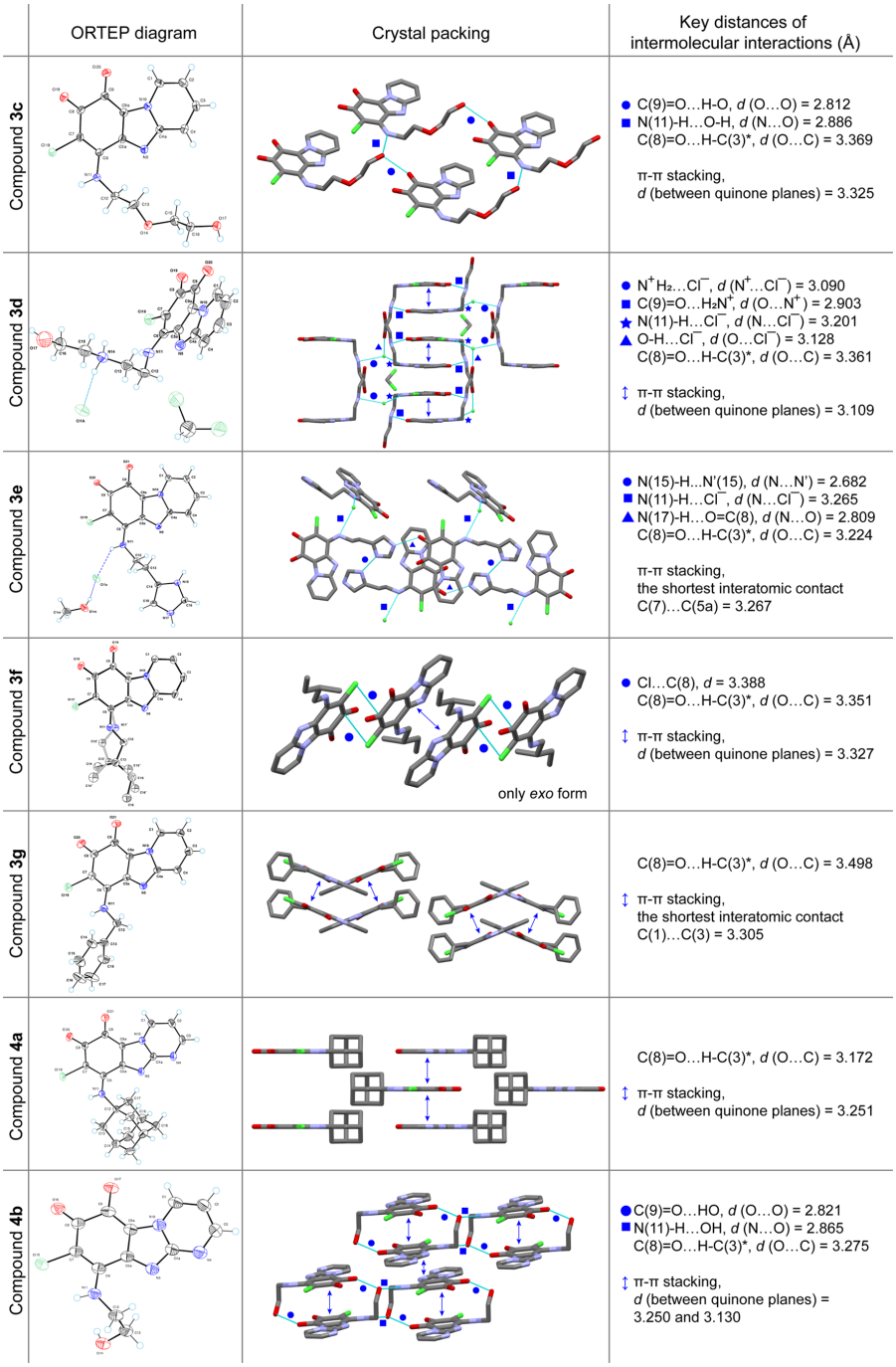


**Figure 1.** Oak ridge thermal ellipsoid plot (ORTEP) diagrams of the asymmetric unit for compounds **3c**−**g** and **4b** and the molecule of compound **4a** showing thermal ellipsoids at the 50% probability level. For the sake of clarity, all hydrogen atoms were omitted in the ORTEP diagram of compound **3f** and methanol molecules were omitted in the crystal packing of compound **3e**. Crystal packing with H-bonds and $\pi-\pi$ stacking marked with graphical symbols; key distances are listed, respectively. * This interaction is not shown in crystal packing.



https://doi.org/10.1021/acsomega.3c07005
ACS Omega 2023, 8, 40960−40971

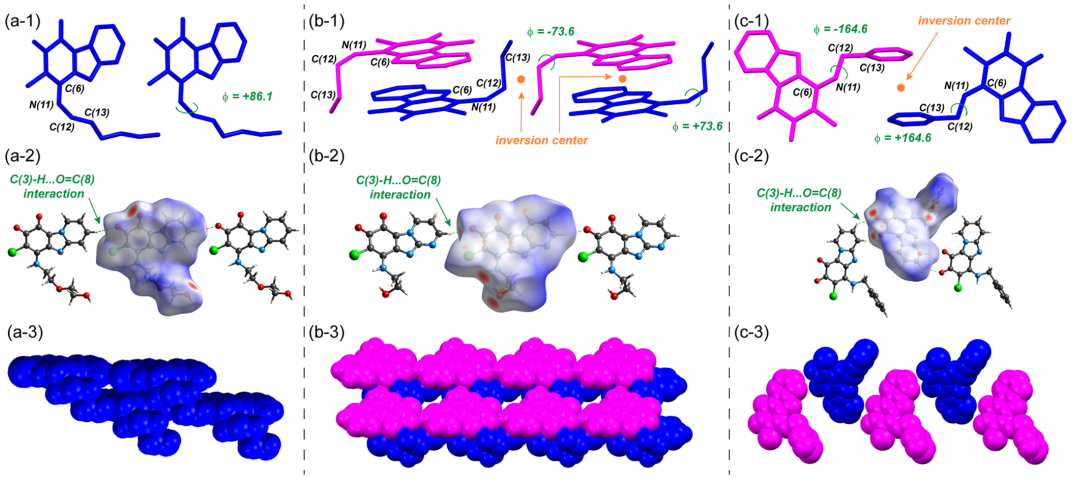


**Figure 2.** Crystal structures of (a) compound **3c**, (b) compound **4b**, and (c) compound **3g** were chosen as representatives of the (1) torsion angles of (+)-conformer (colored in blue) and (−)-conformer (colored in magenta). (2) Top view of Hirshfeld surfaces and 1D molecular chains with C(8)═O···H−C(3) contacts. (3) 1D hydrogen bonding motif: the (+)-conformer chain is shown in blue and the (−)-conformer chain is shown in magenta.

implemented in the CrystalExplorer21.5 program (Figures S52−S60).[28]

In the crystal structure of compounds **3c−g** and **4a,b**, a complicated balance between the various intermolecular forces was observed: in general, molecules of heterocyclic quinone derivatives are associated through strong to moderate[29] C(8)═O···H−C(3) H-bonds resulting in the formation of one-dimensional (1D) molecular chains. Heterocyclic quinone planes are held together by the $\pi-\pi$ stacking interactions that lead to the formation of layered motifs (2D structure). Functional groups of the amino substituent at the C(6) position determine different forms of intermolecular H-bonding of the side chains that resulted in three-dimensional (3D) H-bonded assemblies (Figures 1 and 2).

**Crystal Structures.** *Compound 3c.* Analysis of X-ray data showed that an achiral and conformationally flexible compound **3c** spontaneously crystallized into a noncentrosymmetric chiral crystal with the space group *P*1[30] with the Flack parameter close to zero. It is known[31] that the generation of chirality in the crystallization of achiral compounds is rare. Screening of 10 single crystals showed that the chirality of four of them corresponds to that of the crystal structure. For six single crystals, the crystal structure should be inverted. Thus, this substance represents a racemic conglomerate.

In the crystal packing of compound **3c**, a typical head-to-head columnar stacking was observed, which is essential for chiral crystallization.[31] H-bond networks were formed by the intermolecular interaction of OH···O═C(9) as well as NH···OH.

The architecture of crystal packing depends on the structure of the amino alcohol (e.g., distance from the OH group to the core), and changes such as replacement of the oxygen atom in the compound **3c** by the NH group (compound **3d**) lead to significant changes in intermolecular interactions.

*Compound 3d.* Compound **3d** was isolated as a salt with protonation occurring at the N(14) position due to the more pronounced basicity of this nitrogen compared to the other nitrogen atoms in the molecule. A complex 3D H-bond network was formed by C(9)═O···$NH_2^+$ interactions as well as intermolecular contacts between the chloride ion and proton-donor groups of three separate molecules simultaneously (Figure 1, vide infra Figure 4a).

*Compound 3e.* The X-ray data showed that chloride anions associated with molecular cations by means of H-bonds of the N(11)H···$Cl^-$ type and imidazole hydrogens are not involved in this bond. The imidazole cycle is in the fully staggered position to N(11) through the $CH_2-CH_2$ group. The protonated imidazole ring has two NH protons, both participating in the formation of strong intermolecular H-bonds. One of the imidazole hydrogens takes part in the H-bond with the nitrogen atom of another imidazole ring that are typical for imidazole derivatives.[32] In the crystal structure of compound **3e**, methanol molecules lie on the second-order rotation axes of symmetry. Since such axes do not refer to the own symmetry of methanol molecules, the molecules can be only disordered. Thus, in compound **3e** occurred a so-called disorder by symmetry. Methanol molecules with chloride anions form strong enough hydrogen bonds of the OH···Cl type with the length of 3.113 Å (H(1m)···Cl(1a) = 2.19 Å, and O(1m)−H(1m)···Cl(1a) = 168°). Since molecules of $CH_3OH$ lie on the 2-fold symmetry axis, the occupancy *g*-factors of all atoms of the molecules are equal to 0.5, i.e., the substance **3e** is a methanol semisolvate. It should be noted that the occupancy *g*-factor for the H(15) atom is 0.5 (as well as for the chloride anion, which lies on the 2-fold rotation axis of symmetry). Thus, compound **3e** represents a basic salt (Figure S42).

*Compound 3f.* Compound **3f** contains the aminoalkyl substituent at the C(6) position with the diastereotopic $CH_2$ group attached to N(11)H. The crystal structure of compound **3f** is achiral, and both configurations (*R* and *S*) of the C(13) atom are present since the racemic reagent **2f** was used. Interestingly, two molecular forms are found in crystals: *exo* and *endo* (vide infra, Figure 5a). The *endo* form is stabilized by an intramolecular H-bond of the NH···N type with the


https://doi.org/10.1021/acsomega.3c07005
ACS Omega 2023, 8, 40960−40971

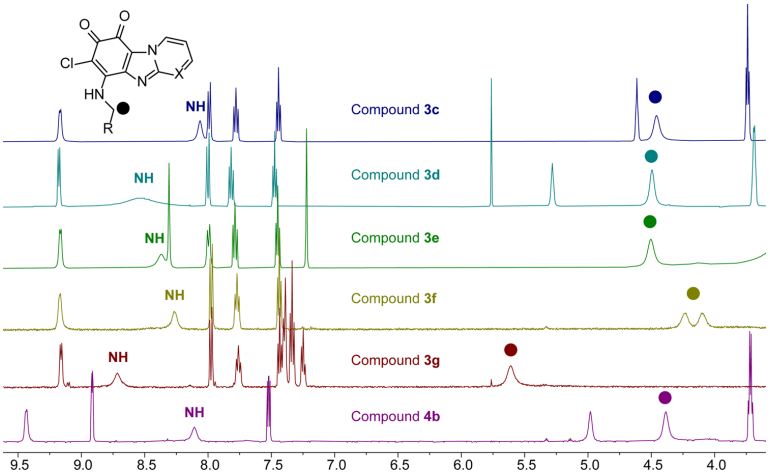


**Figure 3.** $^1$H NMR (500 MHz, DMSO-$d_6$) spectra of compounds **3c**−**g** and **4b**; signals of $\alpha CH_2$ protons are marked with circles.

following parameters: D···A *d* N(11′)···N(5) = 2.640 Å, N(11′)−H(11′)···N(5) = 114°. Because the *exo* and *endo* molecules or their mirror-image forms exist in the same crystallographic position, the crystal structure may be described with the help of the occupancy *g*-factors of the corresponding atoms. The main form (*exo* form) occupies 80%, while the *endo* form occupies 20%. The occupancy *g*-factors of atoms in the crystal structure (*g* = 0.8 and 0.2) were specified and fixed since at such values the thermal displacement parameters of the disordered atoms are close and have realistic values. At other values of *g*-factors, the thermal parameters become physically less realistic.

In the *exo* form, the methyl group (atom C(14)) is in the *gauche* position to nitrogen N(11), while the ethyl group (atoms C(15) and C(16)) is in the fully staggered position. In contrast, for the *endo* form, the methyl group (atom (C14′)) is in the fully staggered position to the amine nitrogen N(11′), but the ethyl group (atoms C(15′) and C(16′)) is in the *gauche* position. Despite the presence of the intramolecular H-bond, the *endo* form is a minor form in the crystals, which can be explained by an elongated C(6)−N(11′) bond in order to form an intramolecular H-bond (Table S3). Additionally, no strong intermolecular interactions were detected with the exception of the contact Cl···C(8), which can be interpreted as an $\pi$-hole interaction of medium strength.

*Compound* ***3g***. In the solid state of compound **3g**, head-to-tail columnar stacking is found. Each of the C−H hydrogens of the methylene group has intermolecular H-bonds with carbonyl groups of the quinone fragment (C−H···O═C′(8) and C−H···O═C″(9)). A complicated balance between repulsion interactions of phenyl rings and heterocyclic quinone planes stacked through $\pi$−$\pi$ stacking was observed (Figure S47). It is worth mentioning that in crystals of compound **3g**, a quite strong anisotropy of the imaginary part of the refraction index is observed. This leads to the fact that these crystals look red from one angle and greenish from another.

*Compound* ***4a***. The main intermolecular interaction in the case of compound **4a** is the H-bond between C(3)-H···O═C(8) and stabilizing interlayer interactions between bulky adamantyl substituents.

*Compound* ***4b***. In the case of compound **4b**, two modes of dimeric interactions were found in the crystal packing: H-bonds between the OH group of the substituent and carbonyl groups C(9)═O of *o*-quinone (centrosymmetric $R_2^2(20)$ dimer[33]) as well as H-bonds between aminoethanol side chains (centrosymmetric $R_2^2(8)$ dimer[33]). As a result, head-to-tail columnar stacking was accompanied by $\pi$−$\pi$ stacking.

Crystal packing analysis revealed similarities and differences between intermolecular interactions in the crystal structures. In general, X-ray data showed that nitrogen (N(11)) at the C(6) position of all studied compounds has a planar configuration as the sum of angles (C(6)−N(11)−H, H−N(11)−C(12), and C(12)−N(11)−C(6)) is close to 360° (Table S3). This observation can lead to the conclusion that partially charged merocyanine exists in the O═C(8)−C(7)−C(6)−N(11)H fragment (Scheme 1b) and formation of conformers in the solid state can be explained by the restricted rotation along the C(6)−N(11) axis. The Mayer bond order of the C(6)−N(11) bond was calculated using *Multiwfn*[34] software from single-crystal X-ray analysis data of compounds **3c**−**g** and **4b**. Calculations proved the partial double-bond character of the C(6)−N(11) bond (Table S3). It is known that derivatives of **1a** tend to form compounds that can be characterized as coupled polymethines.[23] The partially charged merocyanine fragment can facilitate the formation of the resonance-assisted hydrogen bond.[35]

Analysis of X-ray data showed that the achiral compound **3c** crystallized into a noncentrosymmetric chiral crystal that contains only (+) synclinal conformers (Figure 2a-1). Crystallization of derivatives **3d**−**g** and **4b** resulted in the formation of centrosymmetric and, hence, achiral crystals. From the crystallography point of view, such structures can be interpreted as a single rotamer (one of a set of conformers arising from the restricted rotation about a single bond[36]) accompanied by its inverse equivalent. Because of torsional differences at C(6)−N(11)−C(12)-C(13) fragment, molecules of compounds **3d** and **4b** in centrosymmetric crystals acquire both (+) and (−) synclinal (30−90°), molecules of compound **3e**- (+) and (−) anticlinal (90−150°), and molecules of compounds **3f**,**g**- (+) and (−) antiperiplanar


https://doi.org/10.1021/acsomega.3c07005
ACS Omega 2023, 8, 40960−40971

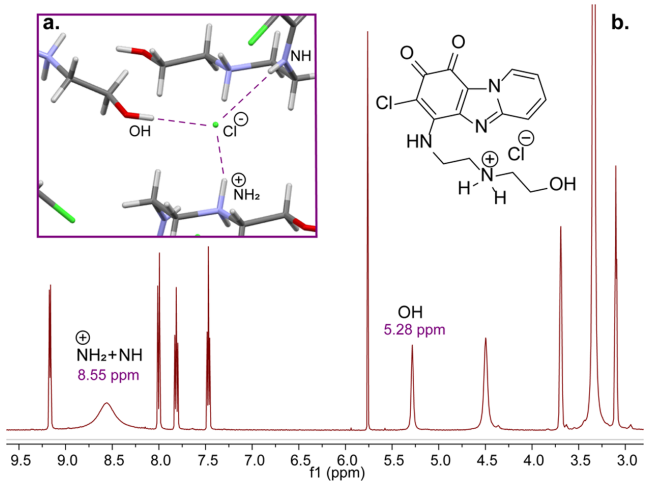


**Figure 4.** (a) Fragment of the H-bond network in the crystal packing of compound **3d** and (b) a fragment of the $^{1}$H-spectrum of the compound **3d**.

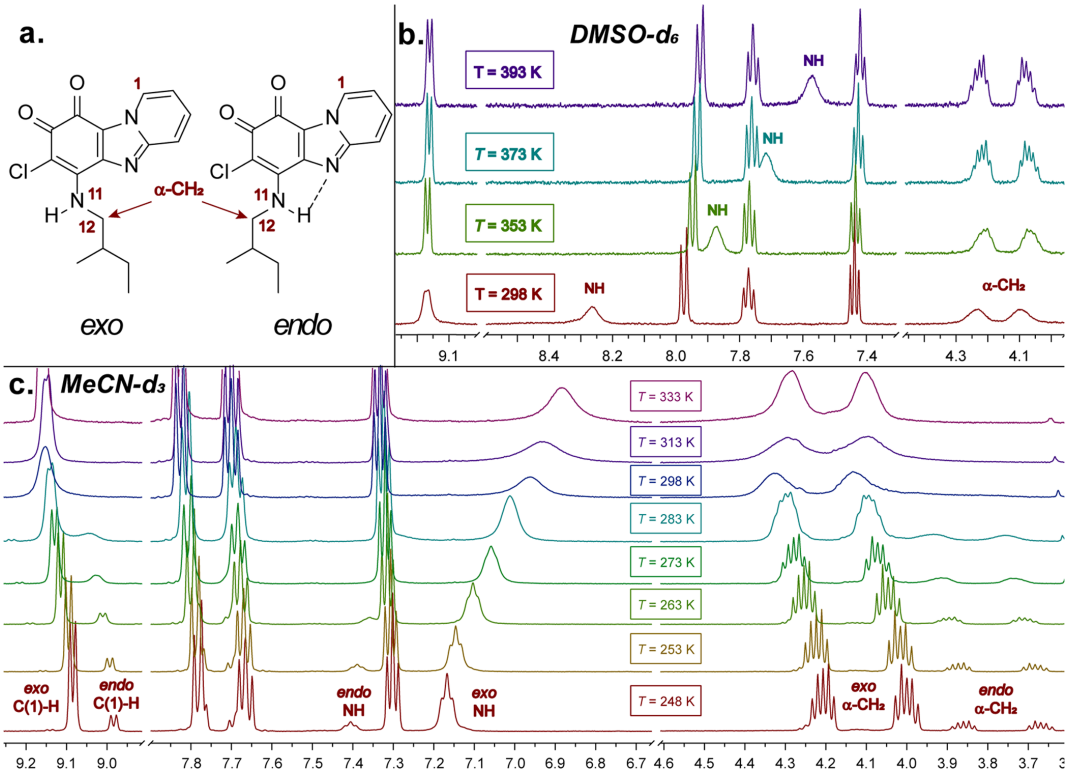


**Figure 5.** (a) Structures of *exo* and *endo* forms of compound **3f**. (b) Fragments of the VT $^{1}$H NMR spectrum (500 MHz, DMSO-$d_6$) of compound **3f** in the temperature range of 298−393 K and (c) fragments of the VT $^{1}$H NMR spectrum (500 MHz, MeCN-$d_3$) of compound **3f** in the temperature range of 248−333 K.

(150−180°) conformations (Figure 2a and Table S3). It was observed that antiperiplanar orientations were found in the crystal structure of compounds **3f** and **3g**, which bear a nonpolar substituent. Figure 2 shows a pair of conformers



https://doi.org/10.1021/acsomega.3c07005
ACS Omega 2023, 8, 40960−40971

connected by the inversion centers: blue-colored (+)-conformation and magenta-colored (−)-conformation. No conformers were detected in the case of compound **4a** due to the symmetrical structure of the introduced substituent and the absence of $-CH_2-$fragment necessary for the formation of a flexible moiety.

Molecules in the crystal structures of heterocyclic quinone derivatives (compounds **3c−g** and **4a,b**) are associated through strong to moderate[29] C(8)═O···H−C(3) H-bonds that lead to the formation of 1D molecular chains (Figures 1 and 2). Along this H-bond, 1D chains can be classified according to Kikkawa et al.[17] into two patterns: a straight pattern ([(+) or (−)] single conformer chains formed by H-bonds) observed in the case of compounds **3c−d,f** and **4b** (Figure 2a-3,b-3) and a zigzag pattern (chains that are formed through H-bonds and consisting of (+)- and (−)-conformers alternately associated with glide) in the case of compounds **3e** and **3g** (Figure 2c-3).

A common feature for all compounds is the $\pi-\pi$-stacking interaction that stabilizes head-to-head (compound **3c**) or head-to-tail (compounds **3d−g** and **4a,b**) columns. Distances between quinone planes lie in a range between 3.109 and 3.327 Å and are shorter than the sum of the van der Waals (vdW) radii (C 3.40 Å[37]). According to energy frameworks analysis, molecules are stacked in columns with dispersion dominated stacking. However, crystal structures of compound **3c** (Figure S53) and compound **4b** (Figure S57) represent balanced energy frameworks between electrostatic and dispersion contributions. Electrostatic energy is the largest for interaction between polar functional groups of flexible side chains; however, dispersion is the largest for the stacking motif between heterocyclic quinone planes.

**NMR Spectroscopy.** Analysis of $^1$H NMR spectra (DMSO-$d_6$) (**3b−g** and **4b**) showed two remarkable features corresponding to the $-NH-\alpha CH_2-$ (i.e., $-N(11)-H-C(12)H_2-$) fragment: protons of $\alpha CH_2$ appeared as broad-downfielded signals and NH proton signals were observed in the 7.99−8.72 ppm range (Figure 3).

Additionally, in the case of the hydrochloride salt **3d** NH and OH group signals were shifted downfield. It can be supposed that the trifurcated bond between the $Cl^-$anion, OH, and both $NH/NH_2^+$ groups (proved by single-crystal X-ray analysis in the solid state) exists in solution as well (Figure 4b).

To investigate the character of $-NH-\alpha CH_2-$ group signals, $^1$H NMR spectra were recorded at 298 K in several solvents of different polarities and abilities to form H-bonds with the substrate. Compounds **3f** and **3g** were chosen due to their better solubility in less polar solvents such as MeCN-$d_3$ and $CDCl_3$. MeCN and $CHCl_3$ are solvents with a lower polarity and H-bond basicity[38] than DMSO, and chemical shifts of NH and $\alpha CH_2$ protons can be sensitive to the solvent. Additionally, the existence of both forms (*endo* and *exo*) in solution (detected in the solid state in the case of compound **3f**, vide supra) was under consideration. To specify the diastereotopic protons of the $\alpha CH_2$ group of compound **3f**, $^1$H NMR resonance signals were assigned using 2D $^1$H−$^1$H COSY and $^1$H−$^{13}$C HSQC NMR spectra (Figures S17 and S18).

In DMSO-$d_6$ and MeCN-$d_3$ solutions at room temperature (298 K), signals of the *endo* form of compound **3f** were not detected. However, in a $CDCl_3$ solution, signals of both forms (*exo* and *endo*, Figure 5a) of compound **3f** were observed (Table 1 and Figure S15) with an *exo*/*endo* ratio of 70:30, which is close to the ratio observed in the crystal structure.

**Table 1. Chemical Shifts ($\delta$) of NH and $\alpha CH_2$ Protons in the $^1$H NMR Spectra (298 K) of Compounds 3f,g in Different Solvents**

| | | | chemical shifts ($\delta$), ppm | |
|---|---|---|---|---|
| cmpd. | solvent | hydrogen-bond basicity of solvents ($\beta_1$)[38] | N<u>H</u> | HN-$\alpha$C<u>H</u>$_2$ |
| **3f** | DMSO-$d_6$ | 0.71 | 8.26 | 4.10, 4.23 |
| | MeCN-$d_3$ | 0.37 | 6.96 | 4.33, 4.13 |
| | $CDCl_3$ | 0 | 6.24$^{exo}$ | 4.09, 4.28$^{exo}$ |
| | | | 6.79$^{endo}$ | 3.74, 3.92$^{endo}$ |
| **3g** | DMSO-$d_6$ | 0.71 | 8.72 | 5.69 |
| | MeCN-$d_3$ | 0.37 | ∼7.30 | 5.63 |
| | $CDCl_3$ | 0 | 6.34 | 5.50 |

Interestingly, compound **3g** showed no separate signals of the *endo* form in the $^1$H NMR spectra at 298 K in all three solvents used.

Solvent-dependent chemical shift of the NH signal is another notable feature. The formation of the solute−solvent complexes[39] between the NH proton and the solvent could explain a downfield shift of the NH signals in DMSO-$d_6$ relative to those in MeCN-$d_3$ and $CDCl_3$ for compounds **3f** and **3g**. Chemical shifts of the NH proton correlated well with the $\beta_1$ value (hydrogen-bond basicity)[38] of these solvents (Figures S16 and S28). Stabilization of the *exo* form by intermolecular interactions and formation of solute−solvent complexes in DMSO can compete with stabilization by an intramolecular H-bond that is well pronounced in less basic solvents.

The most remarkable feature of the $^1$H NMR spectra of compounds **3b−g** and **4b** is a broad-downfielded signal of the $\alpha CH_2$ protons in the DMSO-$d_6$ solution (Figure 3) as well as in MeCN-$d_3$ and $CDCl_3$ for compounds **3f** and **3g**. As the $^1$H NMR spectra of all compounds containing the NH-$\alpha CH_2$ fragment have a broad signal of the $\alpha CH_2$ protons, we supposed that compounds with no $\alpha CH_2$ group can have a different behavior in solution. With this idea in mind, compounds **3a** and **4a** were synthesized. As expected, their $^1$H NMR spectra can be easily interpreted and have no evidence of signal broadening (Figures S1 and S2) as well as no conformers detected in the crystal structure (vide supra).

Compounds **3b−e** and **4b** have the $-NH-\alpha CH_2-\underline{CH_2}$ fragment and signals of <u>the $CH_2$</u> group had clear splitting, suggesting that the broadening of the $\alpha CH_2$ signal is not affected by the rest of the side chain. Several factors may explain the character of the $\alpha CH_2$ signal, e.g., delocalization of electrons between N(11)H and C(8)═O groups (formation of the merocyanine fragment), which leads to a partially charged nitrogen.

In order to test the hindered rotation of the flexible side chain around the N(11)−C(12) bond in solution, quantum chemical calculations were utilized.[40] Geometry from X-ray data was used as initial structures for calculations of theoretical rotation barriers; conformation geometries were obtained by manually scanning along the torsion angle around the bond in question without relaxation of the remaining structure of the molecule. These structures were generated with Open Babel software.[41] For the (single-point) energy calculations, we used Gaussian 16, rev. C.01 computational software,[42] with a meta-hybrid functional MN15[43] and a double-hybrid functional DSD-PBEP86-D3(BJ),[44] which are reported in the literature to


https://doi.org/10.1021/acsomega.3c07005
ACS Omega 2023, 8, 40960−40971

be particularly suitable for computing both energy barriers and noncovalent interactions.[45,46] The results of these calculations (Figure S61) showed that the rotational barrier height ($\Delta G^{\ddagger}$) is around 2−4 kcal/mol for both compounds **3c** and **4b**, while a higher $\Delta G^{\ddagger}$ is observed for the compound **3d** (7 kcal/mol), as expected for cations. As the result of quantum chemical calculations, no evidence for high rotational barriers at the N(11)−C(12) bond of compounds **3c−d** and **4b** was provided; hence, dynamic rotational processes were excluded from consideration.

The cause of signal broadening could be nonequivalence of the $\alpha CH_2$ protons because of the outcome of the unsymmetrical structure[47] or existence of *exo* and *endo* forms at room temperature, despite the fact that only the *exo* form crystallized in all cases with the exception of compound **3f**.

Typically, intramolecularly H-bonded structures are more stable; still, X-ray data showed that in cases of compounds **3c−g** and **4b** the *exo* form is major in the solid state. However, the existence of trace amounts of the *endo* form cannot be excluded and can explain the unusually strong widening of the $\alpha CH_2$ resonance signal at room temperature. It is known[48] that intermolecular/intramolecular H-bonds are affected by elevated/low temperatures; thus, variable-temperature (VT) $^1$H NMR experiments were carried out.

The impossibility of cooling the DMSO solution prevents full variable-temperature study for the compound **3c**; therefore, it was studied only at elevated temperatures (Figure S7). First, $^1$H NMR resonance signals were assigned using a 2D $^1$H−$^1$H-COSY spectrum (Figure S6). At 353 K the broad signal of the $\alpha CH_2$ signal splits into a broad doublet. However, the NH proton is shifted upfield and the OH signal (initially appeared at 4.61 ppm) overlaps with the signal of water. The $^1$H NMR spectrum of the cooled solution was identical to the first one acquired at room temperature except for the signal of the OH proton. Thus, protons of $\alpha CH_2$, NH, and OH groups participate in the formation of intermolecular H-bonds in solution that were destroyed upon heating and restored back to room temperature.

We were able to follow the behavior of compounds **3f−g** (Figures 5, S21, and S29) with VT $^1$H NMR experiments due to their sufficient solubility in MeCN-$d_3$ at temperatures lower than room temperature. $^1$H NMR spectra (MeCN-$d_3$, 298 K) of both compounds **3f,g** (Figures 5c, S14, and S26) exhibited a set of broad signals corresponding to the signal of the NH group, $\alpha CH_2$ protons as well as a signal of the proton at the C(1) position of the heterocyclic core.

The $^1$H NMR spectrum of **3f** recorded in the MeCN-$d_3$ solution at 248 K showed narrowing and splitting of all broad signals (Figure 5c). An additional set of signals of low intensity (corresponding to the *endo* form) appeared, approving the existence of two forms (similar to the $^1$H NMR spectrum in the $CDCl_3$ solution at room temperature). A low-intensity signal of the NH group appeared at 7.41 ppm ($\Delta\delta$ = 0.24 ppm with respect to the *exo* form) that apparently belongs to the intramolecularly H-bonded *endo* form. The ratio of the observed *exo*/*endo* forms at 248 K in the MeCN-$d_3$ solution was 85:15, which is in good agreement with the *exo*/*endo* ratio in the solid state. In general, the intermolecular H-bond is weaker[49] and, in turn, NH signals involved in such a type of H-bonding are more temperature-dependent than NH signals of the intramolecularly bonded group. Correlation between the NH proton (*exo* form) chemical shift and temperature is linear for solutions in DMSO-$d_6$ (298−393 K, $R^2$ = 0.99) and in MeCN-$d_3$ (248−333 K, $R^2$ = 0.97) (Figures S20 and S22). Diastereotopic protons of the *endo* form ($\alpha CH_2$) showed clearly identifiable signals at 3.67 and 3.86 ppm and the signal of the C(1)-H proton appeared at 8.98 ppm with similar multiplicities as $\alpha CH_2$ and C(1)-H of the *exo* form: as a result, C(1)-H and $\alpha CH_2$ signals of the *endo* form shifted upfield (shielded), but the NH signal is downfield shifted (deshielded) relative to the signals of the *exo* form.

A single form of the compound **3f** was observed in the $^1$H NMR spectrum upon heating in a DMSO-$d_6$ solution at 393 K. The multiplicity of each signal ($\alpha CH_2$ group protons and C(1) proton) is similar to the multiplicity of the same signals in $^1$H NMR spectra recorded at cooling for MeCN-$d_3$ solutions. It can be supposed that only the monomer *exo* form was found upon heating in DMSO-$d_6$ as H-bonds are weakened at elevated temperatures (Figure 5b). Cooling the solution of compound **3f** in DMSO-$d_6$ to room temperature restored the original spectrum acquired initially.

It should be mentioned that chemical shifts and multiplicity of signals of heterocyclic core protons (with the exception of C(1)-H) as well as the side-chain protons (with the exception of $\alpha CH_2$ group protons) remained essentially unchanged during the cooling/heating processes.

The *endo* form of compound **3g** was also detected upon cooling in a MeCN-$d_3$ solution (Figure S30). At 253 K, $\alpha CH_2$ protons of the *endo* form exhibited a doublet ($J$ = 7.2 Hz) at 5.17 ppm and at the same time a doublet ($J$ = 7.1 Hz) of the *exo* form appeared at 5.61 ppm. The ratio of *exo*/*endo* forms of compound **3g** was similar to the ratio of *exo*/*endo* forms for compound **3f** at low temperatures.

Temperature - gradients ($\Delta\delta_{HN}/\Delta T$)[48,49] were calculated for compounds where temperature dependence of the NH proton chemical shift was observed (Table S1). These results confirm our previous findings about stabilization of different solvate−solvent interactions by the solvent and do not exclude the influence of the rest of the side chain on the strength of H-bonds.

## CONCLUSIONS

In summary, we synthesized pyrido- and pyrimido-[1,2-*a*]benzimidazole-8,9-dione derivatives in the reaction with simple primary amines and amino alcohols, providing the formation of the C−N bond. In the solid state, the derived compounds exist as partially charged merocyanines that lead to the restricted rotation along the C(6)−N(11) axis.

Crystallization of the resulting compounds led to different crystal structures where the noncentrosymmetric chiral crystal (**3c**) and centrosymmetric achiral crystals (**3d−g, 4a,b**) were detected. In the unit cell of centrosymmetric crystals, one rotamer and its inversion symmetry equivalent (with the opposite sign of torsion angle in the side chain) were found. Formation of 3D bonded networks due to multiple hydrogen bonds as well as other intermolecular interactions such as $\pi-\pi$ stacking and $\pi$−hole interaction was observed.

In the crystal structure of compound **3f**, two sets of different forms were observed: (1) (+)- and (−)-conformations characteristic to all derivatives with the −NH−$CH_2$− fragment; and (2) two forms with different relative orientations of the N−H bond with respect to quinone core: major *exo* (without an intramolecular H-bond) and minor *endo* (stabilized by an intramolecular H-bond) forms. Crystals of compounds **3c−e**, **3g**, and **4b** contain only the *exo* form. In a solution, due to intermolecular interactions of quinone



https://doi.org/10.1021/acsomega.3c07005
ACS Omega 2023, 8, 40960−40971

derivatives **3b−g** and **4b** with a proton-accepting solvent, the *exo* form is dominating; however, a less basic solvent (in the case of compound **3f**) increases the concentration of the *endo* form.

The selected compounds (**3f−g**) were chosen for the explanation of the unusual broadening of signals in $^1$H NMR spectra in a series of heterocyclic quinone derivatives with the −NH−$CH_2$− fragment in the side chain. A combination of X-ray analysis, $^1$H NMR, and VT $^1$H NMR data was used. The observed broadening of the signals can be interpreted by the presence of a minor *endo* form at room temperature, despite the fact that only the *exo* form crystallized in all cases with the exception of compound **3f**. Our results suggest that caution should be exercised when interpreting such spectra.

The formation of a chiral crystal can be expected in the case of unsymmetrical merocyanine with a flexible side chain (−NH−$CH_2$− fragment); however, this assumption requires a more detailed investigation on a greater number of pyrido- and pyrimido-[1,2-*a*]benzimidazole-8,9-diones derivatives as well as different crystallization conditions should be explored.

## METHODS

**Reagents.** Reagents and solvents were purified by standard means or used without further purification.

**Analytical Methods and Apparatus.** Melting points were measured on a Kruess KSP 11 Melting Point Analyzer. $^1$H NMR and $^{13}$C NMR spectra were recorded on the Bruker Avance 300 spectrometer or on the Bruker Avance 500 spectrometer (Bruker BioSpin GmbH, Rheinstetten, Germany) in DMSO-$d_6$, MeCN-$d_3$, or $CDCl_3$ solutions. Chemical shifts ($\delta$) were reported in parts per million and coupling constants ($J$) in Hz. The proton signals for residual nondeuterated solvents ($\delta$ 7.26 for $CDCl_3$, $\delta$ 2.50 for DMSO-$d_6$, $\delta$ 1.94 for MeCN-$d_3$) and carbon signals ($\delta$ 77.1 for $CDCl_3$, $\delta$ 39.5 for DMSO-$d_6$) were used as an internal standard- 50 for $^1$H NMR and $^{13}$C NMR spectra, respectively. Elemental CHN analysis was carried on a Euro Vector EA 3000 analyzer. IR spectra were recorded on a PerkinElmer Spectrum 100 FTIR spectrometer. The UV−vis absorption spectra were acquired with a PerkinElmer 35 UV/vis spectrometer using 1 cm length quartz cuvettes with a concentration of compound $c = 2.5 \times 10^{-5}$ M. Low-resolution mass spectra were acquired on a Waters EMD 1000MS mass detector (ESI+ mode, voltage 30 V) with an Xterra MS C18 5 $\mu$m 2.1 100 mm column and a gradient eluent mode using 0.1% HCOOH in deionized water and MeCN or MeOH.

**General Procedures and Characterization of Products.** 6,7-Dichloropyrido[1,2-*a*]benzimidazole-8,9-dione **1a** and 6,7-dichloropyrimido[1,2-*a*]benzimidazole-8,9-dione **1b** were prepared according to previously reported procedures.[24]

Compounds **3a−g**, **4a,b** are too insoluble to record a qualitative $^{13}$C NMR spectrum.

*Synthesis of Compounds **3a** and **4a**.* 1-Adamantanamine hydrochloride (precursor of **2a**, 0.53 g, 2.82 mmol) was dissolved in MeOH (5 mL), and a solution of KOH (0.16 g, 2.82 mmol) in MeOH was added. The resulting solution was stirred and then was added to a solution of 6,7-dichloropyrido-[1,2-*a*]benzimidazole-8,9-dione (**1a**) or 6,7-dichloropyrimido-[1,2-*a*]benzimidazole-8,9-dione (**1b**) (0.25 g, 0.94 mmol) in dichloromethane (DCM) (250 mL). The reaction mixture was stirred at room temperature for 72 h, and then, the reaction mixture was washed with water twice. The organic layer was dried over anhydrous $CaCl_2$ and evaporated under vacuum to get a dark-colored crude product. The precipitate was recrystallized from the DCM/*n*-hexane mixture and dried in air.

*6-(Adamantan-1-ylamino)-7-chlorobenzo[4,5]imidazo-[1,2-a]pyridine-8,9-dione (**3a**).* **Yield:** 0.12 g (34%), dark crystals. **MP**: 290 °C. **MS:** $C_{21}H_{20}ClN_3O_2$ requires $[M + H]^+$ 382.12; found $[M + H^+]^+$ 382.3. **$^1$H NMR (300 MHz, $CDCl_3$):** $\delta$ 9.28 (d, $J$ = 6.5 Hz, 1H, H-1), 7.83 (d, $J$ = 9.0 Hz, 1H, H-4), 7.61 (m, 1H, H-3), 7.23 (t, $J$ = 6.8 Hz, 1H, H-2), 6.56 (br.s, 1H, exchanges with $D_2O$, NH), 2.42 (s, 6H, $CH_2$ × 3), 2.24 (s, 3H, CH × 3), 1.79 (m, 6H, $CH_2$ × 3). **IR (KBr pellet, cm$^{-1}$):** 3348, 3100, 3035, 2989, 2910, 2846, 1655, 1626, 1572, 1499, 1449. **Anal. Calcd** for $C_{21}H_{20}ClN_3O_2$ + 0.5 $H_2O$: C, 64.53; H, 5.42; N, 10.75; found C, 64.45; H, 5.17; N, 10.72.

*9-(Adamantan-1-ylamino)-8-chlorobenzo[4,5]imidazo-[1,2-a]pyrimidine-6,7-dione (**4a**).* **Yield:** 0.22 g (64%), dark crystals. **MP**: >300 °C. **MS:** $C_{20}H_{19}ClN_4O_2$ requires $[M + H]^+$ 383.12; found $[M + H^+]^+$ 383.3. **$^1$H NMR (300 MHz, $CDCl_3$):** $\delta$ 9.50 (d, $J$ = 5.2 Hz, 1H, H-1), 8.86 (dd, $J$ = 3.4; 1.6 Hz, 1H, H-3), 7.32 (dd, $J$ = 5.3; 0.7 Hz, 1H, H-2), 6.66 (br.s, 1H, exchange with $D_2O$, NH), 2.45 (s, 6H, $CH_2$ × 3), 2.26 (s, 3H, CH × 3), 1.81 (dd, $J$ = 25.7, 12.1 Hz, 6H, $CH_2$ × 3). **IR (KBr pellet, cm$^{-1}$):** 3434, 3343, 3108, 3075, 3014, 2907, 2850, 1658, 1633, 1615, 1572, 1522, 1459, 1425. **Anal. Calcd** for $C_{20}H_{19}ClN_4O_2$: C, 62.74; H, 5.00; N, 14.63; found C, 62.86; H, 5.14; N, 14.57.

*Synthesis of Compounds **3b** and **4b**.* 6,7-Dichloropyrido-[1,2-*a*]benzimidazole-8,9-dione (**1a**) or 6,7-dichloropyrimido-[1,2-*a*]benzimidazole-8,9-dione (**1b**) (0.2 g, 0.75 mmol) was dissolved in DCM (250 mL). Then, aminoethanol (**2b**, 0.14 mL, 2.25 mmol) was added to the resulting solution. A precipitate was formed after stirring the reaction mixture for 3 h. The solution was filtered, and the dark solid was washed with EtOH and MeCN three times.

*7-Chloro-6-((2-hydroxyethyl)amino)benzo[4,5]imidazo-[1,2-a]pyridine-8,9-dione (**3b**).* **Yield:** 0.13 g (62%), dark crystals. **MP**: >300 °C. **MS:** $C_{13}H_{10}ClN_3O_3$ requires $[M + H]^+$ 292.04; found $[M + H^+]^+$ 292.2. **$^1$H NMR (300 MHz, DMSO-$d_6$):** $\delta$ 9.16 (d, $J$ = 6.0 Hz, 1H, H-1), 7.99 (d, $J$ = 9.0 Hz, 2H, H-4 and NH (exchange with $D_2O$)), 7.78 (t, $J$ = 8.0 Hz, 1H, H-3), 7.44 (t, $J$ = 6.8 Hz, 1H, H-2), 4.96 (br.s, 1H, exchange with $D_2O$, OH), 4.36 (s, 2H, $CH_2$), 3.74 (q, $J$ = 5.3 Hz, 2H, $CH_2$). **IR (KBr pellet, cm$^{-1}$):** 3380, 3195, 3087, 3024, 2967, 2922, 2874, 1650, 1616, 1571. **Anal. Calcd** for $C_{13}H_{10}ClN_3O_3$: C, 53.53; H, 3.46; N, 14.41; found C, 53.12; H, 3.70; N, 14.28.

*8-Chloro-9-((2-hydroxyethyl)amino)benzo[4,5]imidazo-[1,2-a]pyrimidine-6,7-dione (**4b**).* **Yield:** 0.08 g (37%), dark crystals. **MP**: 228−230 °C. **MS:** $C_{13}H_{10}ClN_3O_3$ requires $[M + H]^+$ 292.0; found $[M + H^+]^+$ 292.2. **$^1$H NMR (300 MHz, DMSO-$d_6$):** $\delta$ 9.43 (d, $J$ = 5.4 Hz, 1H, H-1), 8.91 (dd, $J$ = 4.0; 1.6 Hz, 1H, H-3), 7.52 (dd, $J$ = 6.5; 4.5 Hz, 1H, H-2), 5.00 (br.s, 1H, exchange with $D_2O$, OH), 4.37 (s, 2H, $CH_2$), 3.71 (m, 2H, $CH_2$). **IR (KBr pellet, cm$^{-1}$):** 3391, 3184, 1654, 1611, 1563, 1524, 1473, 1427. **Anal. Calcd** for $C_{13}H_{10}ClN_3O_3$+0.5$H_2O$ C, 47.77; H, 3.34; N, 18.57; found C, 47.84; H, 3.66; N, 18.25.

*7-Chloro-6-((2-(2-hydroxyethoxy)ethyl)amino)benzo[4,5]-imidazo[1,2-a]pyridine-8,9-dione (**3c**).* To a solution of 6,7-dichloropyrido[1,2-*a*]benzimidazole-8,9-dione (**1a**, 0.2 g, 0.75 mmol) in DCM (300 mL), 2-(2-aminoetoxy)ethanol (**2c**, 0.19 mL, 1.88 mmol) was added. The solution was stirred for 4 h, and then, the reaction mixture was washed with water. The


https://doi.org/10.1021/acsomega.3c07005
ACS Omega 2023, 8, 40960−40971

organic layer was dried over anhydrous $CaCl_2$ and evaporated under vacuum to get a dark-colored crude product. The precipitate was recrystallized from MeCN and dried in air. **Yield:** 0.15 g (60%), dark crystals. **MP**: 218−220 °C. **$^1$H NMR (500 MHz, DMSO-$d_6$):** $\delta$ 9.17 (d, $J$ = 5.6 Hz, 1H, H-1), 8.06 (br.s, 1H, exchange with $D_2O$, NH), 7.99 (d, $J$ = 9.0 Hz, 1H, H-4), 7.78 (t, $J$ = 8.0 Hz, 1H, H-3), 7.44 (t, $J$ = 6.8 Hz, 1H, H-2), 4.61 (s, 1H, exchange with $D_2O$, OH), 4.46 (s, 2H, $CH_2$), 3.74 (t, $J$ = 5.9 Hz, 2H, $CH_2$), 3.50 (s, 4H, $CH_2$). **IR (KBr pellet, cm$^{-1}$):** 3396, 3228, 3084, 2947, 2867, 1715, 1651, 1626, 1569, 1425. **Anal. Calcd** for $C_{15}H_{14}ClN_3O_4$: C, 53.66; H, 4.20; N, 12.52; found C, 53.80; H, 4.23; N, 12.61.

*2-((7-Chloro-8,9-dioxo-8,9-dihydrobenzo[4,5]imidazo-[1,2-a]pyridin-6-yl)amino)-N-(2-hydroxyethyl)-ethanaminium chloride (**3d**).* To a solution of 6,7-dichloropyrido[1,2-*a*]benzimidazole-8,9-dione (**1a**) (0.15 g, 0.56 mmol) in DCM, 2-(2-aminoethylamino)ethanol (**2d**, 0.14 mL, 1.40 mmol) was added. The solution was stirred for 4 h. A dark-colored precipitate was formed and filtered. The precipitate was washed with EtOH and MeCN three times and dried in air. **Yield:** 0.13 g (65%), dark crystals. **MP**: 229−232 °C. **$^1$H NMR (500 MHz, DMSO-$d_6$):** $\delta$ 9.17 (d, $J$ = 6.6 Hz, 1H, H-1), 8.55 (br.s, 3H, exchange with $D_2O$, NH), 8.00 (d, $J$ = 9.0 Hz, 1H, H-4), 7.81 (t, $J$ = 8.0 Hz, 1H, H-3), 7.47 (t, $J$ = 6.9 Hz, 1H, H-2), 5.28 (s, 1H, exchange with $D_2O$, OH), 4.43 (s, 2H, $CH_2$), 3.69 (s, 2H, $CH_2$), 3.36 (overlaps with $H_2O$ signal, t, $J$ = 5.8 Hz, 2H, $CH_2$), 3.10 (t, $J$ = 5.1 Hz, 2H, $CH_2$). **IR (KBr pellet, cm$^{-1}$):** 3368, 3187, 3040, 2826, 1648, 1616, 1563, 1535, 1522, 1497, 1447. **Anal. Calcd** for $C_{15}H_{16}Cl_2N_4O_3$+0.5$CH_2Cl_2$: C, 45.79; H, 4.08; N, 13.35; found C, 45.41; H, 4.46; N, 13.76.

*6-((2-(1H-Imidazol-4-yl)ethyl)amino)-7-chlorobenzo[4,5]-imidazo[1,2-a]pyridine-8,9-dione (**3e**).* Histamine dihydrochloride (precursor of **2e**, 0.2 g, 1.12 mmol) was dissolved in MeOH (5 mL), and a solution of KOH (0.12 g, 2.24 mmol) in MeOH was added. The resulting solution was added to a solution of 6,7-dichloropyrido[1,2-*a*]benzimidazole-8,9-dione (**1a**, 0.15 g, 0.56 mmol) in DCM (250 mL). The reaction mixture was stirred at room temperature for 72 h. The organic layer was evaporated under vacuum until 20 mL to get a dark-colored crude product. The dark-colored precipitate was filtrated, recrystallized from MeOH, and dried in air. **Yield:** 0.12 g (63%), dark powder. **MP**: 225−227 °C. **MS:** $C_{16}H_{12}ClN_5O_2$ requires $[M + H]^+$ 342.1; found $[M + H^+]^+$ 342.3. **$^1$H NMR (500 MHz, DMSO-$d_6$):** $\delta$ 9.17 (d, $J$ = 5.7 Hz, 1H, H-1), 8.37 (br.s, 1H, exchange with $D_2O$, NH), 8.31 (s, 1H, $CH_{imidazole}$), 8.00 (d, $J$ = 8.8 Hz, 1H, H-4), 7.79 (t, $J$ = 8.0 Hz, 1H, H-3), 7.45 (t, $J$ = 6.9 Hz, 1H, H-2), 7.22 (s, 1H, $CH_{imidazole}$), 4.50 (s, 2H, $CH_2$), 3.05 (t, $J$ = 6.7 Hz, 2H, $CH_2$). **IR (KBr pellet, cm$^{-1}$):** 3291, 3145, 2886, 2814, 163, 1660, 1609, 1547, 1514. **Anal. Calcd** for $C_{16}H_{12}ClN_5O$ + 0.5 Cl + 0.5 $CH_3OH$ ($C_{33}H_{29}Cl_3N_{10}O_5$ known from X-ray analysis) C, 52.71; H, 3.89; N, 18.63; found C, 52.74; H, 4.04; N, 18.42.

*7-Chloro-6-((2-methylbutyl)amino)benzo[4,5]imidazo-[1,2-a]pyridine-8,9-dione (**3f**).* 6,7-Dichloropyrido[1,2-*a*]-benzimidazole-8,9-dione (**1a**) (0.2 g, 0.75 mmol) was dissolved in DCM (250 mL). Then, isopentylamine (**2f**, 0.16 mL, 1.88 mmol) was added to the resulting solution. The reaction mixture was stirred at room temperature for 2 h. Then, the reaction mixture in DCM was washed with water twice. The organic layer was dried over anhydrous $CaCl_2$ and evaporated under vacuum to get a dark-colored crude product. The precipitate was recrystallized from a toluene/*n*-hexane mixture and was dried in air. **Yield:** 0.11 g (65%), dark powder. **MP**: 174−176 °C. **MS:** $C_{16}H_{16}ClN_3O_2$ requires $[M + H]^+$ 318.1; found $[M + H^+]^+$ 318.4. **$^1$H NMR (500 MHz, DMSO-$d_6$):** $\delta$ 9.17 (d, $J$ = 3.5 Hz, 1H, H-1), 8.27 (br.s, 1H, exchange with $D_2O$, NH), 7.97 (d, $J$ = 9.0 Hz, 1H, H-4), 7.77 (t, $J$ = 7.9 Hz, 1H, H-3), 7.44 (t, $J$ = 6.9 Hz, 1H, H-2), 4.10 (s, 1H, $CH_2$ (diastereotopic)), 4.23 (s, 1H, $CH_2$ (diastereotopic)), 1.86 (dq, $J$ = 12.9, 6.6 Hz, 1H, CH), 1.48 (dt, $J$ = 12.8, 6.8 Hz, 1H, $CH_2$ (diastereotopic)), 1.20 (dd, $J$ = 13.9, 7.3 Hz 1H, $CH_2$ (diastereotopic)), 0.92 (dd, $J$ = 7.3, Hz, 6H, 2 × $CH_3$). **IR (KBr pellet, cm$^{-1}$):** 3468, 3371, 3082, 3022, 2962, 2875, 1655, 1626, 1571, 1494. **Anal. Calcd** for $C_{16}H_{16}ClN_3O_2$ C, 60.47; H, 5.08; N, 13.22; found C, 60.81; H, 5.22; N, 13.05.

*6-(Benzylamino)-7-chlorobenzo[4,5]imidazo[1,2-a]-pyridine-8,9-dione (**3g**).* 6,7-Dichloropyrido[1,2-*a*]-benzimidazole-8,9-dione (**1a**) (0.2 g, 0.75 mmol) was dissolved in DCM (250 mL). Then, benzylamine (**2g**, 0.14 mL, 2.25 mmol) was added to the resulting solution. The reaction mixture was stirred at room temperature for 24 h and then was washed with water twice. The organic layer was dried over anhydrous $CaCl_2$ and evaporated under vacuum to get a dark-colored crude product. The precipitate was recrystallized from the DCM/*n*-hexane mixture and was dried in air. **Yield:** 0.14 g (67%), dark powder. **MP**: 174−177 °C. **MS:** $C_{18}H_{12}ClN_3O_2$ requires $[M + H]^+$ 338.1; found $[M + H^+]^+$ 338.3. **$^1$H NMR (500 MHz, DMSO-$d_6$):** $\delta$ 9.16 (d, $J$ = 6.4 Hz, 1H, H-1), 8.72 (br.s, 1H, exchange with $D_2O$, NH), 7.98 (d, $J$ = 9.0 Hz, 1H, H-4), 7.76 (t, $J$ = 8.1 Hz, 1H, H-3), 7.43 (t, $J$ = 6.9 Hz, 1H, H-2), 7.40 (d, $J$ = 7.4 Hz, 2H, $CH_{arom.}$), 7.34 (t, $J$ = 7.6 Hz, 2H, $CH_{arom.}$), 7.25 (t, $J$ = 7.2 Hz, 1H, $CH_{arom.}$), 5.61 (s, 1H, $CH_2$). **IR (KBr pellet, cm$^{-1}$):** 3438, 3359, 3105, 3040, 2885, 1665, 1623, 1569, 1497. **Anal. Calcd** for $C_{18}H_{12}ClN_3O_2$ C, 64.01; H, 3.58; N, 12.44; found C, 63.61; H, 3.74; N, 12.37.

*6-Amino-7-chlorobenzo[4,5]imidazo[1,2-a]pyridine-8,9-dione (**5**).* **Yield:** 0.04 g (51%), dark-red crystals. **MP**: >300 °C. **MS:** $C_{11}H_6ClN_3O_2$ requires $[M + H]^+$ 248.1; found $[M + H^+]^+$ 248.3. **$^1$H NMR (500 MHz, DMSO-$d_6$):** $\delta$ 9.10 (d, $J$ = 6.7 Hz, 1H, H-1), 8.65 (br.s, 1H, exchange with $D_2O$, NH), 8.15 (br.s, 1H, exchange with $D_2O$, NH), 7.95 (d, $J$ = 9.0 Hz, 1H, H-4), 7.78 (m, 1H, H-3), 7.43 (t, $J$ = 6.9 Hz, 1H, H-2). **$^{13}$C NMR (125 MHz, DMSO-$d_6$):** 171.9, 168.6, 148.9, 148.5, 147.3, 132.1 (CH), 128.6 (CH), 119.2, 118.6 (CH), 118.3 (CH), 114.9. **IR (KBr pellet, cm$^{-1}$):** 3448, 3246, 3204, 1657, 1628, 1583, 1542, 1501, 1448. **Anal. Calcd** for $C_{11}H_6ClN_3O_2$ C, 53.80; H, 2.44; N, 16.97; found C, 53.87; H, 2.71; N, 16.65.

## ■ ASSOCIATED CONTENT

### Data Availability Statement

The data underlying this study are available in the published article and its Supporting Information.

### Supporting Information

The Supporting Information is available free of charge at https://pubs.acs.org/doi/10.1021/acsomega.3c07005.

Figures of $^1$H NMR spectra (for compounds **3a**−**g**, **4a**,**b**, and **5**), 2D $^1$H−$^1$H COSY NMR spectra (for compounds **3c**−**f**), $^1$H−$^{13}$C HSQC NMR spectra (for compound **3f**) as well as full VT $^1$H NMR spectra for compound **3c** (in DMSO-$d_6$ solution), compound **3f** (in DMSO-$d_6$ and MeCN-$d_3$ solutions), and compound **3g** (in MeCN-$d_3$ solution); single-crystal X-ray analysis data with ORTEP diagrams of the asymmetric unit for compounds **3c**−**g** and **4a**,**b**; and figures of Hirshfeld



https://doi.org/10.1021/acsomega.3c07005
ACS Omega 2023, 8, 40960−40971

surfaces and energy frameworks calculated with CrystalExplorer software (PDF)

## AUTHOR INFORMATION


### Corresponding Author

**Nelli Batenko** − *Riga Technical University, Faculty of Materials Science and Applied Chemistry, Riga LV-1048, Latvia*; Email: nelli.batenko@rtu.lv

### Authors

**Anastasija Gaile** − *Riga Technical University, Faculty of Materials Science and Applied Chemistry, Riga LV-1048, Latvia*; orcid.org/0000-0001-7268-573X

**Sergey Belyakov** − *Latvian Institute of Organic Chemistry, Riga LV-1006, Latvia*

**Vitālijs Rjabovs** − *Riga Technical University, Faculty of Materials Science and Applied Chemistry, Riga LV-1048, Latvia*

**Igors Mihailovs** − *Riga Technical University, Faculty of Computer Science and Information Technology, Riga LV-1048, Latvia; University of Latvia, Institute of Solid State Physics, Riga LV-1063, Latvia*

**Baiba Turovska** − *Latvian Institute of Organic Chemistry, Riga LV-1006, Latvia*

Complete contact information is available at: https://pubs.acs.org/10.1021/acsomega.3c07005


### Author Contributions

N.B.: Supervision, conceptualization, writing—original draft, review and editing. A.G.: Investigation, writing—original draft, review and editing, visualization, funding acquisition. S.B., V.R., and B.T.: Investigation. I.M.: Formal analysis. All authors approved the final version of the manuscript.

### Notes

The authors declare no competing financial interest.

## ACKNOWLEDGMENTS

This work was supported by the European Social Fund within Project No. 8.2.2.0/20/I/008 ≪Strengthening of PhD students and academic personnel of Riga Technical University and BA School of Business and Finance in the strategic fields of specialization≫ of the Specific Objective 8.2.2 ≪To Strengthen Academic Staff of Higher Education Institutions in Strategic Specialization Areas≫ of the Operational Programme ≪Growth and Employment≫. This research/publication was supported by Riga Technical University's Doctoral Grant program (DOK.LKI/21).

## REFERENCES


(1) De Causmaecker, S.; Douglass, J. S.; Fantuzzi, A.; Nitschke, W.; Rutherford, A. W. Energetics of the Exchangeable Quinone, Q_B, in Photosystem II. *Proc. Natl. Acad. Sci. U.S.A.* **2019**, *116* (39), 19458−19463.

(2) Anand, A.; Chen, K.; Yang, L.; Sastry, A. V.; Olson, C. A.; Poudel, S.; Seif, Y.; Hefner, Y.; Phaneuf, P. V.; Xu, S.; Szubin, R.; Feist, A. M.; Palsson, B. O. Adaptive Evolution Reveals a Tradeoff between Growth Rate and Oxidative Stress during Naphthoquinone-Based Aerobic Respiration. *Proc. Natl. Acad. Sci. U.S.A.* **2019**, *116* (50), 25287−25292.

(3) Ji, Q.; Zhang, L.; Jones, M. B.; Sun, F.; Deng, X.; Liang, H.; Cho, H.; Brugarolas, P.; Gao, Y. N.; Peterson, S. N.; Lan, L.; Bae, T.; He, C. Molecular Mechanism of Quinone Signaling Mediated through S-Quinonization of a YodB Family Repressor QsrR. *Proc. Natl. Acad. Sci. U.S.A.* **2013**, *110* (13), 5010−5015.

(4) Bolton, J. L.; Dunlap, T. Formation and Biological Targets of Quinones: Cytotoxic versus Cytoprotective Effects. *Chem. Res. Toxicol.* **2017**, *30* (1), 13−37.

(5) Salazar, C. A.; Flesch, K. N.; Haines, B. E.; Zhou, P. S.; Musaev, D. G.; Stahl, S. S. Tailored Quinones Support High-Turnover Pd Catalysts for Oxidative C−H Arylation with O 2. *Science* **2020**, *370* (6523), 1454−1460.

(6) Piera, J.; Bäckvall, J.-E. Catalytic Oxidation of Organic Substrates by Molecular Oxygen and Hydrogen Peroxide by Multistep Electron Transfer—A Biomimetic Approach. *Angew. Chem., Int. Ed.* **2008**, *47* (19), 3506−3523.

(7) Wang, F.; Sheng, H.; Li, W.; Gerken, J. B.; Jin, S.; Stahl, S. S. Stable Tetrasubstituted Quinone Redox Reservoir for Enhancing Decoupled Hydrogen and Oxygen Evolution. *ACS Energy Lett.* **2021**, 1533−1539.

(8) Son, E. J.; Kim, J. H.; Kim, K.; Park, C. B. Quinone and Its Derivatives for Energy Harvesting and Storage Materials. *J. Mater. Chem. A* **2016**, *4* (29), 11179−11202.

(9) Han, C.; Li, H.; Shi, R.; Zhang, T.; Tong, J.; Li, J.; Li, B. Organic Quinones towards Advanced Electrochemical Energy Storage: Recent Advances and Challenges. *J. Mater. Chem. A* **2019**, *7* (41), 23378−23415.

(10) Sieuw, L.; Jouhara, A.; Quarez, É.; Auger, C.; Gohy, J.-F.; Poizot, P.; Vlad, A. A H-Bond Stabilized Quinone Electrode Material for Li−Organic Batteries: The Strength of Weak Bonds. *Chem. Sci.* **2019**, *10* (2), 418−426.

(11) Tuttle, M. R.; Davis, S. T.; Zhang, S. Synergistic Effect of Hydrogen Bonding and $\pi-\pi$ Stacking Enables Long Cycle Life in Organic Electrode Materials. *ACS Energy Lett.* **2021**, *6* (2), 643−649.

(12) Lin, Z.; Shi, H.-Y.; Lin, L.; Yang, X.; Wu, W.; Sun, X. A High Capacity Small Molecule Quinone Cathode for Rechargeable Aqueous Zinc-Organic Batteries. *Nat. Commun.* **2021**, *12* (1), No. 4424.

(13) Tong, L.; Jing, Y.; Gordon, R. G.; Aziz, M. J. Symmetric All-Quinone Aqueous Battery. *ACS Appl. Energy Mater.* **2019**, *2* (6), 4016−4021.

(14) Wang, C. Weak Intermolecular Interactions for Strengthening Organic Batteries. *Energy Environ. Mater.* **2020**, *3* (4), 441−452.

(15) Zheng, S.; Shi, D.; Sun, T.; Zhang, L.; Zhang, W.; Li, Y.; Guo, Z.; Tao, Z.; Chen, J. Hydrogen Bond Networks Stabilized High-Capacity Organic Cathode for Lithium-Ion Batteries. *Angew. Chem., Int. Ed.* **2023**, *62* (9), No. e202217710, DOI: 10.1002/anie.202217710.

(16) Langis-Barsetti, S.; Maris, T.; Wuest, J. D. Triptycene 1,2-Quinones and Quinols: Permeable Crystalline Redox-Active Molecular Solids. *J. Org. Chem.* **2018**, *83* (24), 15426−15437.

(17) Kikkawa, S.; Masu, H.; Katagiri, K.; Okayasu, M.; Yamaguchi, K.; Danjo, H.; Kawahata, M.; Tominaga, M.; Sei, Y.; Hikawa, H.; Azumaya, I. Characteristic Hydrogen Bonding Observed in the Crystals of Aromatic Sulfonamides: 1D Chain Assembly of Molecules and Chiral Discrimination on Crystallization. *Cryst. Growth Des.* **2019**, *19* (5), 2936−2946.

(18) Corpinot, M. K.; Bučar, D.-K. A Practical Guide to the Design of Molecular Crystals. *Cryst. Growth Des.* **2019**, *19* (2), 1426−1453.

(19) Formen, J. S. S. K.; Wolf, C. Chiroptical Switching and Quantitative Chirality Sensing with (Pseudo)Halogenated Quinones. *Angew. Chem., Int. Ed.* **2021**, *60* (52), 27031−27038.

(20) Helmers, I.; Ghosh, G.; Albuquerque, R. Q.; Fernández, G. Pathway and Length Control of Supramolecular Polymers in Aqueous Media via a Hydrogen Bonding Lock. *Angew. Chem., Int. Ed.* **2021**, *60* (8), 4368−4376.

(21) Edwards, A. J.; Mackenzie, C. F.; Spackman, P. R.; Jayatilaka, D.; Spackman, M. A. Intermolecular Interactions in Molecular Crystals: What's in a Name? *Faraday Discuss.* **2017**, *203*, 93−112.

(22) Mutai, T.; Muramatsu, T.; Yoshikawa, I.; Houjou, H.; Ogura, M. Development of Imidazo[1,2-a]Pyridine Derivatives with an Intramolecular Hydrogen-Bonded Seven-Membered Ring Exhibiting

Bright ESIPT Luminescence in the Solid State. *Org. Lett.* **2019**, *21* (7), 2143−2146.
(23) Gaile, A.; Belyakov, S.; Turovska, B.; Batenko, N. Synthesis of Asymmetric Coupled Polymethines Based on a 7-Chloropyrido[1,2- a ]Benzimidazole-8,9-Dione Core. *J. Org. Chem.* **2022**, *87* (5), 2345−2355.
(24) Batenko, N.; Belyakov, S.; Kiselovs, G.; Valters, R. Synthesis of 6,7-Dichloropyrido[1,2-a]Benzimidazole-8,9-Dione and Its Analogues and Their Reactions with Nucleophiles. *Tetrahedron Lett.* **2013**, *54* (35), 4697−4699.
(25) Batenko, N.; Kricka, A.; Belyakov, S.; Turovska, B.; Valters, R. A Novel Method for the Synthesis of Benzimidazole-Based 1,4-Quinone Derivatives. *Tetrahedron Lett.* **2016**, *57* (3), 292−295.
(26) Dolomanov, O. V.; Bourhis, L. J.; Gildea, R. J.; Howard, J. A. K.; Puschmann, H. OLEX2: A Complete Structure Solution, Refinement and Analysis Program. *J. Appl. Crystallogr.* **2009**, *42* (2), 339−341.
(27) Turner, M. J.; Thomas, S. P.; Shi, M. W.; Jayatilaka, D.; Spackman, M. A. Energy Frameworks: Insights into Interaction Anisotropy and the Mechanical Properties of Molecular Crystals. *Chem. Commun.* **2015**, *51* (18), 3735−3738.
(28) Spackman, P. R.; Turner, M. J.; McKinnon, J. J.; Wolff, S. K.; Grimwood, D. J.; Jayatilaka, D.; Spackman, M. A. CrystalExplorer : A Program for Hirshfeld Surface Analysis, Visualization and Quantitative Analysis of Molecular Crystals. *J. Appl. Crystallogr.* **2021**, *54* (3), 1006−1011.
(29) Giacovazzo, C.; Monaco, H.; Artioli, G.; Viterbo, D.; Ferraris, G.; Gilli, G.; Zanotti, G.; Catti, M. *Fundamentals of Crystallography*, 2nd ed.; Oxford University Press, 2002.
(30) Adawy, A. Functional Chirality: From Small Molecules to Supramolecular Assemblies. *Symmetry* **2022**, *14* (2), 292.
(31) Matsuura, T.; Koshima, H. Introduction to Chiral Crystallization of Achiral Organic Compounds: Spontaneous Generation of Chirality. *J. Photochem. Photobiol., C* **2005**, *6* (1), 7−24.
(32) Miao, Y.; Fu, R.; Zhou, H.-X.; Cross, T. A. Dynamic Short Hydrogen Bonds in Histidine Tetrad of Full-Length M2 Proton Channel Reveal Tetrameric Structural Heterogeneity and Functional Mechanism. *Structure* **2015**, *23* (12), 2300−2308.
(33) Etter, M. C.; MacDonald, J. C.; Bernstein, J. Graph-set Analysis of Hydrogen-bond Patterns in Organic Crystals. *Acta Crystallogr., Sect. B: Struct. Sci.* **1990**, *46* (2), 256−262.
(34) Lu, T.; Chen, F. Multiwfn: A Multifunctional Wavefunction Analyzer. *J. Comput. Chem.* **2012**, *33* (5), 580−592.
(35) Steiner, T. The Hydrogen Bond in the Solid State. *Angew. Chem., Int. Ed.* **2002**, *41*, 48−76.
(36) Eliel, L. E.; Wilen, H. S. *Stereochemistry of Organic Compounds*; John Wiley & Sons, Inc.: New York, 1994.
(37) Mantina, M.; Chamberlin, A. C.; Valero, R.; Cramer, C. J.; Truhlar, D. G. Consistent van Der Waals Radü for the Whole Main Group. *J. Phys. Chem. A* **2009**, *113* (19), 5806−5812.
(38) Laurence, C.; Legros, J.; Chantzis, A.; Planchat, A.; Jacquemin, D. A Database of Dispersion-Induction DI, Electrostatic ES, and Hydrogen Bonding A1and Δ1solvent Parameters and Some Applications to the Multiparameter Correlation Analysis of Solvent Effects. *J. Phys. Chem. B* **2015**, *119* (7), 3174−3184.
(39) Sigalov, M.; Shainyan, B.; Chipanina, N.; Ushakov, I.; Shulunova, A. Intra- and Intermolecular N□H···O Hydrogen Bonds in Pyrrolyl Derivatives of Indane-1,3-Dione—Experimental and Theoretical Study. *J. Phys. Org. Chem.* **2009**, *22* (12), 1178−1187.
(40) Institute of Solid State Physics. *The Computations Were Performed on Latvian SuperCluster (LaSC)*; University of Latvia, 2023 The computations were performed on Latvian SuperCluster (LaSC), located in the Institute of Solid State Physics, University of Latvia.
(41) O'Boyle, N. M.; Banck, M.; James, C. A.; Morley, C.; Vandermeersch, T.; Hutchison, G. R. Open Babel: An Open Chemical Toolbox. *J. Cheminform.* **2011**, *3* (1), 33.
(42) Frisch, M. J.; Trucks, G. W.; Schlegel, H. B.; Scuseria, G. E.; Robb, M. A.; Cheeseman, J. R.; Scalmani, G.; Barone, V.; Petersson, G. A.; Nakatsuji, H.; Li, X.; Caricato, M.; Marenich, A. V.; Bloino, J.; Janesko, B. G.; Gomperts, R.; Mennucci, B.; Hratchian, H. P.; Ortiz, J. V.; Izmaylov, A. F.; Sonnenberg, J. L.; Williams; Ding, F.; Lipparini, F.; Egidi, F.; Goings, J.; Peng, B.; Petrone, A.; Henderson, T.; Ranasinghe, D.; Zakrzewski, V. G.; Gao, J.; Rega, N.; Zheng, G.; Liang, W.; Hada, M.; Ehara, M.; Toyota, K.; Fukuda, R.; Hasegawa, J.; Ishida, M.; Nakajima, T.; Honda, Y.; Kitao, O.; Nakai, H.; Vreven, T.; Throssell, K.; Montgomery, J. A., Jr.; Peralta, J. E.; Ogliaro, F.; Bearpark, M. J.; Heyd, J. J.; Brothers, E. N.; Kudin, K. N.; Staroverov, V. N.; Keith, T. A.; Kobayashi, R.; Normand, J.; Raghavachari, K.; Rendell, A. P.; Burant, J. C.; Iyengar, S. S.; Tomasi, J.; Cossi, M.; Millam, J. M.; Klene, M.; Adamo, C.; Cammi, R.; Ochterski, J. W.; Martin, R. L.; Morokuma, K.; Farkas, O.; Foresman, J. B.; Fox, D. J. *Gaussian 16*, revision C.01; Gaussian, Inc.: Wallington, CT, 2016.
(43) Yu, H. S.; He, X.; Li, S. L.; Truhlar, D. G. MN15: A Kohn−Sham Global-Hybrid Exchange−Correlation Density Functional with Broad Accuracy for Multi-Reference and Single-Reference Systems and Noncovalent Interactions. *Chem. Sci.* **2016**, *7* (8), 5032−5051.
(44) Kozuch, S.; Martin, J. M. L. DSD-PBEP86: In Search of the Best Double-Hybrid DFT with Spin-Component Scaled MP2 and Dispersion Corrections. *Phys. Chem. Chem. Phys.* **2011**, *13* (45), 20104.
(45) Mardirossian, N.; Head-Gordon, M. How Accurate Are the Minnesota Density Functionals for Noncovalent Interactions, Isomerization Energies, Thermochemistry, and Barrier Heights Involving Molecules Composed of Main-Group Elements? *J. Chem. Theory Comput.* **2016**, *12* (9), 4303−4325.
(46) Goerigk, L.; Hansen, A.; Bauer, C.; Ehrlich, S.; Najibi, A.; Grimme, S. A Look at the Density Functional Theory Zoo with the Advanced GMTKN55 Database for General Main Group Thermochemistry, Kinetics and Noncovalent Interactions. *Phys. Chem. Chem. Phys.* **2017**, *19* (48), 32184−32215.
(47) Santos, P. F.; Reis, L. V.; Almeida, P.; Lynch, D. E. Crystal Structures of a Benzoselenazole-Derived Squarylium Cyanine Dye and Three Derivatives Substituted at the Central Squaric Ring. *CrystEngComm* **2011**, *13* (5), 1333−1338.
(48) Andersen, N. H.; Neidigh, J. W.; Harris, S. M.; Lee, G. M.; Liu, Z.; Tong, H. Extracting Information from the Temperature Gradients of Polypeptide NH Chemical Shifts. 1. The Importance of Conformational Averaging. *J. Am. Chem. Soc.* **1997**, *119*, 8547−8561.
(49) Cierpicki, T.; Otlewski, J. Amide Proton Temperature Coefficients as Hydrogen Bond Indicators in Proteins. *J. Biomol. NMR* **2001**, *21* (3), 249−261.
(50) Gottlieb, H. E.; Kotlyar, V.; Nudelman, A. NMR Chemical Shifts of Common Laboratory Solvents as Trace Impurities. *J. Org. Chem.* **1997**, *62* (21), 7512−7515.


https://doi.org/10.1021/acsomega.3c07005
*ACS Omega* 2023, 8, 40960−40971

3. Pielikums
Appendix 3

Anastasija Gaile, Sergey Belyakov, Ramona Durena,

Ņikita Griščenko, Anzelms Zukuls, Nelli Batenko

# Studies of the Functionalized α-Hydroxy-*p*-Quinone Imine Derivatives Stabilized by Intramolecular Hydrogen Bond

*Molecules* **2024**, *29* (7), 1613.

DOI: 10.3390/molecules29071613

*molecules*

MDPI

*Article*

# Studies of the Functionalized α-Hydroxy-*p*-Quinone Imine Derivatives Stabilized by Intramolecular Hydrogen Bond

**Anastasija Gaile [1], Sergey Belyakov [2], Ramona Dūrena [3], Ņikita Griščenko [3], Anzelms Zukuls [3] and Nelli Batenko [1,*]**

[1] Institute of Chemistry and Chemical Technology, Faculty of Natural Sciences and Technology, Riga Technical University, P. Valdena Str. 3, LV-1048 Riga, Latvia; anastasija.gaile@rtu.lv
[2] Latvian Institute of Organic Chemistry, Aizkraukles Str. 21, LV-1006 Riga, Latvia; serg@osi.lv
[3] Institute of Materials and Surface Engineering, Faculty of Natural Sciences and Technology, Riga Technical University, P. Valdena Str. 3, LV-1048 Riga, Latvia; ramona.durena@rtu.lv (R.D.); nikita.griscenko@rtu.lv (Ņ.G.); anzelms.zukuls@rtu.lv (A.Z.)
* Correspondence: nelli.batenko@rtu.lv

**Abstract:** In this work, reactions between 6,7-dichloropyrido[1,2-*a*]benzimidazole-8,9-diones with different benzohydrazides were studied. Nucleophilic substitution at C(6) was followed by isomerization and led to α-hydroxy-*p*-quinone imine derivatives. Synthesized compounds represent a combination of several structural motifs: a benzimidazole core fused with α-hydroxy-*p*-quinone imine, which contains a benzamide fragment. X-ray crystallography analysis revealed the formation of dimers linked through OH···O interactions and stabilization of the imine form by strong intramolecular NH···N hydrogen bonds. The protonation/deprotonation processes were investigated in a solution using UV–Vis spectroscopy and a $^1$H NMR titration experiment. Additionally, the electrochemical properties of 6,7-dichloropyrido[1,2-*a*]benzimidazole-8,9-dione and its α-hydroxy-*p*-quinone imine derivative as cathode materials were investigated in acidic and neutral environments using cyclic voltammetry measurements. Cathode material based on 6,7-dichloropyrido[1,2-*a*]benzimidazole-8,9-dione could act as a potentially effective active electrode in aqueous electrolyte batteries; however, further optimization is required.

**Keywords:** quinone; quinone imine; hydrogen bonding; X-ray crystallography; NMR titration; redox



**Citation:** Gaile, A.; Belyakov, S.; Dūrena, R.; Griščenko, Ņ.; Zukuls, A.; Batenko, N. Studies of the Functionalized α-Hydroxy-*p*-Quinone Imine Derivatives Stabilized by Intramolecular Hydrogen Bond. *Molecules* **2024**, *29*, 1613. https://doi.org/10.3390/molecules29071613

Academic Editor: Gianfranco Favi

Received: 6 March 2024
Revised: 25 March 2024
Accepted: 29 March 2024
Published: 3 April 2024



## 1. Introduction

Quinones and quinone derivatives are well known due to the redox activity that is important in a wide range of biological processes, such as photosynthesis [1] and cellular respiration [2]. Quinones represent a class of biologically active compounds with both cytotoxic and cytoprotective effects [3]. Considerable attention to redox-active compounds in general and quinones in particular [4,5] can be explained by growing demands on energy storage devices for portable electronics and renewable energy-powered vehicles [6]. Quinones can potentially be used in different applications connected with energy storage due to their remarkable redox activity: as organic cathode materials for different kinds of rechargeable batteries [7], including redox flow batteries [8] and Zn-ion batteries [9], or as redox mediators in lithium–sulfur batteries [10]. Physical properties of quinones can be modulated by the introduction of heteroaromatics fused with quinone cores [8] and different substituents that affect solubility [11] or affect the form of quinone fragment [12] or can facilitate binding with metal cations [13]. Additionally, redox properties may be tuned to some extent by intra- and intermolecular hydrogen bonding [14].

Redox potentials, solubility, and stability in the case of small quinones can be affected by modification with electron-donating or -withdrawing functional groups or in combination with a side chain that can form hydrogen bonds. Additionally, substituted *o*-quinones, besides their "classical" form, can also exist in various forms [15], like quinone

methides, quinone imines, and zwitterions. This ability to adopt different structures allows modulation of their properties for different applications. Despite progress in the design of quinone derivatives and their wide application as redox-active materials, limited information on molecular-level insights into the bulk properties (e.g., solubility, stability, redox activity, etc.) is available. The investigation of quinone structure at the molecular level, self-assembly in solid state, and behavior in solution will help tune the performance of quinone-functionalized materials.

An approach to modulate the redox properties of quinones is an introduction of nitrogen-containing redox-active groups (e.g., C≡N, C=N, and N=N) or incorporation of unsaturated carbon–nitrogen bonds and π-conjugated aromatic fragments [16].

This work aimed to gain an understanding of the molecular structure and behavior of unsymmetrical heterocyclic *o*-quinones and their derivatives bearing imine moiety. Also, electrochemical studies of selected compounds were conducted to assess their potential applications.

## 2. Results and Discussion

### *2.1. Synthesis and Structural Studies of Quinone Derivatives* 3a–g

6,7-Dichloropyrido[1,2-*a*]benzimidazole-8,9-dione (**1a**) is a representative of unsymmetrical heterocyclic *o*-quinones that contains a combination of two structural motifs, an *o*-quinone fragment and imidazo[1,2-*a*]pyridine core, that possess C=N bonds (Scheme 1). It can be obtained in one-step synthesis from commercially available tetrachloro-1,4-benzoquinone and 2-aminopyridine [17]. During earlier studies [17–19], it was proved that quinone **1a** and some of its derivatives are electrochemically active compounds. Investigation of the reactivity of heterocyclic quinones **1** with *C*- and *N*-nucleophiles (primary amines) indicated that the attack of the nucleophile proceeds selectively at the C(6)-position of quinone. Interestingly, obtained compounds containing different acceptor groups at the C(6)-position can exist in an *o*-quinone form or as *p*-quinone methides, depending on the introduced substituent.

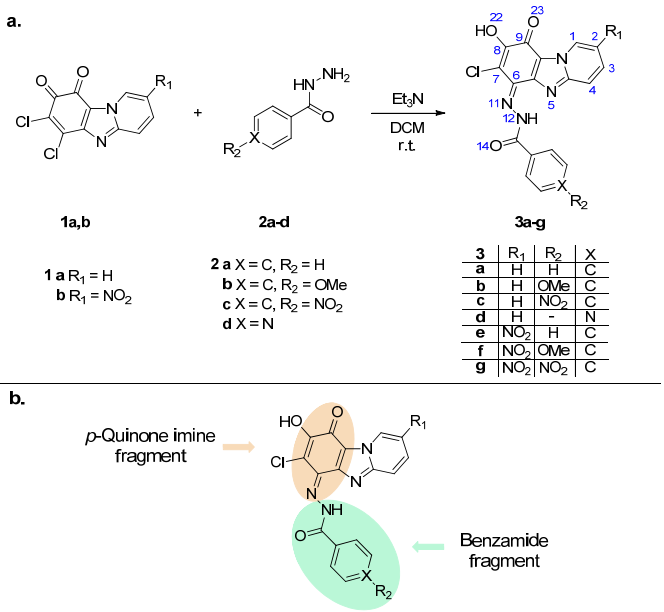


**Scheme 1.** (**a**) Synthesis of compounds **3a–g,** atom numbering of heterocyclic *p*-quinone imine fragment of compounds **3a–g** is shown in blue; (**b**) *p*-Quinone imine and benzamide fragments of obtained compounds **3a–g**.

To expand the scope of redox-active heterocyclic *o*-quinone derivatives, the modification of quinone **1a** with different benzohydrazides was carried out, and structural studies in solid state and solution were conducted.

#### 2.1.1. Synthesis of Quinone Derivatives **3a–g**

Quinone derivatives **3a–g** (Scheme 1a, atoms are numbered according to ORTEP diagram, vide infra) were obtained by the nucleophilic substitution of a chlorine atom of quinone **1a**,**b** by benzohydrazides **2a–d**. Isolated compounds **3a–g** have a red-orange color in the solid state. Interestingly, in the case of aminoderivatives of quinone **1** (a merocyanine on the base of the *o*-quinone form), deep-blue colored crystals were obtained [17,19]. In general, derivatives containing aroyl hydrazine fragments were expected as a result of such substitution [15,20], and a few tautomeric structures can be supposed for the products [21,22]. For the compounds obtained (**3a–g**), the structure determination of the quinone/substituent fragments (Scheme 1b) can explain the observed difference in color of crystals **3a–g** in comparison to aminosubstituted derivatives of quinone **1a**.

#### 2.1.2. Single-Crystal X-ray Analysis of Quinone Derivative **3a**

The use of routine identification procedures (such as $^1$H-NMR and FTIR) to establish the molecular structure of compounds **3a–g** left some room for doubt. To clarify the situation, crystals of compound **3a** were grown from dichloromethane (DCM) solution, and their molecular structure was established using single-crystal X-ray crystallography. Crystal data and refinement details for the studied crystal are presented in Table 1.

**Table 1.** Crystal data and structure refinement details for compound **3a**.

| Crystal Parameter | Compound 3a |
|---|---|
| Empirical formula | $C_{18}H_{11}ClN_4O_3$ |
| Calculated density (g/cm$^3$) | 1.556 |
| Formula weight | 366.766 |
| Color | Red |
| Size/mm$^3$ | 0.18 × 0.03 × 0.01 |
| Temperature/K | 150.0 (1) |
| Crystal system | monoclinic |
| Space group | $P2_1/n$ |
| $a$/Å | 5.65994 (5) |
| $b$/Å | 14.90948 (19) |
| $c$/Å | 18.5815 (2) |
| α/° | 90 |
| β/° | 93.1950 (9) |
| γ/° | 90 |
| $V$/Å$^3$ | 1565.60 (3) |
| Wavelength/Å | 1.54184 |
| Radiation type | Cu K$_\alpha$ |
| Absorption coefficient (mm$^{-1}$) | 2.419 |
| θmin/° | 3.8 |
| 2θmax/° | 155.0 |
| Measured reflections | 17875 |
| Number of independent reflections | 3322 |
| Reflections with I ≥ 2σ($I$) | 3089 |
| $R_{int}$ | 0.0327 |
| Number of refined parameters | 243 |
| Restraints | 0 |
| Largest peak | 0.3476 |
| Deepest hole | −0.3143 |
| Goodness of fit | 1.0362 |
| $wR_2$(all data) | 0.0962 |
| $wR_2$ | 0.0945 |

**Table 1.** *Cont.*

| Crystal Parameter | Compound 3a |
|---|---|
| $R_1$(all data) | 0.0367 |
| $R_1$ | 0.0346 |
| CCDC deposition number | 2238663 |

Figure 1a shows a perspective view of molecule **3a** with thermal ellipsoids and the atom-numbering scheme. The *p*-quinone imine form was confirmed by the inspection of the bond length: bonds between C(9)=O(23) and C(6)=N(11) have double-bond character, and O(22)-C(8) is a single bond (typical bond distances: *d* (Å) (C-O) = 1.34, (C=O) = 1.21, (C-N) = 1.38, (C=N) = 1.28 [23]). Also, an analysis of bond lengths shows that the structure of compound **3a** can be represented as a superposition of mesomeric forms. The main forms are shown in Figure 1b; at that, the non-ionized form has the highest specific weight.

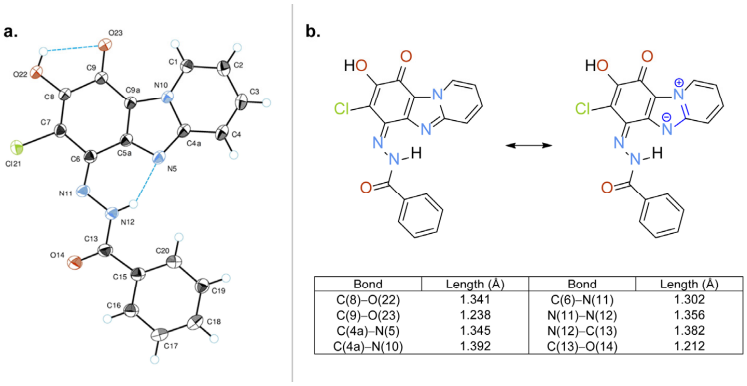


| Bond | Length (Å) | Bond | Length (Å) |
|---|---|---|---|
| C(8)–O(22) | 1.341 | C(6)–N(11) | 1.302 |
| C(9)–O(23) | 1.238 | N(11)–N(12) | 1.356 |
| C(4a)–N(5) | 1.345 | N(12)–C(13) | 1.382 |
| C(4a)–N(10) | 1.392 | C(13)–O(14) | 1.212 |

**Figure 1.** (**a**) ORTEP diagram of compound **3a** showing thermal ellipsoids at the 50% probability level; (**b**) two mesomeric structures of compound **3a** based on the bond distances in the crystal structure.

The molecules of compound **3a** are characterized by a flattened conformation; only the phenyl group is slightly out of the plane of the heterocyclic system (the angle between planes is 5.19°). In the structure of compound **3a,** intramolecular hydrogen bonds NH···N and OH···O were found (Figure 2). The hydroxy group of compound **3a** forms bifurcated hydrogen bonds where O(22)-H···O(23) is an intramolecular bond (Figure 1a) and O(22)-H···O′(23) is an intermolecular one (Figure 2a). By means of these intermolecular H-bonds, the centrosymmetric $R_2^2(10)$ molecular dimers are formed in the crystal structure. Additional intermolecular interactions were found: stacking interaction between the planes of the molecules and a short intermolecular contact between heterocycle (C(3)-H) and the amide group of the substituent (*d* C(3)···O(14) = 3.112 Å, *d* C(3)-H···O(14) = 2.344 Å) (Figure 2b,c).

Hirshfeld surfaces and energy framework calculations (Figures S14 and S15) were obtained in a whole-of-molecule approach using the B3LYP/6-31G(d,p) energy model implemented in CrystalExplorer 21.5 software [24]. The Hirshfeld surface (shown in Figure S14, mapped with $d_{norm}$) investigation is a useful approach to establishing close contacts in a crystal. Areas of close contact are highlighted with different colors (red, white, and blue spots) to show intermolecular contacts with distances less than, equal to, and larger than van der Waal radii. As seen from the Hirshfeld surface analysis of compound **3a**, bright red areas of the same size indicate strong interactions, specifically hydrogen bonds OH···O, between neighboring molecules. Fainter red or white areas suggest relatively weak interactions involving hydrogen atoms from heterocyclic and phenyl rings and chlorine

atoms. Examples include C-H bonds interacting with oxygen (C(3)-H···O(14)), nitrogen (C(3)-H···N(11)), and chlorine (C(4)-H··· Cl and C(phenyl)-H· · · Cl).

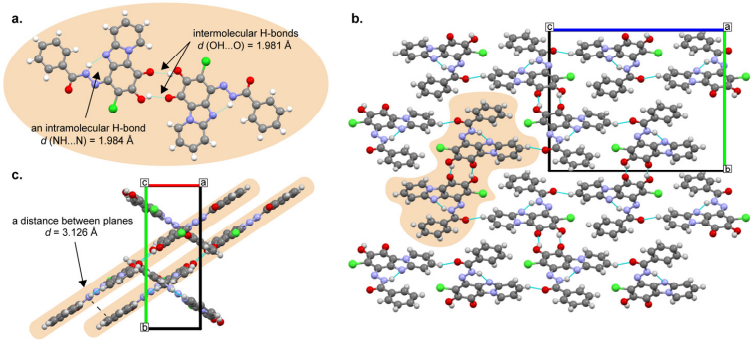


**Figure 2.** (**a**) A dimer (highlighted) formed in the crystal structure of compound **3a**. (**b**) Crystal packing of compound **3a** along the *a* axis. (**c**) Crystal packing of compound **3a** along the *c* axis. Color map: C, grey; N, blue; O, red; Cl, green; H, white.

Energy frameworks provide an opportunity to explore the cooperative effects of intermolecular interactions in the crystal, admitting the electrostatic, dispersion, and total energy between pairs of molecules [25]. In the case of the crystal of compound **3a** (Figure S15), a strong stabilizing interlayer electrostatic interaction was found between molecules involved in the formation of hydrogen-bonded (O–H· · · O) dimers. On the other hand, dispersion energy was more dominant for the intercolumn stacking motif. Overall, the energy framework analysis of the crystal revealed two distinct patterns of electrostatic and dispersion energies, with each contributing similarly.

### 2.1.3. $^1$H NMR Spectroscopy Analysis of Quinone Derivatives **3a–g**

To determine the structure of obtained products in solution compounds **3a–g,** $^1$H NMR spectroscopy data were analyzed, and a set of two broad signals corresponding to NH and OH protons was observed (Figures S1–S7). In the DMSO-$d_6$ solution, signals appeared at 14.36–14.90 ppm and can be assigned to the NH proton, while signals of the OH group were observed at 10.89–11.41 ppm. Additionally, the $^1$H NMR spectrum of compound **3a** was also recorded in $CDCl_3$ solution (a solvent in which hydrogen-bonding interactions are expected to be weaker [26]) (Figure S8), where the NH proton was found at 14.68 ppm (versus 14.71 ppm in DMSO-$d_6$ solution). It can be concluded that a strong intramolecular bond between the NH group proton of the substituent (benzamide group at imine bond) and the nitrogen of the heterocycle (N(12)-H···N(5)) can be found in solution as well as in a solid state (vide supra).

It is known [27] that in the case of α-hydroxyquinone derivatives, an intramolecular hydrogen bond was observed, and an OH proton signal appears at 7.30 ppm in the $CDCl_3$ solution. For compound **3a**, a distinguishable shift was observed for the OH proton signal in the $CDCl_3$ solution (7.20 ppm) in comparison to the DMSO-$d_6$ solution (10.99 ppm), which can indicate the formation of the additional intermolecular interactions between the OH group and a solvent (DMSO-$d_6$) with hydrogen bond acceptor abilities [28].

Moreover, the introduction of various substituents in the phenyl ring (benzamide fragment) showed the linear correlation (Figure S9) between the type of substituent group (represented by the Hammett constant [29] (Table S1)) and OH signal shift in the sets of compounds **3a–c** ($R_1$ = H) and **3e–g** ($R_1$ = $NO_2$). The shift of the OH signal correlates well ($R^2$ = 0.99) with the increasing electron-withdrawing character of the substituent group for both sets of compounds (Figure S9). The presence of an electron-withdrawing group

(EWG) at the heterocyclic fragment ($R_1 = NO_2$) led to a downfield shift in the OH signal compared to molecules without any substituent ($R_1 = H$) on that ring ($\Delta\delta_{OH} \approx 0.3$ ppm).

The most downfield signal of the NH proton (14.90 ppm in DMSO-$d_6$ solution) in the $^1$H NMR spectra was observed for compound **3c** with a $NO_2$ group at the phenyl ring ($R_2$ at benzamide fragment). The most upfield signal of the NH proton (14.36 ppm) was found for compound **3f** with a $NO_2$ group at the heterocyclic fragment ($R_1$) and electron-donating group at the phenyl ring ($R_2$ = OMe). Well-defined linear correlations between the Hammett substituent constant and the NH signal are presented in Figure S9. The variation in the electronic character of the substituent in the *para*-position of the phenyl ring showed the same trend for compounds **3a–c** ($R^2 = 0.96$) and **3e–g** ($R^2 = 0.99$), leading to the downfield shift of the NH signal going from an electron-donating to electron-withdrawing group. Interestingly, the presence of EWG ($R_1 = NO_2$) at the heterocyclic ring caused the NH signal upfield shift ($\Delta\delta_{NH} \approx 0.3$ ppm) compared to a molecule where the same position has a hydrogen atom ($R_1 = H$). In general, the more downfield shifted the NH proton signal, the stronger the intramolecular H-bond [30]. Thus, EWG at the phenyl ring ($R_2 = NO_2$) increases the acidity of the NH proton and increases the intramolecular H-bond strength, but EWG at the heterocyclic fragment ($R_1 = NO_2$) influences the electron density at N(5), affecting intramolecular H-bond in turn.

In the case of compounds **3a–g**, the moiety at the C(6) position can be described as a structural analog of aroyl hydrazone (a different approach [22] to the naming of quinone imine derivatives was observed). A well-known characteristic of compounds containing the carbon–nitrogen double bond is the ability to undergo *E*/*Z* isomerization in the solution activated by light and/or chemical inputs [31,32].

Compounds **3a** and **3b** were chosen for the investigation of the isomerization process. In general, in the case of *E*/*Z* isomerization, an additional set of signals [33,34] is expected to appear. No signals of the second form (isomerization products) were observed in the $^1$H NMR spectra of compound **3a** either in DMSO-$d_6$ or in $CDCl_3$ solution. Also, in the case of compound **3b**, configurational switching was not induced by the addition of excess trifluoracetic acid (TFA) and following irradiation by UV light (365 nm; irradiation by a high-pressure mercury lamp at room temperature) judging from the $^1$H NMR spectra of compound **3b** in DMSO-$d_6$ solution (Figure S10). The formation of a strong intramolecular hydrogen bond N(12)-H···N(5) can explain the existence of a single configuration of substituted imine that agrees with the stabilization of only one form in the presence of an intramolecular hydrogen bond. Additional stabilization of the molecule may be explained by excitation energy dissipation caused by zwitterionic structure.

It is known [35] that for redox properties tests (fabrication of electrodes), a mixture of an organic compound, a conductive additive, and a binder is often prepared using *N*-methyl-2-pyrrolidone (NMP) [36] as a solvent (strongly basic solvent) [37]. This fact prompted us to investigate the influence of the base on the structure of the products **3a–g**.

During preliminary solubility tests of compounds **3a–g,** the color change (from yellow to green or blue) was observed in NMP solution or in the presence of a base. For a better understanding of the effect, a few $^1$H NMR experiments were carried out. Upon addition of an excess of the base (1,8-diazabicyclo(5.4.0)undec-7-ene, DBU), the $^1$H NMR spectrum of compound **3b** in DMSO-$d_6$ solution showed some changes (Figure 3): the signal of OH proton completely disappeared; the sharpened signal of the NH proton (the sharp line can indicate a dynamically stable state) shifted upfield. Additionally, a new minor proton signal at 13.44 ppm was observed. Simultaneously, the yellow-colored solution of compound **3b** became dark blue. It should be noted that the same deprotonation behavior was observed for compound **3a** in $CDCl_3$ solution (Figure S11). After the excess TFA was added, the solution became yellow again, a minor signal at 13.44 ppm disappeared, and the signal of the OH proton was restored. It can be concluded that deprotonation provides the formation of an anionic polymethine dye structure [38] (blue), and protonation restores quinone imine form (yellow); consequently, the equilibrium between the two forms is reversible.

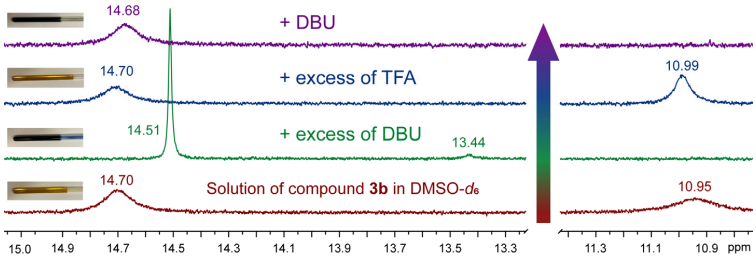


**Figure 3.** An expansion of $^1$H NMR spectra of compound **3b** in DMSO-$d_6$ solution upon sequential addition of base (DBU) and acid (TFA).

To gain more information about the deprotonation process of compound **3b**, a $^1$H NMR titration experiment was carried out. As shown in Figure 4, in the case of compound **3b** deprotonation upon sequential addition of the base (DBU), the $^1$H NMR spectra reveal several features. The broad signal of the OH proton vanished upon the addition of only 0.15 equivalents of the base, which can be explained by the dynamical process as well; color changes were immediate (Figure 4, highlighted in yellow). The signal of the NH proton (benzamide fragment) sharpens and undergoes an upfield shift from 14.70 to 14.51 ppm (Figure 4, highlighted in red).

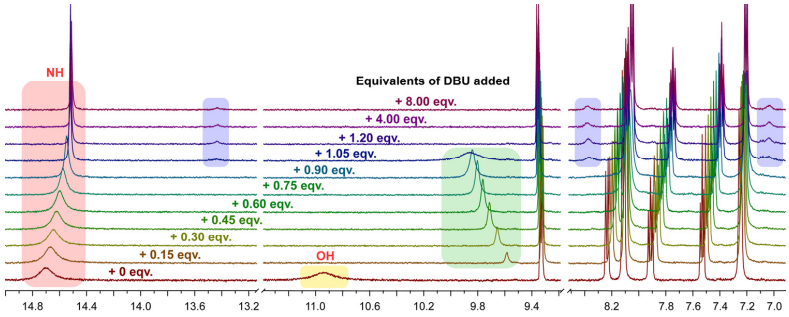


**Figure 4.** $^1$H NMR titration of compound **3b** in DMSO-$d_6$ solution with DBU (0–8 equivalents).

A new signal appeared at 9.58 ppm (+0.15 eqv. of DBU) (Figure 4, highlighted in green), which can be explained by the formation of a hydrogen-bonded complex of protonated DBU ($^1$H NMR spectrum of DBU and TFA mixture in DMSO-$d_6$ solution was recorded; the $NH^+$ signal appears at 9.69 ppm (Figure S12)) with the deprotonated compound **3b**. Upon further addition of the base, this signal was broadened and shifted downfield (9.86 ppm) due to the interaction of protonated DBU ($DBUH^+$) with the anionic compound **3b** through the N–H bond [39].

Upon addition of more than 1.05 eqv. of the base, a second minor form of the compound appears (Figure 4, highlighted in blue); the ratio between major and minor forms is 0.95:0.05, taking into consideration the signals of all protons. Moreover, the addition of an excess amount of the base (4 and 8 eqv.) did not result in the change of the $^1$H NMR spectra of compound **3b** (additional processes as a function of the time and/or temperature in the solution should not be excluded as $^1$H NMR titration experiment was carried out within an hour after addition of DBU to the compound **3b** at room temperature (T = 294 K)).

Also, the presence of two different species (one major and one minor) was detected from the changes in the $^1$H NMR spectra of compounds **3a** and **3c** upon deprotonation with DBU in DMSO-$d_6$ solution (after mixed with more than 1 equivalent of DBU). For compound **3a,** the $^1$H NMR spectrum was also recorded in the presence of NaOH. As a result, the acquired spectrum was identical to the one with an excess of DBU (Figure S13).

Unfortunately, the low solubility of compounds **3a–g** limited the possibility of obtaining qualitative $^{13}C$ NMR spectra.

2.1.4. Electronic Absorption

The UV–Vis absorption spectra of compound **3a** were investigated in solution using solvents of various polarities (DCM and DMSO). Two absorption maxima were found at 381 nm and at 446–449 nm in the absorption spectra of compound **3a** in both solutions (Figure 5a), which can be attributed to the neutral form of the compound. Upon addition of the base (DBU) to the DCM solution of **3a**, the solution instantaneously turned violet, and the absorption revealed a broad band centered at 556 nm. When a base was added to the DMSO solution of compound **3a**, the bathochromic shift was observed with an absorption maxima at 607 nm accompanied by a blue coloration.

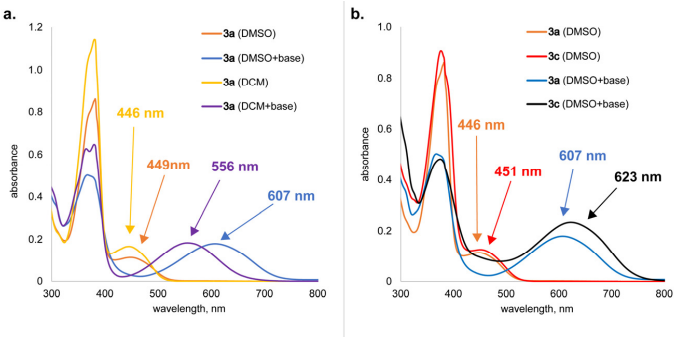


**Figure 5.** (**a**) UV–Vis absorption spectra of neutral (in DMSO or DCM solution) and deprotonated (upon addition base to the DMSO or DCM solution) forms of compound **3a**. (**b**) UV–Vis absorption spectra neutral (in DMSO solution) and deprotonated (upon addition of a base to the DMSO solution) forms of compounds **3a** and **3c**.

The effect of substituents ($R_1$ and $R_2$) on the longwave absorption maximum was examined when DBU was added to the initial solution of compounds **3a–c** (variable $R_2$ while $R_1$ = H) and **3e–g** (variable $R_2$ while $R_1$ = $NO_2$) in $CHCl_3$ (Figure S16, Table S2). It was noticed that the longwave absorption band of deprotonated species of derivatives **3e–g** was red-shifted (λ = 569–578 nm) in comparison to compounds **3a–c** (λ = 556–563 nm). This observation can be explained by the influence of the electron-withdrawing substituent at C(2) on the electron distribution in the heterocyclic fragment. Moreover, a hyperchromic effect was caused by the introduction of the nitro group in the benzamide fragment (compound **3c** in Figure 5b; compounds **3c** and **3g** in Figure S16).

*2.2. Electrochemistry/Redox Chemistry Studies of Quinone Derivatives* **1a** *and* **3a**

Quinone imines contain structural fragments with potentially high redox activity. It was shown by Almeida, R. et al. [40] that *p*-quinone imines are known to undergo a redox cycle through aminophenols [41]. Compound **1a** was previously proved to be electrochemically active [42] when dissolved in the MeCN solution. However, it has not been tested as a cathode material before. To analyze the redox properties of quinone imine **3a** in comparison to initial *o*-quinone **1a**, open-circuit potential (OCP) and cyclic voltammetry (CV) measurements in a solid state were carried out. Preliminary solubility tests showed limited solubility of compounds **1a** and **3a** in aqueous media; compound **1a** was insoluble in water (whole pH range), and at the same time, compound **3a** was insoluble in neutral and acidic environments.

2.2.1. Open-Circuit Potential Measurements

To analyze the electrochemical properties of the compounds, CV measurements and OCP measurements before and after CV were performed (Figure S17). Cathode materials **CM-1a** and **CM-3a** were prepared by combining compounds **1a** and **3a** with Vulcan XC72 CB, respectively (the detailed sample preparation is described in the Experimental section). The OCP of freshly assembled half-cells for cathode materials **CM-1a** and **CM-3a** in the acidic (0.5 M $H_2SO_4$) electrolyte was 0.44 V and 0.37 V vs. Ag/AgCl; however, in a neutral (0.5 M $K_2SO_4$) electrolyte, the potentials of both were 0.28 V vs. Ag/AgCl. After the CV measurements, the OCP of sample half-cells stabilized. For both samples in the acidic electrolyte, they were 0.41 V vs. Ag/AgCl, and in the neutral electrolyte, they were 0.37 V vs. Ag/AgCl. The OCP for both samples is approximately the same, and with decreasing pH, there is a visible shift to higher potential values going from neutral to the acidic electrolyte.

2.2.2. Cyclic Voltammetry Measurements

CV results for samples **CM-1a**, **CM-3a**, and a sample without active material (substrate) in neutral and acidic electrolytes at varying scanning speeds are shown in Figure 6. For the substrate in neutral electrolyte, no visible redox processes were observed. In the acidic electrolyte, a hydrogen evolution reaction can be observed around the potential of −0.3 V vs. Ag/AgCl and one insignificant redox process at faster scan rates around 0.3 V vs. Ag/AgCl. However, when scanning samples with active materials, this substrate process cannot be observed and, therefore, has no electrochemical significance other than providing electrical conductivity.

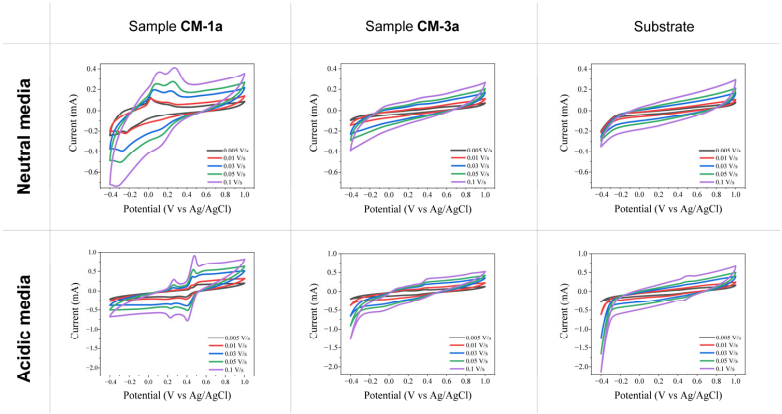


**Figure 6.** CV results at varying scanning speeds for samples **CM-1a**, **CM-3a**, and substrate in neutral (0.5 M $K_2SO_4$) electrolyte and in acidic (0.5 M $H_2SO_4$) electrolyte.

For sample **CM-3a** in a neutral electrolyte (Figure 6), no significant redox processes can be observed. Also, in an acidic electrolyte for sample **CM-3a** (Figure 6), there are no significant processes; however, upon closer inspection (Figure S18), two reversible oxidation (at 0.40 V and 0.07 V vs. Ag/AgCl) and reduction processes (at 0.23 V and −0.06 V vs. Ag/AgCl) can be seen.

Sample **CM-1a** has two redox maxima in the scanned potential window from −0.4 V to 1.0 V vs. Ag/AgCl electrode in both neutral and acidic electrolytes (Figure 6). In a neutral electrolyte (Figure S19), oxidation peaks are at 0.27 V and 0.10 V vs. Ag/AgCl; however, reduction peaks are at 0.14 V and −0.32 V vs. Ag/AgCl. In addition, the oxidation peaks are found at 0.48 V and 0.26 V vs. Ag/AgCl and reduction peaks at 0.40 V and 0.23 V vs. Ag/AgCl in an acidic electrolyte (Figure S20). This indicates a shift in reaction potential to more positive values by increasing $H^+$ ion concentration and thus lowering the pH level of the electrolyte. Both redox processes for sample **CM-1a** correspond to the *o*-quinone

fragment in the molecule. However, by comparing the electrochemical performance of both samples **CM-1a** and **CM-3a**, it can be concluded that by converting *o*-quinone **1a** to α-hydroxy-*p*-quinone imine **3a** accompanied by the additional stabilization by intra- and intermolecular hydrogen bonds, the electrochemical reactivity of the cathode material has been greatly suppressed.

All CV measurement result developments in time can be seen in Figure S21. At the start, samples were cycled at the potential window of −0.4 V to 1.0 V vs. Ag/AgCl reference electrode. Observations indicate that all samples go through the surface activation phase, where the sample-specific capacity increases with each subsequent cycle. During the measurements at different scanning speeds, the stabilization of the system is observed. However, sample **CM-1a** in neutral electrolyte goes through an irreversible oxidation process at 0.11 V vs. Ag/AgCl and a reduction process at −0.32 V vs. Ag/AgCl. This irreversible redox process can be observed during all scan speeds. At an increased potential window (from −1.0 V to 1.5 V), another irreversible process at a scan speed of 0.1 V/s for sample **CM-1a** in a neutral electrolyte can be observed during the oxidation at −0.31 V and reduction at −0.56 V vs. Ag/AgCl. A slight capacity decrease due to the possible dissolution of active materials can be observed for sample **CM-3a** in a neutral electrolyte and sample **CM-1a** in an acidic electrolyte.

### 2.2.3. Raman Measurements

Raman measurements were performed on pure compounds **1a** and **3a**, prepared cathodes (**CM-1a** and **CM-3a**), and after cycling them in acidic and neutral electrolytes (Figure 7). For sample **CM-3a**, the spectra for prepared and cycled cathodes remain as for pure compound **3a**, where an amide band can be seen at 1600–1630 $cm^{-1,}$ as well as bands for aromatic/heteroaromatic rings at 1550 and 1470 $cm^{-1}$ [43]. This indicates that compound **3a** was preserved in the cathode-forming process and did not go through any chemical changes. Also, after CV measurements, the active material is unchanged and present in the samples. For sample **CM-1a**, the spectra for the prepared and cycled cathode in an acidic electrolyte remain as for pure compound **1a** (bands for aromatic/heteroaromatic rings at 1570 and 1450 $cm^{-1}$ and band for carbonyl groups at 1650–1690 $cm^{-1}$) [43]. However, for cathode **CM-1a** cycled in neutral electrolyte, only C and D bands of carbon [44,45] can be seen. Since redox processes are visible for this sample in CV measurements (Figure 6), the active material could have dissolved from the electrode in the electrolyte and gone through the electrochemical reactions from the electrolyte.

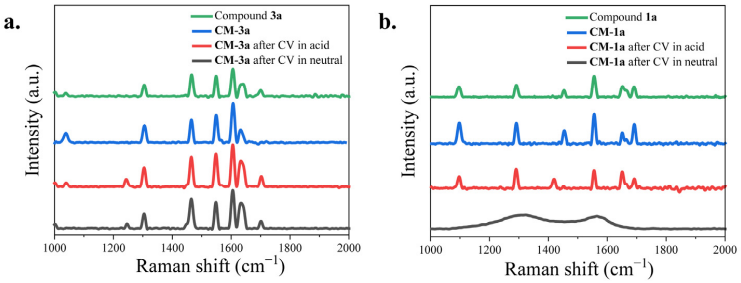


**Figure 7.** (**a**) Raman spectra of pure compound **3a** (green line), prepared cathode **CM-3a** before (blue line) and after cycling in acidic (red line) and neutral (gray line) electrolytes. (**b**) Raman spectra of pure compound **1a** (green line), prepared cathode **CM-1a** before (blue line) and after cycling in acidic (red line) and neutral (gray line) electrolytes.

### 2.2.4. Scanning Electron Microscopy Measurements

Scanning electron microscopy examinations of compounds **1a** and **3a** (Figure S22) were performed to assess the morphology of the products. Compound **1a** consists of needle-like particles with sizes ranging from 1 μm to 10 μm in diameter and 3 μm to 30 μm in length.

Compound **3a** has smaller particles with an overall size of 1 μm in diameter and 5–20 μm in length.

Also, the prepared cathode surfaces with and without active materials before and after cyclic voltammetry are shown in Figure 8. The resemblance of the structures of compounds **1a** and **3a** (as shown in Figure S22) can be seen in the images of cathode disks (samples **CM-1a** and **CM-3a** in Figure 8) before CV measurements. For sample **CM-3a**, these structures can also be seen in images after CV in neutral and acidic electrolytes with some partial dissolution in an acidic electrolyte, as fewer structures can be seen. The formation of non-covalent interactions between compound **3a** and substrate can probably explain the greater stability of **CM-3a** in comparison to **CM-1a**. However, for sample **CM-1a** cycled in neutral and acidic electrolytes, only a few original structures can be seen. This correlates with findings from Raman spectroscopy (Figure 7b) that the active material **1a** dissolves in a neutral electrolyte and goes through electrochemical reactions from it.

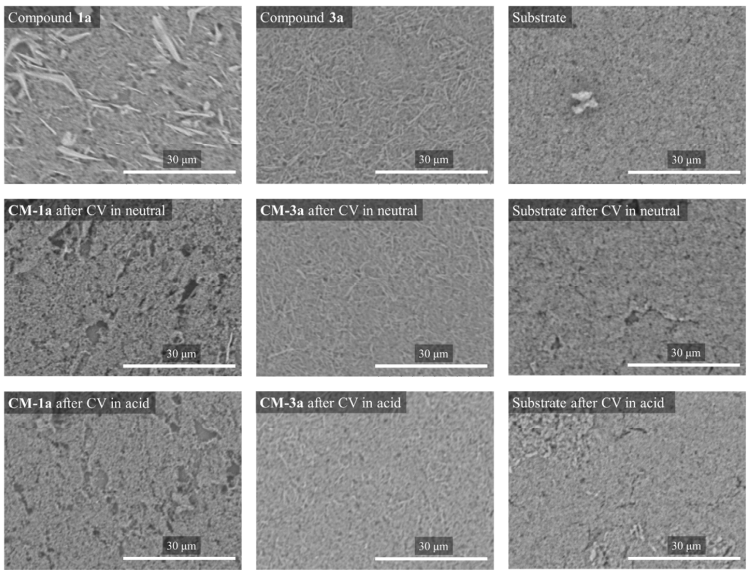


**Figure 8.** Scanning electron microscopy images of samples **CM-1a**, **CM-3a**, and substrate (coating without active material) before and after CV measurements in neutral and acidic electrolytes (magnification of ×2500).

## 3. Materials and Methods

### *3.1. Materials and Instrumentation*

Polyvinylidene fluoride (PVDF) (MW ~530,000) and Dimethylformamide (DMF) were purchased from Merck; Vulcan XC72 Carbon Black (CB) was used, and 0.05 mm thick conductive graphite paper (RERAS, purchased from China and used as electrode substrate) was used to prepare cathode materials.

Melting points were measured on a Kruess KSP 11 Melting Point Analyzer. $^{1}$H NMR spectra were recorded on a Brucker Avance spectrometer at 300 or 500, respectively, in DMSO-$d_6$ or $CDCl_3$ solutions. Chemical shifts were expressed in parts per million (δ, ppm) relative to solvent signal (DMSO-$d_6$: 2.50 ppm $CDCl_3$: 7.26 ppm for $^{1}$H NMR) [46]. Compounds **3a**–**g** are too insoluble to record a qualitative $^{13}$C NMR spectrum. Elemental CHN analysis was carried out on a Euro Vector EA 3000 analyzer. FTIR spectra were recorded on a Perkin-Elmer Spectrum 100 FTIR spectrometer. The UV–Vis absorption spectra were acquired with a Perkin-Elmer 35 UV/Vis spectrometer using 1 cm length quartz cuvettes with a concentration of compound $c = 2.5 \times 10^{-5}$ M. Low-resolution mass

spectra were acquired on a Waters EMD 1000MS mass detector (ESI + mode, voltage 30 V) with an Xterra MS C18 5 μm 2.1 × 100 mm column and gradient eluent mode using 0.1% HCOOH in deionized water and MeCN or MeOH.

### *3.2. X-ray Crystallography Analysis*

For compound **3a**, diffraction data were collected at a low temperature (T = 150.0(1) K) on Rigaku, XtaLAB Synergy, Dualflex, HyPix diffractometer using copper monochromated Cu-Kα radiation (λ = 1.54184 Å). The crystal structure was solved with the help of the ShelXT structure solution program [47] using the Intrinsic Phasing solution method. The model was refined with version of the program olex2.refine using Levenberg–Marquardt minimization [48]. All nonhydrogen atoms were refined in anisotropical approximation. For further details, see crystallographic data for compound **3a** deposited at the Cambridge Crystallographic Data Centre as Supplementary Publications Numbers CCDC 2238663 (for compound **3a**). These data can be obtained free of charge via https://www.ccdc.cam.ac.uk/structures/ (accessed on 1 April 2024) or from the CCDC, 12 Union Road, Cambridge CB2 1EZ, U.K.; Fax: +44 1223 336033; e-mail: deposit@ccdc.cam.ac.uk). For crystal packing visualization, the program *Mercury* [49] was used.

### *3.3. Cathode Material Preparation*

Quinone derivatives **1a** or **3a** were combined with Vulcan XC72 CB at a mass ratio of 5:4. The resulting powder was dried overnight at 80 °C. Then, a binder solution of PVDF:DMF (mass ratio 1:9) was added so the quinone to PVDF mass ratio would be 5:1. Stirring and ultra-sonication were used to create the ink slurry. Extra DMF was added to the slurry to form homogeneous ink (the total weight ratio of DMF to quinone was approximately 12:1). A manual doctor blade coater (with a 25 μm gap size) was employed to apply the coating onto carbon paper that was pre-dried at 120 °C for an hour. Coated cathode substrates were then dried in air to evaporate DMF. For further material characterization, cathode disks were cut out using a hollow punch.

### *3.4. Cyclic Voltammetry*

To analyze the electrochemical properties of the different sample compounds, cyclic voltammetry (CV) measurements were performed using a 3-electrode measuring cell "TSC Surface" (from rhd instruments). For different measurements, the prepared thin-layer electrodes on carbon paper (with or without compound **1a** or **3a**) were used as working electrodes placed in 1 mL of electrolyte with the platinum counter electrode and Ag/AgCl (3 M KCl) reference electrode. Two different pH electrolyte solutions were used for measurements: neutral 0.5 M $K_2SO_4$ and acidic 0.5 M $H_2SO_4$ solutions. The CV measurements were performed from −0.4 to +1.0 V with the following program: (1) open-circuit measurement (OCP) of freshly assembled half-cell before the CV measurements; (2) ten cycles with scan speed of 0.075 V/s to stabilize the half-cell; (3) 5 cycles of 5 scans with scan rates ranging from 0.005 V/s to 0.1 V/s; and (4) OCP measurement after CV.

### *3.5. Raman Spectroscopy*

Raman measurements were performed using a Renishaw In-ViaV727 spectrometer in a backscattering geometry at room temperature at 100× magnification. For phonon excitation, a red laser (He-Ne, λ = 633 nm, grating—1200 $mm^{-1}$, 125 μW) was used, and the sample exposure time was 10 s.

### *3.6. Scanning Electron Microscopy*

A Hitachi TM3000 Tabletop scanning electron microscope (SEM) with an acceleration voltage of 5 kV was used to obtain surface information of the obtained electrode and sample materials. To characterize the obtained samples, different magnifications were used.

### *3.7. Synthesis of Quinone Derivatives* **1a**,**b** *and* **3a**–**g**

6,7-Dichloropyrido[1,2-a]benzimidazole-8,9-dione (**1a**) and 6,7-dichloro-2-nitropyrido[1,2-*a*]benzimidazole-8,9-dione (**1b**) were prepared according to the previously reported procedure [17,42].

General method for synthesis of compounds **3a**–**g**. To a stirring solution of 6,7-dichloropyrido[1,2-*a*]benzimidazole-8,9-dione (**1a**, 1 eq) or 6,7-dichloro-2-nitropyrido[1,2-*a*]benzimidazole-8,9-dione (**1b**, 1 eq) in dichloromethane (DCM) at room temperature, a solution of benzhydrazide derivative (**2a**–**d**, 2 eq) in DCM or DMF was added. Triethylamine (1 eq) was added to the reaction mixture, which was then stirred at room temperature for 8 h. After completion of the reaction, the reaction mixture was filtered through a filter paper, and the solvent was distilled in vacuo to a residual volume of 20 mL. The resulting orange-colored precipitate was collected, recrystallized from DCM/*n*-hexane, washed with hot ethanol (20 mL), and dried at room temperature.

**Compound 3a.** Prepared using 6,7-dichloropyrido[1,2-*a*]benzimidazole-8,9-dione (150 mg, 0.56 mmol, 1 eq), benzohydrazide (153 mg, 1.12 mmol, 2 eq), and triethylamine (*d* = 0.73 g/mL, v = 78 µL, 0.56 mmol, 1 eq). **Yield:** 59%, orange powder. **M.P.**: 258–260 °C. **MS:** $C_{18}H_{11}ClN_4O_3$ requires $[M + H]^+$ 367.1; found $[M + H]^+$ 367.2. **$^1$H NMR (500 MHz, DMSO-$d_6$):** 14.71 (br.s., 1H, exchange with $D_2O$, NH), 10.98 (br.s., 1H, exchange with $D_2O$, OH), 9.29 (d, *J* = 6.6 Hz, 1H, H-1), 8.16 (d, *J* = 9.0 Hz, 1H, H-4), 8.11 (d, *J* = 7.4, 2H, $CH_{Ph}$), 7.89 (t, *J* = 8.0, 1H, H-3), 7.73 (m, 3H, $CH_{Ph}$), 7.51 (d, *J* = 6.8 Hz, 1H, H-2). **FTIR (KBr, cm$^{-1}$):** 3331, 3094, 3033, 1708, 1628, 1604, 1548, 1437, 1351, 1247. **Anal. Calcd.** for $C_{18}H_{11}ClN_4O_3$: C, 58.95; H, 3.02; N, 15.28; found C, 58.82; H, 3.02; N, 15.31.

**Compound 3b.** Prepared using 6,7-dichloropyrido[1,2-*a*]benzimidazole-8,9-dione (150 mg, 0.56 mmol, 1 eq), 4-methoxybenzohydrazide (187 mg, 1.12 mmol, 2 eq), and triethylamine (*d* = 0.73 g/mL, v = 78 µL, 0.56 mmol, 1 eq). **Yield:** 36%, orange solid. **M.P.**: >300 °C. **MS:** $C_{19}H_{13}ClN_4O_4$ requires $[M + H]^+$ 397.1; found $[M + H]^+$ 397.2. **$^1$H NMR (500 MHz, DMSO-$d_6$):** 14.70 (br.s., 1H, exchange with $D_2O$, NH), 10.95 (br.s., 1H, exchange with $D_2O$, OH), 9.33 (d, *J* = 6.7 Hz, 1H, H-1), 8.24 (d, *J* = 9.0 Hz, 1H, H-4), 8.11 (d, *J* = 8.6 Hz, 2H, $CH_{Ph}$), 7.91 (m, 1H, H-3), 7.53 (t, *J* = 6.8 Hz, 1H, H-2), 7.25 (d, *J* = 8.5 Hz, 2H, $CH_{Ph}$), 3.91 (s, 3H, -$OCH_3$). **FTIR (KBr, cm$^{-1}$):** 3468, 3301, 3083, 3024, 2975, 2832, 1690, 1630, 1609, 1582, 1552, 1504, 1351, 1325, 1259. **Anal. Calcd.** for $C_{19}H_{13}ClN_4O_4$: C, 57.51; H, 3.30; N, 14.12; found C, 57.58; H, 3.35; N, 13.82.

**Compound 3c.** Prepared using 6,7-dichloropyrido[1,2-*a*]benzimidazole-8,9-dione (150 mg, 0.56 mmol, 1 eq), 4-nitrobenzohydrazide (204 mg, 1.12 mmol, 2 eq), and triethylamine (*d* = 0.73 g/mL, v = 78 µL, 0.56 mmol, 1 eq). **Yield:** 52%, orange solid. **M.P.**: 275–278 °C. **MS:** $C_{18}H_{10}ClN_5O_5$ requires $[M + H]^+$ 412.1; found $[M + H]^+$ 412.2. **$^1$H NMR (300 MHz, DMSO-$d_6$):** 14.95 (br.s., 1H, exchange with $D_2O$, NH), 11.07 (br.s., 1H, exchange with $D_2O$, OH), 9.29 (d, *J* = 6.5, 1H, H-1), 8.53 (m, 2H, $CH_{Ph}$), 8.32 (d, *J* = 8.3, 3H, H-4 un $CH_{Ph}$), 7.91 (m, 1H, H-3), 7.53 (m, 1H, H-2). **FTIR (KBr, cm$^{-1}$):** 3618, 3306, 3113, 3089, 3016, 1703, 1626, 1605, 1573, 1556, 1519, 1346, 1275. **Anal. Calcd.** for $C_{18}H_{10}ClN_5O_5$: C, 52.51; H, 2.45; N, 17.01; found C, 52.20; H, 2.58; N, 16.73.

**Compound 3d.** Prepared using 6,7-dichloropyrido[1,2-*a*]benzimidazole-8,9-dione (150 mg, 0.56 mmol, 1 eq), isonicotinohydrazide (154 mg, 1.12 mmol, 2 eq), and triethylamine (*d* = 0.73 g/mL, v = 78 µL, 0.56 mmol, 1 eq). **Yield:** 50%, orange crystals. **M.P.**: >250 °C (decomp.). **MS:** $C_{17}H_{10}ClN_5O_3$ requires $[M + H]^+$ 368.1; found $[M + H]^+$ 368.2. **$^1$H NMR (300 MHz, DMSO-$d_6$):** 14.52 (br.s., 1H, exchange with $D_2O$, NH), 10.90 (br.s., 1H, exchange with $D_2O$, NH), 9.31 (d, *J* = 6.7, 1H, H-1), 8.91 (d, *J* = 3.8, 2H, $CH_{Py}$), 8.18 (d, *J* = 8.9, 1H, H-4), 7.97 (d, *J* = 4.6, 2H, $CH_{Py}$), 7.89 (t, *J* = 8.0, 1H, H-3), 7.52 (t, *J* = 6.7, 1H, H-2). **FTIR (KBr, cm$^{-1}$):** 3420, 3055, 1709, 1647, 1568, 1555, 1331, 1280. **Anal. Calcd.** for $C_{17}H_{10}ClN_5O_3 + 0.5H_2O$: C, 54.20; H, 2.94; N, 18.59; found C, 54.29; H, 2.88; N, 18.30.

**Compound 3e.** Prepared using 6,7-dichloro-2-nitropyrido[1,2-a]benzimidazole-8,9-dione (150 mg, 0.48 mmol, 1 eq), benzohydrazide (131 mg, 0.96 mmol, 2 eq), and triethylamine (*d* = 0.73 g/mL, v = 67 µL, 0.48 mmol, 1 eq). **Yield:** 61%, yellow solid. **M.P.**: >250 °C (decomp.). **MS:** $C_{18}H_{10}ClN_5O_5$ requires $[M + H]^+$ 412.1; found $[M + H]^+$ 412.4. **$^1$H NMR**

**(300 MHz, DMSO-$d_6$):** 14.42 (br.s., 1H, exchange with $D_2O$, NH), 11.30 (br.s., 1H, exchange with $D_2O$, OH), 10.06 (d, *J* = 2.3 Hz, 1H, H-1), 8.56 (dd, *J* = 9.8, 2.1 Hz 1H, H-3), 8.40 (d, *J* = 9.7 Hz, 1H, H-4), 8.12 (m, 2H, $CH_{Ph}$), 7.72 (d, *J* = 7.7, 3H, $CH_{Ph}$). **FTIR (KBr, cm$^{-1}$):** 3397, 3091, 3033, 1690, 1642, 1552, 1525, 1351, 1311, 1268. **Anal. Calcd.** for $C_{18}H_{10}ClN_5O_5$: C, 52.51; H, 2.45; N, 17.01; found C, 52.21; H, 2.67; N, 16.76.

**Compound 3f.** Prepared using 6,7-dichloro-2-nitropyrido[1,2-a]benzimidazole-8,9-dione (150 mg, 0.48 mmol, 1 eq), 4-methoxybenzohydrazide (160 mg, 0.96 mmol, 2 eq), and triethylamine (*d* = 0.73 g/mL, v = 67 µL, 0.48 mmol, 1 eq). **Yield**: 42%, yellow crystals. **M.P.**: >250 °C (decomp.). **MS:** $C_{19}H_{12}ClN_5O_6$ requires $[M + H]^+$ 442.1; found $[M + H]^+$ 442.2. **$^1$H NMR (300 MHz, DMSO-$d_6$):** 14.36 (br.s., 1H, exchange with $D_2O$, NH), 11.23 (br.s., 1H, exchange with $D_2O$, OH), 10.05 (s, 1H, H-1), 8.56 (d, *J* = 9.7 Hz, 1H, H-3), 8.42 (d, *J* = 10.8 Hz, 1H, H-4), 8.10 (d, *J* = 7.1 Hz, 2H, $CH_{Ph}$), 7.24 (d, *J* = 8.3 Hz, 2H, $CH_{Ph}$), 3.90 (s, 3H, $OCH_3$). **FTIR (KBr, cm$^{-1}$):** 3399, 3085, 3028, 1687, 1640, 1605, 1555, 1523, 1350, 1310, 1266. **Anal. Calcd.** for $C_{19}H_{12}ClN_5O_6$: C, 51.66; H, 2.74; N, 15.85; found C, 51.35; H, 2.68; N, 15.61.

**Compound 3g.** Prepared using 6,7-dichloro-2-nitropyrido[1,2-a]benzimidazole-8,9-dione (150 mg, 0.48 mmol, 1 eq), 4-nitrobenzohydrazide (174 mg, 0.96 mmol, 2 eq), and triethylamine (*d* = 0.73 g/mL, v = 67 µL, 0.48 mmol, 1 eq). **Yield**: 36%, orange solid. **M.P.**: >250 °C (decomp.). **MS:** $C_{18}H_9ClN_6O_7$ requires $[M + H]^+$ 457.0; found $[M + H]^+$ 457.1. **$^1$H NMR (300 MHz, DMSO-$d_6$):** 14.61 (br.s., 1H, exchange with $D_2O$, NH), 11.41 (br.s., 1H, exchange with $D_2O$, OH), 10.03 (s, 1H, H-1), 8.58 (d, *J* = 10.8 Hz, 2H, H-4 and H-3), 8.51 (m, 2H, $CH_{Ph}$), 8.32 (d, *J* = 8.3 Hz, 2H, $CH_{Ph}$). **FTIR (KBr, cm$^{-1}$):** 3340, 3114, 3081, 1707, 1626, 1602, 1547, 1518, 1344, 1306, 1266. **Anal. Calcd.** for $C_{18}H_9ClN_6O_7$: C, 47.33; H, 1.99; N, 18.40; found C, 47.24; H, 2.02; N, 18.14.

## 4. Conclusions

To summarize, a set of heterocyclic α-hydroxy-*p*-quinone imine derivatives was obtained via one-step nucleophilic substitution of 6,7-dichloropyrido[1,2-*a*]benzimidazole-8,9-diones **1a**,**b** with different benzohydrazides **2a**–**d** followed by isomerization. The α-Hydroxy-*p*-quinone imine form of the synthesized products was proved by X-ray crystallography analysis of compound **3a**. The formation of a strong intramolecular hydrogen bond N(12)-H···N(5) in a solid state and in solution can explain the stabilization of only one configuration of the C=N bond of the substituted imine. The $^1$H NMR acid-base titration experiment showed that deprotonation/protonation processes are reversible. Deprotonation led to the electronic delocalization in the molecule, which is accompanied by distinct changes in the UV–Vis spectra.

Sample **CM-1a** has a distinct maximum of two redox reactions. In an acidic environment, both peaks are stable, while in a neutral environment, only one of them is stable and remains unchanged after several CV cycles. Moreover, for the stable redox reactions, the potential difference is only up to 0.2 V. This indicates that the sample **CM-1a** could act as an effective active electrode in aqueous electrolyte batteries. However, the dissolution of the sample in the electrolyte was observed, so the potential application as cathode material for aqueous batteries would require compound **1a** to be attached to the polymer backbone.

Attempts to modulate redox properties by incorporation of additional unsaturated carbon–nitrogen bonds to the heterocyclic quinone **1a** structure led to changes in the redox-active fragment and the formation of *p*-quinone imine **3a**. As a result, the electrochemical behavior is changed, as it is no longer possible to observe pronounced redox peaks in CV measurements. Structural changes of the quinone fragment (probably induced by the formation of intramolecular H-bond) decreased the redox activity of the derivative despite the introduction of an additional C=N bond; at the same time, the introduced substituent enhanced the stability of the cathode material, which was confirmed by Raman spectroscopy measurements. Therefore, further structure optimizations for the elaboration of effective cathode material should include the analysis of the possible tautomerization, the formation of intramolecular H-bonds, the effect of substituents and interaction with basic solvents versus redox properties, and the stability of the compound.

**Supplementary Materials:** The following supporting information can be downloaded at: https://www.mdpi.com/article/10.3390/molecules29071613/s1. Figures S1–S8: $^1$H NMR spectra (for compounds **3a**–**g** in DMSO-$d_6$ solution and for compound **3a** in $CDCl_3$ solution). Figure S9 and Table S1: Correlations between the Hammett constants ($\sigma_p$) of substituent ($R_2$) and the chemical shifts of NH or OH signals of compounds **3a**–**c** and **3e**–**g**. Figure S10: Additional $^1$H NMR spectra for compound **3b** upon acid addition and irradiation. Figures S11 and S13: $^1$H NMR spectra for compounds **3a**–**c** upon base addition. Figure S12: $^1$H NMR spectrum of DBU and TFA mixture. Figures S14 and S15: Hirshfeld surfaces and energy frameworks calculated with CrystalExplorer software. Figure S16 and Table S2: UV–Vis spectroscopy data of compounds **3a**–**c**, **3e**–**g**. Figures S17–S22: CV curves of samples **CM-1a** and **CM-3a** in neutral and acidic electrolytes at various scan speeds (PDF).

**Author Contributions:** Conceptualization, N.B.; formal analysis, A.G.; investigation, A.G., S.B., R.D., Ņ.G. and A.Z.; writing—original draft preparation, A.G., S.B., R.D., A.Z. and N.B.; writing—review and editing, A.G. and N.B.; visualization, A.G., R.D., Ņ.G. and A.Z.; supervision, N.B.; funding acquisition, A.G. All authors have read and agreed to the published version of the manuscript.

**Funding:** This work has been supported by the European Social Fund within project no 8.2.2.0/20/I/008, «Strengthening of PhD students and academic personnel of Riga Technical University and BA School of Business and Finance in the strategic fields of specialization» of the Specific Objective 8.2.2, «To Strengthen Academic Staff of Higher Education Institutions in Strategic Specialization Areas» of the Operational Programme «Growth and Employment». This research/publication was supported by Riga Technical University's Doctoral Grant program (DOK.LKI/23).

**Institutional Review Board Statement:** Not applicable.

**Informed Consent Statement:** Not applicable.

**Data Availability Statement:** Data are contained within the article or Supplementary Materials.

**Conflicts of Interest:** The authors declare no conflicts of interest.

## References

1. Cao, P.; Bracun, L.; Yamagata, A.; Christianson, B.M.; Negami, T.; Zou, B.; Terada, T.; Canniffe, D.P.; Shirouzu, M.; Li, M.; et al. Structural basis for the assembly and quinone transport mechanisms of the dimeric photosynthetic RC–LH1 supercomplex. *Nat. Commun.* **2022**, *13*, 1977. [CrossRef] [PubMed]
2. Gutiérrez-Fernández, J.; Kaszuba, K.; Minhas, G.S.; Baradaran, R.; Tambalo, M.; Gallagher, D.T.; Sazanov, L.A. Key role of quinone in the mechanism of respiratory complex I. *Nat. Commun.* **2020**, *11*, 4135. [CrossRef] [PubMed]
3. Bolton, J.L.; Dunlap, T. Formation and Biological Targets of Quinones: Cytotoxic versus Cytoprotective Effects. *Chem. Res. Toxicol.* **2017**, *30*, 13–37. [CrossRef]
4. Mansha, M.; Anam, A.; Khan, S.A.; Alzahrani, A.S.; Khan, M.; Ahmad, A.; Arshad, M.; Ali, S. Recent Developments on Electroactive Organic Electrolytes for Non-Aqueous Redox Flow Batteries: Current Status, Challenges, and Prospects. *Chem. Rec.* **2023**, *24*, e202300233. [CrossRef] [PubMed]
5. Go, C.Y.; Shin, J.; Choi, M.K.; Jung, I.H.; Kim, K.C. Switchable Design of Redox-Enhanced Nonaromatic Quinones Enabled by Conjugation Recovery. *Adv. Mater.* **2023**, 2311155. [CrossRef] [PubMed]
6. Simon, P.; Gogotsi, Y. Perspectives for electrochemical capacitors and related devices. *Nat. Mater.* **2020**, *19*, 1151–1163. [CrossRef] [PubMed]
7. Shea, J.J.; Luo, C. Organic Electrode Materials for Metal Ion Batteries. *ACS Appl. Mater. Interfaces* **2020**, *12*, 5361–5380. [CrossRef]
8. Jethwa, R.B.; Hey, D.; Kerber, R.N.; Bond, A.D.; Wright, D.S.; Grey, C.P. Exploring the Landscape of Heterocyclic Quinones for Redox Flow Batteries. *ACS Appl. Energy Mater.* **2023**, *7*, 414–426. [CrossRef] [PubMed]
9. Blanc, L.E.; Kundu, D.; Nazar, L.F. Scientific Challenges for the Implementation of Zn-Ion Batteries. *Joule* **2020**, *4*, 771–799. [CrossRef]
10. Tsao, Y.; Lee, M.; Miller, E.C.; Gao, G.; Park, J.; Chen, S.; Katsumata, T.; Tran, H.; Wang, L.-W.; Toney, M.F.; et al. Designing a Quinone-Based Redox Mediator to Facilitate $Li_2S$ Oxidation in Li-S Batteries. *Joule* **2019**, *3*, 872–884. [CrossRef]
11. Sieuw, L.; Jouhara, A.; Quarez, É.; Auger, C.; Gohy, J.-F.; Poizot, P.; Vlad, A. A H-bond stabilized quinone electrode material for Li–organic batteries: The strength of weak bonds. *Chem. Sci.* **2018**, *10*, 418–426. [CrossRef] [PubMed]
12. Sugumaran, M. Reactivities of Quinone Methides versus o-Quinones in Catecholamine Metabolism and Eumelanin Biosynthesis. *Int. J. Mol. Sci.* **2016**, *17*, 1576. [CrossRef] [PubMed]
13. Poddel'Sky, A.I.; Druzhkov, N.O.; Fukin, G.K.; Cherkasov, V.K.; Abakumov, G.A. Bifunctional iminopyridino-catechol and its o-quinone: Synthesis and investigation of coordination abilities. *Polyhedron* **2017**, *124*, 41–50. [CrossRef]
14. Astaf'eva, T.V.; Arsenyev, M.V.; Rumyantcev, R.V.; Fukin, G.K.; Cherkasov, V.K.; Poddel'sky, A.I. Imine-Based Catechols and o-Benzoquinones: Synthesis, Structure, and Features of Redox Behavior. *ACS Omega* **2020**, *5*, 22179–22191. [CrossRef]

15. Ribeiro, R.C.B.; Ferreira, P.G.; Borges, A.D.A.; Forezi, L.D.S.M.; Silva, F.D.C.D.; Ferreira, V.F. 1,2-Naphthoquinone-4-sulfonic acid salts in organic synthesis. *Beilstein J. Org. Chem.* **2022**, *18*, 53–69. [CrossRef]
16. Wu, Z.; Liu, Q.; Yang, P.; Chen, H.; Zhang, Q.; Li, S.; Tang, Y.; Zhang, S. Molecular and Morphological Engineering of Organic Electrode Materials for Electrochemical Energy Storage. *Electrochem. Energy Rev.* **2022**, *5*, 1–67. [CrossRef]
17. Batenko, N.; Belyakov, S.; Kiselovs, G.; Valters, R. Synthesis of 6,7-dichloropyrido[1,2-a]benzimidazole-8,9-dione and its analogues and their reactions with nucleophiles. *Tetrahedron Lett.* **2013**, *54*, 4697–4699. [CrossRef]
18. Gaile, A.; Belyakov, S.; Turovska, B.; Batenko, N. Synthesis of Asymmetric Coupled Polymethines Based on a 7-Chloropyrido[1,2-a]benzimidazole-8,9-dione Core. *J. Org. Chem.* **2022**, *87*, 2345–2355. [CrossRef] [PubMed]
19. Gaile, A.; Belyakov, S.; Rjabovs, V.; Mihailovs, I.; Turovska, B.; Batenko, N. Investigation of Weak Noncovalent Interactions Directed by the Amino Substituent of Pyrido- and Pyrimido-[1,2-a]benzimidazole-8,9-diones. *ACS Omega* **2023**, *8*, 40960–40971. [CrossRef]
20. Yamada, T.; Yamashita, T.; Nakamura, M.; Shimamura, H.; Yamaguchi, A.; Takaya, M. Synthesis and Hemostatic Activity of 1, 2-Naphthoquinones. *Yakugaku Zasshi* **1980**, *100*, 799–806. [CrossRef]
21. Carroll, F.I.; Miller, H.W.; Meck, R. Thiosemicarbazone and amidinohydrazone derivatives of some 1,4-naphthoquinones. *J. Chem. Soc. C Org.* **1970**, *3*, 1993–1996. [CrossRef]
22. Dudley, K.H.; Miller, H.W.; Schneider, P.W.; McKee, R.L. Potential naphthoquinone antimalarials. 2-Acylhydrazino-1,4-naphthoquinones and related compounds. *J. Org. Chem.* **1969**, *34*, 2750–2755. [CrossRef]
23. Smith, M.B.; March, J. *March's Advanced Organic Chemistry: Reactions, Mechanisms, and Structure*, 6th ed.; John Wiley & Sons: Hoboken, NJ, USA, 2006; Volume 9780471720.
24. Spackman, P.R.; Turner, M.J.; McKinnon, J.J.; Wolff, S.K.; Grimwood, D.J.; Jayatilaka, D.; Spackman, M.A. CrystalExplorer: A program for Hirshfeld surface analysis, visualization and quantitative analysis of molecular crystals. *J. Appl. Crystallogr.* **2021**, *54*, 1006–1011. [CrossRef] [PubMed]
25. Turner, M.J.; Thomas, S.P.; Shi, M.W.; Jayatilaka, D.; Spackman, M.A. Energy frameworks: Insights into interaction anisotropy and the mechanical properties of molecular crystals. *Chem. Commun.* **2014**, *51*, 3735–3738. [CrossRef] [PubMed]
26. Catalán, J. Toward a Generalized Treatment of the Solvent Effect Based on Four Empirical Scales: Dipolarity (SdP, a New Scale), Polarizability (SP), Acidity (SA), and Basicity (SB) of the Medium. *J. Phys. Chem. B* **2009**, *113*, 5951–5960. [CrossRef] [PubMed]
27. Shapet'Ko, N.N.; Shigorin, D.N. NMR study of intramolecular hydrogen bond protons in quinoid structures. *J. Struct. Chem.* **1968**, *8*, 474–476. [CrossRef]
28. Kamlet, M.J.; Taft, R.W. The solvatochromic comparison method. I. The .beta.-scale of solvent hydrogen-bond acceptor (HBA) basicities. *J. Am. Chem. Soc.* **1976**, *98*, 377–383. [CrossRef]
29. Hansch, C.; Leo, A.; Taft, R.W. A survey of Hammett substituent constants and resonance and field parameters. *Chem. Rev.* **1991**, *91*, 165–195. [CrossRef]
30. Su, X.; Lõkov, M.; Kütt, A.; Leito, I.; Aprahamian, I. Unusual para-substituent effects on the intramolecular hydrogen-bond in hydrazone-based switches. *Chem. Commun.* **2012**, *48*, 10490–10492. [CrossRef]
31. Su, X.; Aprahamian, I. Hydrazone-based switches, metallo-assemblies and sensors. *Chem. Soc. Rev.* **2014**, *43*, 1963–1981. [CrossRef]
32. Johnson, J.E.; Morales, N.M.; Gorczyca, A.M.; Dolliver, D.D.; McAllister, M.A. Mechanisms of Acid-Catalyzed Z/E Isomerization of Imines. *J. Org. Chem.* **2001**, *66*, 7979–7985. [CrossRef] [PubMed]
33. Su, X.; Aprahamian, I. Switching Around Two Axles: Controlling the Configuration and Conformation of a Hydrazone-Based Switch. *Org. Lett.* **2010**, *13*, 30–33. [CrossRef] [PubMed]
34. Ryabchun, A.; Li, Q.; Lancia, F.; Aprahamian, I.; Katsonis, N. Shape-Persistent Actuators from Hydrazone Photoswitches. *J. Am. Chem. Soc.* **2019**, *141*, 1196–1200. [CrossRef]
35. Kim, J.; Ling, J.; Lai, Y.; Milner, P.J. Redox-Active Organic Materials: From Energy Storage to Redox Catalysis. *ACS Mater. Au* **2024**. [CrossRef]
36. Wang, M.; Dong, X.; Escobar, I.C.; Cheng, Y.-T. Lithium Ion Battery Electrodes Made Using Dimethyl Sulfoxide (DMSO)—A Green Solvent. ACS Sustain. *Chem. Eng.* **2020**, *8*, 11046–11051. [CrossRef]
37. Laurence, C.; Legros, J.; Chantzis, A.; Planchat, A.; Jacquemin, D. A Database of Dispersion-Induction DI, Electrostatic ES, and Hydrogen Bonding α1 and β1 Solvent Parameters and Some Applications to the Multiparameter Correlation Analysis of Solvent Effects. *J. Phys. Chem. B* **2015**, *119*, 3174–3184. [CrossRef]
38. Matsui, M. Polymethine Dyes. In *Progress in the Science of Functional Dyes*; Ooyama, Y., Yagi, S., Eds.; Springer: Singapore, Singapore, 2021; pp. 3–19. [CrossRef]
39. Miran, M.S.; Kinoshita, H.; Yasuda, T.; Susan, A.B.H.; Watanabe, M. Hydrogen bonds in protic ionic liquids and their correlation with physicochemical properties. *Chem. Commun.* **2011**, *47*, 12676–12678. [CrossRef] [PubMed]
40. Almeida, R.G.; Valença, W.O.; Rosa, L.G.; de Simone, C.A.; de Castro, S.L.; Barbosa, J.M.C.; Pinheiro, D.P.; Paier, C.R.K.; de Carvalho, G.G.C.; Pessoa, C.; et al. Synthesis of quinone imine and sulphur-containing compounds with antitumor and trypanocidal activities: Redox and biological implications. *RSC Med. Chem.* **2020**, *11*, 1145–1160. [CrossRef] [PubMed]
41. Klopčič, I.; Dolenc, M.S. Chemicals and Drugs Forming Reactive Quinone and Quinone Imine Metabolites. *Chem. Res. Toxicol.* **2018**, *32*, 1–34. [CrossRef]
42. Batenko, N.; Kricka, A.; Belyakov, S.; Turovska, B.; Valters, R. A novel method for the synthesis of benzimidazole-based 1,4-quinone derivatives. *Tetrahedron Lett.* **2015**, *57*, 292–295. [CrossRef]

43. Smith, E.; Dent, G. *Modern Raman Spectroscopy—A Practical Approach*; John Wiley & Sons: Chichester, UK, 2004. [CrossRef]
44. Kudin, K.N.; Ozbas, B.; Schniepp, H.C.; Prud'Homme, R.K.; Aksay, I.A.; Car, R. Raman Spectra of Graphite Oxide and Functionalized Graphene Sheets. *Nano Lett.* **2007**, *8*, 36–41. [CrossRef] [PubMed]
45. Saravanan, M.; Ganesan, M.; Ambalavanan, S. An in situ generated carbon as integrated conductive additive for hierarchical negative plate of lead-acid battery. *J. Power Sources* **2014**, *251*, 20–29. [CrossRef]
46. Gottlieb, H.E.; Kotlyar, V.; Nudelman, A. NMR Chemical Shifts of Common Laboratory Solvents as Trace Impurities. *J. Org. Chem.* **1997**, *62*, 7512–7515. [CrossRef] [PubMed]
47. Sheldrick, G.M. Crystal structure refinement with SHELXL. Acta Crystallogr. *Sect. C Struct. Chem.* **2015**, *71*, 3–8. [CrossRef] [PubMed]
48. Bourhis, L.J.; Dolomanov, O.V.; Gildea, R.J.; Howard, J.A.K.; Puschmann, H. The anatomy of a comprehensive constrained, restrained refinement program for the modern computing environment–Olex2dissected. Acta Crystallogr. *Sect. A Found. Adv.* **2015**, *71*, 59–75. [CrossRef]
49. Macrae, C.F.; Sovago, I.; Cottrell, S.J.; Galek, P.T.A.; McCabe, P.; Pidcock, E.; Platings, M.; Shields, G.P.; Stevens, J.S.; Towler, M.; et al. Mercury 4.0: From visualization to analysis, design and prediction. *J. Appl. Crystallogr.* **2020**, *53*, 226–235. [CrossRef]

4. Pielikums

Appendix 4

Anastasija Gaile, Nelli Batenko

# Synthesis of heterocyclic ring-fused quinones (microreview)

*Chem. Heterocycl. Compd.* **2021**, *57* (11), 1076–1078.

DOI: 10.1007/s10593-021-03027-w

DOI 10.1007/s10593-021-03027-w

*Chemistry of Heterocyclic Compounds* **2021**, *57*(11), 1076–1078

HETEROCYCLES IN FOCUS

# Synthesis of heterocyclic ring-fused quinones (microreview)

**Anastasija Gaile**[1], **Nelli Batenko**[1]*

[1] *Institute of Applied Chemistry, Faculty of Materials Science and Applied Chemistry, Riga Technical University, 3/7 Paula Valdena St., Riga LV-1048, Latvia; e-mail: nelli.batenko@rtu.lv*

Published in Khimiya Geterotsiklicheskikh Soedinenii, 2021, *57*(11), 1076–1078

Submitted October 10, 2021
Accepted after revision November 12, 2021

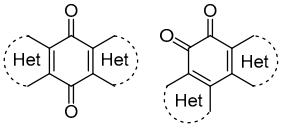


This microreview presents the data on the methods of synthesis of heterocyclic ring-fused quinones over the period from 2015 to 2021.

## Introduction

Quinones are organic chromophores and potent bioactive compounds exhibiting antitumor, antibacterial as well as antifungal activities.[1] The diverse biological effects caused by combination of quinone with heterocyclic fragment has already led to the development of some heterocyclic ring-fused quinones having pronounced biological activity.[2] For example, a well-known antitumor drug Mitomycin C is a derivative of *p*-quinone fused with nitrogen-containing heterocycle.[3] Due to their relevant biological applications, preparation of heterocyclic ring-fused quinones has attracted considerable attention.

## Cycloaddition reactions

Quinones as dipolarophiles represent a privileged platform for the synthesis of ring-fused pyrazoles *via* [3+2] cycloaddition reaction. Pyrazole-fused quinones **3** were obtained by base-promoted [3+2] cycloaddition reaction of *p*-naphthoquinone (**1**) with electron-deficient $CF_3$-substituted iminonitriles, which were generated *in situ* from compounds **2**.[4] Another method for the preparation of pyrazole-fused quinones **5** includes photogeneration of the iminonitrile from 2,5-diaryltetrazole **4**, followed by the sequential 1,3-dipolar cycloaddition/enolization and oxidation processes.[5]

Pyrazole-fused isoquinoline-5,8-diones **8a**,**b** were prepared *via* 1,3-dipolar cycloaddition of *N*-aryl-*C*-heteroarylimino-nitriles (generated *in situ* from compounds **7**) and substituted isoquinoline-5,8-diones **6**. Regioisomeric ratio **8a**:**8b** = = 20:80 was obtained using $Ag_2CO_3$ as a base. Isolated yields of the major regioisomer were 45–72%.[6]

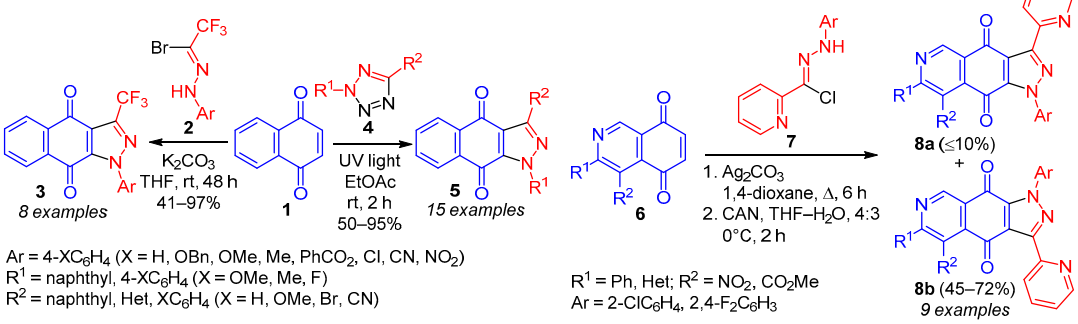


**Nelli Batenko** received her PhD in Chemistry from the Riga Technical University (RTU) in 2005. Currently she is an associate professor at the Faculty of Materials Science and Applied Chemistry, RTU. Her scientific interests include chemistry and properties of quinone derivatives and heterocyclic compounds.

**Anastasija Gaile** received her MSc degree in Chemistry from the Riga Technical University (RTU) in 2020. Currently she is working toward PhD thesis under supervision of associate professor Nelli Batenko and professor Valdis Kampars at the Faculty of Materials Science and Applied Chemistry, RTU. Her research focuses on reactions of heterocyclic quinones and their properties.

**Cycloaddition reactions** (continued)

A formal [3+3] cycloaddition reaction of methyl (*Z*)-3-[(2-hydroxyethyl)amino]but-2-enoate (**10**) and acylnaphthoquinones, which were generated *in situ* from naphthalene-1,4-diols **9** using $Ag_2O$, yielded the corresponding 1,2-dihydrobenzo[*g*]isoquinoline-5,10-diones **11**.[7]

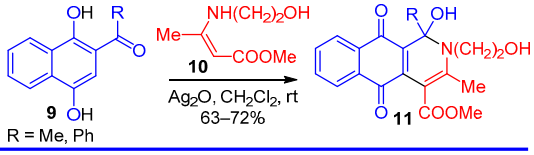


**Multicomponent reactions**

Naphthoquinone-fused indolizines **15** were prepared in moderate yield by multicomponent reaction of quinone **12** with 1,3-indandione (**13**) and substituted pyridines **14** in boiling MeCN followed by oxidation with $H_2O_2$.[8]

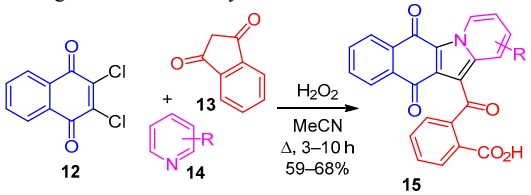


Pseudo four-component one-pot reaction of 2-hydroxy-1,4-naphthoquinone (**16**) with aniline derivatives **17** and 2 equivalents of formaldehyde under ultrasound irradiation in $H_2O$ led to naphthoquinone-fused oxazine derivatives **18**. When aniline derivatives with a strong electron-withdrawing group were used, lower product yield was observed and longer reaction time was required.[9]

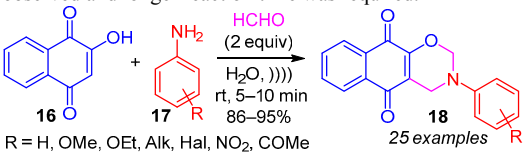


**Oxidation of heterocycles**

Specific oxidative quinone formation during the total synthesis of calothrixin B (**20**) was reported by Liu et al.[10] Screening of oxidation conditions revealed that the installation of a quinone carbonyl groups at the C ring of quino[4,3-*b*]carbazole **19** was efficient using DMP (Dess–Martin periodinane) in DMSO. Under these conditions, calothrixin B (**20**) was synthesized in 91% yield.

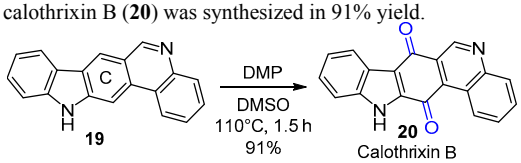


Begunov et al.[11] reported synthesis of hetero-fused *p*-quinones **22** from 3*H*-imidazo[4",5":4',5']benzo[1',2':4,5]imidazo[1,2-*a*]-pyridines **21**. The method included nitration of compounds **21** with $KNO_3$ in $H_2SO_4$ under rather mild conditions (30°C, 1.5 h) and subsequent reduction of the nitro derivatives with 10% HCl and $TiCl_3$ (40°C, 0.5 h). Resulting aminoheterocycles were then oxidized at 25°C using $KNO_3/H_2SO_4$ oxidation system.

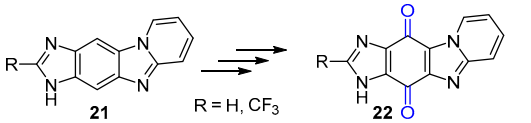


Similar approach was reported by Zhou et al.,[12] using heterocycle **23**, which yielded C-6- and C-7-nitro derivatives upon treating with $NaNO_2$ in AcOH. After catalytic reduction of the nitro group with $H_2$ (Pd/C), the corresponding amines were oxidized by Fremy's salt to yield two isomeric perimidinediones **24a** and **24b**, which could be separated by column chromatography.

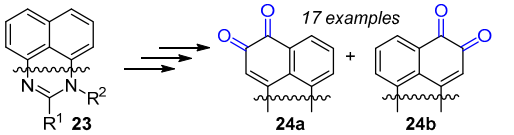


**Reactions of tetraamino-*p*-benzoquinone**

Tetraamino-*p*-benzoquinone (**25**) is a good substrate for the synthesis of quinones fused with five- or six-membered azaheterocycles. Benzo[1,2-*d*:4,5-*d*']bis([1,2,3]triazole)-4,8(2*H*,6*H*)-dione (**26**) was prepared by diazotization of quinone **25**, followed by an intramolecular cyclization reaction. Additionally, its π-extended analog bis([1,2,3]-triazolo)[4,5-*b*:4',5'-*i*]phenazine-4,6,10,12(2*H*,8*H*)-tetraone (**27**), was obtained in the same reaction due to intermolecular coupling of two intermediate diazonium salt molecules.[13] Double condensation of quinone **25** with compound **28** in refluxing AcOH led to planar polycyclic quinone **29** in 59% yield.[14]

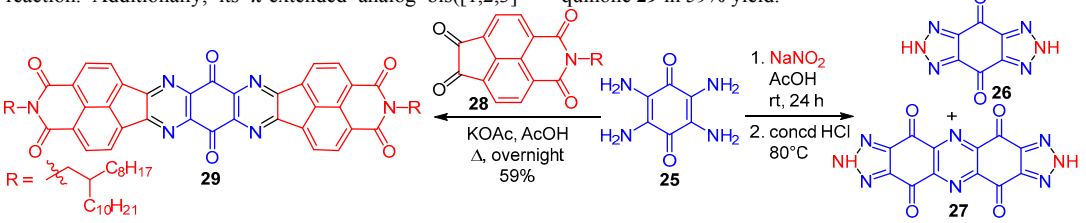

**Miscellaneous**

In general, *p*-quinones can be prepared from dimethoxybenzene derivatives *via* oxidative demethylation, using different oxidation reagents (CAN, NBS/$H_2SO_4$, PhI$(OCOCF_3)_2$ (PIFA), etc.). Halogenated (bibenzimidazole)tetraone derivatives were prepared using NaX/Oxone (X = Cl, Br) system by one-pot electrophilic aromatic substitution and oxidative demethylation reactions.[15]

Novel quinone-indolizine hybrids **31** were prepared *via* domino Michael addition/aldol condensation/aromatization sequence, using $Et_3N$-promoted reaction of *p*-naphthoquinone (**1**) and *N*-substituted pyrrole-2-carboxaldehydes **30**. Quinone-indolizine hybrids revealed potent anticancer effects.[16]

Benzimidazole- and imidazopyrimidine-based *o*-quinones **33** were synthesized through a condensation reaction of 2,3-dichloro-*p*-naphthoquinone derivatives **12** with 2-aminoazines **32** in dry *s*-BuOH. The reaction was carried out at high temperature under argon atmosphere in a closed pressure vessel for 36 h. Electron-withdrawing groups ($R^2$ = $NO_2$, $CF_3$) on 2-aminoazine complicated the cyclization process making it longer.[17]

Intermolecular Michael addition of deprotonated 3-(phenylsulfonyl)isobenzofuran-1(3*H*)-one (**34**) to 2-nitrobenzofuran derivatives **35** followed by Dieckmann cyclization and elimination of a sulfonyl anion and nitro group afforded naphthoquinone-fused benzofurans **36** in 70–87% yield.[18]

Naphthoquinone-fused pyran-2-one derivatives **39** were obtained from 3-hydroxynaphthoquinone-2-carbaldehyde (**37**) and nitrile **38** in $H_2O$ under mild conditions and short reaction time. Application of nonpolar or polar aprotic solvents led to the lower product yields.[19]

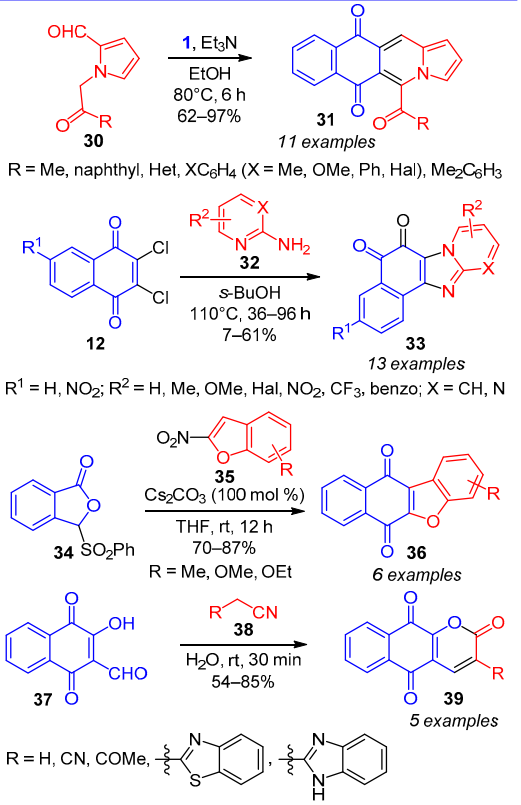


*This publication was supported by Riga Technical University's Doctoral Grant programme (34-14800-DOK.LKI/20).*

## References


1. Asche, C. *Mini-Rev. Med. Chem.* **2005**, *5*, 449.
2. Garuti, L.; Roberti, M.; Pizzirani, D. *Mini-Rev. Med. Chem.* **2007**, *7*, 481.
3. Bass, P. D.; Gubler, D. A.; Judd, T. C.; Williams, R. M. *Chem. Rev.* **2013**, *113*, 6816.
4. Utecht-Jarzynska, G.; Nagła, K.; Mloston, G.; Heimgartner, H.; Palusiak, M.; Jasinski, M. *Beilstein J. Org. Chem.* **2021**, *17*, 1509.
5. Ortiz-Rojano, L.; Rojas-Martín, J.; Rodríguez-Diaz, C.; Carreño, M. C.; Ribagorda, M. *Chem.–Eur. J.* **2019**, *25*, 15050.
6. Bertuzzi, G.; Crotti, S.; Calandro, P.; Bonini, B. F.; Monaco, I.; Locatelli, E.; Fochi, M.; Zani, P.; Strocchi, E.; Mazzanti, A.; Chiariello, M.; Franchini, M. *ChemMedChem* **2018**, *13*, 1744.
7. Valderrama, J. A.; Garrido, J.; Delgado, V.; Benites, J.; Theoduloz, C. *Molecules* **2017**, *22*(12), 1.
8. Batenko, N.; Neibolte, I.; Belyakov, S.; Valters, R. *J. Fluoresc.* **2016**, *26*, 23.
9. Cao, Y.-Q.; Li, X.-R.; Wu, W.; Zhang, D.; Zhang, Z.-H.; Mo, L.-P. *Res. Chem. Intermed.* **2017**, *43*, 3745.
10. Liu, Y.; Xu, M.; Xie, K.; Liu, S. *Adv. Synth. Catal.* **2021**, *363*, 737.
11. Begunov, R. S.; Sokolov, A. A.; Filimonov, S. I. *Russ. J. Org. Chem.* **2020**, *56*, 1383. [*Zh. Org. Khim.* **2020**, *56*, 1222.]
12. Zhou, D.-C.; Lu, Y.-T.; Mai, Y.-W.; Zhang, C.; Xia, J.; Yao, P.-F.; Wang, H.-G.; Huang, S.-L.; Huang, Z.-S. *Bioorg. Chem.* **2019**, *91*, 103131.
13. Sato, M.; Takeda, T.; Hoshino, N.; Akutagawa, T. *CrystEngComm* **2017**, *19*, 910.
14. Wang, Z.; Peng, Q.; Huang, X.; Ma, Q.; Shen, Q.; Shao, J. *Mater. Technol.* **2020**. DOI: 10.1080/10667857.2020.1810925.
15. Conboy, D.; Kielty, P.; Bear, J. C.; Cockcroft, J. K.; Farràs, P.; McArdle, P.; Singer, R. J.; Smith, D. A.; Aldabbagh, F. *Org. Biomol. Chem.* **2021**, *19*, 2716.
16. Joshi, D. R.; Seo, Y.; Heo, Y.; Park, S.-h.; Lee, Y.; Namkung, W.; Kim, I. *J. Org. Chem.* **2020**, *85*, 10994.
17. Šarlauskas, J.; Peciukaityte-Alskne, M.; Miseviciene, L.; Maroziene, A.; Polmickaite, E.; Staniulyte, Z.; Cenas, N.; Anusevicius, Z. *Bioorg. Med. Chem. Lett.* **2016**, *26*, 512.
18. Wood, J. M.; Satam, N. S.; Almeida, R. G.; Cristani, V. S.; de Lima, D. P.; Dantas-Pereira, L.; Salomão, K.; Menna-Barreto, R. F. S.; Namboothiri, I. N. N.; Bower, J. F.; da Silva, E. N., Jr. *Bioorg. Med. Chem.* **2020**, *28*, 115565.
19. Patil, S. R.; Choudhary, A. S.; Sekar, N. *Tetrahedron Lett.* **2016**, *57*, 3100.

5. Pielikums

Appendix 5

Nelli Batenko, Anastasija Gaile

# Chemosensors Based on 5-Ethylidene-Substituted Barbituric Acid Derivatives (Microreview)

*Chem. Heterocycl. Compd.* **2022**, *58* (2–3), 97–99.

DOI: 10.1007/s10593-022-03061-2

*Chemistry of Heterocyclic Compounds* **2022**, *58*(2/3), 97–99

HETERO CYCLES IN FOCUS

# Chemosensors based on 5-ethylidene-substituted barbituric acid derivatives (microreview)

**Nelli Batenko[1]*, Anastasija Gaile[1]**

[1] *Institute of Applied Chemistry, Faculty of Materials Science and Applied Chemistry, Riga Technical University, 3/7 Paula Valdena St., Riga LV-1048, Latvia; e-mail: nelli.batenko@rtu.lv*

Published in Khimiya Geterotsiklicheskikh Soedinenii, 2022, *58*(2/3), 97–99

Submitted February 8, 2022
Accepted February 20, 2022

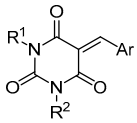

This microreview presents the data on the general synthetic methods for 5-ethylidene-substituted barbituric acid derivatives and their application as chemosensors or probes for detection of ionic species, explosives, gases, and biomolecules over the period from 2018 to 2021.

## Introduction

Barbituric acid (BA) is well-known pyrimidine derivative with pronounced electron-withdrawing properties and planar structure.[1] 5-Ethylidene-substituted BAs show phenomenon of aggregation-induced emission (AIE) and can be termed as AIEgens.[2] Employing AIEgens as sensors will become a future trend for analyte identification.[3] AIEgens were used in the development of sensitive and selective chemosensors/probes for different types of analytes: ionic species, explosives, gases, and biomolecules.[2] According to Krämer et. al.,[4] chemosensors are the systems that reversibly bind the target analyte through a combination of noncovalent binding interactions, while probes are the systems that form strong irreversible bonds with the target analyte.

Typical AIEgens are often large molecules, macromolecules or polymers, implying complex synthetic procedures and/or high costs. BA forms a large variety of derivatives by simple Knoevenagel condensation, which can be used as organic fluorescent dyes. Fluorescence probes have two modes of action: fluorescence enhancement ("turn-on") or fluorescence quenching ("turn-off"). Creation of AIEgens with a donor–acceptor (D–A) structure as well as introduction of typical AIEgens (triphenylamine, tetraphenylethene) into D–A system can improve photophysical properties such as long-wavelength emission, solvatochromism, etc.[5] D–A systems based on BA can be readily created by incorporating different electron-rich functional groups.

## Synthesis

The Knoevenagel condensation is experimentally simple and environmentally friendly synthesis method for 5-ethylidene-substituted BA derivatives **2**. To accomplish this reaction, an aldehyde **1** and commercially available BA ($R^1$ = $R^2$ = H) or 1,3-dimethylBA ($R^1$ = $R^2$ = Me) are widely used.

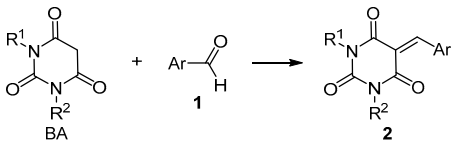


$R^1$, $R^2$ = H, Me, Alk, Ar
Ar = aryl, hetaryl

**Nelli Batenko** received her Dr. chem. degree from Riga Technical University (RTU) in 2005. Currently she is an associate professor at the Faculty of Materials Science and Applied Chemistry, RTU. Her scientific interests include chemistry and properties of heterocyclic compounds and quinone derivatives.

**Anastasija Gaile** received her M. Sc. degree in chemistry from RTU in 2020. Currently she is working toward PhD thesis under supervision of associate professor Nelli Batenko and professor Valdis Kampars at the Faculty of Materials Science and Applied Chemistry, RTU. Her research focuses on reactions of heterocyclic compounds, quinone derivatives and their properties.

**Synthesis** (continued)

Other symmetrical 1,3-disubstituted BAs can be prepared, for example, in two steps by the reaction of a primary amine with carbonyldiimidazole in *t*-BuOH giving rise to *N*,*N*-disubstituted urea and its subsequent cyclization with malonyl chloride. The synthesis of asymmetrical 1,3-disubstituted BAs can be realized *via* the reaction of an amine and substituted isocyanate generating asymmetrical urea **3** as an intermediate. Being treated with malonyl chloride (**4**) the latter forms asymmetrically *N*,*N*'-disubstituted BA.[6]

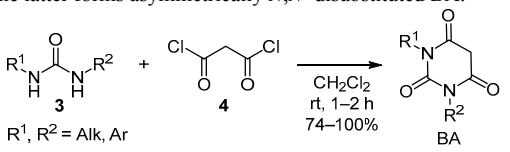


**Detection of hydrazine**

Hydrazine has high toxicity and strong irritant effect. That is why convenient and reliable methods for hydrazine detection are in high demand. Probes **2a**,**b** were synthesized by condensation of BA and corresponding heterocyclic aldehyde.[7,8] In both cases the enhancement of fluorescence ("turn-on") was observed in the presence of hydrazine.

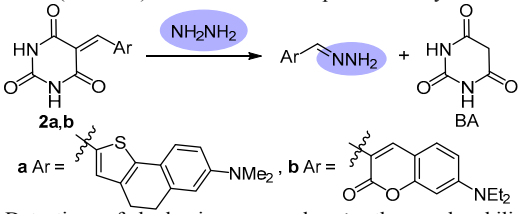


Detection of hydrazine proceeds *via* the nucleophilic addition of hydrazine to the C=C bond of the arylidene substituent, resulting in the removal of BA.[7] Compounds **2a**,**b** can be successfully implemented to indicate the presence of hydrazine in biological samples. Additionally, in solution probe **2b** showed a change of UV absorption spectrum and turn-off fluorescence upon addition of $ClO^-$. Coumarin-based compound **2b** showed dual-mode detection capability for sensing $ClO^-$ and $N_2H_4$.

**Detection of nitroaromatics**

Arylidene derivatives of BA were investigated on the ability to detect electron-deficient nitroaromatic explosives (NACs) using 2,4-dinitrotoluene and picric acid as a model system. A common feature of BAs **2c** is that they do not emit (or have weak emittance) in solution, but strong fluorescence is observed in the aggregated state. Detection of NACs is based on the quenching of fluorescence ("turn-off").

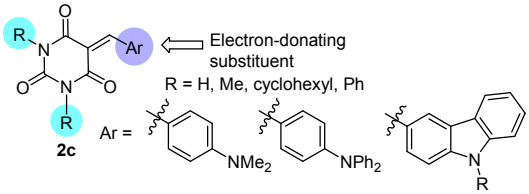


It should be noted that substituents at 1,3-positions of BA have an influence on the properties of derivatives **2c** and size of aggregates: in the case of R = H, intermolecular hydrogen bonding leads to the formation of large aggregates. Lower photostability and decrease of fluorescence intensity was observed in the case of 1,3-unsubstituted derivative **2c** (R = H) due to lactam–lactim tautomerization.[9] The enhance of AIE effect can be provided by increase of hydrophobic properties of electron-donating substituent Ar.[10]

Electron-rich aryl groups in compounds **2c** promote the interaction with electron-deficient nitroaromatics. It was found[11] that the fluorescence intensity of compounds **2c** was significantly decreased with the increased concentration of nitroaromatics. Authors[11,12] suppose that the main fluorescence quencher is photoinduced electron transfer (PET) between the LUMO of the fluorophore (limited to BA core) and LUMO of electron-deficient NACs.

The AIE quenching effect, observed by authors[9,13] had the same pattern for water samples from diverse environments and was nonsensitive to the presence of different metal ions. It is known[2,12] that compounds with AIE properties are an important source of mechanochromic fluorescence (MCF) materials. It was showed[11,14] that some derivatives **2c** have pronounced MCF properties.

**Detection of cyanide**

Different colorimetric and fluorescent turn-on probes **2d** containing D–π–A structure and sensitive to the presence of cyanide were elaborated.[15–20] The sensing mechanism is based on the nucleophilic addition of a cyanide ion to the arylidene C=C bond resulting in the interrupted π-conjugation and blocked intramolecular charge transfer (ICT) process.[17] The addition of common anions had no effect on the $CN^-$ detection.

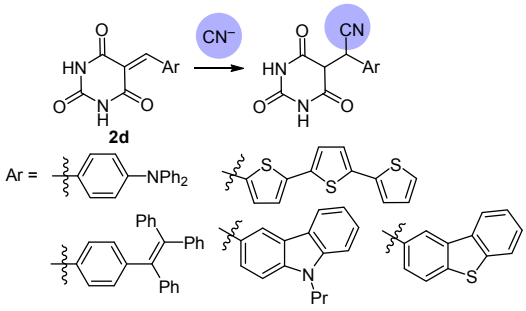


Probe **2e**, synthesized by the reaction of 4,4'-diformyltriphenylamine with an excess of BA and containing two fragments of BA, showed high sensitivity toward $CN^-$.[21]

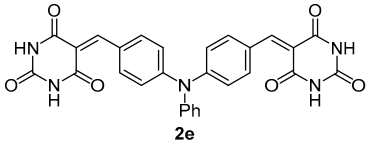

## Detection of cations

Julolidine–BA hybrids **2f**[22] form well-organized by intermolecular hydrogen bonding hexameric structure with the cavity that allows the metal ion coordination. The chemosensors were selective toward $Hg^{2+}$ (X = O, S) and $Ag^{+}$ (X = S) ions. Compounds **2f** provide the signal by means of color change. Silatrane-based compound **2g**[23] showed UV-Vis absorbance changes upon addition of a silver ion. Potential binding sites are triazole nitrogen atom and carbonyl oxygen of the BA. Interestingly, compound **2d** (Ar = 4-(diphenylamino)phenyl) also displays sensitivity for $Hg^{2+}$ ions in aqueous solution.[16]

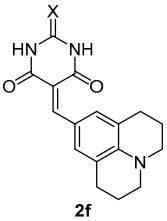


**2f**

X = O, S

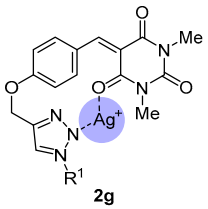


**2g**

$R^1 = (CH_2)_3Si(OCH_2CH_2)_3N$

## Detection of chlorine

Modification of compounds **2c** by typical for AIEgens *N*-[4-(1,2,2-triphenylvinyl)phenyl] fragment leads to asymmetrical donor – acceptor – another donor (D–A–D') derivatives **2h** that showed dramatic decrease of fluorescence intensity after exposure to $Cl_2$ gas.[24]

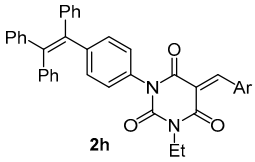


**2h**

## Detection of biothiols

Dihydrophenazine–BA hybrids **2i** were designed as colorimetric and ratiometric fluorescent probes for the ultrasensitive and selective detection of biothiols. An acceptor – donor – another acceptor (A–D–A') structure with two different routes of ICT process was established.[25]

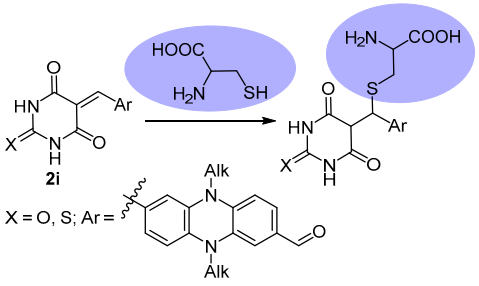


**2i**

X = O, S; Ar =

## Conclusions

5-Ethylidene-substituted barbituric acids are versatile platforms for the elaboration of different chemosensors and probes due to simple synthesis, possible modification of hydrophilic/hydrophobic interactions with environment, and clear response to an analyte.

## References


1. Ding, S.; Yao, B.; Schobben, L.; Hong, Y. *Molecules* **2019**, *25*, 32.
2. Mei, J.; Leung, N. L. C.; Kwok, R. T. K.; Lam, J. W. Y.; Tang, B. Z. *Chem. Rev.* **2015**, *115*, 11718.
3. Zhao, E.; Lai, P.; Xu, Y.; Zhang, G.; Chen, S. *Front. Chem.* **2020**, *8*, Article 288. https://doi.org/10.3389/fchem.2020.00288.
4. Krämer, J.; Kang, R.; Grimm, L. M.; De Cola, L.; Picchetti, P.; Biedermann, F. *Chem. Rev.* **2022**, *122*, 3459.
5. Mei, J.; Hong, Y.; Lam, J. W. Y.; Qin, A.; Tang, Y.; Tang, B. Z. *Adv. Mater.* **2014**, *26*, 5429.
6. Portier, F.; Solier, J.; Halila, S. *Eur. J. Org. Chem.* **2019**, 6158.
7. Du, J.; Li, X.; Ruan, S.; Li, Y.; Ren, F.; Cao, Y.; Wang, X.; Zhang, Y.; Wu, S.; Li, J. *Analyst* **2020**, *145*, 636.
8. Wu, H.; Zhang, W.; Wu, Y.; Liu, N.; Meng, F.; Xie, Y.; Yan, L. *Microchem. J.* **2020**, *159*, 105461.
9. Zhang, H.-J.; Tian, Y.; Tao, F.-r.; Yu, W.; You, K.-Y.; Zhou, L.-R.; Su, X.; Li, T.-d.; Cui, Y.-Z. *Spectrochim. Acta, Part A* **2019**, *222*, 117168.
10. Zhang, H.; Tao, F.; Cui, Y.; Xu, Z. *J. Mol. Liq.* **2020**, *302*, 112550.
11. Xu, J.; Zhang, H.; Xu, Z.; Tao, F.; Cui, Y. *J. Lumin.* **2021**, *232*, 117865.
12. Xu, J.; Zhang, H.; Xu, Z.; Tao, F.; Cui, Y.; Yu, W. W. *J. Nanomater.* **2020**, 7826231.
13. Li, K.; Yu, R.-H.; Shi, C.-M.; Tao, F.-R.; Li, T.-D.; Cui, Y.-Z. *Sens. Actuators, B* **2018**, *262*, 637.
14. Zhang, H.; Cui, Y.; Tao, F.; Zhang, D.; Xu, Z.; Guo, L. *Spectrochim. Acta, Part A* **2019**, *223*, 117320.
15. Zou, Q.; Tao, F.; Xu, Z.; Ding, Y.; Tian, Y.; Cui, Y. *Anal. Methods* **2019**, *11*, 5553.
16. Wen, X.; Yan, L.; Fan, Z. *Spectrochim. Acta, Part A* **2020**, *241*, 118664.
17. Li, D.; Ma, J.; Wang, H.; Liu, L.; Yang, H. *J. Mater. Sci.* **2021**, *56*, 1373.
18. Guo, Z.; Niu, Q.; Yang, Q.; Li, T.; Chi, H. *Anal. Chim. Acta* **2019**, *1065*, 113.
19. Zou, Q.; Tao, F.; Wu, H.; Yu, W. W.; Li, T.; Cui, Y. *Dyes Pigm.* **2019**, *164*, 165.
20. Sun, T.; Niu, Q.; Li, Y.; Li, T.; Hu, T.; Wang, E.; Liu, H. *Sens. Actuators, B* **2018**, *258*, 64.
21. Zuo, B.; Liu, L.; Feng, X.; Li, D.; Li, W.; Huang, M.; Deng, Q. *Dyes Pigment.* **2021**, *193*, 109534.
22. Yuvaraj, P.; Ajantha, J.; Karuppusamy, M.; Easwaramoorthi, S.; Rao, J. R. *ACS Sustainable Chem. Eng.* **2021**, *9*, 10309.
23. Singh, G.; Singh, A.; Satija, P.; Sharma, G.; Shilpy; Singh, J.; Singh, J.; Singh, K. N.; Kaur, A. *New J. Chem.* **2019**, *43*, 5525.
24. Ma, L.; Li, C.; Liang, Q.; Wang, S.; Cao, D. *Dyes Pigm.* **2018**, *149*, 543.
25. Zhang, X.; Yan, Y.; Hang, Y.; Wang, J.; Hua, J.; Tian, H. *Chem. Commun.* **2017**, *53*, 5760.

6. Pielikums

Appendix 6

Anastasija Gaile, Ramona Durena, Ņikita Griščenko, Anzelms Zukuls, Nelli Batenko

# Uz 6,7-dihlorpirido[1,2-*a*]benzimidazola-8,9-diona atvasinājumu bāzes izgatavotu katodu materiālu pētījumi

# Studies of cathode materials based on 6,7-dichloropyrido[1,2-*a*]benzimidazole-8,9-dione derivatives

*Nepublicētie rezultāti / Unpublished results*

# Supporting information

# Studies of cathode materials based on 6,7-dichloropyrido[1,2-*a*]benzimidazole-8,9-dione derivatives

**Table of contents:**



## 1. Synthesis of the compounds

Procedures for the preparation of the compounds **10**, **7H** and 6-amino-7-chloropyrido[1,2-*a*]benzimidazole-8,9-dione (**Q-NH$_2$**) (Fig. S1) were described previously.[1,2]

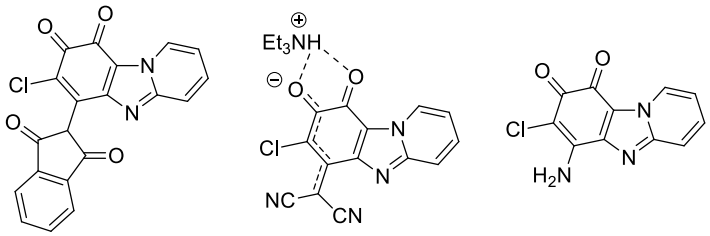


Fig. S1. Structures of the investigated compounds **7H**, **10** and **Q-NH$_2$**.

## 2. Cathode material preparation

Quinone derivatives **10**, **7H** or **Q-NH$_2$** were combined with *Vulcan XC72 CB* at a mass ratio of 5:4. The resulting powder was dried overnight at 80 °C. Then a binder solution of PVDF:DMF (mass ratio 1:9) was added, so the quinone to PVDF mass ratio would be 5:1. Stirring and ultra-sonication were used to create the ink slurry. Extra DMF was added to the slurry to form homogenous ink (the total weight ratio of DMF to quinone was approximately 12:1). Manual doctor blade coater (with a 25 µm gap size) was employed to apply the coating onto carbon paper that was pre-dried at 120 °C for an hour. Coated cathode substrates were then dried in air to evaporate DMF. For further material characterization cathode disks were cut out using a hollow punch.

## 3. Cyclic voltammetry (CV)

To analyze the electrochemical properties of the different sample compounds cyclic voltammetry (CV) measurements were performed using a 3-electrode measuring cell "TSC Surface" (from rhd instruments). For different measurements, the prepared thin layer electrodes on carbon paper (with quinone derivatives **10**, **7H** or **Q-NH$_2$**) were used as working electrodes placed in 1 mL of electrolyte with the platinum counter electrode and Ag/AgCl (3 M KCl) reference electrode. Acidic electrolyte solution (0.5 M $H_2SO_4$) was used for measurements. The CV measurements were performed from –0.4 to +1.0 V with the following program: ten cycles with scan speed of 0.075 V/s to stabilize the half-cell and 5 cycles of 5 scans with scan rates ranging from 0.005 V/s to 0.1 V/s.

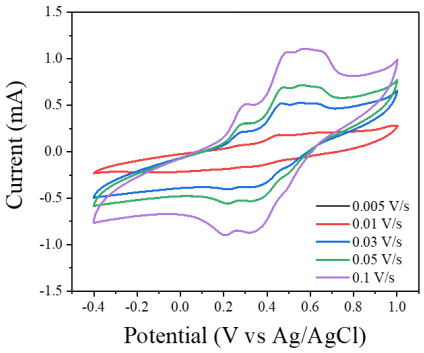


Fig. S2. CV of sample **CM-7H**.

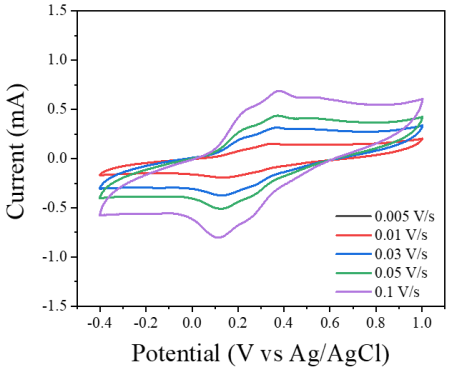


Fig. S3. CV of sample **CM-10**.

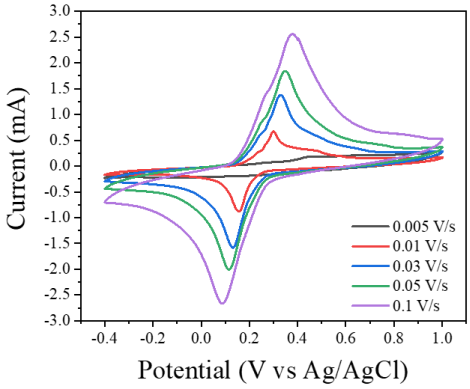


Fig. S4. CV of sample **CM-Q-NH2**.

## 4. Scanning electron microscopy (SEM)

Hitachi TM3000 Tabletop scanning electron microscope (SEM) with an acceleration voltage of 5 kV was used to obtain surface information of the obtained electrode and sample materials. To characterize the obtained samples different magnifications were used.

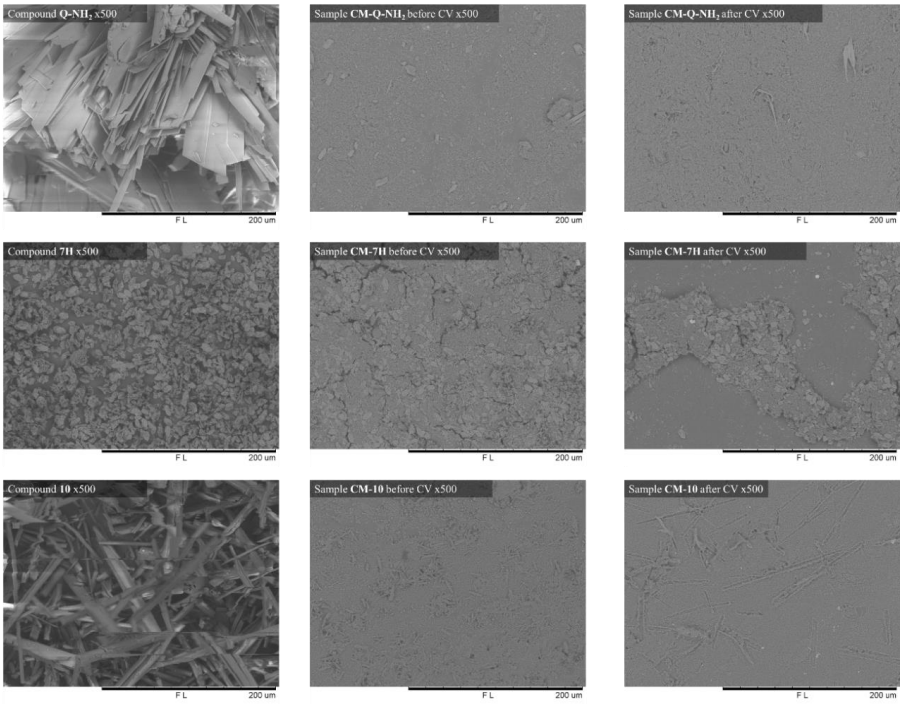


Fig. S5. Scanning electron microscopy images of compounds **7H**, **10** and **Q-NH2** and prepared cathode surfaces **CM-7H**, **CM-10** and **CM-Q-NH2** before and after CV measurements in acidic electrolyte (magnification of x500).

## 5. References


(1) Gaile, A.; Belyakov, S.; Turovska, B.; Batenko, N. Synthesis of Asymmetric Coupled Polymethines Based on a 7-Chloropyrido[1,2- a ]Benzimidazole-8,9-Dione Core. *J. Org. Chem.* **2022**, *87* (5), 2345–2355. https://doi.org/10.1021/acs.joc.1c02196.

(2) Gaile, A.; Belyakov, S.; Rjabovs, V.; Mihailovs, I.; Turovska, B.; Batenko, N. Investigation of Weak Noncovalent Interactions Directed by the Amino Substituent of Pyrido- and Pyrimido-[1,2- a ]Benzimidazole-8,9-Diones. *ACS Omega* **2023**, *8* (43), 40960–40971. https://doi.org/10.1021/acsomega.3c07005.

**Anastasija Gaile** dzimusi 1995. gadā Rīgā. Rīgas Tehniskajā universitātē (RTU) ieguvusi dabaszinātņu bakalaura grādu (2018) un maģistra grādu (2020) ķīmijā. Kopš 2020. gada strādā Dabaszinātņu un tehnoloģiju fakultātes Lietišķās ķīmijas institūtā (no 2024. gada – Ķīmijas un ķīmijas tehnoloģijas institūts; ĶĶTI), ieņemot zinātniskā asistenta amatu. Doktorantūras studiju laikā iesaistījusies darbā ar studentiem vecākā laboranta amatā, kā arī vadījusi skolēnu zinātniski pētnieciskos darbus. Patlaban ir RTU ĶĶTI zinātniskā asistente. Zinātniskās intereses saistītas ar organisko savienojumu strukturālajiem pētījumiem un to potenciālo lietojumu virzieniem.

**Anastasija Gaile** was born in 1995 in Riga. She obtained a Bachelor's degree (2018) and a Master's degree (2020) in Natural Sciences in Chemistry from Riga Technical University (RTU). Since 2020, she has been working at the Institute of Applied Chemistry (since 2024, the Institute of Chemistry and Chemical Technology (ICCT)) at the Faculty of Natural Sciences and Technology, holding the position of a research assistant. During her doctoral studies, she has been involved in working with students in the position of a laboratory assistant, as well as has supervised one secondary school scientific research project. Currently, she is a research assistant at RTU ICCT. Her scientific interests are related to structural studies of organic compounds and their potential applications.